JESSICA ALINE SOUSA BARROS

DECIPHERING THE CARBON STARVATION RESPONSE IN *Arabidopsis thaliana*: AUTOPHAGY, ALTERNATIVE RESPIRATION AND BEYOND

Thesis presented to the Universidade Federal de Viçosa, as part of the requirement of the Plant Physiology Graduate Program to obtain the degree of *Doctor Scientiae*.

Adviser: Wagner L. Araújo

VIÇOSA - MINAS GERAIS
2020

Ficha catalográfica elaborada pela Biblioteca Central da Universidade Federal de Viçosa - Campus Viçosa

T
B277d
2020

Barros, Jessica Aline Sousa, 1991-
Deciphering the carbon starvation response in *Arabidopsis thaliana* : autophagy, alternative respiration and beyond / Jessica Aline Sousa Barros. – Viçosa, MG, 2020.
133 f. : il. (algumas color.) ; 29 cm.

Orientador: Wagner Luiz Araújo.
Tese (doutorado) - Universidade Federal de Viçosa.
Inclui bibliografia.

1. Autofagia. 2. Metabolismo energético. 3. Senescência. I. Universidade Federal de Viçosa. Departamento de Biologia Vegetal. Programa de Pós-Graduação em Fisiologia Vegetal. II. Título.

CDD 22. ed. 571.2

JESSICA ALINE SOUSA BARROS

DECIPHERING THE CARBON STARVATION RESPONSE IN *Arabidopsis thaliana*: AUTOPHAGY, ALTERNATIVE RESPIRATION AND BEYOND

Thesis presented to the Universidade Federal de Viçosa, as part of the requirement of the Plant Physiology Graduate Program to obtain the degree of *Doctor Scientiae*.

APPROVED: November 18th, 2020.

Assent:

Jessica Aline Sousa Barros
Author

Wagner L. Araújo
Adviser

To my beloved father,

I hope you are proud wherever you are.

and to my little sister,

that all this time apart had resulted in something worth it.

ACKNOWLEDGMENTS

First of all, I would like to thank God for guiding me and helped me in all instances of my life, without Him none of this would be possible.

I want to thank my mom, Goreth, for supporting me in everything that I decided to do, and for always be there for me no matter what.

I want to thank the UFV, and to the Plant physiology program for the opportunity to complete my formation in an environment with excellent professionals and infrastructure.

This study was financed in part by the Coordenação de Aperfeiçoamento de Pessoal de Nível Superior – Brasil (CAPES) – Finance Code 001.

I am also thankful for the scholarships provided by National Council for Scientific and Technological Development (CNPq), and Council for Higher Education (Malag-Israel).

I sincerely thank my adviser Wagner Araújo for all guidance since my masters. Thanks for the scientific support and advices, for being the positivity person in this team, and for all encouragement and support in new challenges. I am lucky to have had an exceptional person to guide me throughout this journey.

I would like to thank my overseas supervisor Tamar Avin-Wittenberg for all support before, during, and after my PhD sandwich. I am very grateful for the experience that I had in Israel, both scientifically and culturally. I will not forget her effort to make me feel welcomed.

I want to thank João Henrique Cavalcanti, who assisted my first steps in the "scientific world", and for all friendship during this time. We surely make a very good team.

I am thankful to Prof. Adriano Nunes-Nesi for his co-supervision and for scientific contribution to this research.

I also express here my gratitude to the professors and technicians of Plant Biology Department (UFV) and Life Science Institute (Hebrew University) for the support offered.

I want to thank all my UCP colleagues, former and current members, for all the help provided in the lab. A special thanks go to Karla Gobbi, Willian Silva, David Medeiros, Hellen Oliveira, Elias Feitosa, Dora Martins, Jorge Condori and Roberto Neri for their assistance.

I am also grateful to all my Israeli co-workers, specially Sahar, Shahar, and Yoram. Surely all your help was essential for the work developed in HUJI, but most importantly was the friendship which certainly made easier to live so far from my country.

I want to thank all my friends in Viçosa, especially Jonas Vargas, Luana Luz, and Franciele Oliveira for all friendship and uncounted happy moments that we have lived here. I am grateful to have who to count on, thanks for be kind of family here.

I am especially grateful to João Antonio Siqueira for being by my side during this time. Thanks for all encouragement and support both, scientifically but specially no-scientifically. Having a partner like you surely makes my journey smooth and happier.

To all who had ever contributed to this work or support me along this time and were not nominated here, my sincere thanks.

ABSTRACT

BARROS, Jessica Aline Sousa, D.Sc., Universidade Federal de Viçosa, November, 2020. **Deciphering the carbon starvation response in *Arabidopsis thaliana*: autophagy, alternative respiration and beyon**d. Advisor: Wagner Luiz Araújo.

Throughout their life, plants are constantly challenged with environmental changes that compromises carbohydrate production. Energy deprivation triggers massive reprogramming of transcription, which further supports cellular energetic homeostasis. Therefore, catabolic pathways are generally activated leading to the catabolism of protein, lipid, and chlorophyll. Although our current understanding of plant mechanisms to overcome low energy conditions has significantly enhanced, there are still many open questions to be addressed. This thesis is therefore largely focused on understanding (i) the importance of autophagy as a mechanism of lipids and chloroplast recycling; and (ii) the transcriptional regulation of respiratory alternative pathways during low energy stress. Compelling evidence demonstrated that autophagy and amino acid catabolism are important factors of plant response to energy deprivation. This fact aside, the importance of autophagy on the remobilization of lipid substrates to sustain energy production remains unclear. Thus, we first summarized and discussed novel findings demonstrating the multifaceted roles of autophagy in lipid metabolism. Next, we provided experimental evidence of autophagy requirement to ensure lipid homeostasis during energy starvation conditions. Our findings revealed that autophagy disruption affects proper membrane mobilization and activates a general chloroplast lipid degradation program while failing to produce cytosolic lipid droplets. The degradation of chloroplasts is a hallmark of natural and stress-induced senescence, and a key role of autophagy in this process has been demonstrated elsewhere. Notably, the marked degradation of chloroplast components in mutants with disruption of autophagy (*atg* mutants) reported by several previous studies, raised the question whether other pathways of chloroplast degradation may also have a role in the remobilization of chloroplast components. It has been previously reported that the chloroplast vesiculation (CV) pathway is highly induced in *atg* mutants contributing with their early senescence phenotype during energy starvation. Thus, in the second part of this thesis the importance of CV and its coordination with autophagy under extended darkness was investigated. By using CV RNAi lines it was demonstrated that CV pathway plays a relatively minor role on Arabidopsis starvation response. However, further characterization of double mutants for CV and autophagy pathways highlighted the requirement of CV for chloroplast remodeling

of *atg* mutants under darkness. Within the last chapter novel insights concerning the regulatory components that modulates plant survival under low energetic conditions are shown. To this end, the WRKY45 transcription factor was identified as a potential regulator of metabolic reprogramming, by precisely adjusting amino acid and organic acid response via a possible regulation of mitochondrial stress signaling components. Collectively, the results obtained here describe novel mechanisms underlying plant responses to low energy conditions. These findings are discussed in the context of our current knowledge concerning energetic metabolism, autophagy, and senescence in plants.

Keywords: Autophagy. Energetic stress. Lipids. Metabolism. Senescence.

RESUMO

BARROS, Jessica Aline Sousa, D.Sc., Universidade Federal de Viçosa, novembro de 2020. **Decifrando a resposta à limitação de carbono em *Arabidopsis thaliana*: autofagia, respiração alternativa e além**. Orientador: Wagner Luiz Araújo

Durante seu ciclo de vida, plantas são constantemente expostas a mudanças ambientais que comprometem a produção de carboidratos. A depleção de energia resulta em acentuada reprogramação transcricional que sustenta a manutenção da homeostase energética. Dessa forma, vias catabólicas são geralmente ativadas levando a degradação de proteínas, lipideos e clorofila. Embora nossa compreensão atual acerca dos mecanismos que compõem a resposta de plantas ao déficit de energia tenha melhorado significativamente, ainda há muitas questões a serem abordadas. Portanto, essa tese é amplamente focada na compreensão (i) da autofagia como mecanismo de reciclagem de lipídeos e cloroplastos, (ii) da regulação transcricional das vias respiratórias alternativas durante condições de déficit de energia. Evidências tem demonstrado que a autofagia e o catabolismo de aminoácidos são peças-chaves na resposta de plantas à privação de energia. Apesar disso, pouco se sabe acerca do papel da autofagia na remobilização de substratos lipídicos para sustentar a produção de energia. Assim, primeiramente, sumarizamos estudos recentes que demonstram as múltiplas funções da autofagia no metabolismo lipídico. Em seguida, fornecemos evidências experimentais da importância da autofagia para a homeostase lipídica durante condições de déficit de energia. Nossos resultados demonstram que a ausência da autofagia afeta a mobilização de lipídeos de membrana e ativa degradação de lipídeos do cloroplasto, ao mesmo tempo que a produção de corpos lipídicos no citosol é comprometida. A degradação de cloroplastos é uma característica marcante da senescência natural e induzida por estresse, e o papel central da autofagia nesse processo foi amplamente caracterizado. Notavelmente, a degradação acentuada de componentes do cloroplasto em mutantes da autofagia (mutantes *atg*) reportada em vários estudos anteriores, sugere que outras vias de degradação do cloroplasto também atuem na remobilização dos componentes do cloroplasto. Dessa forma, foi observado anteriormente que a via de vesiculação do cloroplasto (CV) é altamente induzida em mutantes *atg*, contribuindo para seu fenótipo de senescência precoce durante condições de déficit de energia. Portanto, na segunda parte desta tese investigou-se a importância da via CV e sua coordenação com a autofagia durante condições de escuro prolongado. Assim, usando linhas mutantes RNAi para o gene CV, foi demonstrado que essa via desempenha um papel minoritário na resposta ao déficit de energia em Arabidopsis. A

caracterização adicional de duplos mutantes para as vias CV e autofagia revelou a importância de CV na remodelação estrutural do cloroplasto de mutantes *atg* no escuro prolongado. No último capítulo, novas informações sobre componentes regulatórios que modulam a sobrevivência das plantas em condições de baixa energia foram revelados. Nesse contexto, o fator de transcrição WRKY45 foi identificado como um potencial componente da reprogramação metabólica sob escuro prolongado, atuando nos níveis de aminoácidos e ácidos orgânicos por meio de vias relacionadas ao estresse mitocondrial. Coletivamente, os dados obtidos descrevem novos mecanismos inerentes às respostas de plantas a condições de baixa energia. Os resultados são discutidos no contexto do conhecimento atual acerca metabolismo energético, autofagia e senescência em plantas.

Palavras-chave: Autofagia. Estresse energético. Lipídeos. Metabolismo. Senescência.

TABLE OF CONTENT

GENERAL INTRODUCTION

Energy generation in plants is primarily dependent of carbohydrate oxidation by glycolysis and tricarboxylic acid cycle (TCA) in mitochondria (Fernie et al., 2004; Paxton and Podesta, 2006). Notwithstanding, under certain circumstances, including a wide range of environmental stress conditions, changes in the carbohydrate supply might occurs and, consequently, ATP production and energy availability is compromised (Usadel et al., 2008; Baena González and Sheen 2008; Tomé et al., 2014). Therefore, understanding how plants adapt to sugar starvation is important to develop new avenues for improving plant abiotic stress tolerance. Among the metabolic changes associated to energy deprivation, the catabolism of alternative substrates, such as lipids and amino acids, provides energy and maintains mitochondrial metabolism active in plants (Araújo et al., 2011; Tomé et al., 2014; Hildebrandt et al., 2015). Previous studies demonstrated that degradation of branched-chain amino acids (BCAA) and lysine serve as alternative electron donors to maintain respiration during extended darkness through the electron-transfer flavoprotein (ETF) and electron-transfer flavoprotein:ubiquinone oxidoreductase (ETFQO) system in Arabidopsis (Ishizaki et al., 2005; Ishizaki et al., 2006; Araújo et al., 2010). Mutants plants with disruption of either amino acid catabolism or ETF/EFQO system have been largely characterized by an early-senescence phenotype and reduced survival rate under carbon starvation induced by darkness (Ishizaki et al., 2005; Ishizaki et al., 2006; Araújo et al., 2010, Launay et al., 2019; Wang et al., 2019).

Among the protein degradation pathways, autophagy was extensively characterized by its role during starvation conditions (Hanaoka et al., 2002; Thompson et al., 2005; Chung et al., 2010; Avin-Wittenberg et al., 2015; Barros et al., 2017). Autophagy is a highly conserved system facilitating vacuolar protein degradation in eukaryotic cells (Avin-Wittenberg et al., 2018; Marshall and Vierstra 2018). The process involves the degradation of cytoplasmic constituents including soluble proteins, protein aggregates or even entire organelles allowing the recycling of cell components into primary molecules (Marshall and Vierstra, 2018). During this process, cell components are sequestered by a double membrane vesicle (the autophagosome) and delivered into the vacuoles where the material is then degraded, and macromolecules are released back into the cytosol for reuse (Marshall and Vierstra 2018). Autophagy is continuously required at a basal level for cellular maintenance during regular growth conditions but is upregulated under environmental stresses to ensure plant survival (Avin-Wittenberg et al., 2018). Compelling evidence had demonstrated that

plants with disrupted autophagy exhibited accelerated cell death and reduced survival during dark treatment (Doelling et al., 2002; Hanaoka et al., 2002; Thompson et al., 2005; Phillips et al., 2008; Chung et al., 2010; Barros et al. 2017). It was recently demonstrated the importance of autophagy for the provision of free amino acids during carbon starvation conditions (Barros et al., 2017; Hirota et al., 2018). The lower levels of amino acids in autophagy deficient mutants (*atg*) compromises the energy production, contributing for the sensitive phenotype of *atg* mutants under these conditions (Barros et al., 2017; Hirota et al., 2018). There is also an evidence that autophagy mostly favors the selective degradation of chloroplast proteins, specially Rubisco, to provide free amino acids during the early stages of carbon starvation (Hirota et al., 2018). In fact, autophagy is a versatile mechanism operating in several types of chloroplast turnover (Ishida et al., 2008; Xie et al., 2015; Izumi et al., 2017, 2018). On the other hand, the typical early-senescence phenotype of *atg* mutants suggests an activation of autophagy-independent catabolic pathways under later period of carbon starvation. In fact, the interconnection of autophagy with different chloroplast degradation pathways has been suggested (Barros et al., 2017; Kikuchi et al., 2020); however, whether these pathways are regulated and converge to determine specific physiological responses to different stress stimuli remains unknown.

Under carbon deprivation conditions, lipids components are also potential alternative substrates to fulfill energetic requirements. Lipids are stored as triacylglycerols (TAGs) packed in lipid droplets (LDs), and correspond to an important energetic carbon reserve (Lu et al., 2020). Apart from its function on protein and amino acid turnover, the importance of autophagy in different aspects of plant lipid metabolism has been revealed lately (McLoughlin et al., 2018, 2020; Have et al., 2019; Fan et al., 2019; Barros et al., 2020). In mammals and algae, autophagy is implicated in both formation and breakdown of LDs during starvation conditions (Ducharme and Bickel, 2008). In plants, the dual role of autophagy in LD biosynthesis and catabolism was recently described in Arabidopsis (Fan et al., 2019). Additionally, multi-omics studies have demonstrated the importance of autophagy in membrane recycling under both stress and non-stressful conditions (McLoughlin et al., 2018,2020; Have et al., 2019). Although recent studies have clearly revealed an interplay between autophagy and lipid metabolism, it remains contentious whether autophagy operates in lipids metabolism and to which extent it contributes to energetic homeostasis under starvation conditions.

At the same time that our knowledge about metabolic aspects of plant starvation response has substantially increased, information concerning cellular reprogramming that

occurs under energy depletion conditions still remains relatively scarce. Several studies have focused on elucidating the function of plant kinase SNRK1, identified as central component of energy starvation response (Baena-González et al., 2007; Baena-González and Sheen, 2008; Crepin and Holland, 2019). Accordingly, SNRK1 plays a key role in energetic metabolism through both enzymatic and transcriptional regulation (Nukarinen et al., 2016; Sheen, 2014). Members of bZIP family have also been characterized in association with energy limitation (Dietrich et al., 2011; Mair et al., 2015; Pedrotti et al., 2018). Therefore, bZIP1, bZIP53 and bZIP63 transcription factors were related to energy deprivation response through transcriptional control of proline dehydrogenase (ProDH), asparagine synthase (ASN) and branch chain aminotransferase 2 (BCAT-2) (Dietrich et al., 2011; Mair et al., 2015). Recently, it was demonstrated that C/S1-bZIPs transcription factors function both as heterodimers of SnRK1 and regulating genes as ETFQO and ProDH (Pedrotti et al., 2018). Over the past decade, members of the WRKY transcription factor family have been additionally characterized as major regulators of senescence and oxidative stress responses (Finatto et al., 2018). Additional evidence demonstrated that WRKY can also be involved in the mitochondrial retrograde response associated with stress (Van Aken et al., 2013; Meng et al., 2020). The connections between WRKY, senescence and mitochondrial metabolism shed light on the potential of this family to be also associated to transcriptional regulation under low energy conditions, however, this assumption remains to be elucidated.

Despite the progress reached in the last years, there are still many open questions concerning the control of plant starvation responses. It is important to mention that previous works have provided a significant contribution to our current understanding regarding the impacts of autophagy and amino acids catabolism to energy provision in plants. However, how autophagy may influence the activation of other protein degradation pathways, as well as how it mediates lipid substrates provision, requires further clarification. Additionally, scanty attention has been given to fully identify the transcriptional mechanism that regulates the diverse aspects of low energy response in plants. This knowledge is fundamental for the understanding of how energy deprivation is transduced to reprogram gene expression, leading to metabolic adaptation upon energy shortage.

Layout and aims of the chapters

This thesis is largely focused to unravel starvation-induced mechanisms governing metabolic adaptation and plant survival during low energy stress. More specifically, the main goals of this work were: *(i)* to gain additional insights into how and to which extent autophagy affects starvation response in terms of lipid turnover and its interconnections with

other degradative pathways and *(ii)* to identify novel players operating on the transcriptional regulation of energy deprivation response. In order to reach these goals different but complementary experimental approaches were taken, and therefore this thesis is organized as a compilation of four independent stand-alone chapters. In each chapter an introduction, a discussion, as well as details of the methods used, are included. At the end of the thesis, the section entitled "Concluding Remarks" summarizes the main findings of this work and a brief discussion about the challenges and open questions concerning the main aspects affecting plants response to low energy conditions is additionally presented.

Chapter 1: Multifaceted roles of plant autophagy in lipid and energy metabolism

The current knowledge about the roles of autophagy in plant lipid degradation is understudied compared to elucidated mechanisms in animals and yeast. The efforts to cover this issue are just beginning and the information acquired until now is somehow fragmented. In this chapter we showcase the compelling evidence indicating that autophagy has not just a punctual participation, but rather can operate in many aspects of lipid and membrane recycling. We posit that autophagy is a pivotal mechanism to balance the release and usage of lipids to guarantee cell survival, particularly under stress conditions. The comprehensive and integrated characterization of multiple autophagy functions will likely provide the first steps to further practical application for metabolic engineering of plant oil reserves.

Chapter 2: Autophagy is required for lipid homeostasis during dark-induced senescence

Research on autophagy roles in energetic metabolism has mostly focused on protein and amino acid degradation while knowledge supporting autophagy in lipids mobilization and turnover remains scarce. By using an extensive lipidomic approach we characterized Arabidopsis mutants with disrupted autophagy process submitted to extended darkness conditions. Our findings revealed that autophagy plays pivotal roles on lipid metabolism, contributing for: proper membrane mobilization, balance of cytosolic lipid droplet/ plastoglobuli formation, and for the regulation of β-oxidation pathways under dark-induced senescence.

Chapter 3: The interplay between autophagy and chloroplast vesiculation pathways under dark-induced senescence

Chloroplast contains a major part of total leaf proteins, thus its degradation is a crucial mechanism allowing plants to cope with stress, especially carbon starvation. Autophagy, Senescence associated-vacuoles (SAVs) and Chloroplast vesiculation (CV) are the main extraplastidial pathways of chloroplast recycling. Based on previous findings, it was hypothesized that CV can operate as a compensatory mechanism during catabolic events in which autophagy is disrupted. Although the association between autophagy and CV has been suggested, the extent to which these pathways interact to provide energetic substrates remains rather unclear. Thus, we investigated the coordination between autophagy and CV pathways in chloroplast degradation. Additionally, the importance of these pathways for energy homeostasis and plant survival under carbon starvation conditions is presented.

Chapter 4: WRKY45 transcription factor is a key regulator of metabolic adjustments during dark-induced leaf senescence in *Arabidopsis thaliana*

Energy deprivation conditions induces substantial changes in central metabolism, particularly concerning protein and amino acid catabolism. However, the regulatory networks and signaling events that modulate transcriptional control of this alternative pathway remains poorly understood. So far, only a reduced number of transcription factors (TF) were associated to plant response to energy stress. Given that members of WRKY TF family have been recognized by its function on senescence and abiotic stress, it was hypothesized that WRKY TFs is also required during energy deprivation conditions. In this chapter, we investigate the pivotal role of WRKY45 TF on plant cellular reprogramming following energy stress. Our results revealed that both amino acids and organic acids levels are significantly affected by the overexpression of WRKY45 during darkness. Further results suggest that this TF is a potential regulator of stress mitochondrial responses to energy deprivation conditions.

REFERENCES

Araújo WL, Ishizaki K, Nunes-Nesi A, Larson TR, Tohge T, Krahnert I, Witt S, Obata T, Schauer N, Graham IA, Leaver CJ, Fernie AR (2010) Identification of the 2-hydroxyglutarate and isovaleryl-CoA dehydrogenases as alternative electron donors linking lysine catabolism to the electron transport chain of Arabidopsis mitochondria. Trends Plant Sci. **22:** 1549-1563

Araújo WL, Tohge T, Ishizaki K, Leaver CJ, Fernie AR (2011) Protein degradation – an alternative respiratory substrate for stressed plants. Trends Plant Sci. **16:** 489-498

Avin-Wittenberg T, Bajdzienko K, Wittenberg G, Alseekh S, Tohge T, Bock R, Giavilasco P, Fernie AR (2015) Global analysis of the role of autophagy in cellular metabolism and energy homeostasis in Arabidopsis seedlings under carbon starvation. Plant Cell **27**: 306–22.

Avin-Wittenberg T, Baluska F, Bozhkov PV, Elander PH, Fernie AR, Galili G, Hassan A, Hofius D, Isono E, Le Bars R et al (2018) Autophagy-related approaches for improving nutrient use efficiency and crop yield protection. J Exp Bot **69**: 1335–1353

Baena-Gonzalez E, Rolland F, Thevelein JM, Sheen J (2007) A central integrator of transcription networks in plant stress and energy signalling. Nature **448:** 938–942

Baena-Gonzalez E, Sheen J (2008) Convergent energy and stress signaling. Trends Plant Sci. **13:** 474–482

Barros JAS, Cavalcanti JHF, Medeiros DB, Nunes-Nesi A, Avi-Wittenberg T, Fernie AR, Araújo WL (2017) Autophagy deficiency compromises alternative pathway of respiration following energy deprivation. Plant Physiol **175**: 62–76

Barros JAS, Siqueira JAB, Cavalcanti JHF, Araújo WL, Avin-Wittenberg T (2020) Multifaceted roles of plant autophagy in lipid and energy metabolism. Trends Plant Sci **25 (11):** 1141-1153

Chung T, Phillips AR, Vierstra RD (2010) ATG8 lipidation and ATG8- mediated autophagy in Arabidopsis require ATG12 expressed from the differentially controlled ATG12A and ATG12B loci. Plant J **62**: 483–493.

Crepin N, Rolland F (2019) SnRK1 activation, signaling, and networking for energy homeostasis. Curr Opin Plant Biol **51**: 29–36

Dietrich K, Weltmeier F, Ehlert A, Weiste C, Stahl M, Harter K, Dröse-Laser W (2011) Heterodimers of the *Arabidopsis* transcription factors bZIP1 and bZIP53 repro- gram amino acid metabolism during low energy stress. Plant Cell **23:** 381–395

Doelling JH, Walker JM, Friedman EM, Thompson AR, Vierstra RD (2002) The APG8/12-activating enzyme APG7 is required for proper nutrient recycling and senescence in Arabidopsis thaliana. Journal of Biological Chemistry **277**: 33105–33114

Ducharme NA, Bickel PE (2008) Lipid droplets in lipogenesis and lipolysis. Endocrinology **149:** 942–949.

Fan J, Yu L, Xu CG (2019) Dual role of autophagy in lipid metabolism in Arabidopsis. Plant Cell **31**: 1598–1613

Fernie AR, Carrari F, Sweetlove LJ (2004) Respiratory metabolism: glycolysis, the TCA cycle and mitochondrial electron transport. Curr Opin Plant Biol **7:** 254-261

Finatto T, Viana V E, Woyann LG, Busanello C, Maia LCD, Oliveira ACD (2018) Can WRKY transcription factors help plants to overcome environmental challenges? Genet Mol Biol **41**: 533–544.

Hanaoka H, Noda T, Shirano Y, Kat T, Hayashi H, Shibata D, Tabata S, Ohsumi Y (2002). Leaf senescence and starvation induced chlorosis are accelerated by the disruption of an Arabidopsis autophagy gene. Plant Physiol **129**: 1181–1193.

Havé M, Luo J, Tellier F, Balliau T, Cueff G, Chardon F, Zivy M, Rajjou L, Cacas JL, Masclaux-Daubresse C (2019) Proteomic and lipidomic analyses of the Arabidopsis atg5 autophagy mutant reveal major changes in endoplasmic reticulum and peroxisome metabolisms and in lipid composition. New Phytol **223**: 1461–1477.

Hildebrandt TM, Nunes-Nesi A, Araujo WL, Braun HP (2015) Amino acid catabolism in plants. Mol Plant **8:** 1563-1579

Hirota T, Izumi M, Wada S, Makino A, Ishida H (2018) Vacuolar protein degradation via autophagy provides substrates to amino acid catabolic pathways as an adaptive response to sugar starvation in Arabidopsis thaliana. Plant Cell Physiol **59:** 1363–1376

Ishida H, Yoshimoto K, Izumi M, Reisen D, Yan Y, Makino A, Ohsumi Y, Hanson MR, Mae T (2008) Mobilization of rubisco and stroma-localized fluorescent proteins of chloroplasts to the vacuole by an ATG gene-dependent autophagic process. Plant Physiol **148:** 142–155

Ishizaki K, Larson TR, Schauer N, Fernie AR, Graham IA, Leaver CJ (2005) The critical role of Arabidopsis Electron-transfer Flavoprotein:ubiquinone oxidoreductase during dark-induced starvation. Plant Cell **17:** 2587–2600

Ishizaki K, Schauer N, Larson TR, Graham IA, Fernie AR, Leaver CJ (2006) The mitochondrial Electron Transfer Flavoprotein Complex is essential for survival of Arabidopsis in extended darkness. Plant J **47:** 751-760

Izumi M, Ishida H, Nakamura S, Hidema J (2017) Entire photodamaged chloroplasts are transported to the central vacuole by Autophagy. Plant Cell **29**: 377–394

Izumi M, Nakamura S (2018) Chloroplast protein turnover: the influence of extraplastidic processes, including autophagy. Int J Mol Sci **19**: 828

Kikuchi Y, Nakamura S, Woodson JD, Ishida H, Ling Q, Hidema J, Jarvis RP, Hagihara S, Izumi M (2020) Chloroplast autophagy and ubiquitination combine to manage oxidative damage and starvation responses. Plant Physiol **183**: 1531–1544.

Launay A, Cabassa-Hourton C, Eubel H, Maldiney R, Guivarc'h A, Crilat E, Planchais S, Lacoste J, Bordenave-Jacquemin M, Clément G, Richard L, Carol P, Braun HP, Lebreton S, Savouré A (2019) Proline oxidation fuels mitochondrial respiration during dark-induced leaf senescence in Arabidopsis thaliana. J Exp Bot **70**: 6203–6214.

Lu J, Xu Y, Wang J, Singer SD, Chen G (2020) The role of triacylglycerol in plant stress response. Plants **9**: 472

Mair A, Pedrotti L, Wurzinger B, Anrather D, Simeunovic A, Weiste C, Valerio C, Dietrich K, Kirchler T, Nâgele T, Carbajosa JV, Hanson J, Baena-Gonzalez E, Chaben C, Weckwerth W, Dröge-Laser W, Teige M (2015) SnRK1-triggered switch of bZIP63 dimerization mediates the low-energy response in plants. Elife **4:** doi: 10.7554/ eLife.05828

Chapter 1:

Multifaceted Roles of Plant Autophagy in Lipid and Energy Metabolism

Trends in Plant Science

CellPress
REVIEWS

Review

Multifaceted Roles of Plant Autophagy in Lipid and Energy Metabolism

Jessica A.S. Barros,[1,2] João A.B. Siqueira,[1] João H.F. Cavalcanti,[3] Wagner L. Araújo,[1,4,*] and Tamar Avin-Wittenberg[2,4,*]

Together with sugars and proteins, lipids constitute the main carbon reserves in plants. Lipids are selectively recycled and catabolized for energy production during development and in response to environmental stresses. Autophagy is a major catabolic pathway, operating in the recycling of cellular components in eukaryotes. Although the autophagic degradation of lipids has been mainly characterized in mammals and yeast, growing evidence has highlighted the role of autophagy in several aspects of lipid metabolism in plants. Here, we summarize recent findings focusing on autophagy functions in lipid droplet (LD) metabolism. We further provide novel insights regarding the relevance of autophagy in the maintenance and clearance of mitochondria and peroxisomes and its consequences for proper lipid usage and energy homeostasis in plants.

Highlights

Our understanding of autophagy function in lipid degradation in plants is understudied compared with the elucidated mechanisms in animals and yeast. However, the potential roles of plant autophagy in lipid recycling and metabolism are beginning to come to light.

Macroautophagy is a versatile mechanism involved in lipid metabolism, operating both in the turnover of membrane components and in various aspects of reproduction, like pollen and seed metabolism.

A mechanism resembling yeast microlipophagy was recently proposed in plant cells and is specifically active under starvation.

The interplay between microlipophagy and lipolysis in plants seems to drive the efficient usage of lipid reserves.

The autophagic maintenance of mitochondria and peroxisomes is essential for the optimal operation of these organelles, further enabling proper lipid turnover.

On the Connection between Autophagy, Lipids, and Energy

Lipids are not only essential components of cellular structure and function but also provide backbones for biological membranes and play important roles as signaling molecules [1]. Moreover, lipids are carbon-storage substances with a high potential to generate energy in the form of ATP. When carbohydrate supply is impaired (e.g., carbon starvation, senescence, drought, hypoxia), not only proteins [2,3] but also lipids [4–6] are used as alternative respiratory substrates to cope with cellular metabolic demands. In plants, lipids are stored as triacylglycerols (TAGs) in a specialized organelle, the lipid droplet (LD). TAG is a high-energy compound that can be further catabolized in fatty acid (FA) to be oxidized by peroxisomal **β-oxidation** (see Glossary). The breakdown of stored fat reserves occurs primarily by lipases [7]. However, a type of selective autophagy, known as **lipophagy**, also contributes to lipid catabolism in mammalian and yeast cells (*Saccharomyces cerevisiae*) [8]. Autophagy is an evolutionarily conserved recycling mechanism, functioning in cellular homeostasis under nonstressful conditions and is required for plant tolerance to several stresses [9]. Over the years, many efforts have focused on elucidating the function of autophagy in the turnover of proteins and amino acids for cellular energy supply [10–12]. However, the importance of autophagy in the different aspects of plant lipid metabolism is only beginning to come to light.

A direct connection between lipids and autophagy has been previously characterized as specific lipids are needed for **autophagosome** biogenesis (Box 1). Here, we discuss the newly described mechanisms in a different context, focusing on the role of autophagy in lipid homeostasis and turnover and its impact on general metabolism. We describe the currently proposed mechanisms of LD degradation in plant cells. Furthermore, we address the role of autophagy in the turnover of membrane lipids and its connection to FA accumulation and LD biosynthesis. We additionally highlight unnoticed evidence related to the importance of autophagy in various organelles during lipid catabolism. Surprisingly, both mechanistically and genetically, our understanding of autophagy functions during lipid degradation in plants is somewhat limited compared with the elucidated mechanisms in animals and yeast. Therefore, a comprehensive and integrated characterization

[1]Departamento de Biologia Vegetal, Universidade Federal de Viçosa, 36570-900 Viçosa, MG, Brazil
[2]Department of Plant and Environmental Sciences, Alexander Silberman Institute of Life Sciences, Hebrew University of Jerusalem, Givat Ram, Jerusalem 9190401, Israel
[3]Instituto de Educação, Agricultura e Ambiente, Universidade Federal do Amazonas, Humaitá, Amazonas, Brazil
[4]These authors have contributed equally

*Correspondence:
wlaraujo@ufv.br (W.L. Araújo) and
tamar.avin-wittenberg@mail.huji.ac.il (T. Avin-Wittenberg).

© 2020 Elsevier Ltd. All rights reserved.

of multiple autophagy functions in plants is long overdue and is likely to provide an exciting research avenue in plant lipid management.

Lipid Catabolism: A Paradoxical Question

In plants, the most recognized role of lipid reserves is to provide ATP and carbon skeletons during seedling establishment [13]. Accordingly, dysfunctional β-oxidation mutants exhibit delayed and reduced germination rates, as well as dependency on external sucrose for successful seedling establishment [4,14]. However, equally important and much less addressed is the role of lipids as an alternative respiratory substrate during senescence [6,15,16]. In the absence of carbohydrates, lipid reserves can potentially be degraded and targeted for peroxisomal β-oxidation, generating acetyl-CoA for energy production via mitochondrial respiration [4,6,17]. The induction of transcripts and proteins associated with lipid catabolism was observed in response to both developmental and dark-induced senescence [15,18,19].

The requirement of β-oxidation to overcome starvation conditions was demonstrated with mutant plants deficient in peroxisomal ABC-transporter1 (PXA1) and the keto-acyl-thiolase2 (KAT2) enzyme [4]. The knockout mutants *pxa1* and *kat2* showed higher sensitivity to extended darkness due to impaired lipid catabolism, whereas wild-type plants survived by using ATP generated from FAs [4]. Furthermore, it was recently demonstrated that lipids could be catabolized during carbohydrate fluctuations throughout the plant life cycle [20]. Moreover, arabidopsis (*Arabidopsis thaliana*) mutants deficient in starch synthesis exhibited increased rates of FA synthesis and turnover [20]. The disruption of peroxisomal β-oxidation reduced the growth and delayed the bolting and flowering of these mutants, suggesting that lipids are catabolized to fulfill

Box 1. Lipid Requirement for Autophagosome Biogenesis

During autophagy, a double-membrane structure called the 'autophagosome' sequesters cargo molecules. The process involves the operation of ATG proteins and lipid recruitment. To date, only PI 3-phosphate (PI3P) and PE have been characterized as players in autophagosome formation [72] (Figure I).

Autophagy initiation comprises the formation of a pre-autophagosomal structure, the phagophore, from the assembly of a shaped membrane in membrane origin sites. [73]. In mammals, the ATG1 complex is recruited to ER subdomains enriched in PI3P to initiate this process [74]. Although the interaction between the ATG1 complex and PI3P remains elusive in plants, it has been demonstrated that PI3P-enriched ER subdomains participate in the early steps of phagophore formation and regulation [75–78]. Phagophore enrichment with PI3P recruits and stabilizes the membrane binding of ATG18 [79], participating in the recruitment of ATG9 vesicles, possibly from Golgi compartments, to ER sites for autophagosome extension [79]. Notably, ATG9 is not essential for autophagy in plants, suggesting that other membranes might contribute to autophagosome formation [79,80].

ATG8 and PE mediate the elongation and closure of the phagophore. The protease ATG4 processes ATG8 and the ATG5/ATG12/ATG16 ubiquitin-like complex, together with ATG7 and ATG3, conjugates it to PE [73]. The conjugation/deconjugation of ATG8 to PE is needed for autophagosome biogenesis and dynamics [81]. Moreover, ATG8-PE anchoring might ensure the stability of phagophore membrane shapes [82]. Additionally, the interaction of ATG8-PE and PI3P with SH3 DOMAIN-CONTAINING PROTEIN2 (SH3P2) sustains high curvature at the edges of the phagophore [83]. After autophagosome formation, ATG8-PE on the outer membrane is delipidated by ATG4, releasing ATG8 [78,84].

Starved *atg5*- and *atg7*-mutant seedlings displayed altered levels of PE and PI. The low PE levels were associated with disrupted autophagosome biogenesis and a minor PE requirement [46]. Conversely, *atg* mutants accumulated PI under starvation conditions [46] as well as low-N and low-S treatments [52]. It remains unclear how autophagy influences the dynamics of PI and PE thus regulating membrane trafficking pathways in plants.

Besides PI and PE, the composition of the lipid backbone of the autophagosome remains under debate. Membrane contact sites (MCSs) have emerged as potential lipid sources since the donor organelle membrane can directly transfer lipids to the phagophore [85]. Compelling recent evidence points to the initiation of the plant autophagosome at ER–plasma membrane MCSs [86]. However, ER–mitochondria and ER–Golgi contact sites are also likely participants in autophagosome formation [87,88]. Further studies are required to decipher alternative sources of autophagosome membrane biogenesis.

Glossary

Autolysosome: structure generated from the fusion of an autophagosome with a vesicle that contains hydrolases – the lysosome – in animal cells.
Autophagosome: double-membrane-bound vesicle formed during macroautophagy that engulfs cytoplasmic contents and delivers it to the vacuole for degradation.
Lipid droplet (LD)-associated proteins: proteins inserted into or attached on the surface of the LD that perform specific structural and/or enzymatic functions. Oleosins, steroleosins, and caleosins are the three major families characterized to date.
Lipophagy: selective degradation of LDs by autophagy.
Lipotoxicity: generally, it can be defined as an increased concentration of free FAs that impairs cellular homeostasis and disrupts cell function
Macroautophagy: degradation pathway of cytoplasmic components mediated by the autophagosome, through cargo engulfment and transport to the vacuole (in plants); corresponds to the most characterized and general type of autophagy in plants and is referred to throughout the text as autophagy.
Macroautophagy machinery: conserved machinery of core autophagy-related (ATG) proteins participating in macroautophagy. ATG1, ATG13, ATG11, and ATG101 operate in promoting phagophore nucleation and expansion. The transmembrane protein ATG9 recruits lipids for phagophore elongation along with ATG2 and ATG18. Expansion and closure of the phagophore membranes require two ubiquitination-like systems. ATG8 is initially processed by ATG4 then conjugated to the lipid PE by ATG3. The second comprises ATG12, which is conjugated to ATG5 by ATG10. ATP-dependent activating enzyme ATG7 operates in both conjugation systems. The ATG12-ATG5-ATG16 conjugate promotes the lipidation of ATG8 with PE and its anchorage into the phagophore membrane. The closed autophagosome is further transported to the vacuole.
Microautophagy: direct vacuolar engulfment of cytoplasmic components by invagination or protrusion of the vacuolar membrane.
Retromer: a multiprotein complex involved in the intracellular trafficking of cargo proteins. It comprises two subcomplexes, the core retromer

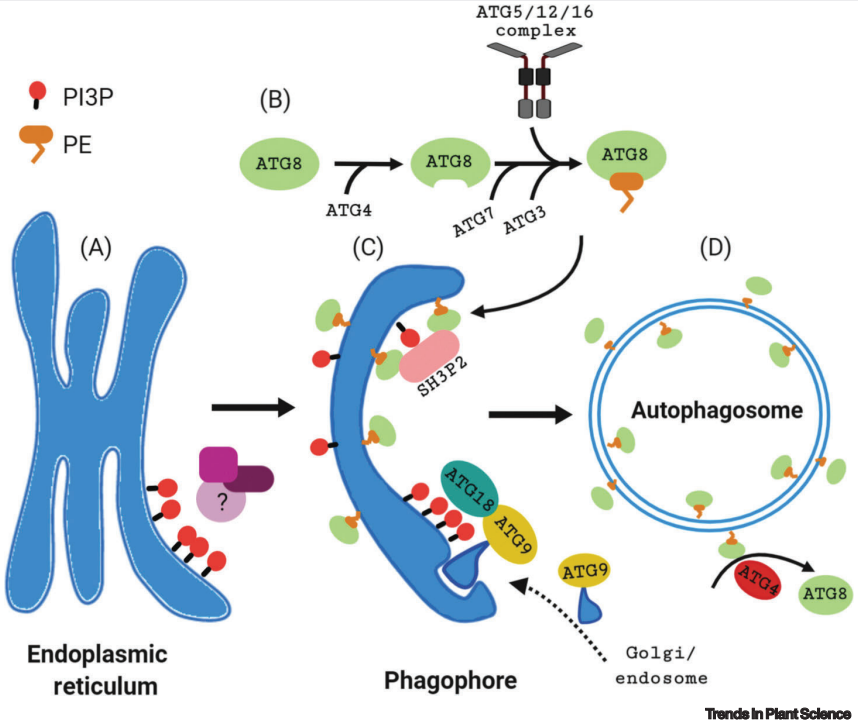

Figure I. A Simplified Model of Lipid Signaling during Autophagosome Formation. (A) Autophagy is initiated by the recruitment of the activated ATG1 complex in the phosphatidylinositol 3-phosphate (PI3P)-enriched domains of the endoplasmic reticulum (ER) in animals. In plants, this interaction was not demonstrated so far (marked question). (B) On the activation of autophagy, ATG8 is conjugated to phosphatidylethanolamine (PE) by successive reactions catalyzed by ATG4, ATG7, ATG3, and the ATG5/12/16 complex to be attached to the phagophore membrane. (C) The phagophore decoration with PI3P mediates the anchoring of ATG18. This protein is required for the recruitment of ATG9 vesicles, the main membrane source for phagophore elongation. At the same time, PI3P, in conjunction with ATG8-PE, interacts with SH3 domain-containing protein2 (SH3P2) to stimulate phagophore curvature. (D) In the last step, the double-membrane autophagosome is closed, the ATG8-PE on the outer membrane is cleaved by ATG4, and only ATG8 anchored in the inner membrane is retained. The figure was created using BioRender (https://biorender.com).

constituted by the VPSs and a dimer of sorting nexins (SNXs).
β-Oxidation: the breakdown of FAs, exclusively occurring in peroxisomes in plants. The hydrolysis of lipid reserves releases free FAs, which enter the peroxisome through PXA1. Inside peroxisomes, FAs are reactivated by long-chain acyl-CoA synthetase (LACS), which adds a CoA moiety generating Acyl-CoA. The following steps of β-oxidation comprise sequential oxidation by acyl-CoA oxidase (ACX) isozymes. The resultant molecules of 2-trans-enoyl-CoA are then hydrolyzed to produce 3-ketoacyl-CoAs via 3-hydroxyacyl-CoAs by the action of multifunctional protein 2 (MFP2). Finally, a 3-ketoacyl-CoA thiolase (KAT) releases acetyl-CoA and a shortened fatty acyl-CoA, which can undergo further rounds of β-oxidation.

energetic requirements [20]. Similarly, the overexpression of phospholipid diacylglycerol acyltransferase1 (PDAT1), an enzyme in TAG biosynthesis, resulted in increased lipid reserves, leading to growth improvement of starchless mutant plants [21].

The catabolism of cellular lipid components, during either stress or senescence, produces free FAs [4,17,22]. An excess of FAs is seemingly toxic to cells because they can either generate damaging bioactive lipids or disrupt mitochondrial membrane integrity [5]. LDs are considered a safe deposit of neutral lipids. Thus, their production has been proposed as a strategic mechanism of plant survival due to their potential to scavenge FAs and prevent lipotoxicity [5,17,22,23]. The restriction of LD hydrolysis by disruption of the cytosolic lipase SUGAR DEPENDENT1 (SDP1) prevented cytosolic FA and reactive oxygen species (ROS) overload, enhancing plant tolerance to extended darkness [17]. The impairment of FA import into peroxisomes also affected plant responses to salt stress, as observed by the increased salt tolerance of *pxa1* mutants compared with wild-type plants [24]. By contrast, increasing the flux of FAs into β-oxidation had the opposite effect in mutants overexpressing the *PDAT1* gene, which were more sensitive

to salt [24]. Collectively, these results indicate that β-oxidation of FAs generates oxidative stress thereby eliciting a negative impact on plant performance under adverse environmental conditions, and reinforce the role of LD production as a protective mechanism against FA lipotoxicity.

Nevertheless, it has been previously demonstrated that a balanced flux between TAG production and β-oxidation is essential to maintain the concentration of FAs below toxic levels under prolonged conditions of darkness [4]. The reversal of the *pxa1* sensitive phenotype by sucrose addition highlights the notion that carbon substrates can overcome the energetic failure triggered by the impairment of FA β-oxidation. Interestingly, the addition of sucrose triggered a drop in FA levels in *pxa1* plants as well as mitigated the mutant phenotype [4]. Furthermore, the disruption of TAG hydrolysis by SDP1 disruption reverted the *pxa1* phenotype under darkness [17]. The interplay between energy production and toxic FA clearance is an apparent double-edged question in lipid metabolism. We posit that proper regulation between lipid degradation and scavenging mechanisms is required to ensure plant survival under suboptimal conditions.

Lipophagy: Eating Away Plant Lipid Reserves

During recent years, we have witnessed a growing body of evidence describing the critical functions of lipophagy. This pathway was initially observed in starved mouse hepatocytes in which LDs were captured into autophagosomes for subsequent degradation in **autolysosomes** [25]. In yeast, different from animal cells, LDs are directly delivered into the vacuole by **microautophagy**, a process denominated microlipophagy [26,27]. Later, it was observed that microlipophagy is activated in yeast cells under sudden glucose restriction and promotes survival during acute nutritional stress [28]. Intriguingly, this response was not activated by gradual glucose or amino acid starvation and failed to provide the energy required for long-term survival [28].

The intricate relationship between lipophagy induction and starvation and/or stress conditions has also been demonstrated in various algal species. Accordingly, in the green alga *Auxenochlorella protothecoides*, LDs were directly sequestered by a microautophagy-like mechanism during the transition from heterotrophic to autotrophic conditions [29]. By contrast, in starved cells of *Micrasterias denticulata*, the degradation of LDs involved sequestration by double-membrane vesicles, in a process that resembles **macroautophagy** [30]. More recently, fusion events between LDs and autophagosomes were demonstrated in *Chlamydomonas reinhardtii* cells under prolonged nutrient deficiency, suggesting that a macroautophagy-type mechanism is most likely to be involved in LD turnover in this alga [31].

In plants, LDs are especially prominent in seeds, further metabolized during post-germinative growth until the acquisition of photoautotrophism. Similarly, pollen accumulates LDs, which might serve as an energy source that drives pollen germination and pollen tube growth. Although they are barely observed in mature leaves, LD numbers increase during both natural senescence and abiotic stress, accumulating lipids derived from the dismantlement of membranes [32–34]. The vast majority of studies of plant LD hydrolysis have been focused on the process mediated by lipases during the early stages of seedling development [35–39]. To date, the dominant plant lipases characterized are SDP1 and the related SDP1-like (SDP1-L). Together, they are responsible for most of the TAG hydrolysis in arabidopsis seeds [35]. SDP1 mediates the hydrolysis of LDs in arabidopsis seedlings through a process dependent on LD–peroxisome contact [36]. To this end, SDP1 is transported from the peroxisome to LDs trough peroxisome tubular extensions associated with a **retromer** enzyme named vacuolar protein-sorting protein (VPS) 29 [36]. Then, SDP1 catabolizes LD TAGs into FAs, further imported by PXA1 to be metabolized via peroxisomal β-oxidation (Figure 1A). Recently, an LD-associated degradation (LDAD) system was described in arabidopsis, mediating the turnover of **LD-associated**

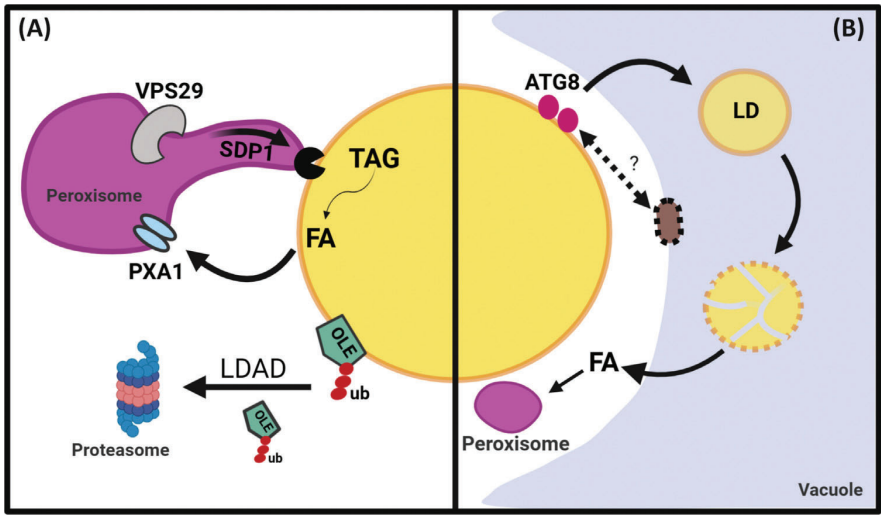

Figure 1. Removal of Cellular Lipid Droplets (LDs) in Plants Is Dependent on Both Lipolysis and Lipophagy. (A) Lipolysis is mediated by sugar-dependent 1 (SDP1) during post-germinative seedling growth. LDs are protected by the surface oleosin (OLE). Before lipolysis occurs, OLE is ubiquitinated and degraded in the proteasome by the LD-associated degradation (LDAD) system. After the removal of OLE, SDP1 is transferred from the peroxisome to the LD surface via peroxisomal extensions. This process is dependent on the retromer subunit vacuolar protein-sorting protein 29 (VPS29). Fatty acids (FAs) from triacylglycerol (TAG) hydrolysis are then imported into the peroxisome by peroxisomal ABC-transporter1 (PXA1). (B) The current model of the microlipophagy-type mechanism indicates that, in later stages of starvation, LDs are fully internalized in the vacuole by an autophagy-dependent process. The degradation of LDs generates FAs that are further oxidized in peroxisomes. The direct interaction of autophagy-related protein 8 (ATG8) (pink circle) with the LD surface is seemingly the signal for degradation. It remains unknown whether other ATG proteins (brown circle) operate as ATG8 cargo receptors or in tonoplast remodeling. The figure was created using BioRender (https://biorender.com).

proteins [37,38]. These proteins are crucial regulators of LD dynamics as their initial degradation is required for the LD breakdown process [39].

In addition to significant advances in our current understanding of lipolysis in the past few years, the first experimental evidence of plant lipophagy was recently described in plants submitted to extended periods of darkness [40]. Under this condition, the association of the ATG8 protein with LDs was verified in leaves of plants ectopically expressing oleosin fused with GFP (OLE1-GFP) in either a *tgd1* or a wild-type background. Oleosin is the most characterized LD protein in seed and trigalactosyl diacyl glycerol1 (TGD) is involved in lipid transfer from the endoplasmic reticulum (ER) to the chloroplast. Also, immunoelectron microscopy of *sdp1*-knockout mutant plants with ATG8 antibody revealed the localization of ATG8 proteins on the LD surface under darkness [40].The disruption of autophagy by mutations in the *ATG5* or *ATG2* gene inhibited vacuolar LD degradation and triggered an increase of TAG levels in *sdp1* mutants [40]. Despite the recognized participation of these ATG proteins in the **macroautophagy machinery**, no autophagosome-like structure was observed, suggesting that lipophagy in arabidopsis probably occurs through a microautophagy-like mechanism (Figure 1B). This type of lipophagy has been characterized mostly in yeast and comprises the direct engulfment of LDs by vacuolar structures [27,28]. In yeast, ATG6 and ATG14 proteins, components of the phosphatidylinositol (PI) 3-kinase (PI3K) complex I involved in autophagosome biogenesis, were characterized as essential players in microlipophagy [28]. Under acute glucose starvation, ATG14 shifts the ER to the vacuole

membrane where, in cooperation with ATG6, it mediates the formation of vacuolar microdomains to support the engulfment of LDs [28]. The suggested microlipophagy-type process in plants is also dependent on autophagy core genes [40]. However, by contrast to that observed in yeast, ATG8 was reported to interact directly with LDs, and no ATG protein was localized to the tonoplast. The possible role of ATG8 as a specific receptor for lipophagy, as well as the dual mechanism and the proteins controlling tonoplast remodeling for LD capture in plants, remains to be investigated.

Importantly, this initial study of lipophagy in plants was executed in different mutant backgrounds with altered lipid metabolism. The ectopic expression of OLE1 triggered TAG accumulation and induced the formation of clusters of small LDs in leaves [41]. Features such as LD size, organization, and composition can directly influence LD catabolic mechanisms [42,43]. Further investigation using solely autophagy-affected plants is required before overall conclusions can be made about the functions of lipophagy in plants.

The characterization of *atg5 sdp1* double mutants pointed out new connections in plant TAG metabolism [40]. It demonstrated the potential role of autophagy in the late reduction of levels of TAG accumulated in *sdp1* mutants after extended darkness [40]. At the same time, the disruption of SDP1 did not affect autophagic flux under either optimal growth or starvation conditions [40]. Collectively, these results imply that autophagy plays a more significant role in TAG hydrolysis under acute carbon deprivation conditions.

Although connections between lipolysis and lipophagy have been reported in mammals and yeast [44], the existence of this association in plants remains to be elucidated. SDP1 was characterized as the main LD catabolic pathway in arabidopsis young tissues, given that, during seedling establishment, almost no TAG degradation is observed following SDP1 disruption [45]. Therefore, lipophagy might not contribute significantly to TAG breakdown during seedling establishment under optimal conditions. However, autophagy disruption triggered delayed seedling development together with the accumulation of several FAs and TAG species in both *atg5-1* and *atg7-2* mutants subjected to carbon deprivation [46]. The fact that autophagy has a significant impact on seedling lipid homeostasis, mostly during carbon starvation, suggests that autophagy and SDP1 can be differently regulated according to the conditions.

Recent reports also pointed out the existence of possible connections between autophagy and phospholipases. Multiomics analysis of maize (*Zea mays*) *atg12* mutants revealed a general induction of transcripts and proteins of phospholipases A, C, and D regardless of the condition imposed [47]. Transcript data from microarray analysis performed on arabidopsis *atg5* [48] also revealed the upregulation of phospholipases A and D on nitrogen depletion. By contrast to SDP1, phospholipase activity is associated with membrane recycling rather than LD degradation. Collectively, these data provide compelling evidence for connections between autophagy and lipid degradation mechanisms. More research is required to fully decipher not only the contributions of lipophagy and lipases in different tissues and conditions but also the differential regulation of these processes and how this interplay contributes to lipid homeostasis.

The Distinct Roles of Autophagy in Plant Lipid Metabolism

Besides the different autophagy mechanisms participating in LD degradation described in mammals and yeast, autophagy had also been reported to function in LD biogenesis [5,49]. Moreover, autophagic degradation of intracellular membranes generates free FAs, which are channeled to the production of neutral lipids and stored in LDs in starved mouse cells [49]. This dual role of autophagy was recently discussed in plants, in which autophagy mediates LD degradation under starvation conditions while it participates in leaf TAG synthesis in arabidopsis under

nonstress conditions [8,40]. The disruption of basal autophagy resulted in lower TAG accumulation in mature and senescent arabidopsis leaves [40]. Furthermore, it was shown that the reduced levels of TAG were triggered by the prevention of FA mobilization from organelle membranes in *atg5* and *atg2* mutants [40]. Interestingly, it was reported that autophagy had no impact on dark-induced TAG synthesis, which is mostly derived from plastid membranes, suggesting that other pathways operate in the mobilization of these organelle components [40].

Beyond operating LD degradation in *C. reinhardtii* under acute starvation, the same study revealed the potential role of autophagy in LD biogenesis in this alga. The close contact between autophagosomes and LDs without fusion events was observed during the early stage of starvation, indicating that autophagy may supply lipid substrates for LD biogenesis under mild carbon stress [31]. Autophagy was previously reported to play an essential role in LD and TAG synthesis in *C. reinhardtii* under nitrogen limitation [50,51].

Recently, the accumulation of lipid breakdown intermediates was observed in both arabidopsis *atg5* and maize *atg12* mutants, suggesting a general impairment of membrane recycling in these plants [47,52]. These reports point out the requirement of autophagy for proper membrane recycling, also suggesting its possible role in LD synthesis. The accumulation of partially disassembled lipids in maize *atg12* mutants implied that autophagy is not required for the initial stages of membrane turnover, which is probably mediated by phospholipases (see section, 'Lipophagy: Eating Away Plant Lipid Reserves'), but it seems likely to be necessary for the complete recycling of its products [52].

In mammalian cells, the strategic mechanism of TAG accumulation during starvation has been associated with autophagy, wherein the formation of LDs is likely to be mediated by lipids released from autophagic degradation of organellar membranes [49]. Despite the evidence of the role of autophagy in the recycling of membrane components, further studies are required to ascertain whether autophagy also participates in membrane component remobilization during starvation events and to what extent these components are channeled to LD production.

Besides the function of autophagy in membrane homeostasis, the requirement of autophagy in lipid metabolism has been previously shown during plant reproductive stages and seed and/or seedling metabolism. In rice (*Oryza sativa*) pollen cells, autophagy mediates the degradation of specific lipids and is essential for pollen development and plant fertility [53]. Recently, the requirement of autophagy to metabolize lipid reserves during pollen tube growth and pollen germination was also reported in tobacco [54]. In arabidopsis, the overexpression of autophagy genes triggered an increase in seed FA content and seed oil yield per plant [55]. By contrast, *atg5*- and *atg7*-knockout plants displayed changes in seed FA composition in conjunction with lower FA content [55]. In addition, transcriptomic analysis of *atg5* and *atg7* plants revealed higher levels of transcripts involved in lipid degradation, suggesting that the lipid response observed in *atg*-knockout mutants is likely to be more related to altered lipid catabolism than to lipid synthesis [55].

Autophagy is, therefore, emerging as a key player in lipid metabolism, participating in various steps, including the modulation of TAG levels, LD synthesis and/or catabolism, and the degradation of membrane lipid components (Figure 2). Nevertheless, the conditions and regulatory mechanisms governing autophagy function in LD synthesis or degradation remain to be elucidated. Besides that, the recent discoveries regarding the importance of autophagy in lipid metabolism in reproductive organs open new avenues concerning the targeted manipulation of autophagy as a biotechnological strategy to enhance the productivity of oil crops (for a review see [56]).

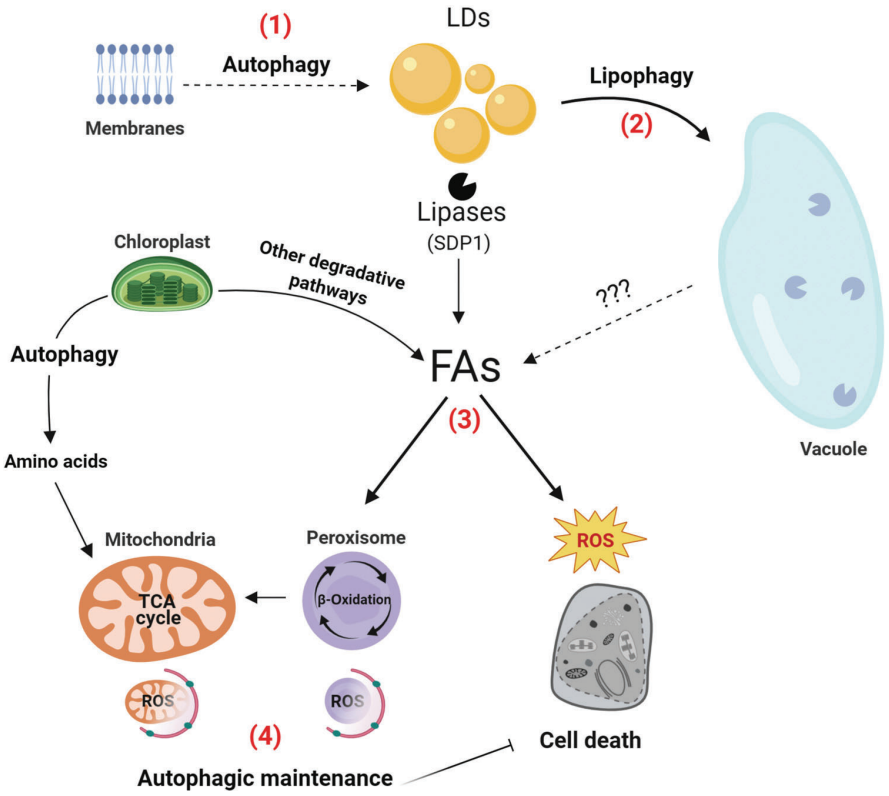

Figure 2. Possible Roles of Autophagy in the Modulation of Lipid Catabolism. (1) Autophagy mediates the degradation of organelle membrane lipids and contributes to lipid droplet (LD) formation. (2) LDs can either be directly catabolized by cytosolic lipases or selectively transported by lipophagy for subsequent vacuole degradation. (3) The disruption of autophagy affects proper lipid metabolism, generating fatty acids (FAs) that are overloaded in the cytosol, triggering reactive oxygen species (ROS) accumulation and leading to cell death. (4) Autophagy is required for the proper maintenance of peroxisomes and mitochondria, assuring that β-oxidation of FA and acetyl-CoA oxidation sustain energy generation. The figure was created using BioRender (https://biorender.com). Abbreviations: SDP1, sugar-dependent 1; TCA, tricarboxylic acid.

Beyond LDs: Autophagic Maintenance of Lipid-Catabolizing Organelles

Besides LD catabolism, obtaining energy from lipids comprises two spatially separated steps: degradation of FAs to acetyl-CoA and ATP generation from products of β-oxidation. Accordingly, a balance between LD degradation, β-oxidation in peroxisomes, and mitochondrial respiration is crucial for the appropriate usage of lipids. Both mitochondria and peroxisomes are potential ROS sources and their quality control and maintenance depend on proper autophagy operation [57,58].

In plants, peroxisomes harbor the entire pathway of FA β-oxidation, generating acetyl-CoA, and hydrogen peroxide (H_2O_2) as byproducts [59]. Although antioxidative enzymes can detoxify ROS, peroxisomes are still likely to be damaged and require turnover. The selective degradation of peroxisomes by autophagy (pexophagy) is crucial for quality control of plant peroxisomes [60]. Impaired pexophagy triggers the accumulation of dysfunctional peroxisome aggregates containing inactive catalase in arabidopsis seedlings [61,62]. Pexophagy has also been shown to function in the transition of glyoxysomes into leaf peroxisomes during photomorphogenesis [63–65]. Besides this, higher activity of peroxisomes also occurs during developmental and stress-induced

senescence, pointing out the relevance of peroxisomal maintenance under these conditions [61,66,67].

The selective autophagic degradation of mitochondria, mitophagy, has been extensively documented in both yeast and mammalian cells as a central clearance mechanism [68]. The identification of mitophagy players in plants remains contentious, although several candidates have been suggested [57]. Besides those, various studies point out the existence of the selective turnover of plant mitochondria by autophagy [57,69,70]. In general, mitophagy is active at basal levels to continuously replace dysfunctional mitochondria. However, a stronger mitophagy response was observed under conditions of higher mitochondrial activity, including oxidative stress and senescence [69,70].

During developmental and carbon-induced senescence, the metabolism of chloroplasts, mitochondria, and peroxisomes is remodeled to catabolize alternative substrates to meet the energy requirements of the cell [16]. Chloroplasts can be considered a significant reservoir of proteins and lipids and unsurprisingly are the first cellular components to be recycled during both developmental and induced senescence [16]. Autophagy plays several roles in the turnover of chloroplast proteins; however, compelling evidence highlighted that autophagy-independent pathways are more likely to mediate chloroplast-lipid turnover (Box 2). Different from chloroplasts, both the integrity and the activity of mitochondria and peroxisomes must be conserved until later stages of senescence. This is due to the apparent reorganization of cellular metabolism to support the catabolism of amino acids and FAs instead of sugars [16].

Recently, experimental evidence has shed light on the connections between autophagy, organelle maintenance, and lipid metabolism. Lipidomic and proteomic analyses of maize and arabidopsis autophagy mutants showed remarkable accumulation of mitochondrial and peroxisomal proteins coupled with changes in the lipid profile [47,52]. Maize *atg12* mutants were characterized by

Box 2. Chloroplast Lipid Reserves and Autophagy

Chloroplasts contain high amounts of glycerolipids in their membranes as well as harboring unique lipid structures: the plastoglobuli (PGs). PGs are globular LDs comprising a membrane lipid monolayer that is physically connected to the stroma leaflet of the thylakoid membrane [89]. This organization permits lipid exchange between the PGs and the thylakoid membrane [90]. During senescence, both PG numbers and size increase concomitantly with thylakoid disassembly and pigment breakdown [91]. This response is associated with the accumulation of FA phytyl esters (FAPEs) produced by esterification of lipids released from the chloroplast and phytol from chlorophyll degradation [91]. The production of FAPEs in PGs can be interpreted as a strategic mechanism to prevent the accumulation of toxic substances (e.g., free FAs, phytol).

Moreover, chloroplast lipid reserves can be used as an energy source for plants under carbon starvation [4]. The disruption of β-oxidation triggers FA and PG accumulation, culminating in early cell death [4]. Although PGs can serve as lipid storage to be catabolized in other organelles, little is known about PG export from the chloroplast. Ultrastructural analyses of senescing watermelon leaves suggested that PGs can be expelled into the cytoplasm by vesicles containing PGs produced at the chloroplast envelope [92]. However, the precise mechanism underlying this transport remains unclear.

Autophagy is known to operate in the turnover of chloroplasts during stress and senescence. Several pathways of autophagy-mediated chloroplast degradation have been characterized [93]. Controversially, chloroplast breakdown and loss of thylakoid proteins are a marked phenotype of *atg* mutants under stress conditions [11,12,70,94]. It is postulated that autophagy deficiency disrupts chloroplast homeostasis, triggering its catabolism. Chlorophagy-derived vesicles have been mostly associated with the sequestration of chloroplastic proteins [95,96] and there is no current evidence that autophagy can transport chloroplast lipids. Recently, substantial changes in the lipid profile of plants lacking autophagy were described [47,52]. These studies revealed generally low levels of the main chloroplast lipids, mono- and digalactoyldiglycerides (MGDGs and DGDGs), in both arabidopsis *atg5* and maize *atg12* mutants, highlighting the chloroplast-dismantling phenotype regardless of the growth conditions. In addition, *atg12* maize mutants showed decreased levels of PG-associated proteins but no difference in PG-associated metabolites [47]. Therefore, this evidence supports the hypothesis that autophagy is required for chloroplast maintenance rather than for lipid metabolism in this organelle. Other autophagy-independent pathways might preferentially operate in the mobilization of chloroplast lipids and PGs.

increased peroxisomal proteins, together with high levels of free FAs and lipid-breakdown intermediate products [47]. This suggests an impairment of FA oxidation, also implying that the high levels of β-oxidation proteins in *atg12* plants is most likely to represent an accumulation of dysfunctional peroxisomes triggered by impairment of autophagy rather than as a result of higher peroxisomal activity [47]. Similarly, proteomic analysis of *atg5* arabidopsis mutants showed accumulation of peroxisomal, mitochondrial, and ER proteins under regular or low nitrate and/or sulfate availability [52]. More specifically, an increase of proteins related to the tricarboxylic acid (TCA) cycle, β-oxidation, and glycolysis was observed in the mutants. However, this response, associated with the reduction of chloroplast lipids and undetectable levels of TAG, was related with more active peroxisomal and/or mitochondrial activity rather than a disruption of organellar autophagy, as previously suggested in maize [52].

Overall, an increase of proteins related to ER and ER stress was also verified in arabidopsis *atg5* mutants [52]. The ER is not only a pivotal site of lipid production and autophagosome biogenesis but is itself a target for selective autophagy [71]. The disruption of ER homeostasis triggered by the absence of autophagy might also affect lipid and LD production. The accumulation of the PDAT1 protein, related to TAG and LD assembly in the ER, was observed in mutants lacking autophagy [52]. Although higher LD turnover was suggested given that TAG levels were undetectable, further analyses of LD dynamics are needed to address this scenario. Considering that the ER is connected with autophagosome biogenesis, the impairment of autophagosome formation might also trigger an unusual accumulation of nonused lipids at the ER. PI and phosphatidylethanolamine (PE) are the main lipid species involved in autophagosome formation (Box 1). An increase of both PI and PE was observed in *atg5* mutants [52]. Although ER stress is recognized to be a result of the unfolded protein response, it will be interesting to investigate how lipid imbalance triggered by autophagosome biogenesis affects overall lipid metabolism in the ER.

Collectively, these studies indicate that autophagy broadly affects lipid homeostasis in conjunction with peroxisomal, mitochondrial, and ER protein accumulation. However, further effort must be made to elucidate whether this response is triggered by higher organellar activity to catabolize lipid components or just represents oxidized organelles that cannot be recycled correctly in the absence of autophagy. Further studies will determine whether the accumulation of phospholipids is triggered by impairment of LD biogenesis or disruption of organellar autophagy and how LD production is affected by autophagy-mediated ER maintenance.

Concluding Remarks

Novel discoveries have greatly expanded the importance of autophagy during lipid metabolism. An emerging model suggests that autophagy can operate in various aspects of lipid and membrane recycling (Figure 2). Current evidence also highlights the complexity of this system, given that autophagy is required for energy-producing organelle maintenance under stress conditions. This is of paramount importance because the removal of damaged and potentially ROS-overproducing energy organelles can circumvent cell death and promote lipid catabolism. At present, only fragmented experimental information is available regarding the mechanism governing lipophagy in plants and the impact of the different selective autophagy pathways in lipid homeostasis. Collectively, the overview presented here emphasizes that a better understanding of these mechanisms is likely to be translated into practical methods, in view of improvement of plant performance under energy-limited conditions such as senescence and abiotic stress. It also clearly points to the necessity for further studies to establish the regulation and physiological functions of the exciting complexity governing plant lipid metabolism (see Outstanding Questions). The recent studies highlighted here also indicate that the regulation of lipid metabolism undoubtedly remains a potential target for metabolic engineering in the management of plant oil reserves.

Outstanding Questions

Is there crosstalk between lipophagy and other cytosolic lipases? Which mechanism controls the differential activation of these pathways?

Considering that the autophagic degradation of LDs in plants resembles microlipophagy in yeast, does the process also occur through the formation of microdomains in the tonoplast? If so, which proteins are responsible for it?

How do plant cells switch between autophagic routes of LD biosynthesis and lipophagy?

How essential is the autophagic maintenance of peroxisomes and mitochondria for efficient lipid catabolism? What is its impact on energy homeostasis and plant survival under particular environmental conditions?

How does the plant cell modulate autophagy to optimize lipid catabolism under suboptimal conditions?

Acknowledgments

This work was made possible through financial support from the Serrapilheira Institute, Brazil (grant Serra-1812-27067). We also thank the scholarships granted by the National Council for Scientific and Technological Development (CNPq-Brazil) and the Council for Higher Education (Malag-Israel) to J.A.S.B. and the Foundation for Research of the State of Minas Gerais (FAPEMIG-Brazil) to J.A.B.S. Research fellowships granted by CNPq-Brazil to W.L.A. are also gratefully acknowledged. Work at the T.A-W. group is supported by the Israeli Science Foundation, grant number 1942/19.

References

1. Nakamura, Y. (2017) Plant phospholipid diversity: emerging functions in metabolism and protein–lipid interactions. *Trends Plant Sci.* 22, 1027–1040
2. Araújo, W.L. *et al.* (2011) Protein degradation – an alternative respiratory substrate for stressed plants. *Trends Plant Sci.* 16, 489–498
3. Hildedrandt, T.M. *et al.* (2015) Amino acid catabolism in plants. *Mol. Plant* 8, 1563–1579
4. Kunz, H.H. *et al.* (2009) The ABC transporter PXA1 and peroxisomal β-oxidation are vital for metabolism in mature leaves of *Arabidopsis* during extended darkness. *Plant Cell* 21, 2733–2749
5. Rambold, A.S. *et al.* (2015) Fatty acid trafficking in starved cells: regulation by lipid droplet lipolysis, autophagy, and mitochondrial fusion dynamics. *Dev. Cell* 32, 678–692
6. Law, S.R. *et al.* (2018) Darkened leaves use different metabolic strategies for senescence and survival. *Plant Physiol.* 177, 132–150
7. Pyc, M. *et al.* (2017) Turning over a new leaf in lipid droplet biology. *Trends Plant Sci.* 22, 596–609
8. Elander, P.H. *et al.* (2018) Autophagy in turnover of lipid stores: trans-kingdom comparison. *J. Exp. Bot.* 69, 1301–1311
9. Avin-Wittenberg, T. (2019) Autophagy and its role in plant abiotic stress management. *Plant Cell Environ.* 42, 1045–1053
10. Izumi, M. (2013) Autophagy contributes to nighttime energy availability for growth in *Arabidopsis*. *Plant Physiol.* 161, 1682–1693
11. Barros, J.A.S. *et al.* (2017) Autophagy deficiency compromises alternative pathway of respiration following energy deprivation. *Plant Physiol.* 175, 62–76
12. Hirota, T. *et al.* (2018) Vacuolar protein degradation via autophagy provides substrates to amino acid catabolic pathways as an adaptive response to sugar starvation in *Arabidopsis thaliana*. *Plant Cell Physiol.* 59, 1363–1376
13. Graham, I.A. (2008) Seed storage oil mobilization. *Annu. Rev. Plant Biol.* 59, 115–142
14. Rylott, E.L. *et al.* (2006) The *Arabidopsis thaliana* multifunctional protein gene (MFP2) of peroxisomal β-oxidation is essential for seedling establishment. *Plant J.* 45, 930–941
15. Watanabe, M. *et al.* (2013) Comprehensive dissection of spatiotemporal metabolic shifts in primary, secondary, and lipid metabolism during developmental senescence in *Arabidopsis*. *Plant Physiol.* 162, 1290–1310
16. Chrobok, D. *et al.* (2016) Dissecting the metabolic role of mitochondria during developmental leaf senescence. *Plant Physiol.* 172, 2132–2153
17. Fan, J. *et al.* (2017) A central role for triacylglycerol in membrane lipid breakdown, fatty acid β-oxidation, and plant survival under extended darkness. *Plant Physiol.* 174, 1517–1530
18. Buchanan-Wollaston, V. *et al.* (2005) Comparative transcriptome analysis reveals significant differences in gene expression and signalling pathways between developmental and dark/starvation induced senescence in *Arabidopsis*. *Plant J.* 42, 567–585
19. Troncoso-Ponce, M.A. *et al.* (2013) Lipid turnover during senescence. *Plant Sci.* 205–206, 13–19
20. Yu, L.H. *et al.* (2018) Starch deficiency enhances lipid biosynthesis and turnover in leaves. *Plant Physiol.* 178, 118–129
21. Fan, J. *et al.* (2019) Diversion of carbon flux from sugars to lipids improves the growth of an *Arabidopsis* starchless mutant. *Plants* 8, 229
22. Wang, C.W. (2016) Lipid droplets, lipophagy, and beyond. *Biochim. Biophys. Acta* 1861, 793–805
23. Fan, J. *et al.* (2013) Phospholipid:diacylglycerol acyltransferase-mediated triacylglycerol biosynthesis is crucial for protection against fatty acid-induced cell death in growing tissues of *Arabidopsis*. *Plant J.* 76, 930–942
24. Yu, L.H. *et al.* (2019) Peroxisomal fatty acid β-oxidation negatively impacts plant survival under salt stress. *Plant Signal. Behav.* 14, 2
25. Singh, R. *et al.* (2009) Autophagy regulates lipid metabolism. *Nature* 458, 1131–1135
26. van Zutphen, T. *et al.* (2014) Lipid droplet autophagy in the yeast *Saccharomyces cerevisiae*. *Mol. Biol. Cell* 25, 290–301
27. Vevea, J.D. *et al.* (2015) Role for lipid droplet biogenesis and microlipophagy in adaptation to lipid imbalance in yeast. *Dev. Cell* 35, 584–599
28. Seo, A.Y. *et al.* (2017) AMPK and vacuole associated Atg14p orchestrate μ-lipophagy for energy production and long-term survival under glucose starvation. *Elife* 6, e21690
29. Zhao, L. *et al.* (2014) Autophagy-like processes are involved in lipid droplet degradation in *Auxenochlorella protothecoides* during the heterotrophy–autotrophy transition. *Front. Plant Sci.* 5, 400
30. Schwarz, V. *et al.* (2017) Carbon starvation induces lipid degradation via autophagy in the model alga *Micrasterias*. *J. Plant Physiol.* 208, 115–127
31. Tran, Q.G. *et al.* (2019) Dynamic interactions between autophagosomes and lipid droplets in *Chlamydomonas reinhardtii*. *Cells* 8, 992
32. Shimada, T.L. *et al.* (2015) Oil body-mediated defense against fungi: from tissues to ecology. *Plant Signal. Behav.* 10, e989036
33. Gidda, S.K. *et al.* (2016) Lipid droplet-associated proteins (LDAPs) are required for the dynamic regulation of neutral lipid compartmentation in plant cells. *Plant Physiol.* 170, 2052–2071
34. Huang, A.H.C. (2018) Plant lipid droplets and their associated oleosin and other proteins: potential for rapid advances. *Plant Physiol.* 176, 1894–1918
35. Kelly, A.A. *et al.* (2011) Seed storage oil mobilization is important but not essential for germination or seedling establishment in *Arabidopsis*. *Plant Physiol.* 157, 866–875
36. Thazar-Poulot, N. *et al.* (2015) Peroxisome extensions deliver the *Arabidopsis* SDP1 lipase to oil bodies. *Proc. Natl. Acad. Sci. U. S. A.* 112, 4158–4163
37. Deruyffelaere, C. *et al.* (2018) PUX10 is a CDC48A adaptor protein that regulates the extraction of ubiquitinated oleosins from seed lipid droplets in *Arabidopsis*. *Plant Cell* 30, 2116–2136
38. Kretzschmar, F.K. *et al.* (2018) PUX10 is a lipid droplet-localized scaffold protein that interacts with CELL DIVISION CYCLE 48 and is involved in the degradation of lipid droplet proteins. *Plant Cell* 30, 2137–2160
39. Deruyffelaere, C. *et al.* (2015) Ubiquitin-mediated proteasomal degradation of oleosins is involved in oil body mobilization during post-germinative seedling growth in *Arabidopsis*. *Plant Cell Physiol.* 56, 1374–1387
40. Fan, J. *et al.* (2019) Dual role for autophagy in lipid metabolism in *Arabidopsis*. *Plant Cell* 31, 1598–1613
41. Fan, J. *et al.* (2013) Dual role for phospholipid: diacylglycerol acyltransferase: enhancing fatty acid synthesis and diverting fatty acids from membrane lipids to triacylglycerol in *Arabidopsis* leaves. *Plant Cell* 25, 3506–3518
42. Siloto, R.M. *et al.* (2006) The accumulation of oleosins determines the size of seed oilbodies in *Arabidopsis*. *Plant Cell* 18, 1961–1974
43. López-Ribera, I. *et al.* (2014) The evolutionary conserved oil body associated protein OBAP1 participates in the regulation of oil body size. *Plant Physiol.* 164, 1237–1249
44. Zechner, R. *et al.* (2017) Cytosolic lipolysis and lipophagy: two sides of the same coin. *Nat. Rev. Mol. Cell Biol.* 18, 671–684

45. Eastmond, P.J. (2006) SUGAR-DEPENDENT1 encodes a patatin domain triacylglycerol lipase that initiates storage oil breakdown in germinating *Arabidopsis* seeds. *Plant Cell* 18, 665–675
46. Avin-Wittenberg, T. *et al.* (2015) Global analysis of the role of autophagy in cellular metabolism and energy homeostasis in *Arabidopsis* seedlings under carbon starvation. *Plant Cell* 27, 306–322
47. McLoughlin, F. *et al.* (2018) Maize multi-omics reveal roles for autophagic recycling in proteome remodeling and lipid turnover. *Nat. Plants* 4, 1056–1070
48. Masclaux-Daubresse, C. *et al.* (2014) Stitching together the multiple dimensions of autophagy using metabolomics and transcriptomics reveals impacts on metabolism, development, and plant responses to the environment in *Arabidopsis*. *Plant Cell* 26, 1857–1877
49. Nguyen, T.B. *et al.* (2017) DGAT1-dependent lipid droplet biogenesis protects mitochondrial function during starvation-induced autophagy. *Dev. Cell* 42, 9–21
50. Couso, I. *et al.* (2017) Autophagic flux is required for the synthesis of triacylglycerols and ribosomal protein turnover in *Chlamydomonas*. *J. Exp. Bot.* 69, 1355–1367
51. Pugkaew, W. *et al.* (2017) Role of autophagy in triacylglycerol biosynthesis in *Chlamydomonas reinhardtii* revealed by chemical inducer and inhibitors. *J. Appl. Phycol.* 30, 15–22
52. Havé, M. *et al.* (2019) Proteomic and lipidomic analyses of the *Arabidopsis atg5* autophagy mutant reveal major changes in ER and peroxisome metabolisms and in lipid composition. *New Phytol.* 223, 1461–1477
53. Kurusu, T. *et al.* (2014) OsATG7 is required for autophagy-dependent lipid metabolism in rice postmeiotic anther development. *Autophagy* 10, 878–888
54. Zhao, P. *et al.* (2020) Autophagy-mediated compartmental cytoplasmic deletion is essential for tobacco pollen germination and male fertility. *Autophagy* Published online January 30, 2020. https://doi.org/10.1080/15548627.2020.1719722
55. Minina, E.A. *et al.* (2018) Transcriptional stimulation of rate-limiting components of the autophagic pathway improves plant fitness. *J. Exp. Bot.* 69, 1415–1432
56. Ortiz, R. *et al.* (2020) Oil crops for the future. *Curr. Opin. Plant Biol.* Published online January 22, 2020. https://doi.org/10.1016/j.pbi.2019.12.003
57. Broda, M. *et al.* (2018) Mitophagy: a mechanism for plant growth and survival. *Trends Plant Sci.* 23, 434–450
58. Young, P.G. (2019) A facile forward-genetic screen for *Arabidopsis* autophagy mutants reveals twenty-one loss-of-function mutations disrupting six ATG genes. *Autophagy* 15, 941–959
59. Kao, Y.T. *et al.* (2018) Peroxisome function, biogenesis, and dynamics in plants. *Plant Physiol.* 176, 162–177
60. Olmedilla, A. (2019) Selective autophagy of peroxisomes in plants: from housekeeping to development and stress responses. *Front. Plant Sci.* 10, 1021
61. Shibata, M. *et al.* (2013) Highly oxidized peroxisomes are selectively degraded via autophagy in *Arabidopsis*. *Plant Cell* 25, 4967–4983
62. Yoshimoto, K. *et al.* (2014) Organ-specific quality control of plant peroxisomes is mediated by autophagy. *J. Cell Sci.* 127, 1161–1168
63. Farmer, L.M. *et al.* (2013) Disrupting autophagy restores peroxisome function to an *Arabidopsis lon2* mutant and reveals a role for the LON2 protease in peroxisomal matrix protein degradation. *Plant Cell* 25, 4085–4100
64. Bartel, B. *et al.* (2014) Mutation of the *Arabidopsis* LON2 peroxisomal protease enhances pexophagy. *Autophagy* 10, 518–519
65. Lingard, M.J. and Bartel, B. (2009) *Arabidopsis* LON2 is necessary for peroxisomal function and sustained matrix protein import. *Plant Physiol.* 151, 1354–1365
66. Pan, R. *et al.* (2018) Proteome analysis of peroxisomes from dark-treated senescent *Arabidopsis* leaves. *J. Integr. Plant Biol.* 60, 1028–1050
67. Voitsekhovskaja, O.V. *et al.* (2014) Plant peroxisomes are degraded by starvation-induced and constitutive autophagy in tobacco BY-2 suspension-cultured cells. *Front. Plant Sci.* 5, 629
68. Pickles, S. *et al.* (2018) Mitophagy and quality control mechanisms in mitochondrial maintenance. *Curr. Biol.* 28, 170–185
69. Minibayeva, F. *et al.* (2012) Oxidative stress-induced autophagy in plants: the role of mitochondria. *Plant Physiol. Biochem.* 59, 11–19
70. Li, F. *et al.* (2014) AUTOPHAGY-RELATED11 plays a critical role in general autophagy- and senescence-induced mitophagy in *Arabidopsis*. *Plant Cell* 26, 788–807
71. Zhang, X. *et al.* (2020) Reticulon proteins modulate autophagy of the endoplasmic reticulum in maize endosperm. *Elife* 9, e51918
72. Gomez, R.E. *et al.* (2018) Lipids in membrane dynamics during autophagy in plants. *J. Exp. Bot.* 69, 1287–1299
73. Marshall, R.S. and Vierstra, R.D. (2018) Autophagy: the master of bulk and selective recycling. *Annu. Rev. Plant Biol.* 69, 173–208
74. Nishimura, T. *et al.* (2017) Autophagosome formation is initiated at phosphatidylinositol synthase-enriched ER subdomains. *EMBO J.* 36, 1719–1735
75. Le Bars, R. *et al.* (2014) ATG5 defines a phagophore domain connected to the endoplasmic reticulum during autophagosome formation in plants. *Nat. Commun.* 5, 4121
76. Fujiki, Y. *et al.* (2007) An *Arabidopsis* homolog of yeast ATG6/VPS30 is essential for pollen germination. *Plant Physiol.* 143, 1132–1139
77. Huang, X. *et al.* (2019) Genetic analyses of the arabidopsis ATG1 kinase complex reveal both kinase-dependent and independent autophagic routes during fixed-carbon starvation. *Plant Cell* 31, 2973–2995
78. Chung, T. (2019) How phosphoinositides shape autophagy in plant cells. *Plant Sci.* 281, 146–158
79. Zhuang, X. *et al.* (2017) ATG9 regulates autophagosome progression from the endoplasmic reticulum in *Arabidopsis*. *Proc. Natl. Acad. Sci. U. S. A.* 114, 426–435
80. Shin, K.D. *et al.* (2014) A revised assay for monitoring autophagic flux in *Arabidopsis thaliana* reveals involvement of AUTOPHAGY-RELATED9 in autophagy. *Mol. Cells* 37, 399–405
81. Nair, U.A. *et al.* (2012) A role for Atg8-PE deconjugation in autophagosome biogenesis. *Autophagy* 8, 780–793
82. Knorr, R.L. *et al.* (2014) Membrane morphology is actively transformed by covalent binding of the protein Atg8 to PE-lipids. *PLoS One* 9, e0115357
83. Zhuang, X. *et al.* (2013) A BAR-domain protein SH3P2, which binds to phosphatidylinositol 3-phosphate and ATG8, regulates autophagosome formation in *Arabidopsis*. *Plant Cell* 25, 4596–4615
84. Yoshimoto, K. *et al.* (2004) Processing of ATG8s, ubiquitin-like proteins, and their deconjugation by ATG4s are essential for plant autophagy. *Plant Cell* 16, 2967–2983
85. Prinz, W.A. *et al.* (2020) The functional universe of membrane contact sites. *Nat. Rev. Mol. Cell Biol.* 21, 7–24
86. Wang, P. *et al.* (2019) Plant AtEH/Pan1 proteins drive autophagosome formation at ER–PM contact sites with actin and endocytic machinery. *Nat. Commun.* 10, 5132
87. Hamasaki, M. *et al.* (2013) Autophagosomes form at ER–mitochondria contact sites. *Nature* 495, 389–393
88. Nascimbeni, A.C. *et al.* (2017) ER–plasma membrane contact sites contribute to autophagosome biogenesis by regulation of local PI3P synthesis. *EMBO J.* 36, 2018–2033
89. Rottet, S. *et al.* (2015) The role of plastoglobules in thylakoid lipid remodeling during plant development. *Biochim. Biophys. Acta* 1847, 889–899
90. Kirchhoff, H. (2019) Chloroplast ultrastructure in plants. *New Phytol.* 223, 565–574
91. Van Wijk, K.J. and Kessler, F. (2017) Plastoglobuli: plastid microcompartments with integrated functions in metabolism, plastid developmental transitions, and environmental adaptation. *Annu. Rev. Plant Biol.* 68, 253–389
92. Liu, L. (2016) Ultramicroscopy reveals that senescence induces *in-situ* and vacuolar degradation of plastoglobules in aging watermelon leaves. *Micron* 80, 135–144
93. Izumi, M. *et al.* (2019) Autophagic turnover of chloroplasts: its roles and regulatory mechanisms in response to sugar starvation. *Front. Plant Sci.* 10, 280
94. Thompson, A.R. *et al.* (2005) Autophagic nutrient recycling in *Arabidopsis* directed by the ATG8 and ATG12 conjugation pathways. *Plant Physiol.* 138, 2097–2110

95. Ishida, H. *et al.* (2008) Mobilization of rubisco and stroma-localized fluorescent proteins of chloroplasts to the vacuole by an ATG gene-dependent autophagic process. *Plant Physiol.* 148, 142–155

96. Michaeli, S. *et al.* (2014) Arabidopsis ATG8-INTERACTING PROTEIN1 is involved in autophagy-dependent vesicular trafficking of plastid proteins to the vacuole. *Plant Cell* 26, 4084–4101

Chapter 2:

Autophagy is required for lipid homeostasis during dark-induced senescence

doi:10.1093/plphys/kiaa120 PLANT PHYSIOLOGY 2021: 0: 1–17

Plant Physiology

Research Article

Autophagy is required for lipid homeostasis during dark-induced senescence

Jessica A. S. Barros,[1,2] Sahar Magen,[2] Taly Lapidot-Cohen,[3] Leah Rosental,[3] Yariv Brotman,[3] Wagner L. Araújo [1,†] and Tamar Avin-Wittenberg [2,*,†]

1 Departamento de Biologia Vegetal, Universidade Federal de Viçosa, 36570-900 Viçosa, Brazil
2 Department of Plant and Environmental Sciences, Alexander Silberman Institute of Life Sciences, Hebrew University of Jerusalem, Givat Ram 9190401, Israel
3 Department of Life Sciences, Ben-Gurion University of the Negev, 8410501 Beer-Sheva, Israel

*Author for communication: tamar.avin-wittenberg@mail.huji.ac.il
†Senior authors.

J.A.S.B., W.L.A., and T.A-W. designed the research. J.A.S.B. performed most of the research. T.A.-W. and W.L.A. supervised the project. Y.B. contributed with new reagents/analytic tools for lipid analysis. S.M. contributed with transcript and western blot analysis. T.L.-C. performed lipid profile. L.R. performed the free fatty acid analysis. J.A.S.B., W.L.A., and T.A-W. analyzed the data and wrote the manuscript with contributions of all the authors.
The author responsible for distribution of materials integral to the findings presented in this article in accordance with the policy described in the Instructions for Authors (https://academic.oup.com/plcell) is: Tamar Avin-Wittenberg (tamar.avin-wittenberg@mail.huji.ac.il).

Abstract

Autophagy is an evolutionarily conserved mechanism that mediates the degradation of cytoplasmic components in eukaryotic cells. In plants, autophagy has been extensively associated with the recycling of proteins during carbon-starvation conditions. Even though lipids constitute a significant energy reserve, our understanding of the function of autophagy in the management of cell lipid reserves and components remains fragmented. To further investigate the significance of autophagy in lipid metabolism, we performed an extensive lipidomic characterization of Arabidopsis (*Arabidopsis thaliana*) autophagy mutants (*atg*) subjected to dark-induced senescence conditions. Our results revealed an altered lipid profile in *atg* mutants, suggesting that autophagy affects the homeostasis of multiple lipid components under dark-induced senescence. The acute degradation of chloroplast lipids coupled with the differential accumulation of triacylglycerols (TAGs) and plastoglobuli indicates an alternative metabolic reprogramming toward lipid storage in *atg* mutants. The imbalance of lipid metabolism compromises the production of cytosolic lipid droplets and the regulation of peroxisomal lipid oxidation pathways in *atg* mutants.

Introduction

The precise control of energy homeostasis is crucial for plant survival, particularly under biotic and abiotic stress conditions. Under low energy availability, plants require a strategy other than carbohydrate oxidation to fully sustain energy production. Therefore, proteins, lipids, and chlorophylls can be catabolized instead of sugars to provide alternative substrates for the tricarboxylic acid (TCA) cycle. This assures the continued operation of the mitochondrial electron transport chain (Ishizaki et al., 2005; Kunz et al., 2009; Araújo et al., 2011; Hörtensteiner and Kräutler, 2011).

Among the alternative substrates of respiration in plants, lipids comprise a significant carbon reserve that represents an important alternative source of energy. Although in comparison to carbohydrates, the usage of lipids is less efficient, as assessed by the respiratory quotient, their intracellular storage and utilization are critical for the maintenance of

Received October 22, 2020. Accepted December 14, 2020. Advance access publication 13 January 2021
© American Society of Plant Biologists 2021. All rights reserved. For permissions, please email: journals.permissions@oup.com

cellular energy homeostasis (Araújo et al., 2011; Yang and Benning, 2018). Plants store lipids as the neutral lipid specie TAG (Yang and Benning, 2018). In leaf mesophyll cells, TAG is deposited in specialized storage compartments, namely lipid droplets (LDs) in the cytosol or plastoglobuli (PG) inside chloroplasts (van Wijk and Kessler, 2017). During nutrient deprivation, cellular lipid reserves are hydrolyzed into fatty acids (FAs), which are further catabolized during β-oxidation. Accordingly, mutants with dysfunctional β-oxidation, triggered by the disruption of the PEROXISOMAL ABC TRANSPORTER 1 (PXA1), exhibit hypersensitivity to extended darkness (Kunz et al., 2009). Moreover, several transcripts of the β-oxidation pathway are up-regulated during developmental leaf senescence (Troncoso-Ponce et al., 2013).

Autophagy, one of the primary cellular catabolic process, is involved in the degradation and recycling of cytoplasmic constituents into primary metabolites (Avin-Wittenberg et al., 2018). The autophagy mechanism is governed by autophagy-related (*ATG*) genes that are highly conserved among eukaryotes (Marshall and Vierstra, 2018). Plants with genetic disruption of *ATG* genes (hereafter, *atg* mutants) have been well characterized for sensitivity to several stresses, particularly nutrient starvation (Avin-Wittenberg, 2018). The importance of autophagy in plants has been mostly associated with the recycling of proteins to amino acids under starvation conditions (Izumi et al., 2013; Li et al., 2014, Barros et al., 2017; Hirota et al., 2018; McLoughlin et al., 2018, 2020). By contrast, in mammals and yeast, autophagy has been largely associated with both protein and lipid metabolism (Elander et al., 2018; Barros et al., 2020). Accordingly, it was shown that autophagy supplies FAs for LD biogenesis as well as mediates the selective degradation of LDs in both mammals and yeast (Singh et al., 2009; Rambold et al., 2015; Nguyen et al., 2017).

A growing body of evidence suggests a dual role of autophagy in the lipid metabolism of alga and plants. Thus, in Chlamydomonas (*Chlamydomonas reinhardtii*), it has been postulated that autophagy participates in both TAG biosynthesis and LD formation (Couso et al., 2017; Pugkaew et al., 2017). In addition, microscopic evidence pointed to the autophagy-mediated engulfment of LDs in the algae *Auxenochlorella protothecoides* (Zhao et al., 2014) and *Micrasterias denticulata* (Schwarz et al., 2017). Interestingly, recent data also suggested that autophagy may mediate LD formation during early stages of starvation whereas it likely operates in LD degradation at the later stages of nitrogen starvation in Chlamydomonas (Tran et al., 2019).

In vascular plants, it was demonstrated that autophagy contributes to TAG synthesis via the turnover of organellar membranes in Arabidopsis under normal growth conditions (Fan et al., 2019). On the other hand, it was suggested that the autophagy operates in the degradation of LDs by a selective microautophagy mechanism under extended darkness (Fan et al., 2019). Notably, this study was based on the analysis of Arabidopsis mutants overexpressing the LD marker OLE1-GFP and carrying a knockout mutation affecting the SUGAR DEPENDENT-1 (SDP1) lipase, which are genotypes with altered LD and TAG metabolism (Fan et al., 2013, 2017; Barros et al., 2020). In maize (*Zea mays*), *atg12-1* mutant presented a higher LD number, which could reflect active LD assembly or disruption of LD catabolism (McLoughlin et al., 2020). It remains contentious, however, whether autophagy mediates the biogenesis or degradation of LDs in vegetative tissues (Elander et al., 2018; Barros et al., 2020; Masclaux-Daubresse et al., 2020). Although recent studies have clearly revealed an interplay between autophagy and lipid metabolism (McLoughlin et al., 2018, 2020; Havé et al., 2019; Fan et al., 2019), relatively little is known about the role of autophagy in the mobilization of lipid components under energy-limited conditions.

Here, we investigated the significance of autophagy in lipid metabolism during dark-induced senescence in Arabidopsis. By performing an extensive lipidomic analysis of three independent *atg* mutants, we observed an overall impact of autophagy deficiency on all lipid classes analyzed and the free FA (FFA) profile. The differential pattern of phospholipid levels and TAG accumulation was further coordinated with changes in LD number and PG size. In addition, analysis of β-oxidation genes revealed an induction of lipid oxidation pathways in *atg* mutants. Collectively, our results demonstrate that autophagy is an essential component in the management of lipid reserves, affecting membrane lipid mobilization, the balance of LD and PG formation, and the regulation of β-oxidation pathways under dark-induced senescence.

Results

Differential lipid response of *atg* mutants under dark-induced senescence

To examine the involvement of autophagy in lipid remodeling during dark-induced senescence, we analyzed three previously described Arabidopsis autophagy mutants: *atg5-1* and *atg7-2* with full inhibition of autophagy (Chung et al., 2010), and *atg9-4* that displays a milder reduction of the autophagic process (Shin et al., 2014). The experimental setup consisted of the subjection of 4-week-old plants to extended darkness conditions, a system widely used to induce energetic stress in plants (Ishizaki et al., 2005; Araújo et al., 2010; Barros et al., 2017).

To further investigate the impact of autophagy disruption on lipid homeostasis during dark-induced senescence, we performed Liquid Chromatography–Mass Spectrometry lipidomic analysis of *atg5-1*, *atg7-2*, *atg9-4*, and their corresponding wild-type (WT). We were able to identify 119 lipid species of the following classes: phosphatidylcholine (PC), phosphatidylethanolamine (PE), diacylglycerol (DAG), triacylglycerol (TAG), monogalactosyldiacylglycerol (MGDG), and digalactosyldiacylglycerol (DGDG). We first performed a principal component analysis (PCA) based on the lipid profiles of samples from control and 6 d (d) of darkness (Figure 1). Most of the variance of the dataset was covered

by the first two principal components, explaining 69.1% of the overall data variance (57.8% and 11.3% for PC1 and PC2, respectively). This fingerprint analysis allowed us to obtain a general picture, discerning the main differences between the darkness treatment and the *atg* mutant lines. Briefly, it revealed that under control conditions (before darkness treatment), all genotypes clustered together; however, a clear separation according to the treatment and genotype was observed following darkness, wherein *atg7-2* and *atg5-1* were disconnected of the WT samples (Figure 1). Interestingly, *atg9-4* presented an intermediary distribution, sharing certain metabolic similarities with WT and the other *atg* genotypes. The analysis of all data points also highlighted the delayed response of *atg9-4*, which after 6 and 9 d of darkness, was more closely related to *atg5-1* and *atg7-2* after 3 d of darkness conditions (Supplemental Figure S1).

Our results are in close agreement with the milder impact of the *ATG9* disruption on metabolic features previously reported under dark-induced senescence (Barros et al., 2017). This response was related to residual autophagy activity observed in *atg9* lines (Yoshimoto et al., 2004; Shin et al., 2014), which explains the intermediary lipid response of *atg9-4* genotype. The information of the individual variables that contributed most to PC1 and PC2 (i.e., the lipids with the main impact on the variance of the dataset) is additionally available in Supplemental Table S1. Several lipids accounted for the main changes observed in the PCA. Briefly, PC1 was mainly comprised of MGDG 34:4, MGDG 34:3, PC 38:4(1), and MGDG 34:1 underlining the separation of dark-treated and control samples. On the other hand, TAG 54:9, MGDG 32:3 (1), and TAG 52:6 were the main lipids responsible for changes in PC2 (Supplemental Table S1),

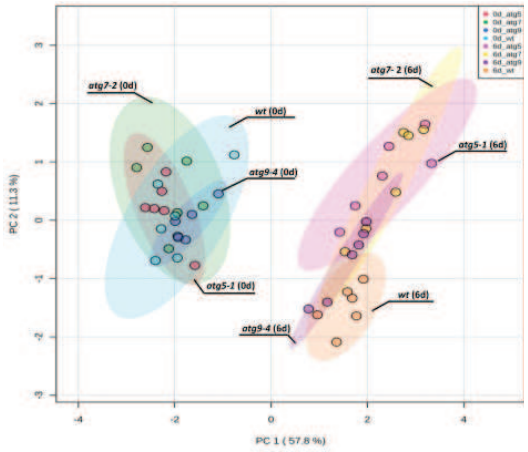

Figure 1 Differential lipid response of *atg* mutants under dark-induced senescence. PCA was performed using the lipid data obtained in samples from 4-week-old Arabidopsis plants immediately before lights were turned off (0 day) and after further treatment for 6 d in darkness. Three loss-of-function mutants of the autophagy pathway, namely *atg5-1*, *atg7-2*, and *atg9-4*, and their WT were analyzed.

contributing to the differences between the genotypes under darkness (Figure 1).

The lack of autophagy affects the dynamics of phospholipids during dark-induced senescence

In order to obtain a more detailed characterization of the lipid composition of *atg* mutants following extended darkness, we analyzed each lipid class separately. We were able to identify the two dominant structural phospholipid species, namely PC and PE. These lipids are components of the plasma membrane, in which PC is associated with the outer leaflet, and PE is concentrated in the inner leaflet. PC and PE are also precursors of lipid mediators, such as phosphatidic acid (PA) and DAG (Wang et al., 2006; Testerink and Munnik, 2011). Additionally, PE plays a crucial role in autophagosome formation (Soto-Burgos et al., 2018; Barros et al., 2020). Interestingly, a slight accumulation of both PC and PE was observed in *atg5-1* and *atg7-2* mutants before darkness treatment (control conditions, Figure 2—0 day). The difference of PC levels under control conditions was marked by the accumulation of 36C PC in *atg5-1* and *atg7-2* mutants, whereas no significant changes were observed in *atg9-4* at this time point (Figure 2, A—0 day). Extended darkness triggered a mixed response of different PC species. Thus, the levels of 32C and 34C mostly increased in WT plants under darkness. However, *atg5-1* and *atg7-2* presented lower accumulation of 34C PC species that contain a combination of 18C and 16C polyunsaturated acyl species, such as 34:5-(18:3-16:2-) and 34:6- (18:3-16:3) during dark treatment. The PC-containing FAs with longer chains, 36C and 38C, were generally reduced in response to extended darkness. However, *atg5-1* and *atg7-2* presented a milder reduction of 36C PC species after 3 and 6 d of darkness, whereas the 38C species (38:3(2), 38:4, 38:5, 38:6) were more reduced in these genotypes after 6 and 9 d of darkness (Figure 2, A).

Following dark treatment, the majority of PE species decreased in WT plants; however, this reduction was milder in *atg* mutant lines after 6 d of darkness (Figure 2, B). On the other hand, after 9 d of darkness, species such as PE 36:2, 34:2, and 36:3(2) were highly reduced in *atg5-1* and *atg7-2* compared with WT. Surprisingly, the PE species 36:5 and 38:3 presented a contrasting pattern, accumulating after 6 and 9 d of darkness in *atg* mutants (Figure 2, B).

Impairment of autophagy accelerates the loss of chloroplast lipids

Since chloroplast lipids are subjected to constant turnover during senescence, we next evaluated the predominant lipid constituents of chloroplast membranes, MGDG and DGDG. An apparent reduction in more than 90% of the detected MGDGs and DGDGs was observed in *atg* mutants exposed to dark treatment (Figure 3). This response was intensified throughout the dark treatment, and thus the levels of some species were below the detection threshold after 9 d. Although *atg9-4* mutants followed the same pattern, the levels of MGDG and DGDG were less reduced in

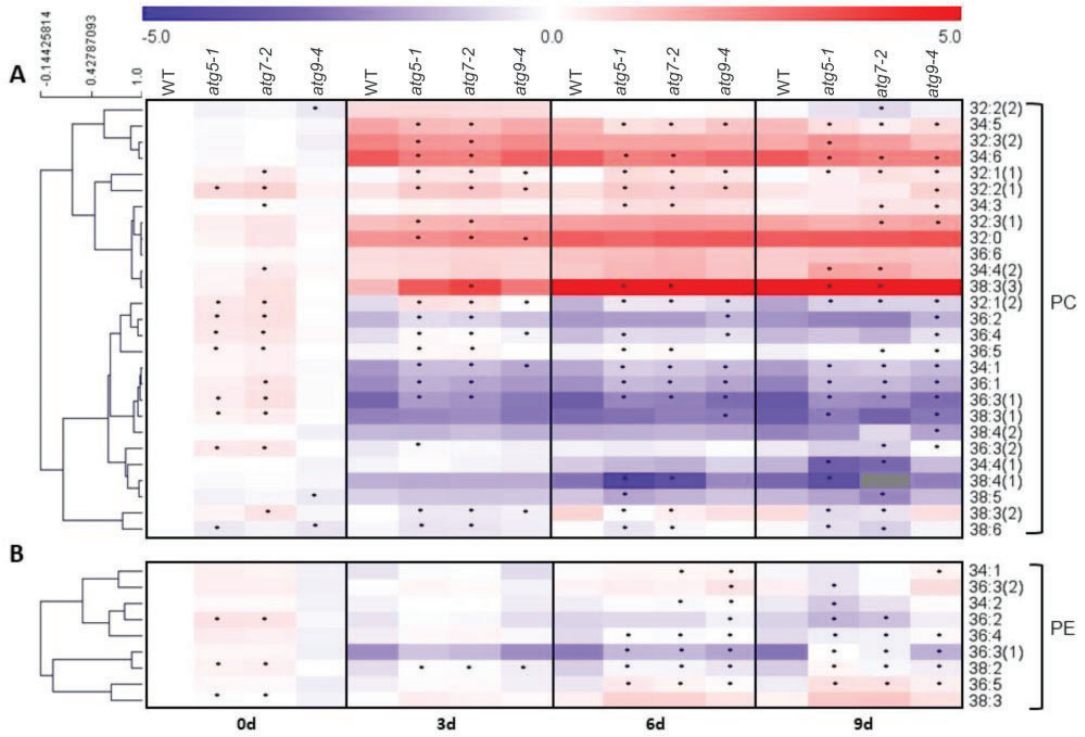

Figure 2 atg mutants present altered phospholipid levels under control and extended darkness conditions. Hierarchical clustering of (A) PC and (B) PE. Values plotted are $\log_2$ fold change. Distances were measured by Pearson correlation using MeV 4.9.0 software. Data were normalized to the mean response calculated for the 0-day dark-treated leaves of the WT. Values presented are means ± SE of five to six biological replicates per genotype; an asterisk (*) designates values that were determined by Student's *t* test to be significantly different ($P < 0.05$) from WT at each time point analyzed.

comparison to *atg5-1* and *atg7-2* mutants (Figure 3). The overall reduction of chloroplast lipids reported here is consistent with the more severe phenotype described previously for *atg5-1* and *atg7-2* mutants lines under extended darkness (Barros et al., 2017). Interestingly, slightly lower levels of unsaturated MGDG and DGDG were also observed in *atg* mutants under control conditions, highlighting the potential role of autophagy in basal chloroplast maintenance, as recently verified in different studies using both Arabidopsis *atg5* and maize *atg12* mutants (McLoughlin et al., 2018, 2020; Havé et al., 2019).

Disruption of autophagy compromises TAG and LD response under dark-induced senescence

The analysis of neutral lipids revealed a general increase in TAG levels during extended darkness. TAGs are composed of three FAs esterified to a glycerol backbone (Yang and Benning, 2018). The dominating accumulated TAG species during dark-induced senescence harbor three FA molecule with 18C with two or three double bonds (54:7 to 54:9 in Figure 4, A), or two FA molecules with 18C with two to three double bonds and 16:3 or 16:0 as a third FA (52:5 to 52:9 in Figure 4, A). Unsaturated C18 FAs (oleic acid, 18:1; linoleic acid, 18:2, and α-linolenic acid, 18:3), palmitic acid (16:0), and unsaturated C16 FAs (16:1 and 16:3) are highly abundant in chloroplasts of Arabidopsis (Hölzl and Dörmann, 2019). Our data indicate that the accumulated TAG species are most likely derived from plastidial lipids. Interestingly, the increase in chloroplast-derived TAG species was less pronounced in both *atg5-1* and *atg7-2* mutants after 3 and 6 d of darkness. Additionally, an increase of other TAG species was observed from 6 d of dark treatment onward in *atg5-1* and *atg7-2* mutants, resulting in general TAG accumulation during the late period of darkness (Figure 4, A).

DAG is a central metabolite in plant lipid metabolism, serving as an intermediate of both TAG and galactolipids (Muthan et al., 2013). Similar to that observed for TAGs, the four DAG molecules identified (34:3, 34:6, 36:5, 36:6) were composed of unsaturated FAs, containing at least one unit of 16:2, 16:3, or 18:3 plastid-derived FA (Figure 4, B). Although no significant differences were observed during

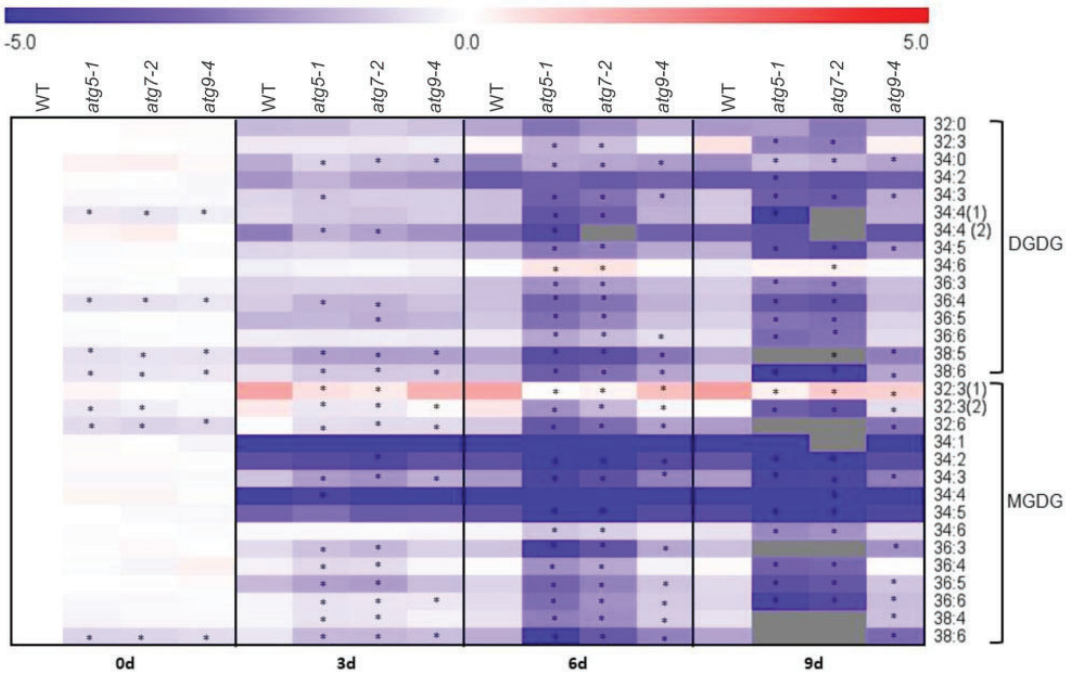

Figure 3 Chloroplast lipids are substantially reduced in *atg* mutants during dark-induced senescence. MGDG and DGDG values plotted are $\log_2$ fold change. Data were normalized to the mean response calculated for the 0-day dark-treated leaves of the WT. Values presented are means ± SE of five to six biological replicates per genotype; an asterisk (*) designate values that were determined by the Student's *t* test to be significantly different ($P < 0.05$) from WT at each time point analyzed.

the early stages of dark treatment, DAGs started to accumulate 6 d after the onset of dark treatment in *atg5-1* and *atg7-2* mutants. At the same time, WT and *atg9-4* plants showed a trend of reduction (Figure 4, B). The accumulation of unsaturated DAG species is likely a result of the degradation of chloroplast membranes in *atg* mutants serving as a precursor for the general TAG accumulation in the late stages of dark-induced senescence.

TAG is the central lipid reserve of the plant cell, stored in LDs (Pyc et al., 2017). To further investigate how the altered levels of TAGs in *atg7-2* and *atg5-1* mutants affect LD metabolism during dark-induced senescence, we visualized the abundance of LDs in leaf tissues by staining with the neutral-lipid-selective fluorescent dye, BODIPY493/503. An increased number of LDs was observed after 3 d of darkness in WT plants (Figure 5). However, no accumulation of LDs was observed in *atg5-1* and *atg7-2* mutants (Figure 5). Notably, the multiple *z*-stacked confocal images revealed that LDs are mostly accumulated in the cytosol and not inside chloroplasts (Figure 5, A). The dynamics of LD accumulation corroborates the high levels of the plastid-derived TAG species, which were subsequently reduced after 6 d of darkness in WT. Furthermore, *atg5-1* and *atg7-2* mutants displayed reduced levels of plastid-derived TAG species that can also be associated with the impairment of LD accumulation (Figure 4, A).

The disruption of autophagy triggers activation of PG metabolism

PGs are specialized globular LDs composed by a membrane lipid monolayer surrounding a core of neutral lipids present in the chloroplast membranes (van Wijk and Kessler, 2017). The production of PG is related to the accumulation of products from chlorophyll and chloroplast lipid catabolism such as FA phytyl esters (FAPEs), TAGs, and FAs (Gaude et al., 2007; Lippold et al., 2012). Given that *atg* mutants presented a substantial reduction of chloroplast lipids under extended darkness, which was not translated to an increase in TAGs or LD accumulation, we next investigated PG-related pathways by reverse transcription quantitative PCR (RT-qPCR). The genes phytyl ester synthase 1 (*PES-1*) and *PES-2*, belonging to the esterase/lipase/thioesterase family, are required for FAPE production in Arabidopsis PG during senescence (Lippold et al., 2012). Accordingly, we observed an increase of *PES-1* and *PES-2* transcript levels following dark-induced senescence (Figure 6, A and B). However, higher induction of *PES-1* in *atg5-1* and *atg7-2*, as well as of *PES-2* in *atg7-2*, was observed after 3 and 6 d of darkness (Figure 6, A and B). The production of FAPE relies on both FFA released from chloroplast membranes and phytol from chlorophyll (Lippold et al., 2012). We therefore analyzed the chlorophyll degradation enzyme pheophytin pheophorbide hydrolase (*PPH*). As observed for *PES1* and *PES2*, *PPH* transcript

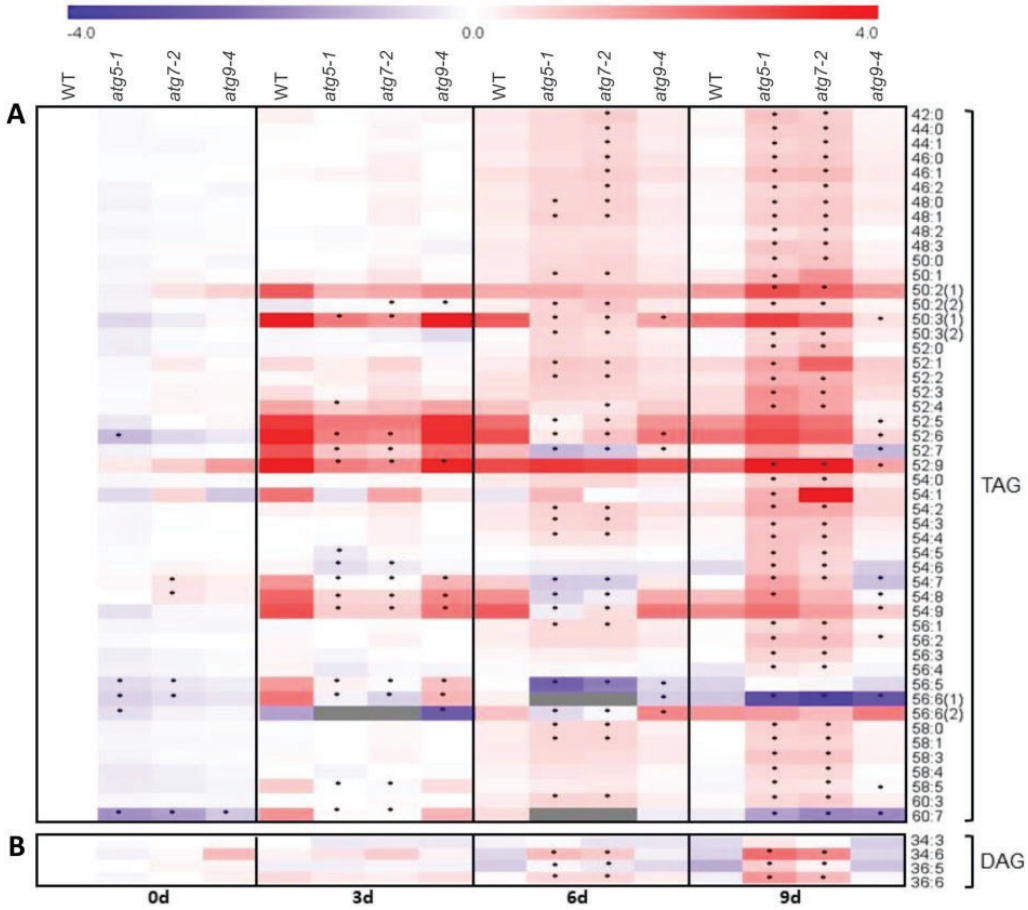

Figure 4 Distinct accumulation of neutral lipids in *atg* mutants during dark-induced senescence. A, TAG and B, DAG. Values plotted are $\log_2$ fold change. Data were normalized to the mean response calculated for the 0-day dark-treated leaves of the WT. Values presented are means ± SE of five to six biological replicates per genotype; an asterisk (*) designates values that were determined by Student's *t* test to be significantly different ($P < 0.05$) from WT each time point analyzed.

accumulated at higher levels in *atg* mutants under dark-induced senescence in comparison to WT levels (Figure 6, D).

PG serves as a lipid deposit and also contain an actively associated proteome (Lundquist et al., 2012). The presence of several Absence of Bc1 Complex Kinase (ABC1K) proteins was described in PG, suggesting a central role of these proteins in the regulation of PG metabolism (Ytterberg et al., 2006; Bréhélin et al., 2007). The protein ABC1K7 has been characterized as a PG core component with marked accumulation during late senescence events (Lundquist et al., 2012; Bhuiyan et al., 2016). Despite the unchanged transcript levels of *ABC1K7* in WT, this gene was induced in *atg5-1* and *atg7-2* mutants following extended darkness (Figure 6, C). Although our results demonstrate a boost of PG pathways in the absence of autophagy under dark-induced senescence, *atg* mutants presented a slight but significant up-regulation for all PG-related genes even under control conditions (Figure 6), highlighting intrinsic crosstalk between these processes.

Transmission electron microscopy analysis revealed that the number and size of PG as well as the chloroplast structure are similar in leaves of WT and *atg5-1* plants under control conditions (Figure 7, A). After dark treatment, different chloroplast responses were observed in WT and *atg5-1* plants (Figure 7, A). Whereas WT presented a typical thylakoid stacking response in chloroplasts of dark-treated plants (Wood et al., 2019), *atg5-1* displayed smaller chloroplasts with disrupted structural remodeling, containing structures resembling senescence-associated vacuoles (Otegui et al., 2005). Moreover, a marked presence of PG was observed in *atg5-1* chloroplasts (Figure 7, A). This response was ascribed to an increase in the size of PG, which reached areas up to 0.02 μm^2 (Figure 7, B–C). Otherwise, WT plants also

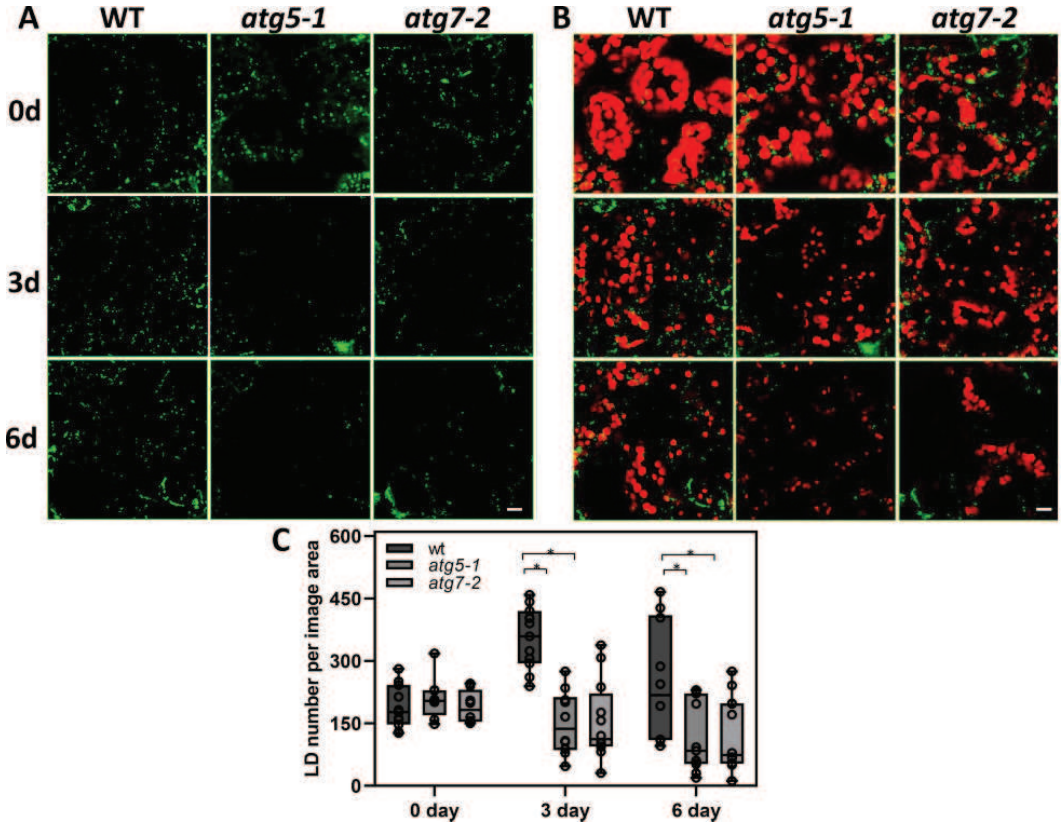

Figure 5 Autophagy deficiency affects LD dynamics during dark-induced senescence. A, Representative confocal images of LDs (BODIPY 493/503 fluorescence, false color [green] in WT, *atg5-1*, and *atg7-2* leaves). B, Merged image of BODIPY and chloroplast autofluorescence (false color red). Images were collected at the same magnification and are projections of *Z*-stacks of 20 optical sections. Bar = 10 μm. C, Number of total LDs per image area. The number of LDs was quantified by ImageJ as BODIPY-stained lipid area in 2-D projections of *Z*-stacks of three images of four biological replicates per genotype and time point.

presented increases in PG size; however, these increases were to a far less extent compared with *atg5-1* (Figure 7, B and C).

Proteomic studies of PG have shown that members of the fibrillin (FBN) family are the most abundant proteins in the PG proteome (Lundquist et al., 2012). Therefore, we next checked the content of the PG core protein FBN1a (FBN 1a), previously characterized as a PG structural component (Austin, 2006, Simkin et al., 2007, Singh and McNellis, 2011). Immunoblotting analysis showed a strong reduction of FBN1a abundance in *atg5-1* mutant compared with WT, which displayed a slight increase of FBN1a abundance after 6 d of dark treatment (Figure 7, D and Supplemental Figure S2). Interestingly, the overexpression of FBN1a homologs resulted in increased numbers and clustering of PGs in tobacco (*Nicotiana tabacum*) leaves and tomato (*Solanum lycopersicum*) fruit (Rey et al., 2000; Simkin et al., 2007). Additionally, FBN overexpression was also associated with the delay of thylakoid disintegration, suggesting its role on protection/maintenance of chloroplast membranes (Simkin et al., 2007; Rottet et al., 2015). The reduction of FBN1a protein abundance is most likely related to the occurrence of supersized PG coupled with the overall degradation of chloroplast membranes in *atg5-1* mutant plants under dark-induced senescence. Collectively, our findings highlight PG as a potential lipid storage site in *atg* mutants subjected to extended darkness conditions. It will therefore be interesting to determine hereafter whether and to what extent FBNs determine PG structural modeling during low-energy conditions.

atg mutants induce lipid oxidation pathways in response to dark-induced senescence

FA oxidation may be of particular significance when the carbon and energy status is rather low. During carbon starvation, the importance of lipid metabolism was demonstrated by the characterization of β-oxidation loss-of-function mutants (Kunz et al., 2009). In addition, autophagy association with peroxisomal protein abundance was recently demonstrated (McLoughlin et al., 2018, 2020; Havé et al., 2019).

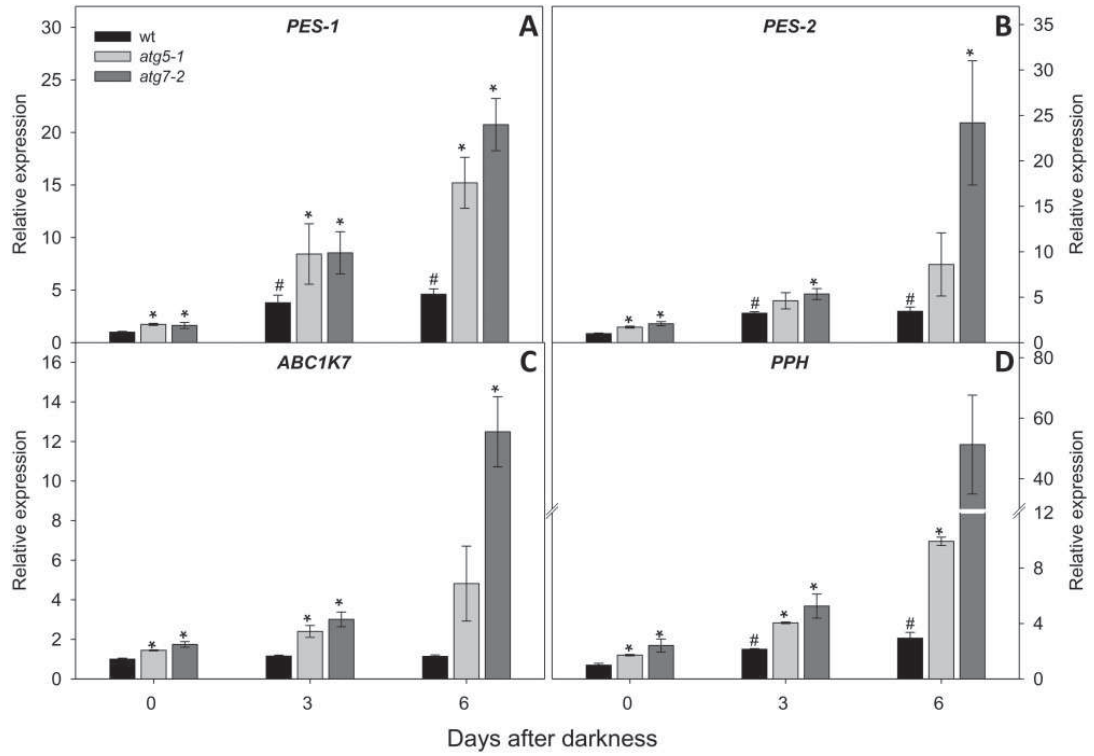

Figure 6 PG-related genes are up-regulated in *atg* mutants during dark-induced senescence. Transcript abundance is shown for genes associated with PG, including *PES-1* (A), *PES-2* (B), *ABC1K7* (C), and *PPH* (D). The *y*-axis values represent the gene expression level relative to the WT. Data were normalized with respect to the mean response calculated for the 0-day dark-treated leaves of the WT. Values presented are means ± SE of three independent biological replicates. An asterisk (*) indicates values that were determined by Student's *t* test to be significantly different ($P < 0.05$) from the WT at each time point analyzed. A hash (#) indicates values determined by Student's *t* test to be significantly different ($P < 0.05$) from WT at 0 day.

The general reduction of chloroplast lipids, together with reduced LD numbers in *atg5-1* and *atg7-2* mutants subjected to extended darkness, raised the question of whether these lipids were being quickly oxidized to be used as energetic substrates in *atg* mutants. We therefore evaluated the expression of genes related to LD catabolism and peroxisomal pathways of FA oxidation (Supplemental Table S2). We observed that the transcript levels of the peroxisomal enzymes acyl-CoA oxidase (*ACX-4*), multifunctional protein 2 (*MFP-2*), ketoacyl-CoA thiolase (*KAT-2*), citrate synthase 1 (*CSY-1*), and peroxisomal malate dehydrogenase (*pMDH-1*) genes were generally higher in *atg5-1* and *atg7-2* under extended darkness (Figure 8, A–E). More specifically, *ACX-4* and *CSY-1* were slightly induced in WT throughout the treatment. However, higher transcript levels were observed in *atg5-1* and *atg7-2* plants after 6 d of darkness (Figure 8, A and B). Despite no major changes in *KAT-2* and *MFP-2* transcript abundance in WT plants, increased expression levels were observed in *atg5-1* and *atg7-2* after 9 d of darkness (Figure 8, C and D). We further confirmed that *pMDH-1* was downregulated following dark-induced senescence (Figure 8, E). *pMDH-1* operates in the reduction of oxaloacetate to malate and enables the re-oxidation of NADH for continued β-oxidation (Pracharoenwattana et al., 2007). Given that *pMDH-1* is not participating directly in β-oxidation, it is possible that an alternative pathway of NADH oxidation becomes operational under carbon starvation.

To investigate whether the reduced number of LDs is a result of the induction of catabolic pathways or impairment in biosynthesis, we next evaluated the expression of *SDP-1*. Despite being characterized as the primary lipase mediating LD catabolism in seeds, compelling evidence has suggested that *SDP-1* also operates in senescent and carbon-starved leaves (Fan et al., 2017, 2019). Indeed, an accumulation of *SDP-1* transcript levels was observed in WT plants during the early stages of darkness (Figure 8, F). Nonetheless, no significant difference in *SDP-1* transcript levels between WT plants and *atg5-1* and *atg7-2* was observed, suggesting that the reduced levels of LDs are likely more related to the impairment of LD biogenesis rather than an induction of LD degradation pathways.

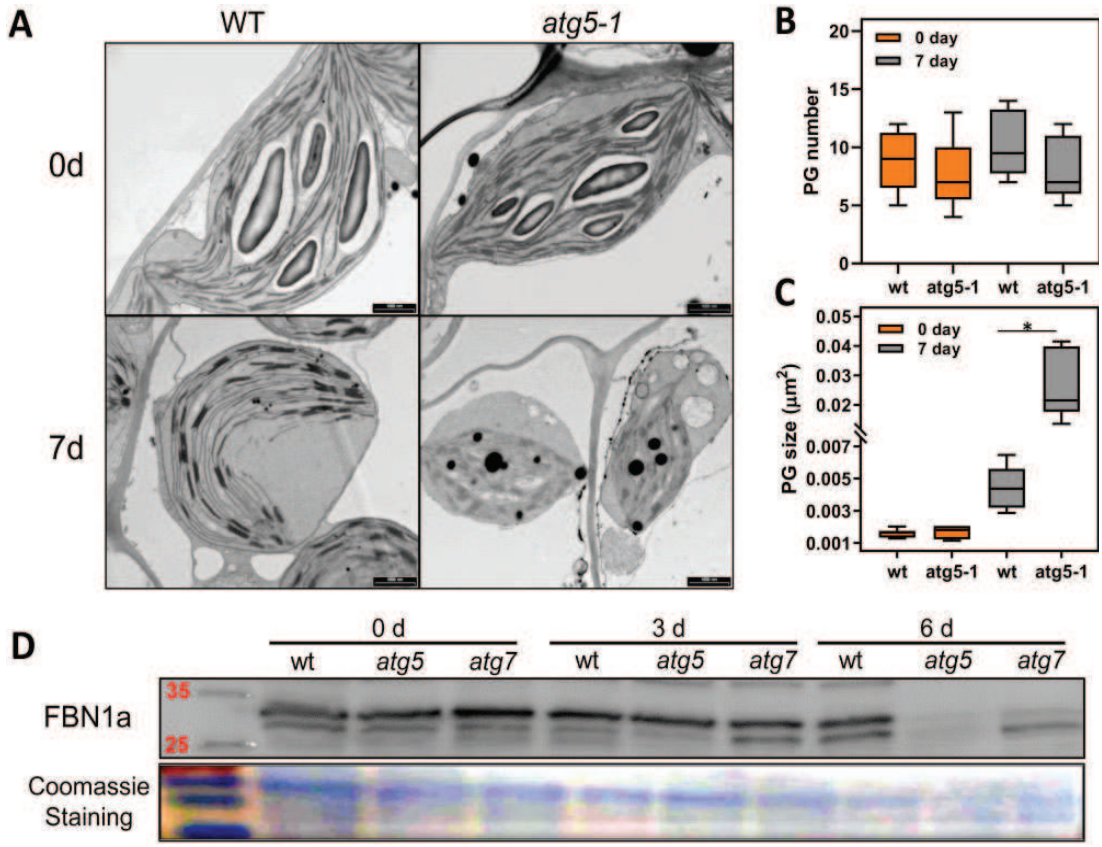

Figure 7 Autophagy disruption triggers altered PG response. A, Transmission electron micrographs of leaves from 4-week-old Arabidopsis plants immediately before lights were turned off (0 day) and after further treatment for 7 d of darkness. Scale bar = 1 µm. Quantification of the number (B) and size (C) of PG per chloroplasts (±SE, n = 6–7 chloroplasts of three independent cells); Analysis shown in A–C was performed in *atg5-1* and its respective WT. D, Immunoblot analysis of the PG protein, FBN1a, was performed in leaves from 4-week-old Arabidopsis *atg5-1*, *atg7-2*, and WT plants immediately before (0 day) and after further treatment for 3 and 6 d in darkness. FBN1a protein displayed a predicted molecular mass of ~30–35 kD. The detection of a second lower band in the region of 30 kD possibly corresponds to FBN1b protein (with high sequence similarity with FBN1a), as previously observed (GiacomelLi et al., 2006; Martinis et al., 2013, 2014).

Altered FFA response of *atg* mutants under dark-induced senescence

Since autophagy deficiency altered cytosolic LD dynamics and β-oxidation pathways, we next evaluated if this response also affected the pool of FFA. Figure 9 shows that long-chain FFA (13C–21C chain length) are more affected by both genotype and darkness, whereas no major changes were observed for very long-chain FFA (>22C). Higher levels of 16:3, 18:1, 18:2, and 18:3 in *atg5-1* and *atg7-2* genotypes under control conditions were observed, reinforcing the functional role of autophagy in basal lipid homeostasis. Upon darkness treatment, the levels of C18 and C20 FFAs were reduced, and unsaturated C16 accumulated in *atg5-1* and *atg7-2* mutants (Figure 9). By contrast, WT plants presented an initial increase followed by later reduction of C16 and C18 FFAs except for 16:3 and 18:1 species FFAs, which were, respectively, accumulated and reduced in darkness (Figure 9). Although unsaturated C16 and C18 FAs are typical components of chloroplast membranes, only 16:3 is exclusively found in the thylakoid lipid MGDG in plant species (e.g., Arabidopsis), and it is, therefore, a chloroplast lipid marker (Ohlrogge et al., 1991; Kunz et al., 2009; Hölzl and Dörmann, 2019). Thus, the overall accumulation of 16:3 is in good agreement with the reduction of galactolipids observed under dark-induced senescence. Additionally, this result suggests that the rate of 16:3 release exceeds its channeling to LD and PG. The higher accumulation of 16:3 in *atg* mutants strengthens our claim that this disbalance is more intense when autophagy is disrupted.

Discussion

It is well established that plant autophagy plays a crucial role in the energetic metabolism mediating the supply of proteins and amino acids under carbon starvation conditions (Avin-Wittenberg et al., 2015; Barros et al., 2017; Hirota et al., 2018; McLoughlin et al., 2020). Furthermore, in both animals and yeast, autophagy is recognized as an important lipid catabolic pathway in starved cells (Singh et al., 2009).

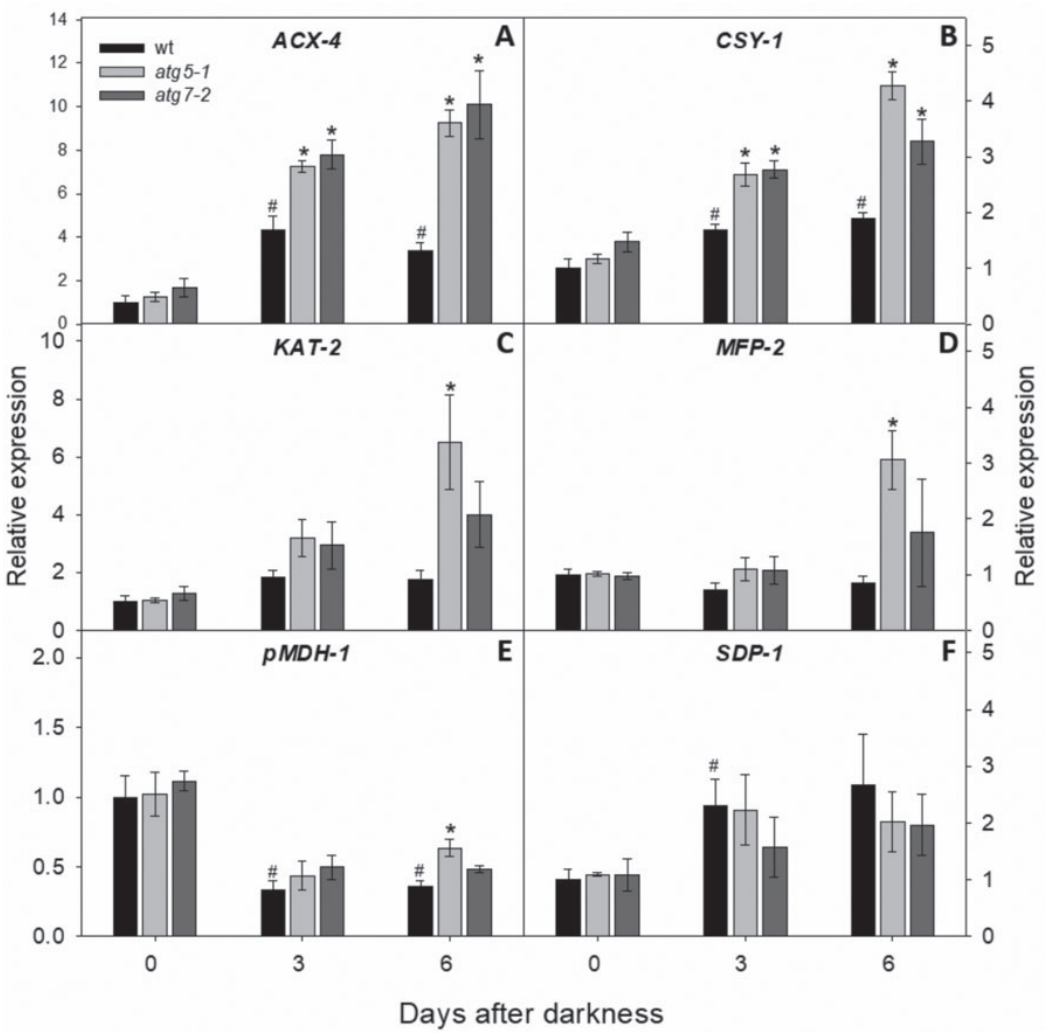

Figure 8 Changes in transcript levels in WT and atg mutants during dark-induced senescence. Transcript abundance is shown for genes associated with lipid catabolic pathways, including ACX-4 (A), CSY-1(B) KAT-2 (C), MFP-2 (D), pMDH-1 (E), SDP-1 (F). The y-axis values represent the expression level relative to the wild type (WT). Data were normalized with respect to the mean response calculated for the 0-d dark-treated leaves of the WT. Values presented are means ± SE of three independent biological replicates. An asterisk (*) indicates values that were determined by Student's t test to be significantly different ($P < 0.05$) from the WT at each time point analyzed. A number sign (#) indicates values determined by Student's t test to be significantly different ($P < 0.05$) from WT at 0d.

In plant leaves, growing evidence has highlighted the role of autophagy in managing cell lipid components and reserves (Avin-Wittenberg et al., 2015; McLoughlin et al., 2018, 2020; Fan et al., 2019; Havé et al., 2019). In fact, the lipid response of *atg* mutants under N starvation has been previously demonstrated (McLoughlin et al., 2018; Havé et al., 2019). More recently, McLoughlin et al. (2020) reported extensive lipid alterations in maize *atg12* mutants subjected to carbon deprivation induced by short-term darkness. Here, we provide further evidence that autophagy broadly affects lipid and LD metabolism during dark-induced senescence in Arabidopsis. Notably, similarities and differences between the aforementioned studies and the findings reported here were observed. The main points are summarized in Supplemental Figure S3, and they will be further discussed throughout the text.

By performing a detailed lipidomics analysis, we revealed that autophagy widely affects the lipid homeostasis of Arabidopsis during dark-induced senescence. The major differences reported here are related to the *atg5-1* and *atg7-2* mutant plants, characterized by a full inhibition of autophagy (Chung et al., 2010). By contrast, *atg9-4*, which is characterized by a partial reduction of autophagy, presented an intermediary impact on lipid metabolism that was more evident during the late stages of extended darkness (Figure 1 and Supplemental Figure S1). The fact that *atg9-4* did not cluster with *atg5-1* and *atg7-2* implies that the lipid response

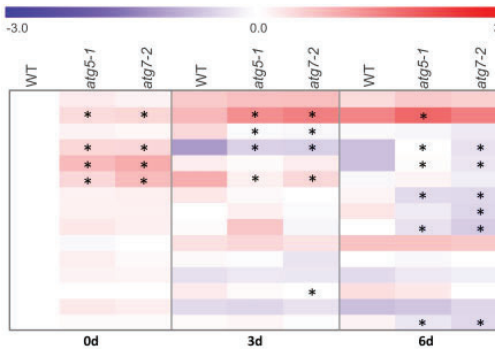

Figure 9 Changes in FFA levels in WT and *atg* mutant plants under dark-induced senescence. Values plotted are $\log_2$ fold change. Data were normalized to the mean response calculated for the 0-day dark-treated leaves of the WT. Values presented are mean ± SE of five to six biological replicates per genotype; an asterisk (*) designates values that were determined by the Student's *t* test to be significantly different ($P < 0.05$) from WT each time point analyzed.

is directly related to autophagy intensity. Indeed, the characterization of Arabidopsis *ATG5* and *ATG7* knockout and overexpression mutants showed a positive correlation between the level of autophagy and seed FA content (Minina et al., 2018). We previously demonstrated that amino acid catabolic pathways were less compromised in *atg9-4* mutants, contributing to its more tolerant phenotype during dark-induced senescence (Barros et al., 2017). Additionally, the limited reproductive phenotype of *atg* mutants is also dependent on autophagy intensity since parameters related to seed and silique production were more compromised in *atg* lines fully defective in autophagy (Barros et al., 2017). Taking into account the fact that Arabidopsis is an oilseed (Li et al., 2006), the results reported here and by others (Minina et al., 2018) suggest that the altered reproductive and carbon starved phenotype of *atg* mutants is a consequence of both impaired protein catabolic process and extensive reprogramming of lipid metabolism.

The detailed analysis of the specific lipid classes revealed an altered lipid phenotype in mutants lacking autophagy under non-stress conditions. These differences are mostly attributed to galactolipids and the phospholipids PC and PE, whereas minor differences were observed for TAGs (Figures 2–4). The galactolipids MGDG and DGDG are prevalent in the chloroplast envelope and the thylakoid membrane (Hölzl and Dörmann, 2019). By contrast, PC and PE are highly abundant in the plasma membrane, mitochondrial membrane, and endoplasmic reticulum (Liu et al., 2015). Hence, the high levels of PC and low levels of MGDG and DGDG reveal an imbalance of cytosolic and plastidial membrane lipids in *atg5-1* and *atg7-2* mutants under normal growth conditions. Similar results were previously reported in Arabidopsis *atg5* mutants, which displayed a general alteration of phospholipid levels under non-stressful conditions (Havé et al., 2019). The accumulation of lipid-breakdown products in maize *atg12* mutants also suggested an induced turnover of membrane components under normal growth conditions (McLoughlin et al., 2018, 2020). In addition, Fan et al. (2019) reported that the disrupted membrane lipid turnover in *atg* mutants affected TAG synthesis. The TAG profile detailed here reveals that only specific TAG species are reduced in *atg5-1*, and *atg7-2* mutants under normal growth conditions, which seems to contribute to the low total TAG content previously reported.

Collectively, our results support the notion that, beyond the role of autophagy in basal lipid metabolism, autophagy is clearly required for lipid remodeling under starvation conditions in Arabidopsis. Upon exposure to extended darkness, PC metabolism is broadly rearranged, presenting different patterns of accumulation and reduction (Figure 2). In general, the majority of 32C and 34C PC species increases, whereas 36C and 38C declines upon darkness (Figure 2). However, an altered response of PC accumulation and degradation was observed in *atg* mutants. The turnover of membrane lipids is a recognized aspect of plant senescence in general (Troncoso-Ponce et al., 2013). It seems that the disruption of autophagy leads to a differential degradation rate of membrane lipid components, most likely affecting the supply of FAs to sustain other cellular processes, including respiration. Alteration of PE levels was also observed in *atg* mutants under our experimental conditions (Figure 2). Noteworthy, PE is an essential component of ATG8 conjugation during autophagosome membrane biogenesis (Soto-Burgos et al., 2018; Barros et al., 2020). The less accentuated reductions and accumulation of several PE species (PE 36:4, 36:3(1), 38:2, 36:5, 38:3) in *atg* mutants might be related to the disrupted usage and recycling of these molecules for autophagosome biogenesis, as previously suggested (Avin-Wittenberg et al., 2015; Havé et al., 2019).

Apart from changes in the extra-plastidial phospholipids, *atg7-2* and *atg5-1* mutants also presented intense degradation of chloroplastic MGDG and DGDG during dark-induced senescence (Figure 5). This data are consistent with the hypersensitive phenotype marked by chloroplast dismantling observed in *atg* mutants subjected to dark-induced senescence (Thompson et al., 2005; Phillips et al., 2008; Barros et al., 2017). Accordingly, autophagy has been characterized to mediate the degradation of chloroplast proteins by different selective processes (Ishida et al., 2008; Wada et al., 2009; MichaeLi et al., 2014; Izumi et al., 2017; Nakamura et al., 2018). This fact aside, the results shown here reinforce the hypothesis that other pathways likely mediate the degradation of chloroplast lipid components in carbon-starved plants and that they are likely to be more active when autophagy is absent. Moreover, this response is not restricted to carbon limitation, as similar results were reported in both Arabidopsis and maize *atg* mutants under low-nitrogen conditions (Supplemental Figure S3; McLoughlin et al., 2018; Havé et al., 2019).

The breakdown of membrane lipid components releases FFAs for further oxidation in peroxisomes. The overaccumulation of FFAs is detrimental to the plant cell. Consequently,

FFAs are first incorporated as neutral lipids to then be directed to peroxisomal FA catabolic pathways (Fan et al., 2017). TAGs stored in LDs are not abundant in leaf mesophyll cells. However, their number substantially increases under abiotic conditions and developmental senescence (Pyc et al., 2017; Yang and Benning, 2018). In agreement with this, we observed a transient LD accumulation after 3 d of darkness in WT plants. In addition, a marked increase of highly unsaturated TAG levels was observed after 3 d of darkness in WT (Figure 3). Despite an increase of some FFA species after 3 d of darkness, this increase was not overloaded to result in a lipotoxic effect since WT plants present favorable performance under dark-induced senescence (Barros et al., 2017). Indeed, the pattern of initial accumulation and later reduction of FFA 16:2, 18:0, 18:2, and 18:3 was similar to that observed for TAG and LD (Figures 4, 5, and 9), suggesting a dynamic equilibrium between membrane consumption, lipid reserve formation, and FA utilization in WT plants. By contrast, in addition to disrupted LD accumulation in *atg5-1* and *atg7-2* mutants, these lines showed lower levels of unsaturated TAGs and higher accumulation of plastidial FFA 16:3 after 3 and 6 d of darkness. Collectively, these results demonstrate that autophagy is required for the proper mobilization of chloroplast lipids destined for cytosolic LD biosynthesis in Arabidopsis energy-starved cells. A recent study of maize *atg12* mutants subjected to carbon deprivation reported distinct LD dynamics (McLoughlin et al., 2020). It was observed that *atg12* mutants contained more cytoplasmic LD under normal growth conditions. In individually dark-treated leaves, LD numbers were not affected in WT and only slightly reduced in the *atg12* mutant. A possible explanation for this discrepancy may stem from the experimental systems utilized. Whereas McLoughlin et al. (2020) analyzed individually dark-treated leaves of maize, we examined Arabidopsis in a whole-plant dark-treatment system. Plants have divergent metabolic strategies in response to different dark treatments (Law et al., 2018). It has been postulated that individually dark-treated leaves still receive sugars from other parts of the plant during short-term dark periods. However, the lipid catabolic response is not activated as long as carbohydrates are available, which likely affects LD dynamics (Kunz et al., 2009; Law et al., 2018). In addition to divergent LD responses according to the dark treatment imposed, the results reported until now also open new avenues regarding contrasting LD responses in different plant species.

In Arabidopsis, autophagy operates in the mobilization of FAs from organelle membranes to TAG synthesis under normal growth conditions (Fan et al., 2019). The same study stated that autophagy has no influence on TAG formation during darkness, but instead operates in LD degradation by lipophagy mechanism. Despite that, general TAG accumulation was observed in *atg* mutants after 6 d of darkness, which was not accompanied by cytosolic LD accumulation (Figures 4, 5). Nonetheless, caution must be taken when comparing the results obtained here with previous findings (Fan et al., 2019) due to differences in the genotypes analyzed (Barros et al., 2020). Thus, although Fan et al. (2019) demonstrated the existence of lipophagy in different mutant backgrounds, we analyzed plants solely lacking autophagy. When considered together, our results, coupled with previously reported data, highlight the potential role of autophagy as a versatile player in LD metabolism, particularly in starved cells.

Beyond the LDs in the cytosol, PG serve as subcompartments for lipid biosynthesis and storage in chloroplasts (Rottet et al., 2015; van Wijk and Kessler, 2017). The analysis of PG-related genes indicates a marked activation of PG metabolism in *atg5-1* and *atg7-2* mutants during dark-induced senescence (Figure 6). In agreement, we observed the presence of large PG in chloroplasts of *atg5-1* mutants under extended darkness conditions (Figure 7, A–C). On the other hand, reduced abundance of the PG core protein FBN1a was observed in *atg* mutants after 6 d of darkness (Figure 7, D and Supplemental Figure S2). It is noteworthy that FBN proteins, localized on the PG surface, were proposed to play both structural and protection roles in chloroplast, preventing the PG coalescence and delaying thylakoid disintegration (Austin et al., 2006; Ytterberg et al., 2006; Simkin et al., 2007; Singh and McNellis, 2011; Rottet et al., 2015). It is tempting to suggest, therefore, that the reduction of FBN1a protein can be associated with the large size of PG as well as the chloroplast-sensitive phenotype of *atg* mutants in response to dark-induced senescence. There is a strong correlation between thylakoid dismantling and supersizing of PG during senescence, which is likely associated with the massive deposit of FAs and phytol released from chloroplast degradation (Lippold et al., 2012; Besagni and Kessler, 2013; Rottet et al., 2015; van Wijk and Kessler, 2017). In light of this, we also verified an increase of *PPH* transcript in *atg5-1* and *atg7-2* mutants compared with WT under darkness (Figure 6, D). It seems reasonable to assume that both the products from the degradation of chlorophyll (Barros et al., 2017) and chloroplast membranes are funneled for PG formation in *atg* mutants subjected to extended darkness (Figures 3, 7, and 10). This response can be presumed as a strategic mechanism preventing the accumulation of lipotoxic intermediaries. Collectively, our results imply that the disruption of autophagy triggers a differential response prompting PG rather than cytosolic LD formation under dark-induced senescence. Nonetheless, whether PG can be remobilized to provide lipid-derived energetic substrates remains to be further investigated.

It is already known that, during extended darkness, FAs are oxidized by β-oxidation, generating acetyl-CoA that, combined with oxaloacetate, produces citrate to be exported to mitochondria for ATP generation (Kunz et al., 2009). To further understand whether the released membrane lipid components were channeled to the maintenance of the energetic status, we paid particular attention to the transcriptional activation of lipid oxidation pathways. Our results show an up-regulation of peroxisomal genes in plants

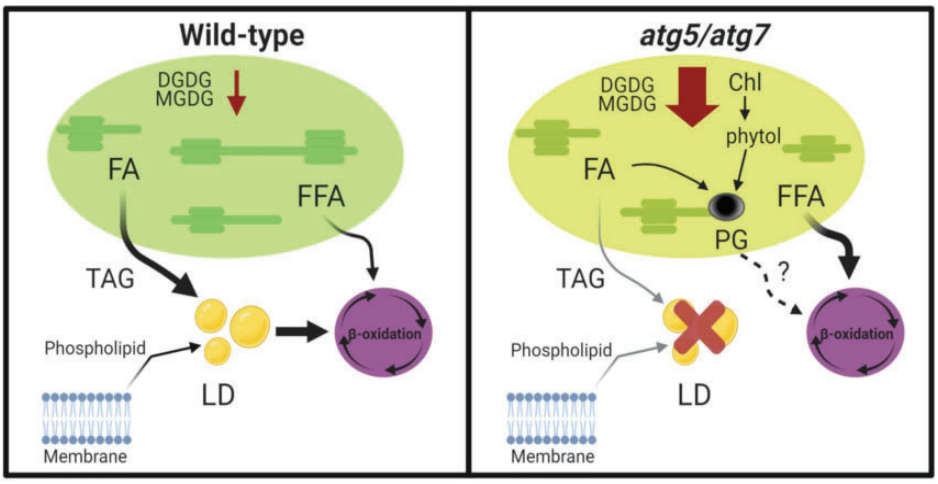

Figure 10 Schematic model of lipid remodeling response of *atg* mutants during extended darkness. Under extended darkness, the plastidial and extraplastidial membranes, composed by MGDG/DGDG and phospholipids, respectively, are degraded, releasing FAs to be stored as TAGs in LD in the cytosol. LDs and transient FFA donate substrates for β-oxidation in peroxisomes. Meanwhile, in *atg* mutants, there is a substantial degradation of chloroplast lipids, whereas the production of cytosolic LDs is impaired. Part of the released plastidial FAs, together with phytol derived from chlorophyll degradation, are channeled to the production of PG in the chloroplast. β-Oxidation pathways are highly induced to consume overloaded plastidial FFA and, possibly, PG lipids (question mark). The figure was created using BioRender (https://biorender.com).

with disrupted autophagy after 6 and 9 d of darkness (Figure 8). Notably, the transcriptional induction of β-oxidation has been correlated to mitochondrial activity in dark-treated leaves (Law et al., 2018). Interestingly, the same *atg* mutants exhibited higher rates of respiration and an elegant metabolic reprogramming under carbon-starvation conditions (Avin-Wittenberg et al., 2015; Barros et al., 2017).

Autophagy also plays a role in peroxisome quality control by the selective degradation of damaged peroxisomes, a process known as pexophagy (Marshall and Vierstra, 2018). The accumulation of peroxisome-related transcripts/proteins in *atg* mutants has been reported lately, and it can represent both activation of peroxisomal metabolism or accumulation of oxidized peroxisome (Supplemental Figure S3; McLoughlin et al., 2018, 2020; Havé et al., 2019). Specifically, under carbon starvation conditions, the enrichment of peroxisomal proteins was followed by an increase of glyoxysomal proteins (McLoughlin et al., 2020). This response suggests that peroxisomes are most likely converted to glyoxysomes to sustain high activation of FA β-oxidation pathways during starvation conditions (McLoughlin et al., 2020). The induction of peroxisomal pathways reported here is positively correlated with the high levels of plastidial FFAs in *atg* mutants, which can be interpreted as a response to control FFA levels concomitantly with energy production. When taken together with our work, these studies suggest that the primary metabolism of *atg* mutants is both rearranged for amino acid catabolism and possibly involved in supporting lipid oxidation pathways. In light of this, further studies are clearly required (i) to investigate whether the disruption of LD dynamics and differential membrane recycling of *atg* mutants impact the supply of lipid substrates for FA oxidation pathways and (ii) to characterize the function of autophagy under a range of environmental stresses during this process.

Conclusions

In the current work, we present compelling evidence regarding the importance of autophagy to lipid homeostasis in Arabidopsis leaves. During carbon starvation, the products of organellar membrane recycling are channeled to cytosolic LD production. This enables the balance of FA production and turnover. The functional lack of autophagy impacts proper membrane mobilization and activates a general chloroplast lipid degradation program while failing to produce cytosolic LDs. Nonetheless, the products of chloroplast membrane dismantling are possibly channeled to PG in *atg* mutants chloroplasts (Figure 10). We postulate that the increased activation of peroxisomal lipid catabolic pathways is part of a complex metabolic response to catabolize the FFAs released from chloroplast dismantling, and possibly, from PG mobilization. Although our results highlight insights regarding the role of autophagy in lipid metabolism, they certainly underestimate the complex crosstalk between autophagy, peroxisomes, mitochondria, and the endoplasmic reticulum. An investigation of the interplay involving autophagy, membrane recycling, and organellar maintenance is required to fully understand the implications of autophagy for the regulation of lipid reserve dynamics and energy homeostasis. The combined results presented here are of potential application for the breeding of crops with higher yield and increased resilience. Moreover, it seems reasonable to assume that there is a timely need to accelerate our understanding of the

mechanisms controlling autophagy and associated processes in response to environmental conditions.

Materials and methods

Plant material and dark treatment

All *Arabidopsis thaliana* (L.) Heynh plants used in this study were of the Columbia ecotype (Col-0). The T-DNA mutant lines *atg9-4* (SALK_145980; Shin et al., 2014), *atg5-1* (SAIL_129B079), (Yoshimoto et al., 2009), and *atg7-2* (GK-655B06; Hofius et al., 2009) were used in this study. Seeds were surface-sterilized and imbibed for 4 d at 4°C in the dark on 0.7% (w/v) agar plates containing half-strength Murashige and Skoog (MS) media (Sigma–Aldrich; pH 5.7). Seeds were subsequently germinated and grown at 22°C under short-day conditions (8-h light/16-h dark), 60% relative humidity with 150 µmol photons m^{-2} s^{-1}. For dark treatments and subsequent induction of dark-induced senescence, 10–14-d-old seedlings were transferred to soil and then grown at 22°C under short-day conditions (8-h light/16-h dark). Four-week-old plants were transferred to darkness in the same growth cabinet. Whole rosettes of two different plants representing an independent replicated by genotype were harvested at intervals of 0, 3, 6, and 9 d after transition to darkness. At least five biological replicates of each genotype were obtained. They were immediately frozen in liquid nitrogen and stored at −80°C until further analysis.

Visualization and analysis of LDs

To visualize LDs in Arabidopsis leaves, LDs were stained with BODIPY 493/503 (Invitrogen; from 4 mg/mL stock in DMSO). The sixth rosette leaf of 4-week-old plants was used for LD visualization and analysis. Leaf discs were stained with BODIPY solution (2 µg/mL) in the dark and under vacuum for 10 min. Confocal images were acquired using the FV-1200 confocal microscope (Olympus, Japan) with a 60 × /1.42 oil immersion objective. Excitation was performed at 488 nm, and emission was collected at 500–540 nm for BODIPY 493/503 and 650–750 nm for chlorophyll autofluorescence. The LD number was quantified using ImageJ (Schneider et al., 2012). Z-stack series of three images from four plants for each genotype were used for the quantification of LDs.

Lipid profiling and FFA analysis

Lipids and natural endogenic FFAs were extracted from six biological replicates using the MTBE method described by Salem et al. (2016). Vacuum-dried organic phases were processed using ultra-performance liquid chromatography (on a C8 reverse-phase column) coupled with Fourier transform mass spectrometry (exactive mass spectrometer; Thermo Fisher Scientific) in positive and negative ionization modes. The FFA was analyzed using ultra-performance liquid chromatography (Waters, Acquity I Class System) coupled with mass spectrometer (Q-Exactive Thermo Fisher Scientific, H-ESI). Processing of chromatograms, peak detection, and integration was performed using REFINER MSH 10 (GeneData). Processing of mass spectrometry data included the removal of the fragmentation information, isotopic peaks, and chemical noise. Selected features were annotated using an in-house lipid database (Lapidot-Cohen et al., 2020). Five–six biological replicates were used for the analysis. The whole data set from the lipid profile is additionally available as Supplemental Table S3.

Expression analysis by RT-qPCR

Total RNA was isolated using TRIzol reagent (Ambion, Life Technology) according to the manufacturer's recommendations. The total RNA was treated with TURBO DNA-free kit (Invitrogen). The integrity of the RNA was checked on 1% (w/v) agarose gels and the concentration was measured using a Nanodrop spectrophotometer. Finally, 1 µg of total RNA was reverse transcribed with SensiFAST cDNA Synthesis Kit (Bioline) according to the manufacturer's recommendations. qPCR reactions were performed in a 384-well microliter using SensiFAST SYBR No-ROX Kit (Bioline). The primers used here were designed using the open-source program QuantPrime-qPCR primer designed tool (Arvidsson et al., 2008) and are described in Supplemental Table S2. The transcript abundance was calculated by the standard curves of each selected gene and normalized using the constitutively expressed genes ACTIN (AT2G37620). Three biological replicates were processed for each experimental condition.

Transmission electron microscopy

Small pieces of leaves were cut and fixed in 3% (v/v) glutaraldehyde in 0.1 M acodylate buffer (pH 7.4) 10 h at room temperature in a desiccator and then transferred to 40°C for the continuation of fixation overnight. The tissues were washed in cacodylate buffer and postfixed and stained with 2% (w/v) osmium tetroxide, and 1.5% (w/v) potassium ferricyanide in 0.1 M cacodylate buffer for 2 h. Tissues were then washed in cacodylate buffer and dehydrated through a graded series of ethanol treatments for 10 min each step, followed by 100% (v/v) anhydrous ethanol three times, 20 min each, and propylene oxide two times, 10 min each. The tissues were infiltrated with increasing concentrations of Agar 100 resin in propylene oxide for 16 h each step. The tissues were embedded in fresh resin and polymerized in a 60°C oven for 48 h. Ultrathin sections, approximately 80-nm thick, were cut on a Leica Reichert Ultracut S microtome, collected onto 200 Mesh carbon-formvar-coated copper grids, and stained with uranyl acetate followed by Reynold's Lead Citrate for 10 min. The sections were examined using Tecnai 12 TEM 100 kV (Phillips, Eindhoven, The Netherlands) equipped with MegaView II CCD camera and Analysis version 3.0 software (Soft Imaging System GmbH, Münstar, Germany).

Immunoblot analyses

Plant leaf tissue (∼100 mg) was ground in liquid nitrogen and total proteins were extracted using a protein extraction buffer previously described (Gruis et al., 2002). After the

addition of buffer and centrifugation for 15 min at 20,000 × *g*, supernatants were collected and samples were incubated immediately for 10 min at 100°C, vortexed, and samples were adjusted in SDS-PAGE sample buffer (Laemmli, 1970). Total proteins were separated by SDS-PAGE and transferred to a polyvinylidene difluoride membrane (GE Healthcare Life science). Equal loading was validated using Coomassie Brilliant Blue staining of the membrane. For immunodetection, antibodies raised against FBN1a (Agrisera; AS06116) was used in combination with horseradish peroxidase-conjugated goat anti-rabbit antibody (Sigma; ab920).

Statistical analyses

The experiments were conducted in a completely randomized design with three to six replicates of each genotype. Data were statistically examined using analysis of variance and tested for significant ($P < 0.05$) differences using Student's *t* tests from an algorithm embedded into Microsoft Excel. PCA was performed to reduce the dataset and identify the variables that best explained the highest proportion of total variance using Metaboanalyst 4.0, an open-source, web-based tool for metabolomics data analysis (Chong et al., 2019). The whole information of variables from the first three principal component is additionally available as Supplemental Table S4.

Accession numbers

The Arabidopsis Genome Initiative locus numbers for the main genes discussed in this article are as follows: *ATG5* (At5g17290), *ATG7* (At5g45900), and *ATG9* (At2g31260).

Supplemental data

The following supplemental materials are available.

Supplemental Figure S1. Lipid response of *atg* mutants throughout dark-induced senescence.

Supplemental Figure S2. Quantification of the FBN1a protein signal.

Supplemental Figure S3. Compared lipidomics of Arabidopsis and maize *atg* mutants under carbon and nitrogen starvation.

Supplemental Table S1. Summary of the main variables of the first three principal component (PC) of *atg* mutants and WT genotypes after 0 and 6 d of dark treatment

Supplemental Table S2. Primers used in the RT-qPCR analyses performed in this study

Supplemental Table S3. Relative lipid content of leaves of Arabidopsis knockout mutants *atg5-1*, *atg7-2*, *atg9-4*, and WT after 0, 3, 6, and 9 d of dark treatment

Supplemental Table S4. Variables of the first three PC of *atg* mutants and WT genotypes after 0 and 6 d of dark treatment

Acknowledgments

The authors thank Prof. Oren Ostersetzer-Biran from The Hebrew University of Jerusalem for providing the facilities allowing transcript analysis, as well as Corinne Best and Sofia Shevtsov, for their assistance with qPCR analyses. They also thank Dr. Naomi Melamed-Book and Dr. Yael Friedmann from the microscopy core facility at The Hebrew University's Life Science core facility for their technical support with confocal and EM analysis. Finally, they thank Prof. Zack Adam from The Hebrew University of Jerusalem for providing them with the anti-FBN1a antibody.

Funding

This work was made possible through financial support from the Serrapilheira Institute [grant Serra-1812-27067] and FAPEMIG (Foundation for Research Assistance of the Minas Gerais State, Brazil, Grant RED-00053-16). Work at the TAW group is supported by the Israeli Science Foundation [grant 1899/16]. Scholarships granted by the National Council for Scientific and Technological Development (CNPq-Brazil) and Council for Higher Education (Malag-Israel) to J.A.S.B. and research fellowships awarded by CNPq-Brazil to W.L.A. are gratefully acknowledged.

Conflict of interest statement. The authors declare no conflict of interest.

References

Araújo WL, Ishizaki K, Nunes-Nesi A, Larson TR, Tohge T, Krahnert I, Witt S, Obata T, Schauer N, Graham IA, et al. (2010) Identification of the 2-hydroxyglutarate and isovaleryl-CoA dehydrogenases as alternative electron donors linking lysine catabolism to the electron transport chain of *Arabidopsis* mitochondria. Plant Cell **22**: 1549–1563.

Araújo WL, Tohge T, Ishizaki K, Leaver CJ, Fernie AR (2011) Protein degradation: an alternative respiratory substrate for stressed plants. Trends Plant Sci **16**: 489–498.

Avin-Wittenberg T, Bajdzienko K, Wittenberg G, Alseekh S, Tohge T, Bock R, Giavalisco P, Fernie AR (2015) Global analysis of the role of autophagy in cellular metabolism and energy homeostasis in Arabidopsis seedlings under carbon starvation. Plant Cell **27**: 306–322.

Avin-Wittenberg T, Baluska F, Bozhkov PV, Elander PH, Fernie AR, Galili G, Hassan A, Hofius D, Isono E, Le Bars R, et al. (2018) Autophagy-related approaches for improving nutrient use efficiency and crop yield protection. J Exp Bot **69**: 1335–1353.

Arvidsson S, Kwasniewski M, Riaño-Pachón DM, Mueller-Roeber B (2008) QuantPrime: a flexible tool for reliable high-throughput primer design for quantitative PCR. BMC Bioinformatics **9**: 465.

Austin JR II, Frost E, Vidi PA, Kessler F, Staehelin LA (2006) Plastoglobules are lipoprotein subcompartments of the chloroplast that are permanently coupled to thylakoid membranes and contain biosynthetic enzymes. Plant Cell **18**: 1693–1703.

Barros JAS, Cavalcanti JHF, Medeiros DB, Nunes-Nesi A, Avi-Wittenberg T, Fernie AR, Araújo WL (2017) Autophagy deficiency compromises alternative pathway 414 of respiration following energy deprivation. Plant Physiol **175**: 62–76.

Barros JAS, Siqueira JAB, Cavalcanti JHF, Araújo WL, Avin-Wittenberg T (2020) Multifaceted roles of plant autophagy in lipid and energy metabolism. Trends Plant Sci **25**: 1141–1153.

Besagni C, Kessler F (2013) A mechanism implicating plastoglobules in thylakoid disassembly during senescence and nitrogen starvation. Planta **237**: 463–470.

Bhuiyan NH, Friso G, Rowland E, Majsec K, van Wijk KJ (2016) The plastoglobule-localized metallopeptidase PGM48 is a positive

regulator of senescence in *Arabidopsis thaliana*. Plant Cell **28**: 3020–3037.

Bréhélin C, Kessler F, van Wijk KJ (2007) Plastoglobules: versatile lipoprotein particles in plastids. Trends Plant Sci **12**: 260–266.

Chong J, Wishart DS, Xia J (2019) Using MetaboAnalyst 4.0 for comprehensive and integrative metabolomics data analysis. Curr Protoc Bioinform **68**: 1–128.

Chung T, Phillips AR, Vierstra RD (2010) ATG8 lipidation and ATG8-mediated autophagy in Arabidopsis require ATG12 expressed from the differentially controlled ATG12a and ATG12b loci. Plant J **62**: 483–493.

Couso I, Perez-Perez ME, Martinez-Force E, Kim HS, He Y, Umen JG, Crespo JL (2017) Autophagic flux is required for the synthesis of triacylglycerols and ribosomal protein turnover in Chlamydomonas. J Exp Bot **69**: 1355–1367.

Elander PH, Minina EA, Bozhkov PV (2018) Autophagy in turnover of lipid stores: trans-kingdom comparison. J Exp Bot **69**: 1301–1311.

Fan J, Yan C, Zhang X, Xu C (2013) Dual role for phospholipid:diacylglycerol acyltransferase: enhancing fatty acid synthesis and diverting fatty acids from membrane lipids to triacylglycerol in Arabidopsis leaves. Plant Cell **25**: 3506–3518.

Fan J, Yu L, Xu C (2017) A central role for triacylglycerol in membrane lipid breakdown, fatty acid b-oxidation, and plant survival under extended darkness. Plant Physiol **174**: 1517–1530.

Fan J, Yu L, Xu CG (2019) Dual role of autophagy in lipid metabolism in Arabidopsis. Plant Cell **31**: 1598–1613.

Gaude N, Bréhélin C, Tischendorf G, Kessler F, Dörmann P (2007) Nitrogen deficiency in Arabidopsis affects galactolipid composition and gene expression and results in accumulation of fatty acid phytyl esters. Plant J **49**: 729–739.

Giacomelli L, Rudella A, van Wijk KJ (2006) High light response of the thylakoid proteome in Arabidopsis wild type and the ascorbate deficient mutant vtc2-2. A comparative proteomics study. Plant Physiol **141**: 685–701.

Gruis DF, Selinger DA, Curran JM, Jung R (2002) Redundant proteolytic mechanisms process seed storage proteins in the absence of seed-type members of the vacuolar processing enzyme family of cysteine proteases. Plant Cell **14**: 2863–2882.

Havé M, Luo J, Tellier F, Balliau T, Cueff G, Chardon F, Zivy M, Rajjou L, Cacas JL, Masclaux-Daubresse C (2019) Proteomic and lipidomic analyses of the Arabidopsis atg5 autophagy mutant reveal major changes in endoplasmic reticulum and peroxisome metabolisms and in lipid composition. New Phytologist **223**: 1461–1477.

Hirota T, Izumi M, Wada S, Makino A, Ishida H (2018) Vacuolar protein degradation via autophagy provides substrates to amino acid catabolic pathways as an adaptive response to sugar starvation in *Arabidopsis thaliana*. Plant Cell Physiol **59**: 1363–1458.

Hofius D, Schultz-Larsen T, Joensen J, Tsitsigiannis DI, Petersen NH, Mattsson O, Jørgensen LB, Jones JD, Mundy J, Petersen M (2009) Autophagic components contribute to hypersensitive cell death in Arabidopsis. Cell **137**: 773–783.

Hölzl G, Dörmann P (2019) Chloroplast lipids and their biosynthesis. Annu Rev Plant Biol **70**: 51–81.

Hörtensteiner S, Kräutler B (2011) Chlorophyll breakdown in higher plants. Biochim Biophys Acta **1807**: 977–988.

Ishida H, Yoshimoto K, Izumi M, Reisen D, Yano Y, Makino A, Ohsumi Y, Hanson MR, Mae T (2008) Mobilization of Rubisco and stroma-localized fluorescent proteins of chloroplasts to the vacuole by an ATG gene-dependent autophagic process. Plant Physiol **148**: 142–155.

Ishizaki K, Larson TR, Schauer N, Fernie AR, Graham IA, Leaver CJ (2005) The critical role of Arabidopsis electron-transfer flavoprotein: ubiquinone oxido reductase during dark-induced starvation. Plant Cell **17**: 2587–2600.

Izumi M, Hidema J, Makino A, Ishida H (2013) Autophagy contributes to nighttime energy availability for growth in Arabidopsis. Plant Physiol **161**: 1682–1693.

Izumi M, Ishida H, Nakamura S, Hidema J (2017) Entire photodamaged chloroplasts are transported to the central vacuole by autophagy. Plant Cell **29**: 377–394.

Kunz HH, Scharnewski M, Feussner K, Feussner I, Flügge UI, Fulda M, Gierth M (2009) The ABC transporter PXA1 and peroxisomal b-oxidation are vital for metabolism in mature leaves of Arabidopsis during extended darkness. Plant Cell **21**: 2733–2749.

Laemmli UK (1970) Cleavage of structural proteins during the assembly of the head of bacteriophage T4. Nature **227**: 680–685.

Lapidot-Cohen T, Rosental L, Brotman Y (2020) Liquid chromatography–mass spectrometry (LC–MS)-based analysis for lipophilic compound profiling in plants. Curr Protoc Plant Biol **5**: e20109.

Law SR, Chrobok D, Juvany M, Delhomme N, Lindén P, Brouwer B, Ahad A, Moritz T, Jansson S, Gardestrom P, et al. (2018) Darkened leaves use different metabolic strategies for senescence and survival. Plant Physiol **177**: 132–150.

Li F, Chung T, Vierstra RD (2014) AUTOPHAGY-RELATED11 plays a critical role in general autophagy and senescence-induced mitophagy in Arabidopsis. Plant Cell **26**: 788–807.

Li YH, Beisson F, Pollard M, Ohlrogge J (2006) Oil content of Arabidopsis seeds: the influence of seed anatomy, light and plantto-plant variation. Phytochemistry **67**: 904–915.

Lippold F, vom Dorp K, Abraham M, Hölzl G, Wewer V, Yilmaz JL, Lager I, Montandon C, Besagni C, Kessler F, et al. (2012) Fatty acid phytyl ester synthesis in chloroplasts of Arabidopsis. Plant Cell **24**: 2001–2014.

Liu Y, Wang G, Wang X (2015) Role of aminoalcoholphosphotransferases 1 and 2 in phospholipid homeostasis in Arabidopsis. Plant Cell **27**: 1512–1528.

Lundquist PK, Poliakov A, Bhuiyan NH, Zybailov B, Sun Q, van Wijk KJ (2012) The functional network of the Arabidopsis plastoglobule proteome based on quantitative proteomics and genome-wide coexpression analysis. Plant Physiol **158**: 1172–1192.

Marshall RS, Vierstra RD (2018) Autophagy: the master of bulk and selective recycling. Annu Rev Plant Biol **69**: 173–208.

Martinis J, Glauser G, Valimareanu S, Kessler F (2013) A chloroplast ABC1-like kinase regulates vitamin E metabolism in Arabidopsis. Plant Physiol **162**: 652–662.

Martinis J, Glauser G, Valimareanu S, Stettler M, Zeeman SC, Yamamoto H, Shikanai T, Kessler F (2014) ABC1K1/PGR6 kinase: a regulatory link between photosynthetic activity and chloroplast metabolism. Plant J **77**: 269–283.

Masclaux-Daubresse C, d'Andrea S, Bouchez I, Cacas J-L (2020) Reserve lipids and plant autophagy. J Exp Bot **71**.

McLoughlin F, Augustine RC, Marshall RS, Li F, Kirkpatrick LD, Otegui MS, Vierstra RD (2018) Maize multi-omics reveal roles for autophagic recycling in proteome remodelling and lipid turnover. Nat Plants **4**: 1056–1070.

McLoughlin F, Marshall RS, Ding X, Chatt EC, Kirkpatrick LD, Augustine RC, Li F, Otegui MS, Vierstra RD (2020) Autophagy plays prominent roles in amino acid, nucleotide, and carbohydrate metabolism during fixed-carbon starvation in maize. Plant Cell.

Michaeli S, Honig A, Levanony H, Peled-Zehavi H, Galili G (2014) Arabidopsis ATG8-INTERACTING PROTEIN1 is involved in autophagy-dependent vesicular trafficking of plastid proteins to the vacuole. Plant Cell **26**: 4084–4101.

Minina EA, Moschou PN, Vetukuri RR, Sanchez-Vera V, Cardoso C, Liu Q, Elander PH, Dalman K, Beganovic M, Yilmaz JL, et al. (2018) Transcriptional stimulation of rate-limiting components of the autophagic pathway improves plant fitness. J Exp Bot **69**: 1415–1432.

Muthan B, Roston RL, Froehlich JE, Benning C (2013) Probing Arabidopsis chloroplast diacylglycerol pools by selectively targeting bacterial diacylglycerol kinase to suborganellar membranes. Plant Physiol **163**: 61–74.

Nakamura S, Hidema J, Sakamoto W, Ishida H, Izumi M (2018) Selective elimination of membrane-damaged chloroplasts via microautophagy. Plant Physiol **177**: 1007–1026.

Nguyen TB, Louie SM, Daniele JR, Tran Q, Dillin A, Zoncu R, Nomura DK, Olzmann JA (2017) DGAT1-dependent lipid droplet biogenesis protects mitochondrial function during starvation-induced autophagy. Dev Cell **42**: 9–21.

Ohlrogge JB, Browse J, Somerville CR (1991) The genetics of plant lipids. Biochim Biophy Acta **1082**: 1–26.

Otegui MS, Noh YS, Martínez DE, Vila Petroff MG, Andrew Staehelin L, Amasino RM (2005) Senescence-associated vacuoles with intense proteolytic activity develop in leaves of Arabidopsis and soybean. Plant J **41**: 831–844.

Phillips AR, Suttangkakul A, Vierstra RD (2008) The ATG12-conjugating enzyme ATG10 is essential for autophagic vesicle formation in *Arabidopsis thaliana*. Genetics **178**: 1339–1353.

Pracharoenwattana I, Cornah JE, Smith SM (2007) Arabidopsis peroxisomal malate dehydrogenase functions in b-oxidation but not in the glyoxylate cycle. Plant J **50**: 381–390.

Pugkaew W, Meetam M, Ponpuak M, Yokthongwattana K, Pokethitiyook P (2017) Role of autophagy in triacylglycerol biosynthesis in *Chlamydomonas reinhardtii* revealed by chemical inducer and inhibitors. J Appl Phycol **30**: 15–22.

Pyc M, Cai Y, Greer MS, Yurchenko O, Chapman KD, Dyer JM, Mullen RT (2017) Turning over a new leaf in lipid droplet biology. Trends Plant Sci **22**: 596–609.

Rambold AS, Cohen S, Lippincott-Schwartz J (2015) Fatty acid trafficking in starved cells: regulation by lipid droplet lipolysis, autophagy, and mitochondrial fusion dynamics. Dev Cell **32**: 678–692.

Rey P, Gillet B, Römer S, Eymery F, Massimino J (2000) Over-expression of a pepper plastid lipid-associated protein in tobacco leads to changes in plastid ultrastructure and plant development upon stress. Plant J **21**: 483–494.

Rottet S, Besagni C, Kessler F (2015) The role of plastoglobules in thylakoid lipid remodeling during plant development. Biochim Biophys Acta **1847**: 889–899.

Salem MA, Juppner J, Bajdzienko K, Giavalisco P (2016) Protocol: a fast, comprehensive and reproducible one-step extraction method for the rapid preparation of polar and semi-polar metabolites, lipids, proteins, starch and cell wall polymers from a single sample. Plant Methods **12**: 45.

Schneider CA, Rasband WS, Eliceiri KW (2012) NIH Image to ImageJ: 25 years of image analysis. Nat Methods **9**: 671–675.

Schwarz V, Andosch A, Geretschläger A, Affenzeller M, Lütz-Meindl U (2017) Carbon starvation induces lipid degradation via autophagy in the model alga Micrasterias. J Plant Physiol **208**: 115–127.

Shin KD, Lee HN, Chung T (2014) A revised assay for monitoring autophagic flux in *Arabidopsis thaliana* reveals involvement of AUTOPHAGY-RELATED9 in autophagy. Mol Cells **37**: 399–405.

Simkin AJ, Gaffe J, Alcaraz JP, Carde JP, Bramley PM (2007) Fibrillin influence on plastid ultrastructure and pigment content in tomato fruit. Phytochemistry **68**: 1545–1556.

Singh R, Kaushik S, Wang Y, Xiang Y, Novak I, Komatsu M, Tanaka K, Cuervo AM, Czaja MJ (2009) Autophagy regulates lipid metabolism. Nature **458**: 1131–1135.

Singh DK, McNellis TW (2011) Fibrillin protein function: the tip of the iceberg? Trends Plant Sci **16**: 432–441.

Soto-Burgos J, Zhuang X, Jiang L, Bassham DC (2018) Dynamics of autophagosome formation. Plant Physiol **176**: 219–229.

Testerink C, Munnik T (2011) Molecular, cellular, and physiological responses to phosphatidic acid formation in plants. J Exp Bot **62**: 2349–2361.

Thompson AR, Doelling JH, Suttangkakul A, Vierstra RD (2005) Autophagic nutrient recycling in Arabidopsis directed by the ATG8 and ATG12 conjugation pathways. Plant Physiol **138**: 2097–2110.

Tran QG, Yoon HR, Cho K, Lee SJ, Crespo JL, Ramanan R, Kim HS (2019) Dynamic interactions between autophagosomes and lipid droplets in *Chlamydomonas reinhardtii*. Cells **8**: 992.

Troncoso-Ponce MA, Cao X, Yang Z, Ohlrogge JB (2013) Lipid turnover during senescence. Plant Sci **205–206**: 13–19.

van Wijk KJ, Kessler F (2017) Plastoglobuli: plastid microcompartments with integrated functions in metabolism, plastid developmental transitions, and environmental adaptation. Annu Rev Plant Biol **68**: 253–289.

Wada S, Ishida H, Izumi M, Yoshimoto K, Ohsumi Y, Mae T, Makino A (2009) Autophagy plays a role in chloroplast degradation during senescence in individually darkened leaves. Plant Physiol **149**: 885–893.

Wang X, Devaiah SP, Zhang W, Welti R (2006) Signaling functions of phosphatidic acid. Prog Lipid Res **5**: 250–278.

Wood WHJ, Barnett SFH, Flannery S, Hunter CN, Johnson MP (2019) Dynamic thylakoid stacking is regulated by LHCII phosphorylation but not its interaction with PSI. Plant Physiol **180**: 2152–2166.

Yang Y, Benning C (2018) Functions of triacylglycerols during plant development and stress. Curr Opin Biotechnol **49**: 191–198.

Yoshimoto K, Hanaoka H, Sato S, Kato T, Tabata S, Noda T, Ohsumi Y (2004) Processing of ATG8s, ubiquitin-like proteins, and their deconjugation by ATG4s are essential for plant autophagy. Plant Cell **16**: 2967–2983.

Yoshimoto K, Jikumaru Y, Kamiya Y, Kusano M, Consonni C, Panstruga R, Ohsumi Y, Shirasu K (2009) Autophagy negatively regulates cell death by controlling NPR1-dependent salicylic acid signaling during senescence and the innate immune response in Arabidopsis. Plant Cell **21**: 2914–2927.

Ytterberg AJ, Peltier JB, van Wijk KJ (2006) Protein profiling of plastoglobules in chloroplasts and chromoplasts. A surprising site for differential accumulation of metabolic enzymes. Plant Physiol **140**: 984–997.

Zhao L, Dai J, Wu Q (2014) Autophagy-like processes are involved in lipid droplet degradation in *Auxenochlorella protothecoides* during the heterotrophy–autotrophy transition. Front Plant Sci **5**: 400.

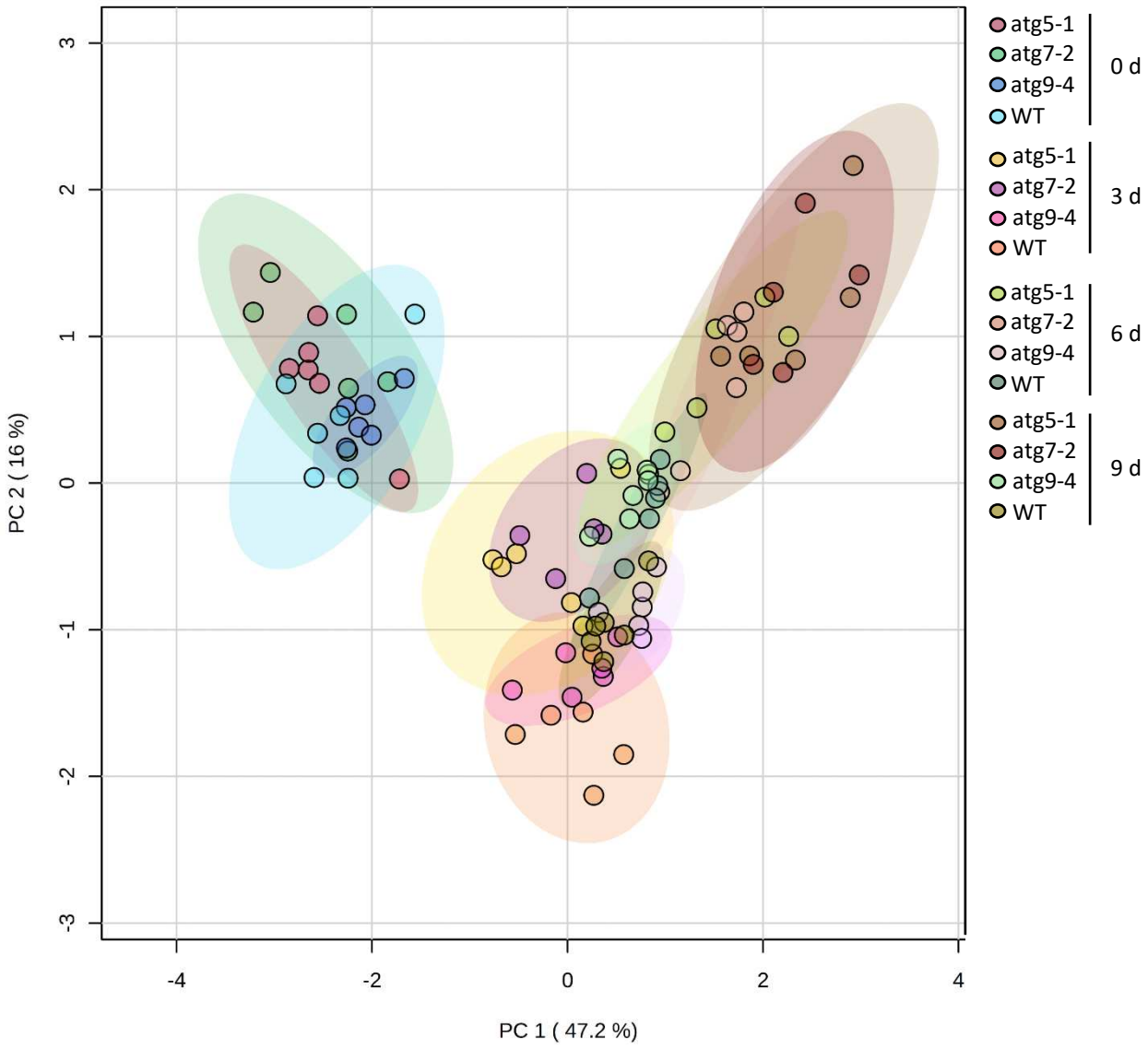

Supplemental Figure S1: Lipid response of *atg* mutants throughout dark-induced senescence. Principal component analysis (PCA) was performed using the lipid data of *atg5-1, atg7-2, atg9-4* and wild type (WT) genotypes after 0 (0d), 3 (3d), (6d), and 9 (9d) days of dark treatment

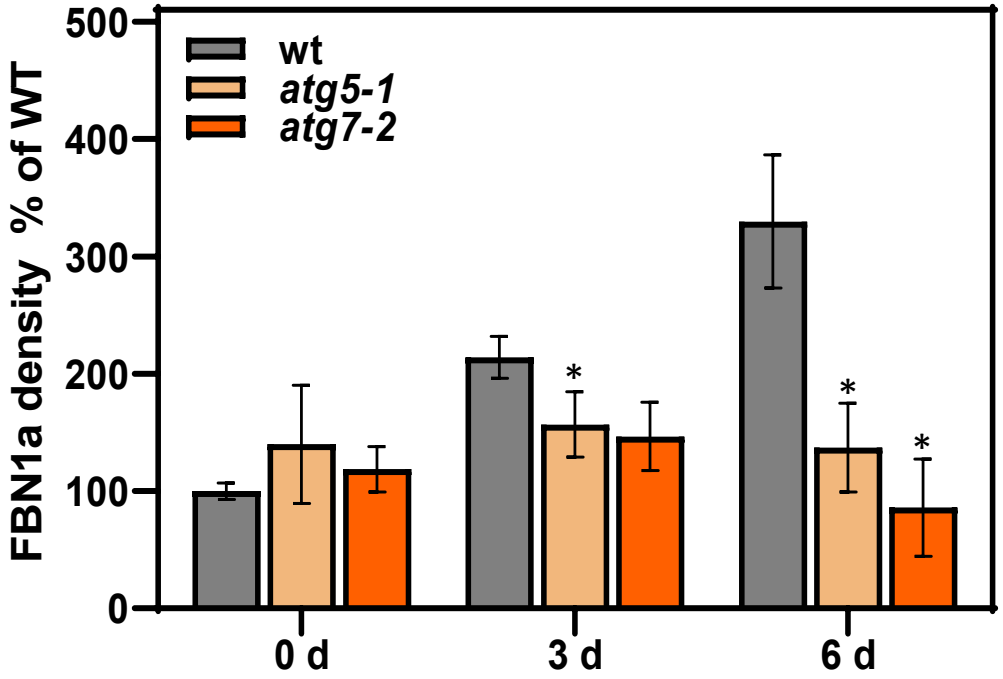

Supplemental Figure S2: Quantification of the FBN1a protein signal

Integrated density values for FBN1a were first normalized to loading control and then expressed as a percentage of the obtained value for the wild type (WT) at 0d. Data represent means ±SE; n= 3 biological replicates. An asterisk (*) indicates values that were determined by Student's t-test to be significantly different ($P < 0.05$) from the WT at each time point analyzed.

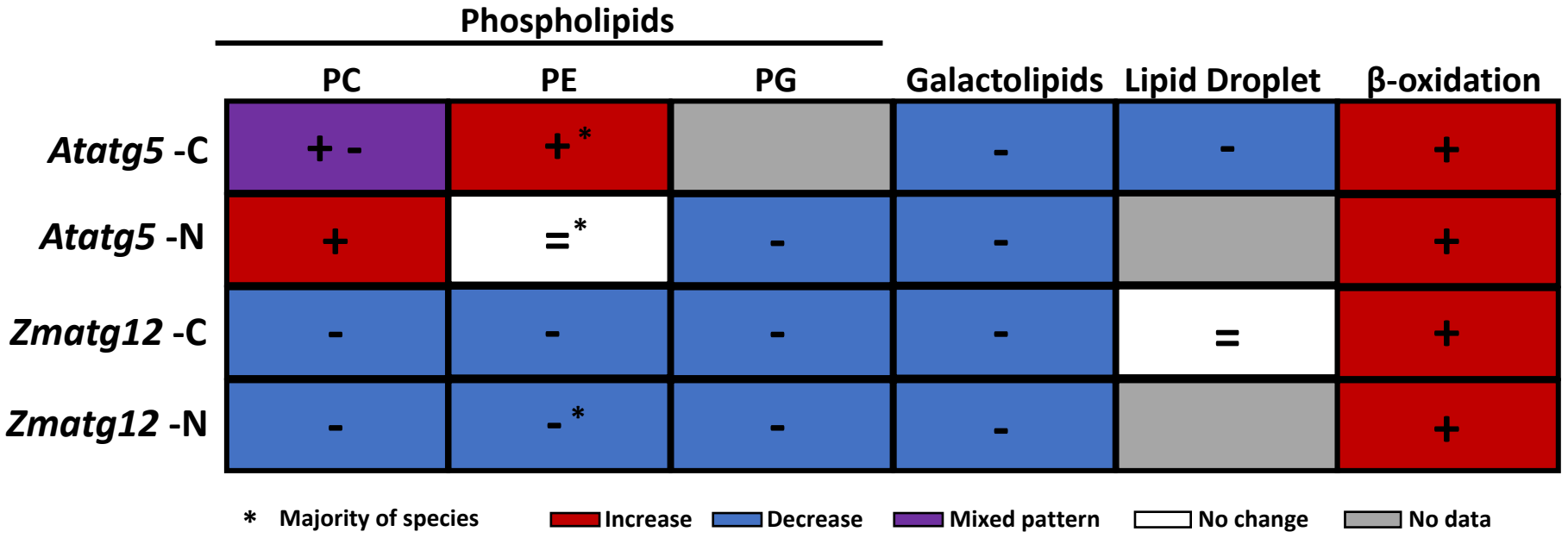

Supplemental Figure S3: Compared lipidomics of Arabidopsis and maize *atg* mutants under carbon and nitrogen starvation.

General representation of the changes in Phospholipids, Galactolipds, Lipid Droplet number, and β-oxidation transcripts reported in Arabidopsis and maize under carbon starvation (this study; McLoughlin et al., 2020) and nitrogen starvation (McLoughlin et al., 2018; Have et al., 2019). The scheme does not take into consideration the experimental differences in these studies. Abbreviations- PC: Phosphatidylcholine; PE-: Phosphatidylethanolamine; PG: phosphatidylglycerol; -C: Carbon starvation; -N: Nitrogen starvation

Supplemental Table S1: Summary of the main variables of the first three Principal Component (PC) of atg mutants and wild type (WT) genotypes after 0 and 6 d of dark treatment.

PC 1 CV = 57.8%		**PC 2** CV= 69.1%		**PC 3** CV=78.6%	
MGDG 34:4	-0.1813	TAG 54:9	-0.2078	TAG 56:4	-0.1958
MGDG 34:3	-0.16	MGDG 32:3(1)	-0.1916	TAG 54:6	-0.184
PC 38:4 (1)	-0.1589	TAG 52:6	-0.1681	TAG 52:4	-0.1819
MGDG 34:1	-0.1554	PC 36:5	0.1856	TAG 54:5	-0.1765

Supplemental Table S2: Primers used in the RT-qPCR analyses performed in this study

Gene	Locus	Forward	Reverse
ABC1K7	AT3G07700	TCCGTGTTCGGGTTCTTGAGTC	TGGCAACAAGCTGACTTCCTTGG
ACT	AT2G37620	CTTGCACCAAGCAGCATGAA	CCGATCCAGACACTGTACTTCCTT
ACX-4	AT3G51840	AGGTCAAGCCAGTTTAGGAAAGGC	AATTCCCGACCTAGCGAAGCAG
CSY-1	AT2G42790	AAGATCATGAGACCACAACAGGTG	TCTCACTGGTGTGTAATGCCTCAG
KAT-2	AT2G33150	TCCCGTTCTTGGTGTATTCAGGAC	ACCCATGATTGCAGGGTCAACAC
MFP-2	AT3G06860	ATGCCAATGGGTCCCTTCAGAC	CGATAAACTGCGTTGCGGTTGC
PES-1	AT1G54570	TGAAGTCTTGGTCCTTGCTAGTGG	AAGTAACCCGTGAAGCCGCTTTG
PES-2	AT3G26840	AAGGACGCTGGCAACATAAGGG	ACCTGCTGTTTCTATTGGTTTGCC
PMDH-1	AT2G22780	TGAGCTTCCCTTCTTCGCATCG	TGCCTTCTCTAATCCCATCCTCTC
PPH	AT5G13800	GGTGAGACCGTTATGGGGAAAG	GCATCAGATAGTTCACCACCTCAG
SDP-1	AT5G04040	TAAGCTCGCGCATCTAGTGGAG	CCGAGCTCTAATACCTGGTTGC

Supplemental Table S3: Relative lipid content of leaves of Arabidopsis knockout mutants *atg5-1, atg7-2, atg9-4* and wild type (WT) after 0, 3, 6 and 9 days of dark treatment

	0 day								3 day								6 day								9 day							
	WT		atg5-1		atg7-2		atg9-1		WT		atg5-1		atg7-2		atg9-1		WT		atg5-1		atg7-2		atg9-1		WT		atg5-1		atg7-2		atg9-1	
Lipid	Mean	SE	Mean	SE	Mean	SE	Mean	SE	Mean	SE	Mean	SE	Mean	SE	Mean	SE	Mean	SE	Mean	SE	Mean	SE	Mean	SE	Mean	SE	Mean	SE	Mean	SE	Mean	SE
DAG 34:3	1	0.1113	0.96207	0.0768	1.00667	0.075	1.06572	0.13	1.01773	0.10278	0.77971	0.06716	0.80572	0.07515	0.78537	0.1066	0.85592	0.04546	0.94044	0.08862	0.7429	0.04707	0.7518	0.09991	0.66444	0.01461	**1.3107**	0.09226	**0.94397**	0.0403	0.59669	0.03474
DAG 34:6	1	0.1834	0.85263	0.0328	1.08713	0.214	2.08405	0.486	1.16658	0.12071	1.33338	0.20327	1.72936	0.53488	1.18311	0.14783	0.65319	0.10089	**2.07428**	0.32649	**1.81432**	0.217	0.84126	0.09786	0.62049	0.07652	**4.85802**	0.31157	**3.64677**	0.49381	0.64645	0.05639
DAG 36:5	1	0.1148	1.0087	0.1099	1.15355	0.084	1.15613	0.087	0.8347	0.04821	0.83209	0.04383	0.89246	0.09093	0.86156	0.04902	0.57694	0.05681	**0.89731**	0.07739	**0.78318**	0.03994	0.66806	0.05429	0.40321	0.02611	**1.73918**	0.17003	**1.15472**	0.06396	**0.52871**	0.04397
DAG 36:6	1	0.1102	0.89439	0.0664	0.98212	0.032	1.20763	0.097	1.50628	0.11613	1.26132	0.09276	1.24607	0.12793	1.42611	0.09808	1.10082	0.08415	**1.53765**	0.10431	**1.54405**	0.14942	1.24394	0.097	0.83423	0.02792	**3.15584**	0.2862	**2.13664**	0.20441	0.90269	0.05353
DGDG 32:0	1	0.2217	0.99919	0.1643	1.11442	0.154	1.09248	0.106	0.39689	0.08141	0.40989	0.03143	0.50526	0.11108	0.45037	0.05164	0.30045	0.11916	0.15213	0.0441	0.21987	0.06507	0.34382	0.09871	0.25005	0.03599	0.26825	0.09169	0.16137	0.02564	0.30352	0.10433
DGDG 32:3	1	0.0787	1.02696	0.1361	1.03338	0.119	0.96358	0.051	0.74049	0.04147	0.74105	0.05422	0.71807	0.06625	0.77523	0.0338	1.16839	0.13518	**0.33771**	0.05158	**0.42573**	0.0863	0.95544	0.06031	1.49601	0.22153	**0.18831**	0.04835	**0.17091**	0.02637	1.25063	0.11
DGDG 34:0	1	0.1051	1.2412	0.0904	1.28694	0.156	1.12766	0.083	0.32146	0.03104	**0.55771**	0.04879	**0.46299**	0.04509	**0.42346**	0.03327	0.17865	0.00972	**0.32195**	0.03607	**0.30637**	0.04091	**0.26798**	0.02724	0.20989	0.01709	**0.41735**	0.05476	**0.36869**	0.02151	**0.28889**	0.02923
DGDG 34:2	1	0.1362	1.06998	0.1455	0.96812	0.124	0.87857	0.126	0.23664	0.04807	0.36443	0.08646	0.26162	0.03075	0.2343	0.04242	0.08904	0.01561	0.1122	0.0183	0.09184	0.01453	0.11371	0.0085	0.08876	0.0106	**0.09135**	0.02399	0.07182	0.01283	0.10201	0.01618
DGDG 34:3	1	0.1008	0.87478	0.0561	0.89737	0.063	0.87778	0.04	0.56627	0.01797	**0.47495**	0.01476	0.5008	0.03041	0.52304	0.02366	0.43025	0.04161	**0.10903**	0.01573	**0.1517**	0.02686	**0.31605**	0.01799	0.47595	0.04253	**0.10362**	0.01921	**0.09518**	0.01153	**0.33501**	0.02484
DGDG 34:4 (1)	1	0.0641	**0.73467**	0.0937	**0.70049**	0.078	**0.78102**	0.07	0.59897	0.0469	0.481	0.03558	0.45071	0.05891	0.51463	0.04305	0.43029	0.03797	**0.07907**	0.01431	**0.10905**	0.02579	0.34951	0.01786	0.48943	0.05183	**0.03392**	0.00875	nd	nd	0.3531	0.045
DGDG 34:4 (2)	1	0.0897	1.2082	0.122	1.29514	0.148	1.02382	0.1	0.17095	0.02463	**0.36622**	0.05876	**0.28334**	0.03328	0.225	0.03754	0.12725	0.02276	**0.05175**	0.01047	nd	nd	0.10718	0.02294	0.10391	0.01317	0.07696	0.0183	nd	nd!	0.07909	0.0153
DGDG 34:5	1	0.0837	0.93255	0.05	0.95774	0.073	0.93848	0.043	0.57142	0.03234	0.60153	0.05672	0.56082	0.02129	0.52973	0.03947	0.37877	0.02843	**0.16013**	0.02966	**0.18101**	0.02732	0.31575	0.02191	0.34976	0.02602	**0.07995**	0.02109	**0.06605**	0.00748	**0.2606**	0.03194
DGDG 34:6	1	0.0448	0.96857	0.0726	1.05732	0.086	1.0053	0.043	0.78044	0.02938	0.84784	0.06633	0.88139	0.05978	0.81056	0.04873	0.95266	0.07658	**1.40571**	0.12431	**1.47952**	0.15169	1.07898	0.07407	0.80452	0.05108	1.19297	0.33465	**1.20314**	0.10934	0.93393	0.05603
DGDG 36:3	1	0.1095	0.88179	0.0614	0.95158	0.095	0.8361	0.072	0.52811	0.02278	0.56147	0.02769	0.54207	0.04595	0.53181	0.03466	0.43563	0.04232	**0.22372**	0.03143	**0.26797**	0.02906	0.40473	0.03582	0.51568	0.05413	**0.18766**	0.02451	**0.17407**	0.01027	0.42013	0.04433
DGDG 36:4	1	0.075	**0.66324**	0.048	**0.66174**	0.081	**0.72478**	0.077	0.49914	0.05034	**0.36631**	0.02052	0.35748	0.02053	0.448	0.0177	0.42322	0.04101	**0.1187**	0.01819	**0.15192**	0.02502	0.35396	0.02676	0.48345	0.04737	**0.09104**	0.02241	**0.07681**	0.00896	0.39673	0.03576
DGDG 36:5	1	0.0854	0.94719	0.0724	0.97433	0.1	0.9325	0.08	0.36996	0.03227	0.38323	0.0461	0.33916	0.03264	0.37139	0.01749	0.47634	0.04307	**0.14624**	0.01897	**0.20304**	0.03526	0.44802	0.03748	0.55185	0.05336	**0.15685**	0.04613	**0.14117**	0.01867	0.54325	0.04404
DGDG 36:6	1	0.0703	0.89286	0.0422	0.94647	0.058	0.94958	0.05	0.77001	0.01982	0.74565	0.04055	0.76855	0.03981	0.7482	0.03731	0.74801	0.03599	**0.29744**	0.04866	**0.39892**	0.06019	**0.63054**	0.02748	0.70365	0.03103	**0.13022**	0.04406	**0.14717**	0.04216	0.62695	0.04419
DGDG 38:5	1	0.0693	**0.66064**	0.0394	**0.6919**	0.084	**0.6777**	0.036	0.39244	0.03547	**0.27789**	0.02666	**0.26947**	0.02024	**0.27579**	0.03127	0.29194	0.02795	**0.06297**	0.00847	**0.06957**	0.02283	**0.15892**	0.01455	0.31997	0.03066	**nd**	nd	nd	nd	**0.17562**	0.02242
DGDG 38:6	1	0.0587	**0.69743**	0.0507	**0.72589**	0.072	**0.73548**	0.027	0.66457	0.03476	**0.48606**	0.03371	**0.49201**	0.03171	**0.49806**	0.03246	0.45253	0.03636	**0.10193**	0.01825	**0.15064**	0.03173	**0.2959**	0.02302	0.52606	0.05362	**0.03492**	0.01276	**0.0368**	0.01111	**0.29097**	0.03372
MGDG 32:3 (1)	1	0.1322	1.16491	0.1457	0.98919	0.152	0.9509	0.204	3.47852	0.39286	**1.5273**	0.16682	**1.36679**	0.26681	2.83926	0.28135	3.52783	0.35214	**1.05294**	0.15141	**1.18192**	0.35395	**2.40713**	0.29371	3.70257	0.26148	**1.25825**	0.43843	**2.07965**	0.47546	**1.90752**	0.0709
MGDG 32:3 (2)	1	0.0662	**0.71662**	0.0358	**0.77827**	0.032	0.89743	0.076	1.37133	0.09806	**0.72227**	0.06118	**0.7351**	0.06106	**1.07737**	0.05878	1.40703	0.12793	**0.22178**	0.02791	**0.39373**	0.11783	**0.86968**	0.02718	1.06972	0.06193	**0.10329**	0.02298	**0.07701**	0.01854	**0.63782**	0.05214
MGDG 32:6	1	0.158	**0.6204**	0.0836	**0.56492**	0.008	0.58991	0.027	0.93775	0.09233	**0.6428**	0.06648	**0.62054**	0.05297	**0.62316**	0.03521	0.48339	0.07417	**0.08699**	0.02012	**0.13819**	0.05595	**0.28639**	0.03394	0.26346	0.03396	nd	nd	nd	nd	**0.15262**	0.02504
MGDG 34:1	1	0.0853	1.08689	0.0861	1.04498	0.104	0.84348	0.062	0.00205	0.00034	0.00583	0.00295	0.00278	0.00047	0.00223	0.00064	0.00561	0.00162	0.00738	0.00093	0.00511	0.00087	0.00295	0.00026	0.00716	0.00294	0.01607	0.00373	nd	nd	0.00468	0.00047
MGDG 34:2	1	0.0717	1.0791	0.0519	1.08235	0.129	0.96313	0.09	0.06966	0.00542	0.05577	0.00948	**0.0482**	0.00755	0.07471	0.00552	0.07099	0.00615	**0.02252**	0.0018	**0.02823**	0.00377	**0.056**	0.00224	0.08094	0.00909	**0.02857**	0.00189	**0.0293**	0.00197	0.06243	0.00181
MGDG 34:3	1	0.058	0.89169	0.0494	0.89357	0.047	0.9167	0.058	0.45066	0.021	**0.26197**	0.01198	**0.22953**	0.01452	**0.33565**	0.01861	0.25013	0.01628	**0.04266**	0.00599	**0.0682**	0.01712	**0.18635**	0.01074	0.25854	0.00701	**0.04088**	0.00466	**0.04291**	0.00455	**0.17322**	0.0153
MGDG 34:4	1	0.0747	1.17846	0.1023	1.18249	0.069	1.06967	0.048	0.01588	0.00336	**0.04369**	0.01097	0.02225	0.0042	0.02017	0.00294	0.01191	0.00155	0.01493	0.00215	0.01334	0.00169	0.01092	0.00086	0.01286	0.00071	0.01345	0.00166	**0.01495**	0.00063	0.01585	0.00192
MGDG 34:5	1	0.1657	1.01197	0.1513	0.91565	0.045	0.8928	0.041	0.11253	0.0152	0.14606	0.03069	0.09499	0.0068	0.09815	0.01239	0.07326	0.01348	**0.01439**	0.00308	**0.02191**	0.00731	0.05575	0.00747	0.05252	0.00641	**0.00717**	0.0019	**0.00693**	0.00115	0.04626	0.00687
MGDG 34:6	1	0.1137	0.97102	0.0684	0.98241	0.05	0.94098	0.046	0.90463	0.02767	0.90027	0.05327	0.92112	0.0261	0.87214	0.04676	0.85017	0.07349	**0.46212**	0.0485	**0.52217**	0.08336	0.75278	0.05937	0.68066	0.03284	**0.19867**	0.05286	**0.22528**	0.03149	0.62592	0.05954
MGDG 36:3	1	0.0468	1.05882	0.0663	1.12512	0.111	1.04416	0.09	0.62709	0.04201	**0.43843**	0.02232	**0.37725**	0.02574	0.54129	0.04005	0.45287	0.03083	**0.04048**	0.00932	**0.07697**	0.02918	**0.30243**	0.01497	0.43575	0.02481	nd	nd	nd	nd	0.22919	0.0201
MGDG 36:4	1	0.0751	0.95624	0.1257	0.84945	0.135	1.25335	0.253	0.82337	0.07038	**0.59615**	0.03712	**0.62193**	0.07339	0.86977	0.06379	0.95839	0.08531	**0.22396**	0.01656	**0.30427**	0.05852	0.82736	0.07635	1.096	0.09006	**0.11146**	0.03577	**0.12486**	0.02124	0.96077	0.03902
MGDG 36:5	1	0.0528	0.99588	0.0714	1.0529	0.079	1.08637	0.128	0.39347	0.04049	**0.28524**	0.03526	**0.26227**	0.04428	0.41389	0.03114	0.5713	0.03158	**0.11818**	0.01027	**0.18525**	0.03965	**0.44937**	0.02389	0.6112	0.05336	**0.06655**	0.0142	**0.08402**	0.01376	**0.46607**	0.01795
MGDG 36:6	1	0.0781	0.88212	0.0474	0.89213	0.049	0.92544	0.056	0.83859	0.04087	**0.67831**	0.03405	**0.70387**	0.03768	**0.71231**	0.04277	0.62664	0.04101	**0.14045**	0.0257	**0.22633**	0.05735	**0.4923**	0.0315	0.57649	0.01428	**0.04057**	0.01179	**0.05415**	0.0146	**0.41142**	0.02977
MGDG 38:4	1	0.0915	0.8343	0.0489	0.87888	0.048	0.89539	0.066	0.86013	0.03914	**0.68153**	0.00826	**0.69371**	0.05665	0.81627	0.04926	0.67616	0.04908	**0.17445**	0.01297	**0.21411**	0.06055	**0.50134**	0.02447	0.66381	0.01049	nd	nd	nd	nd	**0.41935**	0.04056
MGDG 38:6	1	0.1394	**0.56154**	0.0561	**0.57143**	0.03	**0.62877**	0.012	0.72974	0.0427	**0.38165**	0.01896	**0.38087**	0.02214	**0.42697**	0.02591	0.32984	0.03433	**0.03489**	0.0049	**0.08865**	0.02537	**0.18466**	0.01622	0.28809	0.01578	nd	nd	nd	nd	**0.13022**	0.01297
PC 32:0	1	0.2	1.21285	0.1785	1.43139	0.187	1.03235	0.089	4.24248	0.34784	**4.55156**	0.4004	5.13182	0.71314	**5.13291**	0.2535	9.13124	1.49363	7.89598	0.49109	9.51901	0.9968	9.91861	1.101	9.08473	1.30178	9.59383	1.54587	9.89763	1.21507	10.7362	1.45074
PC 32:1 (1)	1	0.0575	1.21901	0.1157	**1.37774**	0.102	0.92741	0.06	0.90987	0.05195	**1.39713**	0.12333	**1.402**	0.13475	**1.17019**	0.05049	0.9946	0.07918	**1.63531**	0.12695	**1.5407**	0.12454	**1.38604**	0.08189	0.95396	0.07079	1.27246	0.16912	1.53361	0.28353	**1.38683**	0.09779
PC 32:1 (2)	1	0.0585	**1.37055**	0.0909	**1.48654**	0.115	1.07589	0.031	0.62006	0.04481	**1.51309**	0.1768	**1.38595**	0.11401	**0.97686**	0.07949	0.35361	0.01568	**0.73301**	0.06537	**0.70524**	0.07899	**0.59196**	0.03151	0.29238	0.02058	0.52107	0.08466	**0.55204**	0.00938	**0.55097**	0.04735
PC 32:2 (1)	1	0.08	**1.67809**	0.1552	**1.83374**	0.222	1.20582	0.079	1.44335	0.14043	**2.06469**	0.16544	**2.19755**	0.21365	**1.82201**	0.11672	1.54198	0.11057	**2.05712**	0.14501	**1.93789**	0.18814	**2.13505**	0.11886	1.41509	0.09751	1.29145	0.28649	1.30377	0.21663	**1.84796**	0.11352
PC 32:2 (2)	1	0.0448	0.83792	0.0718	0.89551	0.066	**0.72953**	0.065	1.72224	0.14119	1.76398	0.15727	1.71976	0.14059	1.64556	0.1121	1.07426	0.06465	1.06626	0.11988	0.99867	0.11831	1.10919	0.07782	0.90302	0.08131	0.66689	0.13163	**0.59457**	0.04875	0.82399	0.07626
PC 32:3 (1)	1	0.0964	1.28254	0.1513	**1.41835**	0.177	1.13234	0.11	2.36821	0.21633	2.68203	0.25726	2.78089	0.31078	**3.0124**	0.22351	3.67872	0.49687	3.88315	0.27167	4.17725	0.41957	4.05565	0.29643	3.43014	0.32264	2.88246	0.30408	3.27887	0.22179	3.61088	0.22934
PC 32:3 (2)	1	0.098	0.88217	0.1031	1.02127	0.113	0.80396	0.097	5.39206	0.36625	**4.17019**	0.30854	**4.01583**	0.43162	4.91676	0.38237	3.53554	0.32333	3.41073	0.21546	3.5385	0.26962	3.19489	0.29675	3.21208	0.29703	**4.45265**	0.33384	3.77112	0.39264	2.39765	0.26922
PC 34:1	1	0.0662	1.14743	0.1101	1.25989	0.149	0.90843	0.076	0.24812	0.0163	**0.40941**	0.03971	**0.41268**	0.04057	**0.30581**	0.0198	0.31028	0.02324	**0.51637**	0.04443	**0.48049**	0.03154	**0.40233**	0.03036	0.26254	0.02657	**0.46208**	0.05241	**0.5031**	0.03687	**0.40631**	0.02397
PC 34:3	1	0.0398	0.9936	0.0604	1.07939	0.082	0.90254	0.046	1.09108	0.042	1.23234	0.09873	1.27342	0.09536	1.20752	0.06699	1.29035	0.06131	**1.57666**	0.08494	**1.64397**	0.1223	1.44769	0.07768	1.18953	0.05295	1.29024	0.14561	**1.46306**	0.06373	**1.44647**	0.07003
PC 34:4 (1)	1	0.127	0.97853	0.0947	1.03402	0.08	0.83985	0.09	0.84708	0.09541	1.06958	0.15996	0.84431	0.12685	0.77874	0.09378	0.49871	0.07009	0.37807	0.02865	0.33911	0.0596	0.54428	0.07081	0.36244	0.03114	**0.10581**	0.03501	**0.12701**	0.01021	0.41765	0.06355
PC 34:4 (2)	1	0.0615	1.16928	0.142	1.3506	0.131	1.09925	0.11	1.52075	0.09251	1.66358	0.15819	1.87032	0.21054	1.69335	0.10435	2.10856	0.22412	2.59931	0.16539	2.74353	0.26583	2.21915	0.16618	2.0519	0.15474	**3.46781**	0.18902	**3.2626**	0.26954	2.39212	0.14605
PC 34:5	1	0.0806	0.92785	0.1251	0.97867	0.105	0.87138	0.111	3.42373	0.14473	**2.56813**	0.12474	**2.41499**	0.21177	3.16785	0.21956	2.7146	0.22173	**1.51201**	0.0782	**1.67033**	0.15574	**2.15536**	0.14601	2.54304	0.22304	**1.55277**	0.15958	**1.29329**	0.20545	**1.65297**	0.15395
PC 34:6	1	0.1203	0.90914	0.1459	1.03394	0.138	0.86504	0.14	9.67346	1.08125	**5.7438**	0.73133	**5.64413**	0.48473	8.57546	0.75665	9.41646	1.21275	**5.69055**	0.50012	**6.06753**	0.29564	7.43589	0.2103	9.59478	1.05557	**6.25772**	0.66839	**5.51824**	1.07975	**5.46157**	0.5054
PC 36:1	1	0.115	1.24353	0.1213	**1.43962**	0.159	0.93777	0.047	0.2046	0.01453	**0.3382**	0.03383	**0.30075**	0.02406	0.25301	0.02381	0.224	0.02434	**0.39796**	0.02553	**0.36891**	0.02833	**0.29836**	0.02189	0.18378	0.01704	**0.40091**	0.0407	**0.39108**	0.04126	**0.30802**	0.02677
PC 36:2	1	0.0479	**1.4066**	0.1141	**1.5057**	0.149	1.04813	0.056	0.37474	0.02792	**0.62673**	0.07592	**0.56604**	0.04644	0.43531	0.04283	0.24891	0.01717	0.26179	0.02379	0.2627	0.03048	**0.36681**	0.02059	0.23444	0.02095	0.19212	0.03125	0.18021	0.02467	**0.3522**	0.03515
PC 36:3 (1)	1	0.055	**1.29013**	0.119	**1.51223**	0.138	0.93492	0.108	0.12556	0.00729	**0.25873**	0.02543	**0.23258**	0.02038	**0.16629**	0.01293	0.10453	0.00958	**0.19886**	0.01906	**0.18197**	0.01614	**0.13863**	0.01107	0.08694	0.00953	**0.22376**	0.01887	**0.20861**	0.02235	**0.13927**	0.01171
PC 36:3 (2)	1	0.0647	**1.35129**	0.0986	**1.40887**	0.166	1.01597	0.065	0.73567	0.02857	**0.89861**	0.07093	0.88186	0.10735	0.79177	0.04831	0.83594	0.0761	0.75961	0.07875	0.7999	0.07487	0.94356	0.07429	0.7556	0.06438	0.52308	0.12832	**0.52578**	0.05328	**0.93842**	0.0646
PC 36:4	1	0.0795	**1.35286**	0.0991	**1.42008**	0.095	1.09531	0.062	0.64099	0.04506	**1.11818**	0.11569	**1.06791**	0.08754	**0.84035**	0.05704	0.41252	0.03455	**0.62119**	0.06802	**0.59144**	0.08232	**0.6611**	0.04432	0.38961	0.02775	0.45503	0.06166	0.35751	0.0683	**0.66461**	0.05156
PC 36:5	1	0.0285	**1.19187**	0.0866	**1.25876**	0.121	1.01595	0.075	0.85153	0.04096	**1.1342**	0.09773	**1.16364**	0.08352	1.02413	0.07601	0.85199	0.05617	**1.058**	0.06116	**1.13221**	0.10355	1.02466	0.07522	0.81976	0.03342	0.98031	0.08643	**0.98528**	0.06295	**1.01466**	0.06501
PC 36:6	1	0.0509	1.04321	0.0806	1.15695	0.13	0.93022	0.1	1.62674	0.11692	1.71	0.19593	1.77455	0.14836	1.74733	0.15503	2.23357	0.18372	2.44478	0.1825	2.66086	0.23369	2.19403	0.16862	2.0547	0.09083	2.15404	0.19216	2.33354	0.15685	2.18804	0.12563
PC 38:3 (1)	1	0.0603	**1.21286**	0.0405	**1.29763**	0.116	0.99029	0.07	0.18604	0.01541	0.19794	0.01678	0.21581	0.02903	0.16089	0.0144	0.13338	0.00889	0.14601	0.02025	0.17561	0.0313	**0.16703**	0.00842	0.09984	0.01376	0.16875	0.02895	0.11395	0.03097	**0.1636**	0.01875
PC 38:3 (2)	1	0.0799	1.19996	0.1325	**1.45689**	0.114	0.8623	0.094	0.97721	0.05938	**0.74368**	0.06391	**0.74521**	0.08435	**0.80092**	0.03681	1.78715	0.195	**1.04332**	0.09017	**1.27919**	0.14681	1.51998	0.09352	1.63709	0.19933	0.62774	0.11302	**0.68154**	0.08336	1.56971	0.09937
PC 38:3 (3)	1	0.3274	1.19772	0.2643	1.48665	0.233	0.99969	0.147	2.5788	0.89396	9.45343	4.28758	**13.2224**	3.17746	6.19292	1.16457	31.5114	7.15299	**134.451**	40.1327	**216.243**	58.1911	50.0064	11.7144	57.5789	16.8396	338.705	102.05	**414.077**	123.599	101.634	36.4711
PC 38:4 (1)	1	0.0857	0.90239	0.0729	1.04757	0.09	0.85502	0.091	0.34146	0.0392	0.32308	0.06104	0.33521	0.06154	0.33298	0.04921	0.14994	0.02758	**0.04689**	0.01145	**0.06812**	0.01339	0.20694	0.03915	0.12767	0.01992	0.06917	0.01268	nd	nd	0.17765	0.02817
PC 38:4 (2)	1	0.1233	0.96744	0.0759	1.03825	0.099	0.80238	0.097	0.38031	0.04389	0.36909	0.04882	0.42687	0.06434	0.33715	0.03417	0.32675	0.02122	0.34371	0.04842	0.37041	0.0538	0.33297	0.02811	0.1955	0.0239	0.2413	0.04153	0.59944	0.36069	**0.2871**	0.02835
PC 38:5	1	0.0832	0.81091	0.062	0.89505	0.08	**0.74299**	0.082	0.53712	0.02699	0.46593	0.04182	0.45161	0.0468	0.46365	0.02795	0.45567	0.03816	**0.30206**	0.02501	0.36204	0.05006	0.45658	0.03076	0.38135	0.02603	0.29409	0.04728	**0.20069**	0.03728	0.40967	0.03747
PC 38:6	1	0.0633	**0.74201**	0.0529	0.83863	0.082	**0.69677**	0.086	0.87488	0.04106	**0.69455**	0.074	**0.70487**	0.06291	0.77371	0.05944	1.03041	0.10155	**0.71265**	0.06186	0.89607	0.11481	0.96033	0.06636	0.90239	0.06996	0.64876	0.08705	**0.53154**	0.07731	0.85158	0.06031

Supplemental Table S3 (Continuation): Relative lipid content of leaves of Arabidopsis knockout mutants *atg5-1, atg7-2, atg9-4* and wild type (WT) after 0, 3, 6 and 9 days of dark treatment.

	0 day								3 day								6 day								9 day							
	WT		atg5-1		atg7-2		atg9-1		WT		atg5-1		atg7-2		atg9-1		WT		atg5-1		atg7-2		atg9-1		WT		atg5-1		atg7-2		atg9-1	
Lipid	Mean	SE	Mean	SE	Mean	SE	Mean	SE	Mean	SE	Mean	SE	Mean	SE	Mean	SE	Mean	SE	Mean	SE	Mean	SE	Mean	SE	Mean	SE	Mean	SE	Mean	SE	Mean	SE
PE 34:1	1	0.14678	1.24465	0.16674	1.2136	0.14163	0.81256	0.1739	0.68993	0.06198	0.95731	0.14199	0.96104	0.16564	0.61649	0.09437	0.94156	0.03226	1.15177	0.22017	1.14767	0.05328	**1.17702**	0.07652	0.86687	0.06919	0.70604	0.12047	0.99689	0.19721	**1.20147**	0.13042
PE 34:2	1	0.10029	1.13012	0.11519	1.11076	0.09946	0.8242	0.12156	0.83195	0.06316	0.97425	0.13408	0.99684	0.17236	0.7679	0.0912	0.77514	0.01984	0.93499	0.10587	**0.91693**	0.04834	**1.03251**	0.07528	0.75715	0.05932	**0.49134**	0.06116	0.67391	0.03926	**1.06125**	0.08387
PE 36:2	1	0.1222	**1.44976**	0.17098	**1.42796**	0.1478	0.89234	0.15865	0.68433	0.05143	0.95356	0.1657	0.89234	0.18585	0.63782	0.09242	0.55772	0.02918	0.59435	0.07198	0.59321	0.03084	**0.81062**	0.07439	0.55046	0.04833	**0.37533**	0.02078	0.4418	0.02023	**0.77341**	0.09411
PE 36:3 (1)	1	0.17647	1.157	0.13654	1.1748	0.13839	0.79039	0.17867	0.21563	0.0305	0.45442	0.11828	0.3902	0.10069	0.21582	0.05819	0.16653	0.01873	**0.38358**	0.06128	**0.39012**	0.05075	**0.29399**	0.04054	0.15638	0.02185	**1.00823**	0.17142	**0.82168**	0.09713	**0.33789**	0.06132
PE 36:3 (2)	1	0.14124	1.2519	0.14207	1.25112	0.15029	0.79452	0.13559	0.97058	0.06132	1.16224	0.21248	1.09721	0.23105	0.82702	0.11005	1.19839	0.05115	1.28951	0.17937	1.23344	0.07706	**1.4443**	0.13537	1.27034	0.11868	**0.70972**	0.05403	**0.9645**	0.04281	1.63082	0.1766
PE 36:4	1	0.12459	1.34663	0.15171	1.27647	0.13583	0.80467	0.12495	0.77276	0.0879	1.14189	0.18422	1.18704	0.24367	0.88133	0.13032	0.58769	0.03619	**1.04862**	0.12585	**0.91788**	0.09769	**0.97624**	0.10332	0.61322	0.06431	**0.77678**	0.02187	**0.8236**	0.05756	**1.08623**	0.15246
PE 36:5	1	0.134	1.12995	0.1258	1.10592	0.13186	0.76343	0.12102	0.78309	0.09239	1.0744	0.17838	1.08498	0.2163	0.79213	0.11446	0.73005	0.0394	**1.37606**	0.15535	**1.22794**	0.11992	**1.07736**	0.09891	0.77216	0.07812	**1.50693**	0.03971	**1.49447**	0.1641	**1.27462**	0.1171
PE 38:2	1	0.04721	**1.23842**	0.10216	**1.27665**	0.12772	0.97588	0.04683	0.6238	0.02613	**1.05781**	0.09643	**0.95403**	0.07087	**0.77609**	0.04437	0.51184	0.03439	**0.87027**	0.04957	**0.85171**	0.09911	**0.72035**	0.03965	0.50526	0.03768	**1.15188**	0.0627	**0.87975**	0.15911	**0.78202**	0.06138
PE 38:3	1	0.0444	0.9576	0.0821	1.018	0.08847	**0.83779**	0.05013	1.04757	0.04064	**1.3103**	0.07851	1.20706	0.09113	1.13869	0.07784	1.26279	0.08355	**1.84656**	0.10387	**1.82704**	0.16907	1.48095	0.11278	1.21956	0.08449	**2.08368**	0.22761	**2.16633**	0.28108	**1.52598**	0.09626
TAG 42:0	1	0.1208	0.90665	0.04176	1.04283	0.05975	0.98718	0.06656	1.19504	0.06578	1.055	0.10223	1.09494	0.09995	1.15489	0.10563	1.30808	0.04271	1.49916	0.15581	**1.71232**	0.06209	1.28236	0.10341	1.07269	0.06933	**1.91121**	0.1984	**1.68242**	0.10153	1.14554	0.08357
TAG 44:0	1	0.13429	0.89918	0.05153	0.94816	0.07691	0.95675	0.10235	0.97091	0.07533	0.98351	0.1086	1.1413	0.07873	1.00769	0.08844	1.2405	0.0701	1.48193	0.16087	**1.5321**	0.12538	1.27134	0.07811	1.13264	0.07213	**1.70124**	0.14146	**1.7161**	0.12317	1.16946	0.09607
TAG 44:1	1	0.13645	0.92013	0.0509	0.8917	0.02886	0.97109	0.08408	0.98752	0.07776	0.9887	0.10363	1.07798	0.08443	0.95003	0.07308	1.29667	0.07809	1.47074	0.1157	**1.51974**	0.09999	1.23661	0.11814	1.0103	0.06772	**1.60989**	0.16344	**1.68718**	0.16342	1.19079	0.11286
TAG 46:0	1	0.13259	0.96083	0.06019	0.96531	0.07234	0.95633	0.09047	0.98545	0.07388	1.03319	0.10669	1.1787	0.0978	1.03539	0.10576	1.24607	0.05798	1.44441	0.09755	**1.60477**	0.12226	1.32416	0.10573	1.05193	0.0769	**1.70506**	0.14911	**1.76015**	0.1918	1.23817	0.10614
TAG 46:1	1	0.09903	0.96408	0.04572	0.96943	0.07096	1.00705	0.07625	1.06249	0.06894	1.14104	0.14532	1.22609	0.0908	1.04259	0.06877	1.39009	0.06184	1.58615	0.12457	**1.69213**	0.11691	1.44593	0.1238	1.16482	0.0802	**1.97299**	0.19487	**2.05043**	0.19999	1.27082	0.07984
TAG 46:2	1	0.14538	0.87144	0.04931	0.98539	0.07372	0.8916	0.05201	0.99216	0.08856	0.99608	0.1342	1.12572	0.09483	0.97491	0.08587	1.27851	0.06162	1.5324	0.12034	**1.60112**	0.11237	1.22251	0.0994	1.11041	0.09807	**1.56788**	0.15715	**1.61962**	0.09906	1.2122	0.08202
TAG 48:0	1	0.12401	0.8641	0.05711	0.93544	0.05828	0.94799	0.06735	1.00631	0.10734	1.00452	0.09537	1.19111	0.08832	1.08159	0.09277	1.28838	0.09505	**1.57155**	0.08948	**1.6382**	0.13943	1.31079	0.1156	1.0868	0.0687	**1.64949**	0.16764	**1.77968**	0.15422	1.27621	0.07115
TAG 48:1	1	0.11599	0.91047	0.05937	0.94641	0.05318	0.97295	0.05442	1.00074	0.08802	1.02718	0.11285	1.1933	0.07591	1.02003	0.09929	1.27758	0.05554	**1.64173**	0.11575	**1.60014**	0.13457	1.27972	0.11161	1.12551	0.08369	**1.7124**	0.13328	**1.76053**	0.15262	1.21356	0.08413
TAG 48:2	1	0.10749	0.87707	0.02423	0.92358	0.04014	0.97066	0.10748	0.95617	0.09127	0.92396	0.10888	1.06635	0.08986	0.962	0.08746	1.20229	0.05852	1.40684	0.13203	1.38064	0.11728	1.22941	0.09493	1.01651	0.0796	**1.38703**	0.09681	**1.53078**	0.15672	1.01097	0.06227
TAG 48:3	1	0.11952	0.92695	0.0704	1.06525	0.09245	1.06703	0.0752	0.99308	0.09092	0.95495	0.17554	1.07455	0.08684	0.85715	0.07795	1.28515	0.09672	1.43306	0.1177	1.51098	0.10462	1.18688	0.11968	1.06136	0.08071	**1.84435**	0.20664	**1.76624**	0.18133	1.14591	0.0712
TAG 50:0	1	0.12954	0.86558	0.05187	0.96413	0.06494	0.87949	0.05265	1.00151	0.10626	1.02123	0.12004	1.16314	0.08493	0.97285	0.08005	1.26048	0.09468	**1.5052**	0.09189	1.59723	0.15203	1.28866	0.09056	1.02542	0.06849	**1.64762**	0.16651	**1.93454**	0.22355	1.2061	0.06591
TAG 50:1	1	0.14051	0.9028	0.05365	1.1466	0.13644	1.00113	0.08128	1.2112	0.28888	1.113	0.13412	1.35254	0.12926	1.06085	0.09256	1.23107	0.06706	**1.60949**	0.15366	**1.59356**	0.0979	1.31888	0.10683	1.31	0.11607	**2.1319**	0.16261	3.33959	1.20633	1.46858	0.08867
TAG 50:2 (1)	1	0.33203	0.84235	0.14635	1.3647	0.21593	1.64478	0.26809	6.11233	2.42996	2.24176	0.3297	2.56367	0.48089	3.47758	0.4749	2.48455	0.6847	2.50719	0.34455	2.07377	0.19722	2.01463	0.23242	2.9939	0.54533	**7.15049**	1.86317	5.4166	0.83906	3.1661	0.88383
TAG 50:2 (2)	1	0.12938	0.86255	0.08777	0.97761	0.07969	0.92293	0.11874	0.77347	0.03875	0.95014	0.10843	**1.05925**	0.05776	0.94107	0.08613	1.20745	0.09306	**1.60978**	0.16477	**1.86438**	0.20408	1.27731	0.10722	0.99788	0.07577	**1.56993**	0.16646	**1.56228**	0.24845	1.15101	0.18667
TAG 50:3 (1)	1	0.25305	0.65125	0.14146	0.79622	0.1364	1.077	0.20767	20.3278	5.66176	**4.22181**	0.96416	**3.23178**	0.65319	15.5	2.21937	6.03931	1.26292	**1.6392**	0.53097	**1.5547**	0.44738	**2.73909**	0.33511	4.38417	0.81115	8.3676	2.11272	5.69347	2.99261	**1.40046**	0.14138
TAG 50:3 (2)	1	0.11355	0.81658	0.06682	0.95154	0.13428	0.98924	0.09621	0.89793	0.14072	0.95924	0.12178	0.85407	0.05405	0.67648	0.08323	1.04841	0.04313	**1.55115**	0.21001	**1.41001**	0.12129	1.21099	0.12761	0.94062	0.06392	**1.54626**	0.12681	**1.69679**	0.27361	1.22866	0.15243
TAG 52:0	1	0.14521	0.80601	0.06021	0.92342	0.1077	0.90789	0.07554	0.92354	0.1247	0.91152	0.09729	1.05964	0.13261	0.88799	0.09045	1.13771	0.14857	1.5282	0.16799	1.45929	0.19864	1.26354	0.11833	0.93841	0.07215	**1.6399**	0.20862	**2.15032**	0.49829	1.04139	0.09554
TAG 52:1	1	0.12576	0.90978	0.05952	1.27017	0.22923	1.01913	0.10034	1.50891	0.60786	1.19659	0.11777	1.59133	0.20447	1.10768	0.07991	1.24092	0.09716	**1.81642**	0.26543	**1.70675**	0.17657	1.40944	0.19418	1.54257	0.19382	**2.74534**	0.32469	5.45584	2.78395	1.72627	0.21197
TAG 52:2	1	0.13392	0.92727	0.06242	1.08291	0.07835	1.09402	0.08676	1.09444	0.12689	1.21499	0.15158	1.31749	0.10684	1.05953	0.09421	1.37033	0.08989	**1.72354**	0.10762	**1.6838**	0.11793	1.33671	0.13594	1.3001	0.08512	**2.35326**	0.25242	**2.31065**	0.09579	1.59849	0.12905
TAG 52:3	1	0.09721	0.95133	0.06921	1.14846	0.08255	1.10328	0.09673	1.44467	0.21654	1.09972	0.08976	1.45603	0.15509	1.22627	0.09647	1.37421	0.09487	1.62127	0.13846	1.54876	0.0972	1.42383	0.12652	1.49519	0.13292	**3.3573**	0.3598	**2.61961**	0.11874	1.42465	0.06619
TAG 52:4	1	0.11522	0.93135	0.05964	1.13987	0.077	1.09364	0.10599	2.64342	0.26938	**1.68144**	0.14921	1.96557	0.24854	2.73913	0.28826	1.9016	0.11038	1.34045	0.27966	**1.32916**	0.12263	1.70622	0.08634	1.50519	0.1443	**3.22041**	0.51073	**2.67878**	0.2005	1.17025	0.09309
TAG 52:5	1	0.19836	0.7731	0.11194	1.00127	0.10657	1.1344	0.15379	8.74632	2.23444	4.3095	0.87226	4.22621	0.77359	10.0338	1.40075	4.78506	0.80808	**1.14636**	0.4729	**1.51283**	0.34498	3.26714	0.19698	3.14125	0.65745	6.34992	2.09645	4.52802	1.06537	**1.25371**	0.1317
TAG 52:6	1	0.2209	**0.47679**	0.05628	0.65436	0.02059	0.78507	0.10178	11.9024	2.85681	**3.9704**	0.76439	**3.51643**	0.48851	10.4341	1.34459	7.0003	0.89233	**1.27729**	0.49539	**1.95325**	0.54046	**4.31598**	0.21822	4.58642	0.8048	7.70315	2.66793	5.6642	1.95648	**1.58927**	0.12554
TAG 52:7	1	0.16059	0.83694	0.09263	0.9354	0.06486	1.00948	0.10254	6.44525	0.82287	**1.87127**	0.23205	**1.57986**	0.1624	4.68432	0.47651	2.066	0.15994	**0.45797**	0.19324	**0.55542**	0.16471	**1.31815**	0.11832	1.081	0.11517	2.57411	0.58021	1.69301	0.59753	**0.47344**	0.02833
TAG 52:9	0.83333	0.242	1.29786	0.64443	1.70632	0.81084	2.96434	1.90288	21.8946	2.84855	**4.05517**	0.62988	**3.42283**	0.44444	**11.4604**	1.11781	7.43477	0.71015	9.04165	2.63453	8.01093	0.48181	6.35442	0.45353	4.57492	0.37184	**45.0002**	8.94319	**29.9937**	8.10974	**2.63215**	0.20227
TAG 54:0	1	0.1431	0.89859	0.04959	0.93901	0.05876	0.95647	0.07165	0.9729	0.07782	0.99834	0.11018	1.09677	0.08008	1.0215	0.08525	1.29646	0.05112	1.54572	0.17259	1.57045	0.1488	1.25302	0.10147	1.05944	0.05201	**1.65004**	0.14015	**1.81731**	0.17419	1.22054	0.1108
TAG 54:1	0.83333	0.26697	0.67424	0.13469	1.59507	1.09175	0.55403	0.07067	4.61132	4.32523	0.73005	0.09594	2.66467	1.37349	1.33094	0.84655	0.76118	0.29078	2.13674	1.17051	0.95021	0.25946	0.88515	0.10674	1.21188	0.29117	**2.35279**	0.31052	25.0199	22.4596	1.53954	0.64558
TAG 54:2	1	0.12286	0.90532	0.04312	1.04362	0.08746	1.04204	0.06849	1.17566	0.23423	1.13498	0.12178	1.29704	0.09566	1.03225	0.07114	1.28064	0.08468	**1.62748**	0.12507	**1.68192**	0.09698	1.3899	0.12891	1.41594	0.15227	**2.50136**	0.35466	**2.47027**	0.25818	1.5628	0.17791
TAG 54:3	1	0.12978	0.892	0.04801	0.96025	0.05846	0.98361	0.08131	1.02281	0.08601	0.9856	0.11181	1.18034	0.091	0.99617	0.08606	1.28165	0.05236	**1.54996**	0.11412	**1.64597**	0.08104	1.23601	0.10972	1.11633	0.04726	**1.87282**	0.17016	**1.87377**	0.11643	1.26072	0.0755
TAG 54:4	1	0.11476	0.89712	0.05925	1.00315	0.06081	0.97499	0.07433	1.00719	0.1116	0.95381	0.1035	1.1889	0.13024	0.94833	0.0767	1.11473	0.05107	**1.37168**	0.1166	**1.39599**	0.12198	1.17631	0.07997	1.10773	0.07296	**1.94119**	0.23167	**1.77943**	0.1657	1.15618	0.0791
TAG 54:5	1	0.08559	0.94001	0.06357	1.04371	0.06902	0.98851	0.06856	1.03303	0.08744	**0.78262**	0.02406	1.08042	0.13128	0.95922	0.08844	1.03659	0.05574	1.09715	0.12355	**1.11442**	0.08189	1.02101	0.06455	0.90284	0.05019	**1.93933**	0.24021	**1.5791**	0.09955	0.89771	0.05679
TAG 54:6	1	0.08677	0.95201	0.09863	1.15309	0.0895	1.07788	0.0947	1.12885	0.08803	**0.69117**	0.05589	**0.80378**	0.09277	0.91417	0.0809	0.89372	0.0529	0.79836	0.13836	0.78034	0.05579	0.80141	0.05739	0.67004	0.04111	**1.91383**	0.28209	**1.52109**	0.11175	0.57932	0.033
TAG 54:7	1	0.11311	1.09617	0.13254	**1.34541**	0.0727	1.20484	0.0824	3.16002	0.29521	**1.0646**	0.10596	**1.01475**	0.0702	**2.22215**	0.20822	1.73893	0.15263	**0.56341**	0.17546	**0.57889**	0.08862	**1.3053**	0.1293	0.9935	0.0732	**2.70381**	0.55703	**1.777**	0.20988	**0.51347**	0.02859
TAG 54:8	1	0.12499	0.99596	0.1102	**1.33188**	0.02929	1.17881	0.08952	5.29715	0.66528	**1.58724**	0.17653	**1.55976**	0.12025	**3.58675**	0.3221	3.39573	0.24297	**0.62602**	0.16253	**0.82979**	0.19671	**2.51464**	0.22684	2.00294	0.13093	**3.52601**	0.84237	2.17117	0.52968	**0.91661**	0.04397
TAG 54:9	1	0.17378	0.71749	0.06172	0.91221	0.06511	0.93231	0.08476	6.82051	0.97564	**1.7224**	0.23852	**1.72339**	0.14115	**4.38699**	0.38457	5.93631	0.35954	**0.83688**	0.18024	**1.4259**	0.4153	**4.51852**	0.32132	3.50383	0.23455	4.67824	1.30555	2.91747	1.13743	**1.75889**	0.11119
TAG 56:1	1	0.15141	0.87157	0.06079	0.88919	0.03593	0.89571	0.08391	0.9247	0.06395	1.02657	0.11918	1.06691	0.07374	0.95841	0.10323	1.2169	0.04809	**1.49416**	0.1071	**1.48315**	0.11793	1.23753	0.09957	1.04653	0.09831	**1.51397**	0.1037	**1.7857**	0.16733	1.10177	0.08579
TAG 56:2	1	0.12497	0.92885	0.04758	1.00349	0.06177	1.00683	0.09719	1.10801	0.17797	1.00804	0.09022	1.17369	0.0827	0.99131	0.09863	1.24981	0.05401	1.50969	0.12934	1.48674	0.12849	1.28153	0.09743	1.0557	0.03788	**1.94051**	0.20737	**1.9411**	0.16976	1.26841	0.07252
TAG 56:3	1	0.09282	0.81844	0.03024	0.88541	0.05993	0.94036	0.09522	1.12848	0.13148	0.88159	0.09061	1.03767	0.08845	0.9933	0.0876	1.1151	0.04914	1.21393	0.08357	1.22848	0.10377	1.0703	0.09336	1.01381	0.05481	**1.58476**	0.16226	**1.55979**	0.10945	1.01357	0.02828
TAG 56:4	1	0.10821	0.84291	0.06564	0.87824	0.04122	0.94874	0.06123	1.14509	0.20208	**0.78408**	0.05722	0.91226	0.10355	0.88174	0.0627	0.94436	0.0918	0.92397	0.07023	0.94793	0.07825	0.91467	0.05876	0.77478	0.05354	**1.32589**	0.14768	**1.1933**	0.05434	0.87294	0.05748
TAG 56:5	1	0.08081	**0.67718**	0.06267	**0.76593**	0.02638	0.82805	0.03097	2.95672	0.27713	**1.18043**	0.12675	**0.95754**	0.11148	**1.99849**	0.16623	1.03639	0.14405	0.17062	0.0349	**0.24171**	0.0929	**0.64953**	0.08592	0.62306	0.07602	0.97631	0.24644	0.91015	0.31675	0.65848	0.21362
TAG 56:6 (1)	1	0.1404	**0.61665**	0.08161	**0.70538**	0.03767	0.75392	0.06748	4.47625	0.45965	**0.86338**	0.10395	**0.62601**	0.07421	**2.23224**	0.15235	1.19565	0.15072	nd	nd	nd	nd	**0.58985**	0.1024	0.536	0.05829	**0.115**	0.0374	0.08551	0.04403	**0.13666**	0.0342
TAG 56:6 (2)	1	0.10655	**0.70077**	0.08138	0.84959	0.07335	0.89594	0.09872	0.36229	0.05447	nd	nd	nd	nd	**0.1551**	0.05539	1.94354	0.22388	**0.66611**	0.11021	0.90849	0.11922	**3.77454**	0.52044	3.17818	0.48288	2.90387	0.70131	2.10065	1.19792	4.19838	0.97198
TAG 58:0	1	0.1414	0.86523	0.04217	0.92926	0.04877	0.95138	0.07466	0.95861	0.08761	0.99358	0.12755	1.12126	0.07338	1.00692	0.10138	1.24392	0.03662	**1.54575**	0.11759	**1.57707**	0.09404	1.21356	0.09272	1.00891	0.07065	**1.63813**	0.14795	**1.74251**	0.14623	1.15608	0.06569
TAG 58:1	1	0.12025	0.89162	0.05334	0.8976	0.05996	0.91989	0.05332	0.93454	0.06994	1.00938	0.09187	1.11153	0.08246	1.01377	0.09614	1.2673	0.02805	**1.54832**	0.1047	**1.56664**	0.12163	1.2851	0.11779	1.00531	0.06212	**1.57053**	0.09926	**1.60304**	0.1972	1.18096	0.09922
TAG 58:3	1	0.15264	0.86672	0.05995	0.93386	0.03641	0.952	0.07311	1.07681	0.08563	0.99872	0.133	1.15399	0.10735	1.02855	0.08999	1.26646	0.05578	1.48357	0.13285	1.43885	0.10534	1.27678	0.11613	1.0492	0.0726	**1.85021**	0.17897	**1.84819**	0.18372	1.19069	0.09486
TAG 58:4	1	0.12952	0.78818	0.04949	0.83254	0.04049	0.9141	0.06345	0.98216	0.07236	0.87085	0.089	0.99005	0.07274	0.95225	0.08954	1.17713	0.04916	1.33647	0.11579	1.31348	0.10376	1.10028	0.07418	0.91596	0.06094	**1.50425**	0.16543	**1.51812**	0.11338	0.97779	0.06361
TAG 58:5	1	0.11831	0.79858	0.03468	0.82818	0.03813	0.88434	0.05764	1.77047	0.14878	0.97148	0.09114	0.92746	0.0701	1.43183	0.12655	1.12078	0.081	1.23061	0.11468	1.28094	0.10861	1.10262	0.07188	0.89623	0.04193	**1.37519**	0.14586	**1.32824**	0.11922	0.94788	0.06677
TAG 60:3	1	0.15723	0.89158	0.06251	0.92216	0.05686	0.89436	0.06992	0.97962	0.06835	**1.00271**	0.13512	**1.06006**	0.06761	0.99924	0.09632	1.23639	0.0484	**1.58475**	0.11	**1.58211**	0.07569	1.22715	0.08982	1.05622	0.05757	**1.54137**	0.12724	**1.72932**	0.17253	1.20423	0.09555
TAG 60:7	1	0.09113	**0.29974**	0.03352	**0.35095**	0.02637	**0.55223**	0.0709	3.23806	0.5718	1.05849	0.11845	1.04472	0.0909	2.23915	0.2394	1.46266	0.16007	nd	nd	nd	nd	**0.82472**	0.08556	0.80636	0.09971	**0.36365**	0.13603	**0.27376**	0.08912	**0.28383**	0.02665

Supplemental Table S4: Variables of the first three Principal Component (PC) of atg mutants and wild type (WT) genotypes after 0 and 6 days of dark treatment

PC 1		PC2		PC3	
MGDG 34:4	-0.18128	TAG 54:9	-0.20776	TAG 56:4	-0.19577
MGDG 34:3	-0.15998	MGDG 32:3(1)	-0.19164	TAG 54:6	-0.184
PC 38:4 (1)	-0.1589	TAG 52:6	-0.16809	TAG 52:4	-0.18187
MGDG 34:1	-0.15535	TAG 54:8	-0.15611	TAG 54:5	-0.17651
DGDG 34:4 2	-0.15172	TAG 52:5	-0.14742	MGDG 32:3 (2)	-0.17009
MGDG 34:2	-0.14786	MGDG 32:3(2)	-0.146	TAG 54:7	-0.16902
DGDG 34:2	-0.14571	TAG 52:7	-0.14509	TAG 56:5	-0.16581
MGDG 34:5	-0.13872	TAG 50:3(1)	-0.12716	TAG 52:7	-0.15016
MGDG 36:5	-0.13142	PC 34:5	-0.10637	TAG 58:5	-0.14444
PC 38:4 2	-0.13077	TAG 54:7	-0.09713	MGDG 36:4	-0.14177
DGDG 34:5	-0.13073	TAG 56:6(2)	-0.09693	TAG 54:8	-0.14136
MGDG 36:3	-0.13005	PC 34:6	-0.09314	MGDG 36:5	-0.14018
PC 38:3 1	-0.12904	TAG 56:5	-0.09101	TAG 54:9	-0.13951
DGDG 36:5	-0.12727	DGDG 32:3	-0.08929	TAG 56:3	-0.13647
PC 36:2	-0.1261	MGDG 36:4	-0.07157	MGDG 36:6	-0.1319
PC 36:3 1	-0.12473	TAG 52:4	-0.06981	TAG 60:3	-0.1268
DGDG 34:0	-0.12465	PC 32:0	-0.06588	MGDG 34:6	-0.12553
PE 36:3 1	-0.11976	DGDG 34:4(1)	-0.0478	DGDG 36:6	-0.12531
DGDG 38:5	-0.11622	MGDG 38:4	-0.0436	TAG 58:4	-0.12478
DGDG 34:4 1	-0.11606	PC 38:3 (2)	-0.04167	MGDG 38:4	-0.12397
MGDG 36:6	-0.11447	MGDG 32:6	-0.0324	TAG 58:0	-0.11953
DGDG 34:3	-0.11372	PC 38:6	-0.03134	TAG 48:3	-0.11416
PC 36:4	-0.11246	MGDG 36:6	-0.03056	TAG 52:6	-0.11314
DGDG 38:6	-0.11037	PC 32:3 (2)	-0.02866	DGDG 36:4	-0.11122
PC 38:5	-0.10614	DGDG 36:6	-0.02312	DGDG 36:5	-0.10928
DGDG 36:3	-0.10549	MGDG 34:6	-0.01862	TAG 52.5	-0.10854
DGDG 36:4	-0.10409	PC 32:3 (1)	-0.01857	TAG 44:0	-0.10795
PC 34:1	-0.10315	DGDG 38:6	-0.01696	MGDG 34:3	-0.10613
PC 34:4 1	-0.10232	DGDG 36:4	-0.01383	TAG 48:2	-0.10585
DGDG 32:0	-0.10207	MGDG 36:5	-0.01009	TAG 58:3	-0.10453
MGDG 38:4	-0.09774	MGDG 38:6	-0.00836	TAG 54:4	-0.10345
PE 36:2	-0.09711	TAG 50:2 (1)	-0.0044	TAG 56:1	-0.1031
DGDG 36:6	-0.09385	TAG 52:9	0.000235	TAG 44:1	-0.10173
PC 36:1	-0.09313	PE 36:3 (2)	0.003421	MGDG 36:3	-0.09982
PC 32:1 2	-0.09012	DGDG 36:5	0.011349	TAG 54:0	-0.09493
MGDG 38:6	-0.08955	MGDG 36:3	0.011967	DGDG 34:3	-0.09304
MGDG 34:6	-0.0771	DGDG 38:5	0.013327	DGDG 34:4(1)	-0.09251
PE 38:2	-0.07262	DGDG 34:3	0.015721	TAG 54:3	-0.09249
MGDG 32:6	-0.07233	PC 32:2 (2)	0.017578	DGDG 38:6	-0.09012
MGDG 36:4	-0.05677	PC 36:6	0.026841	TAG 50:3(1)	-0.0897
DAG 36:5	-0.05492	DGDG 34:5	0.03107	MGDG 38:6	-0.08788
DGDG 32:3	-0.0518	DGDG 36:3	0.032028	TAG 42:0	-0.08533
TAG 56:5	-0.05049	PC 34:4 (1)	0.033785	TAG 56:2	-0.08479
TAG 54:6	-0.05004	MGDG 34:3	0.039807	DAG 34:3	-0.08466
PE 36:4	-0.04708	PC 38:5	0.040199	DGDG 38:5	-0.0843
PC 36:3 2	-0.04368	PC 34:4 (2)	0.041859	DGDG 32:3	-0.08231
PE 34:2	-0.03563	PE 34:1	0.042642	DGDG 32:0	-0.08143
DAG 34:3	-0.03424	TAG 54:1	0.046735	TAG 46:2	-0.08127
MGDG 32:3 2	-0.02881	DAG 34:3	0.047641	TAG 58:1	-0.08001
PC 36:5	-0.02405	PC 36:3 (2)	0.053812	TAG 46:0	-0.07746
TAG 54:7	-0.02068	PC 32:2 (1)	0.05751	TAG 54:2	-0.07658
PE 34:1	-0.00229	DGDG 32:0	0.061166	TAG 52:3	-0.07568
TAG 52:7	0.005835	PE 36:2	0.061311	DGDG 34:5	-0.07512
TAG 54:1	0.011787	MGDG 34:5	0.062306	TAG 48:1	-0.07394
PC 38:6	0.014131	PE 34:2	0.06291	TAG 46:1	-0.07364
PE 36:5	0.015818	TAG 42:0	0.063555	DGDG 36:3	-0.07184

TAG 56:4	0.019379	PC 38:4 (1)	0.064336	MGDG 32:6	-0.06979
PE 36:3 2	0.022045	TAG 58:1	0.064974	MGDG 32:3(1)	-0.06807
PC 38:3 2	0.023602	TAG 56:1	0.067361	TAG 50:3(2)	-0.06574
DAG 34:6	0.028602	DAG 36:6	0.069397	MGDG 34:2	-0.06551
TAG 54:8	0.030643	TAG 50:3 (2)	0.073373	TAG 48:0	-0.06535
TAG 56:6 2	0.03313	TAG 48:1	0.074763	TAG 50:1	-0.06305
PC 32:2 1	0.033329	DAG 36:5	0.077244	MGDG 34:1	-0.05899
PC 32:1 1	0.036131	DGDG 34:4(2)	0.077627	PC 38:6	-0.05869
MGDG 32:3 1	0.041951	TAG 60:3	0.078916	TAG 50:0	-0.05646
TAG 54:5	0.043233	PC 34:3	0.079692	MGDG 34:4	-0.05374
TAG 50:3 1	0.044646	TAG 58:0	0.079822	TAG 56:6(2)	-0.05302
TAG 50:3 2	0.045954	PC 38:3 (3)	0.080279	MGDG 34:5	-0.05157
PC 32:2 2	0.047587	PE 38:3	0.08074	TAG 52:0	-0.04931
DGDG 34:6	0.051625	MGDG 34:2	0.080788	TAG 50:2(2)	-0.04843
TAG 52:5	0.053032	TAG 52:3	0.083795	TAG 52:2	-0.04687
TAG 42:0	0.055256	PC 36:2	0.084386	PC 34:5	-0.03956
TAG 58:0	0.055456	TAG 54:3	0.085512	PC 38:5	-0.03806
TAG 60:3	0.058576	DGDG 34:2	0.085662	DAG 36:5	-0.03725
TAG 50:2 1	0.061646	TAG 54:2	0.086544	DGDG 34:2	-0.03677
TAG 48:1	0.063352	PC 32:1 (1)	0.088481	PC 38:4(1)	-0.03368
TAG 54:3	0.065008	TAG 46:1	0.088506	DAG 34:6	-0.02537
TAG 54:9	0.065144	PC 38:3 (1)	0.090381	TAG 52:1	-0.02533
TAG 56:1	0.065169	PC 38:4 (2)	0.092159	PC 34:6	-0.02459
DAG 36:6	0.065243	TAG 54:6	0.092175	PC 38:3(2)	-0.02224
TAG 54:2	0.065457	TAG 56:4	0.092793	DGDG 34:0	-0.02124
TAG 52:6	0.065645	TAG 52:0	0.093157	PC 34:4(1)	-0.02109
TAG 58:1	0.066838	TAG 58:3	0.095032	DGDG 34:4(2)	-0.01909
TAG 52:1	0.067604	MGDG 34:1	0.095865	TAG 50:2(1)	-0.0177
PC 34:5	0.07377	TAG 50:0	0.099209	DAG 36:6	-0.01724
TAG 52:9	0.076157	MGDG 34:4	0.10037	PC 38:3(1)	-0.01208
TAG 52:0	0.080517	PC 36:3 1()	0.10093	PC 36:3(2)	-0.00059
TAG 48:3	0.084706	TAG 48:2	0.10326	PC 36:1	0.000828
TAG 54:4	0.085174	TAG 58:4	0.1033	TAG 52:9	0.00151
PC 34:6	0.085632	DGDG 34:0	0.10511	PC 36:2	0.004513
PC 38:3 3	0.085948	PE 36:3 (1)	0.10716	PC 32:2(2)	0.009343
TAG 52:4	0.086885	PC 36:1	0.10812	PC 36:3(1)	0.009479
TAG 56:3	0.088818	TAG 44:0	0.10813	TAG 54:1	0.010301
TAG 50:1	0.090451	TAG 52:1	0.10873	PC 38:4(2)	0.012665
TAG 50:2 2	0.090716	TAG 54:0	0.10952	PC 36:4	0.012915
PE 38:3	0.091356	TAG 56:3	0.11088	PC 32:3(2)	0.015315
TAG 52:3	0.091997	TAG 44:1	0.11135	PC 36:6	0.023017
TAG 56:2	0.093022	TAG 48:0	0.11276	PC 34:1	0.032532
TAG 48:2	0.093764	TAG 58:5	0.11287	PC 32:0	0.033226
PC 34:3	0.095682	PC 34:1	0.11316	PC 36:5	0.034821
TAG 58:3	0.098103	PE 36:4	0.1136	PC 34:4(2)	0.035198
TAG 54:0	0.098889	TAG 46:0	0.11369	PC 34:3	0.03897
TAG 44:0	0.099232	TAG 56:2	0.11596	PC 32:3(1)	0.044913
TAG 46:0	0.10032	TAG 48:3	0.11631	PC 32:1(2)	0.050999
TAG 50:0	0.10141	TAG 50:2 (2)	0.11746	PE 38:2	0.058751
TAG 58:4	0.1019	TAG 52:2	0.11819	PC 32:2(1)	0.05957
TAG 58:5	0.10266	TAG 46:2	0.12076	PC 32:1(1)	0.067381
PC 34:4 2	0.10446	DAG 34:6	0.12313	DGDG 34:6	0.070985
TAG 46:2	0.10861	PC 36:4	0.12573	PE 38:3	0.074545
TAG 48:0	0.11153	PE 36:5	0.12575	PE 36:3 (1)	0.082484
TAG 52:2	0.11159	TAG 50:1	0.12788	PC 38:3(3)	0.083653
PC 36:6	0.11291	DGDG 34:6	0.13092	PE 36:2	0.085899
TAG 46:1	0.11552	PC 32:1 (2)	0.13142	PE 36:3(2)	0.12448
TAG 44:1	0.11686	TAG 54:4	0.13754	PE 34:2	0.14052
PC 32:3 1	0.12475	TAG 54:5	0.14102	PE 34:1	0.14758
PC 32:0	0.13208	PE 38:2	0.15074	PE 36:5	0.15755
PC 32:3 2	0.1498	PC 36:5	0.18557	PE 36:4	0.15833

Chapter 3:

The interplay between autophagy and chloroplast vesiculation pathways under dark-induced senescence

Title:

The interplay between autophagy and chloroplast vesiculation pathways under dark induced senescence

Authors:

Jessica A. S. Barros[a], João Henrique F. Cavalcanti[b], Karla G. Pimentel[a], Sahar Magen[c], David B. Medeiros[d], Adriano Nunes-Nesi[a], Alisdair R. Fernie[d], Tamar Avin-Wittenberg[c] and Wagner L. Araújo[a]*

Affiliation:

[a] Departamento de Biologia Vegetal, Universidade Federal de Viçosa, 36570-900 Viçosa, Minas Gerais, Brazil

[b] Instituto de Educação, Agricultura e Ambiente, Universidade Federal do Amazonas, 69800-000, Humaitá, Amazonas, Brazil

[c] Department of Plant and Environmental Sciences, The Alexander Silberman Institute of Life Sciences, Hebrew University of Jerusalem, Givat Ram, Jerusalem 9190401 Israel

[d] Max Planck Institute of Molecular Plant Physiology, Am Mühlenberg 1, D-14476 Potsdam-Golm, Germany

ABSTRACT

In cellular circumstances which carbohydrates are scarce, plants can use alternative substrates for cell energetic maintenance. In plants, the main protein reserve is present in chloroplast, which contains the most part of total leaf proteins and represent a rich source of nitrogen and amino acids. Autophagy plays a key role on chloroplasts dismantling, the well-recognized symptom of both natural and stress-induced plant senescence. Remarkably, an autophagic-independent route of chloroplast degradation associated with the Chloroplast Vesiculation (CV) pathway was recently demonstrated. During extended darkness, CV is highly induced in the absence of autophagy, contributing with the early senescence phenotype of *atg* mutants. To further investigate the role of CV under dark-induced senescence conditions, mutants with low expression of CV (*amircv*) and double mutants *amircv1xatg5* were characterized. Following darkness treatment, no aberrant phenotypic were observed in *amircv* single mutants; however, double mutants showed early senescence and enhanced dismantling of chloroplast and membrane structures under these conditions. The metabolic characterization revealed that the functional lack of both CV and autophagy leads to higher impairment of amino acid release during starvation conditions. The data obtained are discussed in the context of the role of CV and autophagy both with respect to metabolism and to the regulation of chloroplasts dismantling.

Keywords: Autophagy, Carbon starvation, Chloroplast degradation, Senescence.

INTRODUCTION

Under environmental and developmental conditions that leads to carbohydrate limitation, plants require alternative substrates to sustain metabolic reactions (Araujo et al., 2011). Such energetic demands may require both the disassembly of organelles components and the redirection of alternative substrates for respiration. In plants, the major protein reserve is in the chloroplast, as approximately 80% of the total leaf nitrogen corresponds to photosynthetic proteins in C3 plants (Ishida et al., 2008). In fact, the degradation of chloroplasts is a hallmark of both natural and stress induced plant senescence, and their catabolic products are used for energy production during carbon starvation conditions (Wada et al., 2009; Izumi et al., 2013, 2017, 2018). Accordingly, autophagy plays a key role in this process by targeting chloroplast proteins for degradation (Ishida et al., 2008; Xie et al.,2015; Izumi et al.,2017, 2018; Hirota et al., 2018).

Overall, autophagy is a well characterized pathway by which cytosolic components are engulfed and delivered by a specialized double-membrane structure (autophagosome) to the vacuole for recycling (Marshall and Viersta 2018; Avin-Wittenberg et al., 2018). Interestingly, several types of autophagy-mediated chloroplast degradation pathways are differentially activated under distinct conditions (Izumi et al., 2018). The encapsulation of entire chloroplasts into ATG8-decorated autophagic vesicles and their subsequent delivery to the vacuole is termed chlorophagy. This process is dependent on ATG8 lipidation, and it is induced upon UV-B or high light treatments (Izumi et al., 2017; 2018). The Rubisco containing bodies (RCBs) is one specific type of autophagy that provide piecemeal transport of stromal proteins, and it is activated under carbohydrate starvation (Ishida et al. 2008; Izumi et al., 2018; Hirota et al., 2018). By contrast, ATI (ATG8-Interacting 1) bodies, a type of autophagy relying on a specific ATG8-binding protein, are initiated inside the chloroplast, and were associated with thylakoid, envelope, and stroma proteins (Michaeli et al., 2014; 2016). The appearance of plastid-associated ATI bodies has been observed in both senescence leaves and energy-starved seedlings (Michaeli et al., 2014; 2016).

Recent studies have also highlighted the relevance of chloroplast degradation mechanisms that are autophagy-independent, namely the Senescence Associated Vacuoles (SAVs) and Chloroplast Vesiculation (CV) pathways. SAVs are small proteolytic vacuolar compartments that degrade a subset of chloroplast components and are accumulated in senescing leaves (Otegui et al., 2005; Martínez et al., 2008; Gomez et al., 2019). SAVs have been characterized both to contain stromal proteins and for exhibit strong cysteine protease activity evidenced by the presence of Senescence-associated protease, *SAG12* (Otegui et al.,

2005). In addition, CV was unequivocally demonstrated as a chloroplast degradation pathway independent of either SAVs or autophagy (Wang and Blumwald, 2014). CV was first demonstrated to be strongly upregulated under abiotic stress and downregulated by cytokinin in rice (Peleg et al., 2011). Afterwards, by using Arabidopsis mutants where CV was downregulated, CV-containing vesicles (CCVs) were characterized for mobilizing thylakoid and stromal proteins to the vacuole for degradation (Wang and Blumwald, 2014). Furthermore, the disruption of CV has been associated with an increased chloroplast stability, delaying induced-senescence, and enhancing tolerance to abiotic stress whereas its overexpression caused premature leaf senescence (Wang and Blumwald, 2014; Sade et al., 2017). The role of CV in mediating peroxisomal turnover, contributing to the regulation of photorespiration, and N assimilation in rice plants under elevated CO_2 was also recently reported (Umnajkitikorn et al., 2020).

Although our knowledge of chloroplast degradation pathways has increased during the last decade, the relationships and differential regulation among these diverse pathways remains to be elucidated. Autophagy plays a key role in chloroplast degradation events, yet *atg* mutants have been shown to undergo early leaf senescence and accelerated degradation of chloroplast components upon diverse stress conditions (Thompson et al., 2005; Lee et al., 2013; Izumi et al., 2013; Barros et al., 2017; Hirota et al., 2018). These observations argue against the role of autophagy in the dismantling of chloroplasts during senescence and highlight a possible connection between these different chloroplast degradation processes in response to stresses. In this context, we previously observed that *CV* gene is highly induced in the absence of autophagy, contributing to the early-senescence phenotype observed in *atg5* and *atg7* mutants (Barros et al., 2017). Nevertheless, it remains unclear to which extent these pathways interact to control chloroplast stress response.

Here, we investigated the significance of CV pathway during carbon starvation response. To this end, two previously described mutants lines with low expression of CV pathway (*amircv-1* and *amircv-2*) were characterized under dark-induced senescence conditions. Our results demonstrate that the solely impairment of CV has minor effects in plant responses to extended darkness. We further assessed the relationship between CV and autophagy by analyzing double-mutant plants with impairments in both pathways. Although the double mutants showed a hypersensitive phenotype, similarly to the observed in *atg5* mutant under late stages of darkness, both CV and autophagy are likely required for the chloroplast remodeling during these conditions. Our results further support the notion that autophagy is the preferably mechanism of chloroplast turnover under carbon limiting

conditions, while CV likely operates as a compensatory mechanism when autophagy is disrupted.

RESULTS

Phenotypes of *amircv* mutant lines

To examine the metabolic consequences of CV impairment, we used two previously described RNAi mutants lines, namely *amircv-1* and *amircv-2* (Wang and Blumwald 2014). The low expression of *CV* gene was initially confirmed by RT-qPCR (Supplemental Figure S1). We next investigated the physiological consequences of CV impairment under optimal conditions. Thus, photosynthetic parameters were determined in mature plants of *amircv* mutants and WT grown under short-day conditions. No differences were observed in net assimilation rate (Figure 1A), stomatal conductance (Figure 1B), and internal CO_2 concentration (Figure 1C) of *amircv-1* and *amircv-2* lines compared to WT. In fact, CV pathway has been characterized to play significant role in chloroplast degradation mainly under abiotic stress situations (Wang and Blumwald 2014; Sade et al., 2017). Accordingly, rice mutants plants RNAi*OsCV* exhibited higher photosynthesis rates only when submitted to water stress, while similar photosynthetic rates were observed under optimal conditions (Sade et al., 2017).

Given that the induction of *CV* gene during energy depletion conditions has been previously demonstrated (Barros et al 2017), we next transferred 4-week-old plants to extended darkness, a system previously used to prove the metabolic importance of autophagy and alternative pathways of respiration in plants (Ishizaki et al., 2005; Araújo et al., 2010; Barros et al., 2017; Hirota et al., 2018). After 10d of continuous darkness, both WT and *amircv* plants exhibited only limited signs of leaf senescence (Fig. 2A). To obtain a detailed analysis of leaf senescence parameters, we measured the total chlorophyll content and the maximum variable fluorescence/maximum yield of fluorescence (*F*v/*F*m). Chlorophyll loss coupled with reductions of *F*v/*F*m were observed throughout the period of the experiment (Fig. 2B and C). In agreement with the visual phenotype reported, no significant differences of chlorophyll levels and *F*v/*F*m were verified in *amircv* lines under extended darkness conditions.

Down-regulation of *CV* has minor effects on starvation response

To elucidate the role of CV pathway in plant energetic metabolism, we further conducted a metabolic characterization of *amircv* plants. Thus, the levels of starch, protein,

sugars and organic acids were determined (Fig. 3). As might be expected, sugars (sucrose, fructose and glucose) and starch declined rapidly from 3d of dark treatment in all genotypes (Fig. 3A-D). Both fumarate and malate were initially reduced in both WT and *amircv* lines, fumarate levels were further increased throughout the darkness treatment (Fig. 3E-F). This result is in accordance with the dual pattern of TCA intermediates commonly observed during extended darkness conditions (Ishizaki et al., 2005; Araújo et al., 2010; Barros et al., 2017; Kamranfar et al., 2018). During both developmental and induced senescence, plant cells undergo massive changes in cellular metabolism and activated a progressive hydrolysis of macromolecules (Watanabe et al., 2013; Sade et al., 2018). Besides sugars, catabolism of proteins, lipids, and chlorophyll provides energetic substrates that allows continued operation of mitochondrial respiration (Araújo et al., 2011; Hortensteiner Krautler, 2011; Barros et al., 2020). Accordingly, following the exhaustion of carbohydrate reserves a drop of protein content was observed during extended darkness (Fig. 3G). It is worth mentioning that *amircv* mutants presented a slightly higher reduction of protein content in the early stage of darkness. Protein degradation during stress conditions and senescence leads to a general amino acid accumulation (Araujo et al., 2011; Watanabe et al., 2013). Consistently, the enhanced protein degradation resulted in slight increase of total amino acids in *amircv* mutants after 3d of darkness (Fig. 3H). Despite that, *amircv* lines and WT presented similar metabolic responses throughout the darkness treatment.

Amino acids are the main alternative substrates to provide energy to alternative pathways of respiration under carbon starvation (Ishizaki et al., 2005,2006; Araújo et al.,2010,2011). More specifically, branched chain amino acids (BCAA) and lysine have been extensively reported to participate in energy generation by the alternative pathway mediated by the ETF-ETFQO system (Araújo et al., 2010,2011). We previously demonstrated that both CV and alternative respiratory pathways are activated in autophagy mutants submitted to extended darkness (Barros et al., 2017). Thus, to investigate the interplay between these processes, the expression of selected genes related to alternative respiration, BCAA and lysine degradation was investigated in *amircv* mutants (Fig. 4). This analysis revealed that the *ETFQO* gene is clearly induced during the darkness treatment (Fig. 4A). In a similar vein, the transcript levels of *IVDH*, the key enzyme of BCAA degradation, was also up regulated under these conditions (Fig. 4B). The induction of *ETQO* and BCAA catabolism related genes during low energy and senescence conditions have been extensively reported (Izumi et al., 2013, Chrobok et al., 2016; Barros et al., 2017; Hirota et al., 2018). Nevertheless, similar induction of *ETQO* and *IVDH* transcripts was observed in WT and

amircv plants. Furthermore, we analyze the Lys-ketoglutarate reductase/saccharopine dehydrogenase (*LKR/SDH*) gene, that encodes a key enzyme of lysine catabolism. It was observed a strong induction of *LKR/SDH* during darkness in all genotypes, with a trend of minor induction of *LKR/SDH* in *amircv* mutants after 10d of darkness (Fig. 4C). The enzyme LKR/SDH controls most of the lysine homeostasis, presenting a complex regulation both at transcriptional and post-translational level (Arruda and Barreto, 2020). It was recently reported that both *CV* and *LKR/SDH* are activated during ageing and abiotic stress by a common regulator, the RD26 transcript factor (Kamranfar et al., 2018). Additional studies are clearly required to understand the possible connection between CV and lysine metabolism. Collectively, *CV* downregulation plays minor influence on the activation of energetic amino acids catabolism and ETF/ETQO pathways during extended darkness conditions.

Deficiency of CV and Autophagy triggers susceptibility to extended darkness

Taking into account that autophagy has a recognized role on plant energetic homeostasis under carbon starvation conditions (Ishida et al., 2013; Barros et al., 2017; Hirota et al., 2018), we further evaluated the autophagic process in *amircv* plants. For this, we measured the transcript levels of *ATG8h*, that encodes an isoform of ATG8 protein required for the formation of autophagosome membrane. The transcript levels of *ATG8h* gene increased from 3d of darkness in both WT and *amircv* mutants (Fig. 4D), which suggests a general activation of autophagy under these conditions. Although it was previously reported that CV and autophagy pathways are independent, occurring concomitantly in the cell (Wang and Blumwald, 2014), the lack of CV does not trigger any differential autophagy activation under extended darkness. However, *CV* gene is upregulated in plants lacking autophagy during darkness treatment (Barros et al., 2017). Thus, it is tempting to suggest that CV triggers minor effects on energetic metabolism when autophagy is functional.

In order to test the coordination of these two pathways, we next generate double mutants for both CV and autophagy: *amircv1*x*atg5* (Fig. 5A). Double mutant plants and its single mutants backgrounds were grown side-by-side under short-day and further submitted to extended darkness conditions. Interestingly, after 10d of darkness, the double mutants exhibited an early senescence phenotype similar to *atg5* single mutants (Fig. 5B). The sensitivity phenotype was followed by a massive reduction of chlorophyll levels in both *atg5* and *amircv1*x*atg5* mutants (Fig. 5C). Thus, the impairment of CV pathway does not recover

the *atg5* sensitive phenotype, suggesting that other chloroplast catabolic pathways are likely activated in both *atg5* and *amircv1xatg5* plants under darkness.

Effects of autophagy and CV deficiency on metabolic adjustment under extended darkness

To gain more insights on the differential impacts of CV and autophagy deficiency under extended darkness, we further analyzed the metabolic profile of *amircv1xatg5* along with its respective single mutants, *amircv-1* and *atg5*. In good agreement with the phenotype observed, *amircv-1* single mutant presented similar pattern of metabolic changes observed in WT plants, while *atg5* and a*mircv1xatg5* presented more comparable responses (Fig. 6). In general, the majority of the amino acids accumulated during darkness; however, minor accumulation of alanine, glutamate, methionine, pyroglutamate, threonine, tyrosine and valine was observed in *atg5* and *amircvxatg5* after 10d of extended darkness. We also found that TCA intermediates citrate, malate, and 2-oxoglutarate were highly accumulated in *atg5* after 10d of darkness. These results are consistent with previous findings that demonstrated the impairment of amino acids provision coupled with altered respiratory response of *atg* mutants under darkness (Barros et al., 2017; Hirota et al., 2018). Additionally, it was also verified that stress related compounds, such as trehalose and mannitol, accumulated in *atg5* and *amircvxatg5,* and it might contribute for the sensitive phenotype observed in these plants.

Despite the similarities with *atg5* mutant, *amircv1xatg5* also showed specific metabolic signatures. The accumulation of 2-oxoglutarate levels was greatly reduced in *amircv1xatg5* after 10d of darkness, while this organic acid was increased throughout the whole period of darkness in *atg5* plants (Fig. 6). 2-oxoglutarate is a central metabolite of carbon/nitrogen metabolism, participating in both TCA cycle and nitrogen assimilation (Araujo et al., 2014). It has been demonstrated that the accumulation of 2-oxoglutarate in leaves leads to alteration in respiratory and nitrogen metabolism resulting in significant shifts in the amino acids pools in different tissues (Araujo et al., 2008, 2012). Interestingly, after 10d of darkness, *amircv1xatg5* mutants also presents lower levels of amino acids specifically those derived from 2-oxoglutarate (Ornithine and Glutamate), but also asparagine, pyroglutamate, valine and serine (Fig. 6). The coordination between CV and nitrogen assimilation pathways during abiotic stress was previously proposed (Sade et al., 2017). In this way, the CV rice mutant, RNAi*Os*CV, presented generally lower levels of amino acids under water stress conditions (Sade et al., 2017). The authors claim that this response

indicates a delay in nitrogen remobilization in RNAi*Os*CV, plants which affects positively plant response to abiotic stress. On the other hand, the disruption of autophagy impacts the supply of amino acids under carbon depletion (Izumi et al., 2013; Barros et al., 2017; Hirota et al., 2018). Collectively, our results indicate that: (*i*) by contrast to the reported for water stress, the solely impairment of CV has minor effects on plant responses to extended darkness; and (*ii*) the metabolic reprogramming of *atg5* mutants under extended darkness is, at least partially, dependent of CV operation.

CV contributes to abnormal chloroplast structure of *atg5* mutants under extended darkness

Given that both autophagy and CV can mediate chloroplast degradation, we next investigate the effects of simultaneous lack of autophagy and CV on chloroplast structure by using a transmission electron microscopy approach. Before darkness treatment, chloroplasts of all the genotypes appeared undamaged at the ultrastructural level, containing large starch granules, grana, and stroma thylakoids and occasionally occurring small plastoglobules (Fig. 7A-D). After 7d of darkness, WT and single mutant *amircv-1* chloroplasts presented similar structures, containing remodeled thylakoid system and grana stacking (Fig. 7E-F). However, the membrane organization of *amircv1*x*atg5* chloroplast was notably disturbed (Fig. 7H). We previously showed that *ATG5* mutation compromises the chloroplast integrity under darkness (Barros et al., 2021). Interestingly, when comparing *atg5* and *amircv1xatg5* chloroplast differential structural changes between these genotypes were observed (Fig. 7G and H). In addition to the marked supersized plastoglobuli discussed previously, *atg5* chloroplasts lost their normal structure and further exhibited longish and curved shape containing deformed stroma and several vesicles (Fig. 7G). These vesicles structures resemble the senescence associated vacuoles (SAVs), which also mediate the recycle of chloroplast proteins by an autophagy-independent mechanism (Otegui et al., 2005). Additionally, it is clear that *atg5* chloroplast lost the curved thylakoid membrane response observed in WT and *amircv-1* genotypes. Despite the presence of grana stacking in *atg5*, the granum is narrow with more layers (Fig 7I and L). On the other hand, it seems that double mutants partially recovered the curved thylakoid membrane response, yet the presence of grana structure was highly reduced (Fig 7H and M). It is generally accepted that chloroplast stacking is governed by physicochemical forces between membranes and lipid-protein interactions (Armbruster et al., 2013; Johnson and Wientjes, 2019; Mazur et al., 2019). Since CV and autophagy operate in the selective degradation of chloroplast proteins, it is tempting

to suggest that the distinct chloroplast response observed is likely associated to the differential protein degradation in these genotypes.

DISCUSSION

To cope with energetic challenging conditions, plants activated strategic mechanisms of organelles disassembly which generally culminates in a senescence-induced response. During both developmental and stress-induced senescence, chloroplast proteins are massively degraded, and the amino acids released can be either remobilized for other tissues or used as respiratory substrates (Araujo et al., 2011, Watanabe et al., 2013, Hildebrandt et al., 2015; Chrobok et al., 2016). It is well known that chloroplast contains their own proteolytic machinery, comprising several types of proteases which operates in its protein quality control (Buet et al., 2019). This fact aside, recent studies have reported the existence of extraplastidial pathways for chloroplast turnover (Otegui 2017; Izumi and Nakamura, 2018). Three main extraplastidic processes involved in the degradation of chloroplasts were identified: autophagy (Ishida et al., 2008; Wada et al., 2009), SAVs (Otegui et al., 2005; Martínez et al., 2008), and CV (Wang and Blumwald, 2014). It remains unknown, however, how these distinct pathways are regulated and cooperates to ensure the proper chloroplast turnover. We previously suggested that CV might function as a compensatory mechanism contributing to the sensitive phenotype of *atg* mutants under carbon starvation (Barros et al., 2017). Here, we provide additional experimental evidence of the importance of CV and autophagy pathways for both metabolic response and chloroplast remodeling under extended darkness.

We first investigated the effects of solely CV disruption on plant tolerance to extended darkness. Thus, we focused on phenotypic and metabolic characterization of lines with low expression of *CV* gene previously described (Wang and Blumwald, 2014). Accordingly, we verified that WT and *amircv-1* and *amircv-2* plants displayed similar phenotype under extended darkness conditions (Fig. 2). However, the reduced protein content coupled with an elevated total free amino acid levels after 3d of darkness indicates that mechanisms of protein turnover are more rapidly induced in *amircv* mutants (Fig. 3). Furthermore, no metabolic differences were observed between *amircv* mutants and WT plants throughout the darkness treatment (Fig. 3 and 6). Additionally, the accumulation of amino acids was not correlated with a differential activation of alternative pathways of respiration in *amircv* lines (Fig. 4). Collectively, these findings suggest that altered protein

response observed in *amircv* does not trigger major effects on energetic metabolism and, CV has minor importance in plant response to extended darkness conditions.

It was previously demonstrated that silencing CV resulted in chloroplast stability whereas CV overexpression led to chloroplast degradation by destabilization of the photosynthetic apparatus during abiotic stress (Wang and Blumwald, 2014; Sade et al., 2017). By contrast, plants with enhanced autophagy presented better fitness performance and enhanced tolerance to oxidative stress (Minina et al., 2018). Autophagy is a versatile mechanism of chloroplast degradation since it mediates both the turnover of piecemeal stroma components or the degradation of entire chloroplast by the chlorophagy mechanism (Izumi and Nakamura, 2018). Experimental evidence has suggested that the selective degradation of stromal proteins mediated by autophagy, the RCB pathway, is preferentially activated to provide amino acids in energy-starved plants (Hirota et al., 2018; Izumi et al., 2019). Altogether, the results described above coupled with our own results suggest that autophagy is more likely to operate as a pro-survival mechanism by the turnover of stromal components under starvation conditions, while CV leads to a widespread degradation of chloroplast. Additionally, our previous study indicated a higher activation of CV pathway in *atg* mutants submitted to extended darkness (Barros et al., 2017). It is tempting to suggest, therefore, that autophagy operates as a primary chloroplast degradation pathway, while CV is a complementary mechanism which is activated in the absence of autophagy.

In order to unravel how these pathways modulates chloroplast turnover and stress-induced senescence response, we further characterized double mutants for both CV and autophagy pathways. Surprisingly, under extended darkness *amircv1xatg5* plants presented an early senescence response accompanied by reduction of chlorophyll levels, resembling *atg5* single mutant phenotype (Fig. 5). The metabolic analysis also showed that the solely CV mutation has minor effects on metabolic reprogramming, whereas the disruption of both autophagy and CV is more related to the effects of ATG mutation (Fig. 6). Nevertheless, the levels of specific amino acids differed between *amircv1xatg5* and *atg5* genotypes. The double mutants plants showed more reduced levels of asparagine, glutamate, pyroglutamate, ornithine and valine after 10d of darkness compared to *atg5* mutants. Glutamine, glutamate, asparagine, aspartate and their conversion products have been long documented to be key compounds of nitrogen metabolism (Masclaux-Daubresse et al., 2006; Gaufichon et al., 2016). In particular, asparagine plays a primary role in nitrogen recycling, storage and transport during senescence, and it is highly produced during extended darkness (Watanabe et al., 2013; Hildebrandt et al., 2018). The fact that *amircv1xatg5* has reduced levels of both

asparagine and glutamate suggests a possible impairment of N remobilization pathways in *amircv1xatg5* plants. Interestingly, *amircv1xatg5* was also characterized by minor accumulation of 2-oxoglutarate compared to *atg5* after 10d of darkness (Fig. 6). This organic acid can be produced from either sugar respiration or amino acid transamination, and it is a branch-point between carbon and nitrogen metabolism (Araújo et al., 2014). The glutamate dehydrogenase (GDH) enzyme catalyzes the reversible oxidative deamination of glutamate to 2-oxoglutarate, and it is highly induced during senescence (Masclaux-Daubresse et al., 2006). Interestingly, lower expression of Glutamate dehydrogenase (*GDH)*, Glutamine synthetase (*GS1*), and Asparagine synthetase (*AS*) genes was observed in RNAi*Os*CV mutants compared to WT under water stress (Sade et al., 2017). This response was associated with the delay of senescence and amino acids remobilization, ensuring a better performance of RNAi*Os*CV compared to WT. Accordingly, plants overexpressing *CV* were characterized by higher activation of these N remobilization pathways triggering an enhanced susceptibility to environmental stress (Sade et al., 2017). In a context of carbon starvation induced by darkness, the shift in amino acid metabolism by CV disruption is likely capable to compromise plant survival, once amino acids are extensively used as energetic substrates under these conditions. Indeed, the impairment of amino acids release in *atg* mutants leads to energetic failure under extended darkness conditions (Barros et al., 2017). Our findings revealed that amino acid release is more compromised in plants lacking both CV and autophagy pathways. The fact that the disruption of CV only triggers significant metabolic effects in the absence of autophagy further suggests that autophagy has a primary role on chloroplast degradation events, whereas CV is only activated when autophagy is disrupted.

To decipher the importance of autophagy and CV pathways in the chloroplast maintenance, we paid particular attention to the analysis of chloroplast ultrastructure. It was previously reported that *atg5* mutants presented marked changes on chloroplast structure following extended darkness conditions (see Chapter 2). Here, we further demonstrated that the disruption of both CV and autophagy leads to a differential chloroplast ultrastructure phenotype under extended darkness. Accordingly, *atg5* presented deformed chloroplast with a more compromised stromal structure (Fig. 7). Although we observed certain conservation of grana in chloroplast of *atg5*, the thylakoid membrane system is static, and misses the typical reorganization of darkened chloroplast characterized by the curvature of thylakoid membranes observed in WT and *amircv-1*. On the other hand, *amircv1xatg5* chloroplast partially recovered thylakoid membrane organization, despite showing compromised grana stacking (Fig. 7). It was previously observed that *CV* overexpression induced chloroplast

structural changes, characterized by the unstacking and swelling of the thylakoid membranes which impaired chloroplast stability (Wang and Blumwald, 2014). By contrast, under our experimental conditions, the lack of CV triggered a disarranged in thylakoid membranes. It is worth mentioning that CV was previously proposed to mediate the target of PsbO protein altering the structure of the photosystem II, and facilitating the access of the thylakoid-associated proteases, such DEGP1 and FTSH, to chloroplast core proteins (Wang and Blumwald, 2014). The lack of chloroplast repair mediated by proteases results in the accumulation of chloroplast damaged proteins, generating ROS (Kato et al., 2009), which possibly leads to deregulation of chloroplast machinery. Therefore, it is tempting to suggest that the selective turnover of envelope proteins by CV pathway most likely contributes to the chloroplast remodeling in absence of autophagy. It needs to be clarified which mechanisms underlies this response. It should also be highlighted that the lipid composition directly influences the biophysical properties of thylakoid membranes (Mazur et al., 2019). Indeed, recent studies have reported massive changes of galactolipids in plants lacking autophagy (Havé et al., 2019; McLoughlin et al., 2020; Barros et al., 2021, however, the potential roles of CV in chloroplast lipid composition still needs to be addressed.

Collectively, the findings described here refine our understanding of chloroplast degradation events during dark-induced senescence. By contrast to the situation observed when autophagy is disrupted, the impairment of CV has minor impact on plant response to energy deprivation. This highlights the preferential activation of autophagy mediated pathways to ensure chloroplast maintenance and starvation response under extended darkness. Our data further suggest that CV deficiency triggers minor energetic consequences when autophagy is still present and activated. The further characterization of *amircv1xatg5* double mutants revealed a potential role of CV in the metabolic response and chloroplast remodeling of *atg5* mutant during extended darkness. Noteworthy, the early senescence phenotype of *amircv1xatg5* mutants under extended darkness highlights the possible operation of other catabolic pathways. The presence of SAVs in *atg5* chloroplast indicates the relevance of this pathway in chloroplast turnover during these conditions. Dissecting the intertwined mechanisms regulating chloroplast turnover are still required to fully understand the exact relation between autophagy, CV and SAVs on chloroplast maintenance and plant stress tolerance.

METHODS

Plant material and dark treatment

Two *Arabidopsis* RNAi mutant lines for *CV* gene, *amircv-1* and *amircv-2* (Wang and Blumwald, 2014), the T-DNA line *atg5-1* (SAIL_129B079) and its correspondent WT (Columbia 0 ecotype) were used in this study. Seeds were surface-sterilized and imbibed for 4 days at 4°C in the dark and subsequently germinated. Seedlings grown at 22°C under short-day conditions (8 h light/16 h dark), 60% relative humidity with 150 μmol photons m^{-2} s^{-1}. *amircv* mutants were selected by application of Glufosinate-ammonium (120 mg/L) in five-old seedlings. For dark treatments, selected seedlings were grown at 22°C under short-day for 4 weeks. Afterwards, plants were maintained in dark in the same growth cabinet. The rosettes were harvested at intervals of 0, 3, 7 and 10 days after transition to darkness and immediately frozen in liquid nitrogen and stored at -80°C until further analysis.

Measurements of photosynthetic parameters

Gas-exchange measurements were performed with an open-flow infrared gas-exchange analyzer system (Li-Cor 6400XT) with a portable photosynthesis system. Light was supplied from a series of light-emitting diodes located above the cuvette, providing an irradiance of 150 μmol photons m^{-2} s^{-1}, similar to the growth conditions aforementioned. The reference CO_2 concentration was set at 400 mmol CO_2 mol^{-1} air. All measurements were performed at 25°C, and vapor pressure deficit was maintained at 0.2 kPa, while the amount of blue light was set to 10% of photon flux density to optimize stomatal aperture. The determination of the photosynthetic parameters was performed in 4-week-old plants. *F*v/*F*m, which corresponds to the potential quantum yield of the photochemical reactions of PSII and represents a measure of photochemical efficiency, was measured as described previously (Oh et al., 1996).

Biochemical assays

Leaf samples were harvested at the time points indicated, immediately frozen in liquid nitrogen, and stored at -80°C until further analysis. Extraction was performed by rapid grinding of tissue in liquid nitrogen and immediate addition of ethanol as described in Gibon et al. (2004). Photosynthetic pigments were determined as in Porra et al. (1989). The levels of starch were determined exactly as described previously (Fernie et al., 2001). Proteins and amino acids were determined as described previously (Cross et al., 2006).

Metabolite profiling

Metabolite extraction was performed essentially by following an established gas chromatography-mass spectrometry (GC-MS)-based metabolite profiling protocol of Lisec et al. (2006) modified. Approximately 50 mg of homogenized plant materials were aliquoted in tubes and extracted in 100% methanol and internal standard (0.2 mg ribitol mL^{-1} water). 2.0 mL tubes were shaken for 15 min at 70°C and next centrifuged at 14000 rpm for 10 min. The supernatant was transferred to new tubes and, afterwards, 100% chloroform and distilled water were added. Tubes were centrifuged at 4000 rpm for 15 min. Finally, 150 µL of the upper phase of each sample were transferred to new 1.5 mL tubes and let to dry overnight in a vacuum concentrator. Sample derivatization was carried out as previously described (Lisec et al., 2006). A pooled reference sample was made by combining 5 µl aliquots from all samples. Sample injection and subsequent peak annotation were performed as described in Dahtt et al. (2019), using the Fiehn GC/MS Metabolomics RTL Library (G1676AA; Agilent). After blank subtraction, the peak area of each metabolite was normalized to the internal standard (i.e., ribitol) in each sample, as well as fresh weight.

Expression analysis by RT-PCR

Total RNA was isolated using TRIzol reagent (Ambion, Life Technology) according to the manufacturer's recommendations. The total RNA was treated with DNAse I (RQ1 RNase free DNase I, Promega, Madison, WI, USA). The integrity of the RNA was checked on 1% (w/v) agarose gels, and the concentration was measured using a Nanodrop spectrophotometer. Finally, 2 µg of total RNA were reverse transcribed with Superscript II Rnase H2 reverse transcriptase (Invitrogen) and oligo (dT) primer according to the manufacturer's recommendations. Real-time PCR reactions were performed in a 96-well microplate (Applied Biosystems Applera, Darmstadt, Germany), using Power SYBR Green PCR Master Mix. The primers used here were designed using the open-source program QuantPrime-qPCR primer designed tool (Arvidsson et al., 2008) and are described in Table S2. ACTIN (AT2G37620) was used as internal standard. The relative levels of mRNAs were determined using the $2^{-\Delta Ct}$ method (Livak and Schmittgen, 2001). Three biological replicates were processed for each experimental condition.

Transmission Electron Microscopy

Small pieces of leaves were cut and fixed in 3% Glutaraldehyde in 0.1M Cacodylate buffer (pH 7.4) 10 hours at room temperature in a desiccator and then transferred to 40° C for continuation of fixation overnight. Tissues were washed in cacodylate buffer and post fixed and stained with 2% osmium tetroxide, 1.5% potassium ferricyanide in 0.1M

cacodylate buffer for 2 hours. Tissues were then washed in cacodylate buffer and dehydrated through a graded series of ethanol treatments for 10 min each step followed by 100% anhydrous ethanol 3 times, 20 min each, and propylene oxide 2 times, 10 minutes each. The tissues were infiltrated with increasing concentrations of Agar 100 resin in propylene oxide for 16 hours each step. The tissues were embedded in fresh resin in 60°C oven for 48 hours. Ultrathin sections, approximately 80 nm thick, were cut on a Leica Reichert Ultracut S microtome, collected onto 200 Mesh carbon-formvar coated copper grids and stained with Uranyl acetate followed by Reynold's Lead Citrate for 10 min. The sections were examined using Tecnai 12 TEM 100kV (Phillips, Eindhoven, the Netherlands) equipped with MegaView II CCD camera and Analysis® version 3.0 software (SoftImaging System GmbH, Münster, Germany).

Statistical analyses

The experiments were conducted in a completely randomized design with 3-5 replicates of each genotype. Data were statistically examined using analysis of variance and tested for significant ($P < 0.05$) differences using Student's *t* test. All statistical analyses were performed using the algorithm embedded into Microsoft Excel.

ACKNOWLEDGEMENTS

The authors would like to acknowledge Dr. Edward Blumwald (University of California) for sharing the *amircv* seeds used in this work. We also thank Dr. Yael Friedmann from the microscopy core facility at The Hebrew University's Life Science core facility for her technical support with confocal and EM analysis. This work was supported by funding from the National Council for Scientific and Technological Development (CNPq-Brazil, to WLA) and the FAPEMIG (Foundation for Research Assistance of the Minas Gerais State, Brazil, Grant RED-00053-16). Work at the TAW group is supported by the Israeli Science Foundation, grant number 1899/16. Scholarships granted by the National Council for Scientific and Technological Development (CNPq-Brazil) and Council for Higher Education (Malag-Israel) to JASB and research fellowships awarded by CNPq-Brazil to ANN and WLA are also gratefully acknowledged.

Authors contribution

J.A.S.B., T.A-W., and W.L.A. designed the research; J.A.S.B. performed most of the research with the support of J.H.F.C, S.M, D.B.M, and K.G.P; T.A-W. and W.L.A. supervised the project; S.M contributed with transcript analysis; D.B.M and A.R.F.

performed metabolite profile; A.N-N. and A.R.F. contributed with new reagents/analytic tools; D.B.M., A.N-N, and A.R.F. analysed the data, discussed the results, and complemented the writing. J.A.S.B., T.A-W., and W.L.A. analyzed the data and wrote the article, which was later approved by all the others.

REFERENCES

Araújo WL, Nunes-Nesi A, Trenkamp S, Bunik VI, Fernie AR (2008) Inhibition of 2-oxoglutarate dehydrogenase in potato tuber suggests the enzyme is limiting for respiration and confirms its importance in nitrogen assimilation. Plant Physiol. **148**: 1782–1796.

Araújo WL, Ishizaki K, Nunes-Nesi A, Larson TR, Tohge T, Krahnert I, Witt S, Obata T, Schauer N, Graham IA, Leaver CJ, Fernie AR (2010) Identification of the 2-hydroxyglutarate and isovaleryl-CoA dehydrogenases as alternative electron donors linking lysine catabolism to the electron transport chain of Arabidopsis mitochondria. Plant Cell **22:** 1549-1563.

Araújo WL, Tohge T, Ishizaki K, Leaver CJ, Fernie AR (2011) Protein degradation - an alternative respiratory substrate for stressed plants. Trends in Plant Science **16:** 489–498.

Araújo WL, Tohge T, Osorio S, Lohse M, Balbo I, Krahnert I, Sienkiewicz-Porzucek A, Usadel B, Nunes-Nesi A, Fernie AR (2012) Antisense inhibition of the 2-oxoglutarate dehydrogenase complex in tomato demonstrates its importance for plant respiration and during leaf senescence and fruit maturation. Plant Cell **24**: 2328–2351

Araújo WL, Martins AO, Fernie AR, Tohge T (2014) 2-Oxoglutarate: linking TCA cycle function with amino acid, glucosinolate, flavonoid, alkaloid, and gibberellin biosynthesis. Frontiers in Plant Science **5**: 552

Armbruster U, Labs M, Pribil M, Viola S, Xu W, Scharfenberg M, Hertle AP, Rojahn U, Jensen PE, Rappaport F, et al (2013) Arabidopsis CURVATURE THYLAKOID1 proteins modify thylakoid architecture by inducing membrane curvature. Plant Cell **25**: 2661–2678

Arruda P, Barreto P (2020) Lysine catabolism through the saccharopine pathway: enzymes and intermediates involved in plant responses to abiotic and biotic stress. Front. Plant Sci. **11:** 587

Arvidsson S, Kwasniewski M, Riaño-Pachón DM, Mueller-Roeber B (2008) QuantPrime: flexible tool for reliable high-throughput primer design for quantitative PCR. BMC Bioinformatics **9**: 465

Avin-Wittenberg T, Baluska F, Bozhkov PV, Elander PH, Fernie AR, Galili G, Hassan A, Hofius D, Isono E, Le Bars R et al (2018) Autophagy-related approaches for improving nutrient use efficiency and crop yield protection. J Exp Bot **69**: 1335–1353

Barros JAS, Cavalcanti JHF, Medeiros DB, Nunes-Nesi A, Avi-Wittenberg T, Fernie AR, Araújo WL (2017) Autophagy deficiency compromises alternative pathway of respiration following energy deprivation. Plant Physiol **175**: 62–76

Barros JAS, Siqueira JAB, Cavalcanti JHF, Araújo WL, Avin-Wittenberg T (2020) Multifaceted Roles of Plant Autophagy in Lipid and Energy Metabolism. Trends Plant Sci. **25 (11):** 1141-1153

Barros JAS, Magen S, Lapidot-Cohen T, Rosental L, Brotman Y, Araújo WL, Avin-Wittenberg T (2021) Autophagy is required for lipid homeostasis during dark-induced senescence. Plant Physiol, kiaa120, https://doi.org/10.1093/plphys/kiaa120

Buet A; Costa ML; Martínez DE; Guiamet JJ (2019) Chloroplast protein degradation in senescing leaves: Proteases and lytic compartments. Front. Plant Sci. **10**: 747

Chrobok D, Law SR, Brouwer B, Lindén P, Ziolkowska A, Liebsch D, Narsai R, Szal B, Moritz T, Rouhier N, et al (2016) Dissecting the metabolic role of mitochondria during developmental leaf senescence. Plant Physiol **172**: 2132–2153

Cross JM, von Korff M, Altmann T, Bartzetko L, Sulpice R, Gibon Y, Palacios N, Stitt M (2006) Variation of enzyme activities and metabolite levels in 24 Arabidopsis accessions growing in carbon-limited conditions. Plant Physiol **142:** 1574–1588

Dhatt BK, Abshire N, Paul P, Hasanthika K, Sandhu J, Zhang Q, Obata T, Walia H (2019) Metabolic Dynamics of Developing Rice Seeds Under High Night-Time Temperature Stress. Front Plant Sci. **10:** 1443

Fernie AR, Roscher A, Ratcliffe RG, Kruger NJ (2001). Fructose 2,6-bisphosphate activates pyrophosphate: fructose-6-phosphate 1-phosphotransferase and increases triose phosphate to hexose phosphate cycling in heterotrophic cells. Planta **212**: 250-63

Gibon Y, Blaesing OE, Hannemann J, Carillo P, Hohne M, Hendriks JH, Palacios N, Cross J, Selbig J, Stitt MA (2006). Robot-based platform to measure multiple enzyme activities in arabidopsis using a set of cycling assays: comparison of changes of enzyme activities and transcript levels during diurnal cycles and in prolonged darkness. *Plant Cell* **16:** 3304-3325

Gomez FM, Carrion CA, Costa ML, Desel C, Kieselbach T, Funk C, Krupinska K, Guiamet J (2019) Extra-plastidial degradation of chlorophyll and photosystem I in tobacco leaves involving 'senescence-associated vacuoles'. The Plant Journal **99**: 465–477

Havé M, Luo J, Tellier F, Balliau T, Cueff G, Chardon F, Zivy M, Rajjou L, Cacas JL, Masclaux-Daubresse C (2019) Proteomic and lipidomic analyses of the Arabidopsis atg5 autophagy mutant reveal major changes in endoplasmic reticulum and peroxisome metabolisms and in lipid composition. New Phytologist **223**: 1461–1477.

Hildebrandt TM (2018) Synthesis versus degradation: Directions of amino acid metabolism during Arabidopsis abiotic stress response. Plant Molecular Biology **98**: 121–135

Hildebrandt TM, Nunes Nesi A, Araújo WL, Braun HP (2015) Amino acid catabolism in plants. Mol Plant **8**: 1563–1579

Hirota T, Izumi M, Wada S, Makino A, Ishida H (2018) Vacuolar protein degradation via autophagy provides substrates to amino acid catabolic pathways as an adaptive response to sugar starvation in Arabidopsis thaliana. Plant & Cell Physiology 59: 1363–1376

Hörtensteiner S, Kräutler B (2011) Chlorophyll breakdown in higher plants. Biochim Biophys Acta. **1807**: 977-988

Ishida H, Yoshimoto K, Izumi M, Reisen D, Yan Y, Makino A, Ohsumi Y, Hanson MR, Mae T (2008) Mobilization of rubisco and stroma-localized fluorescent proteins of chloroplasts to the vacuole by an ATG gene-dependent autophagic process. Plant Physiol **148:** 142–155

Ishizaki K, Larson TR, Schauer N, Fernie AR, Graham IA, Leaver CJ (2005) The critical role of Arabidopsis electron-transfer flavoprotein: Ubiquinone oxido reductase during dark-induced starvation. The Plant Cell **17:** 2587-2600

Ishizaki K, Schauer N, Larson TR, Graham IA, Fernie AR, Leaver CJ (2006) The mitochondrial electron transfer flavoprotein complex is essential for survival of Arabidopsis in extended darkness. The Plant Journal **47:** 751-760

Izumi M, Hidema J, Makino A, Ishida H (2013) Autophagy contributes to nighttime energy availability for growth in Arabidopsis. Plant Physiology **161**: 1682–1693.

Izumi M, Ishida H, Nakamura S, Hidema J (2017) Entire photodamaged chloroplasts are transported to the central vacuole by Autophagy. Plant Cell **29**: 377–394

Izumi M, Nakamura S (2018) Chloroplast protein turnover: the influence of extraplastidic processes, including autophagy. Int. J. Mol. Sci . **19**: 828

Izumi M, Nakamura S, Li N (2019) Autophagic turnover of chloroplasts: its roles and regulatory mechanisms in response to sugar starvation. Frontiers in Plant Science **10**: 280.

Johnson MP, Wientjes E (2019) The relevance of dynamic thylakoid organisation to photosynthetic regulation. Biochim Biophys Acta doi: 10.1016/j.bbabio.2019.06.011

Kamranfar I, Xue GP, Tohge T, Sedaghatmehr M, Fernie AR, Balazadeh S, Mueller-Roeber, B (2018). Transcription factor RD 26 is a key regulator of metabolic reprogramming during dark-induced senescence. New Phytologist **218**:1543-1557

Lee TA, Vande-Wetering SW, Brusslan JA (2013) Stromal protein degradation is incomplete in Arabidopsis thaliana autophagy mutants undergoing natural senescence. BMC Research Notes **6**: 17–17

Lisec J, Schauer N, Kopka J, Willmitzer L, Fernie AR (2006) Gas chromatography mass spectrometry-based metabolite profiling in plants. Nat Protoc **1**: 387–396

Livak KJ, Schmittgen TD (2001) Analysis of relative gene expression data using real-time quantitative PCR and the 2(−ΔΔC(T)) method. Methods **25**: 402–408.

Marshall RS,Vierstra RD (2018) Autophagy: the master of bulk and selective recycling. Annu. Rev. Plant Biol. **69**: 173-208

Martínez DE, Costa ML, Gomez FM, Otegui MS, Guiamet JJ (2008) 'Senescence-associated vacuoles' are involved in the degradation of chloroplast proteins in tobacco leaves. The Plant Journal **56:** 196–206.

Masclaux-Daubresse C, Reisdorf-Cren M, Pageau K, Lelandais M, Grandjean O, Kronenberger J, Valadier MH, Feraud M, Jouglet T, Suzuki A (2006) Glutamine synthetase–glutamate synthase pathway and glutamate dehydrogenase play distinct roles in the sink–source nitrogen cycle in tobacco. Plant Physiology **140**: 444–456.

Mazur R, Mostowska A, Szach J, Gieczewska K, Wójtowicz J, Bednarska K., et al. (2019). Galactolipid deficiency disturbs spatial arrangement of the thylakoid network in Arabidopsis thaliana plants. J. Exp. Bot. **70**: 4689–4704.

McLoughlin F, Marshall RS, Ding X, Chatt EC, Kirkpatrick LD, Augustine RC, Li F, Otegui MS, Vierstra RD (2020) Autophagy Plays Prominent Roles in Amino Acid, Nucleotide, and Carbohydrate Metabolism During Fixed-carbon Starvation in Maize. Plant Cell. DOI: 10.1105/tpc.20.00226

Michaeli S, Galili G, Genschik P, Fernie AR, Avin-Wittenberg T (2016) Autophagy in plants: what's new on the menu? Trends Plant Sci **21**: 134–144

Michaeli S, Honig A, Levanony H, Peled-Zehavi H, Galili G (2014) Arabidopsis ATG8-INTERACTING PROTEIN1 is involved in autophagy-dependent vesicular trafficking of plastid proteins to the vacuole. Plant Cell **26**: 4084–4101

Minina EA, Moschou PN, Vetukuri RR, Sanchez-Vera V, Cardoso C, Liu Q, Elander PH, Dalman K, Beganovic M, Yilmaz JL, Marmon S, Shabala L, Suarez MF, Ljung K, Novák O, Shabala S, Stymne S, Hofius D, Bozhkov PV (2018) Transcriptional stimulation of rate-limiting components of the autophagic pathway improves plant fitness. J Exp Bot **69**: 1415–1432.

Oh SA, Lee SY, Chung IK, Lee CH, Nam HG (1996) A senescence-associated gene of Arabidopsis thaliana is distinctively regulated during natural and artificially induced leaf senescence. Plant Mol Biol **30**: 739–754

Otegui MS, Noh YS, Martı´nez DE, Vila Petroff MG, Staehelin LA, Amasino RM, Guiamet JJ (2005) Senescence-associated vacuoles with intense proteolytic activity develop in leaves of Arabidopsis and soybean. Plant J 41: 831–844

Otegui MS (2017) Vacuolar degradation of chloroplast components: autophagy and beyond. J. Exp. Bot. **69**: 741–750

Porra RJ, Thompson WA, Kriedemann PE (1989) Determination of accurate extinction coefficients and simultaneous equations for assaying chlorophylls a and b extracted with four different solvents: verification of the concentration of chlorophyll standards by atomic absorption spectroscopy. Biochim Biophys Acta **975**: 384–394

Sade N, Del Mar Rubio-Wilhelmi M, Umnajkitikorn K, Blumwald E (2018) Stress-induced senescence and plant tolerance to abiotic stress. J. Exp. Bot. **69**: 845–853

Sade N, Umnajkitikorn K, Rubio Wilhelmi M, Wright M, Wang S, Blumwald E (2017) Delaying chloroplast turnover increases water-deficit stress tolerance through the enhancement of nitrogen assimilation in rice. J. Exp. Bot. **69:** 867–878

Thompson AR, Doelling JH, Suttangkakul A, Vierstra RD (2005) Autophagic nutrient recycling in Arabidopsis directed by the ATG8 and ATG12 conjugation pathways. Plant Physiol **138**: 2097–2110

Umnajkitikorn K, Sade N, Wilhelmi MDMR, Gilbert ME, Blumwald E (2020) Silencing of OsCV (chloroplast vesiculation) maintained photorespiration and N assimilation in rice plants grown under elevated CO2. Plant Cell Environ. **43:** 920–933

Wada S, Ishida H, Izumi M, Yoshimoto K, Ohsumi Y, Mae T, Makino A (2009) Autophagy plays a role in chloroplast degradation during senescence in individually darkened leaves. Plant Physiology **49**: 885–893

Wang S, Blumwald E (2014) Stress-induced chloroplast degradation in Arabidopsis is regulated via a process independent of autophagy and senescence-associated vacuoles. Plant Cell **26:** 4875–488

Watanabe M, Balazadeh S, Tohge T, Erban A, Giavalisco P, Kopka J, Mueller-Roeber B, Fernie AR, Hoefgen R (2013) Comprehensive dissection of spatio-temporal metabolic shifts in primary, secondary and lipid metabolism during developmental senescence in Arabidopsis thaliana. Plant physiology **162:** 1290-1310

Xie Q, Michaeli S, Peled-Zehavi H, Galili G (2015) Chloroplast degradation: One organelle, multiple degradation pathways. Trends in Plant Science **20**: 264–265

FIGURES

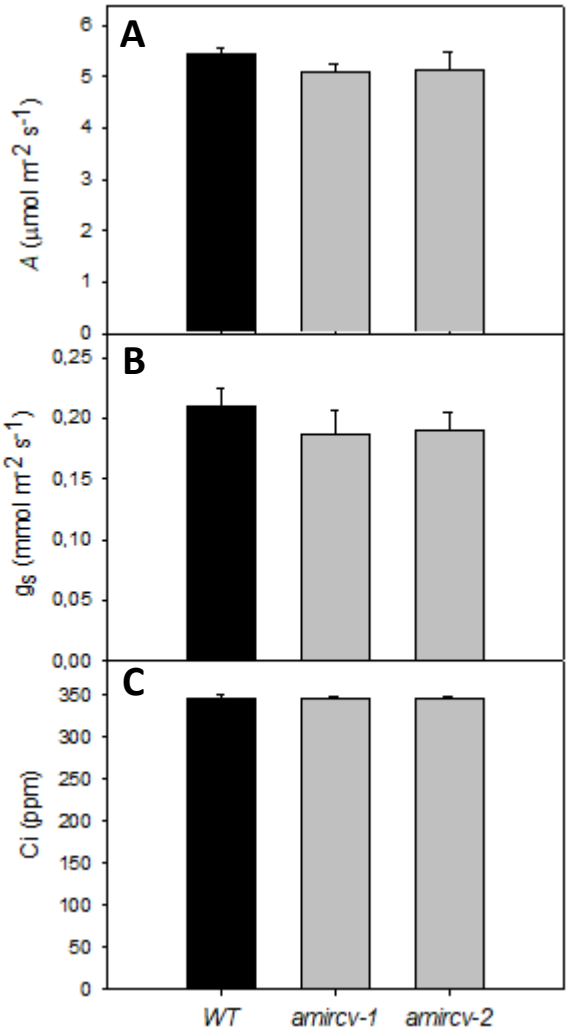

Figure 1. Gas-exchange parameters are not affected in WT and *amircv* mutants.

(A) net CO_2 assimilation rate (A), (B) stomatal conductance (g_s), (C) internal CO_2 concentration (C_i). Values presented are means ± SE of five biological replicates per genotype.

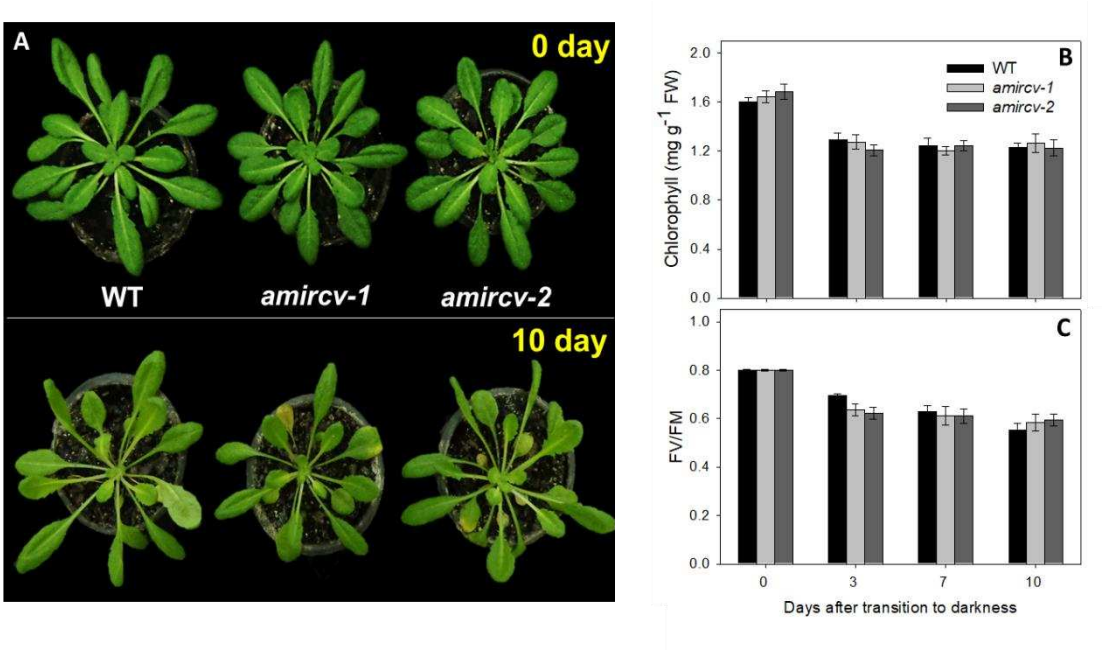

Figure 2: Phenotype of *amircv* Arabidopsis mutants under extended darkness

(A) Images of 4-week-old, short-day-grown Arabidopsis plants immediately (0 day) and after treatment for 10 days in darkness conditions; (B) Chlorophyll content; (C); Fv/Fm, the maximum quantum yield of PSII of leaves of 4-week-old plants after further treatment for 0, 3, 7 and 10 d in darkness. Values are means ± SE of five independent samplings; an asterisk indicates values that were determined by the Student's t test to be significantly different ($P < 0.05$) from WT each time point analyzed; FW, fresh weight.

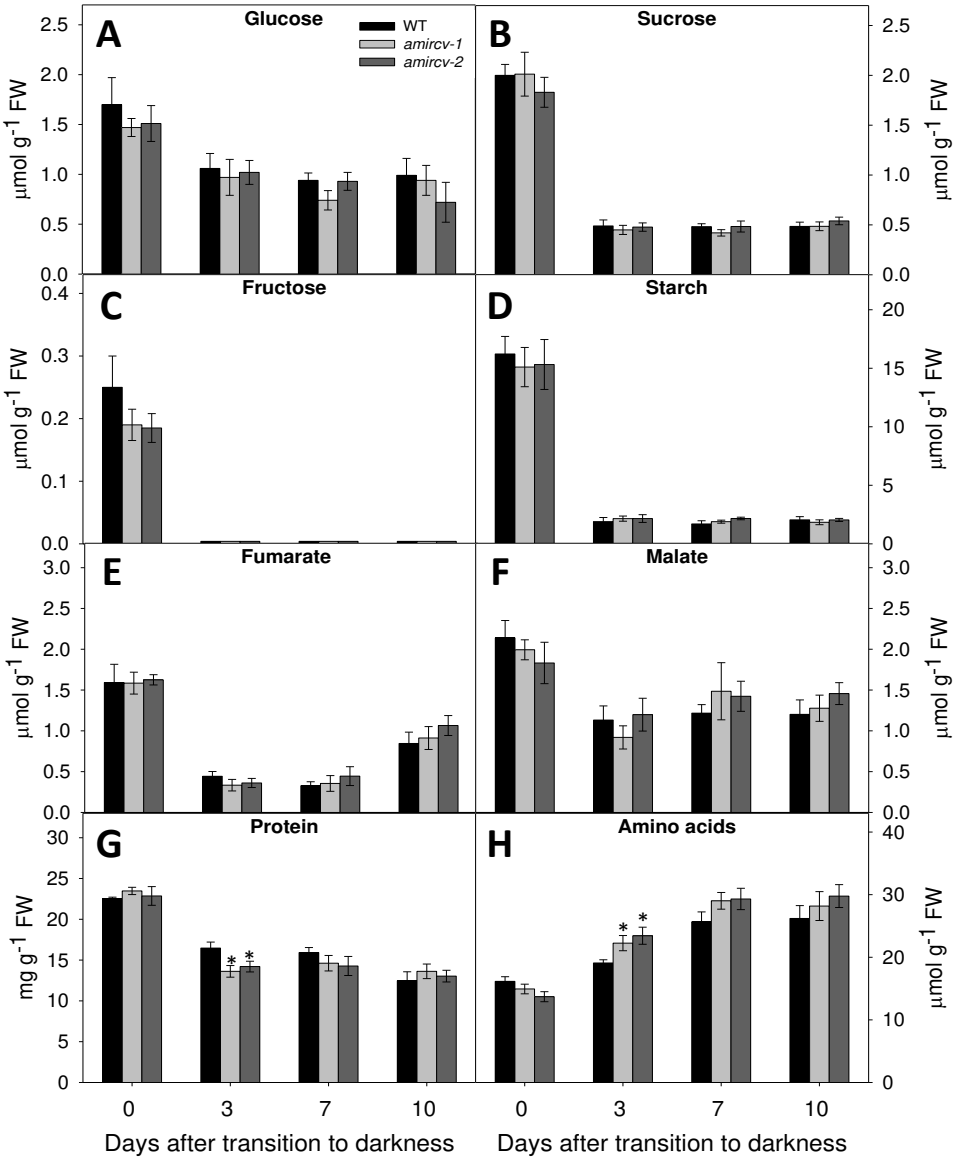

Figure 3: Metabolite levels in *amircv Arabidopsis* mutants under extended darkness

(A) Glucose, (B) Sucrose, (C) Fructose, (D) Starch, (E) Fumarate, (F) Malate, (G) Protein and (H) Amino acids. Values presented are means ± SE of five biological replicates per genotype; an asterisk (*) designate values that were determined by the Student's *t*-test to be significantly different ($P < 0.05$) from the wild-type (WT).

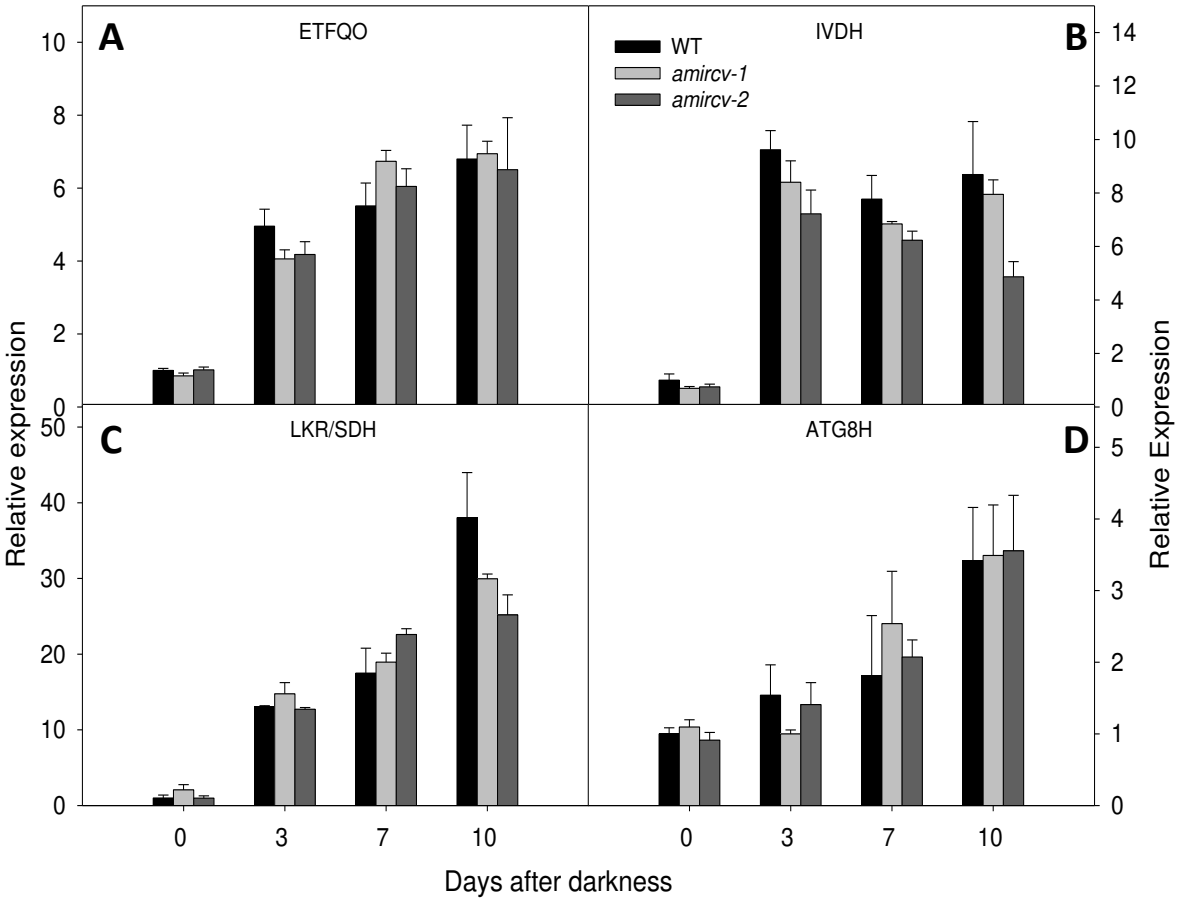

Figure 4: Transcript levels of genes related to alternative pathways of respiration and autophagy in *amircv Arabidopsis* mutants.

(A) Transfer flavoprotein/ ubiquinone oxireductase ETFQO; (B) Isovaleryl-CoA dehydrogenase- IVDH; (C) Lysine-ketoglutarate reductase/sacharopine dehydrogenase- LKR/SDH (D) Autophagy gene -ATG8h. The y-axis values represent the expression level relative to the wild type (WT). Data were normalized with respect to the mean response calculated for the 0-d dark-treated leaves of the WT. Values are average of three independent biological replicates.

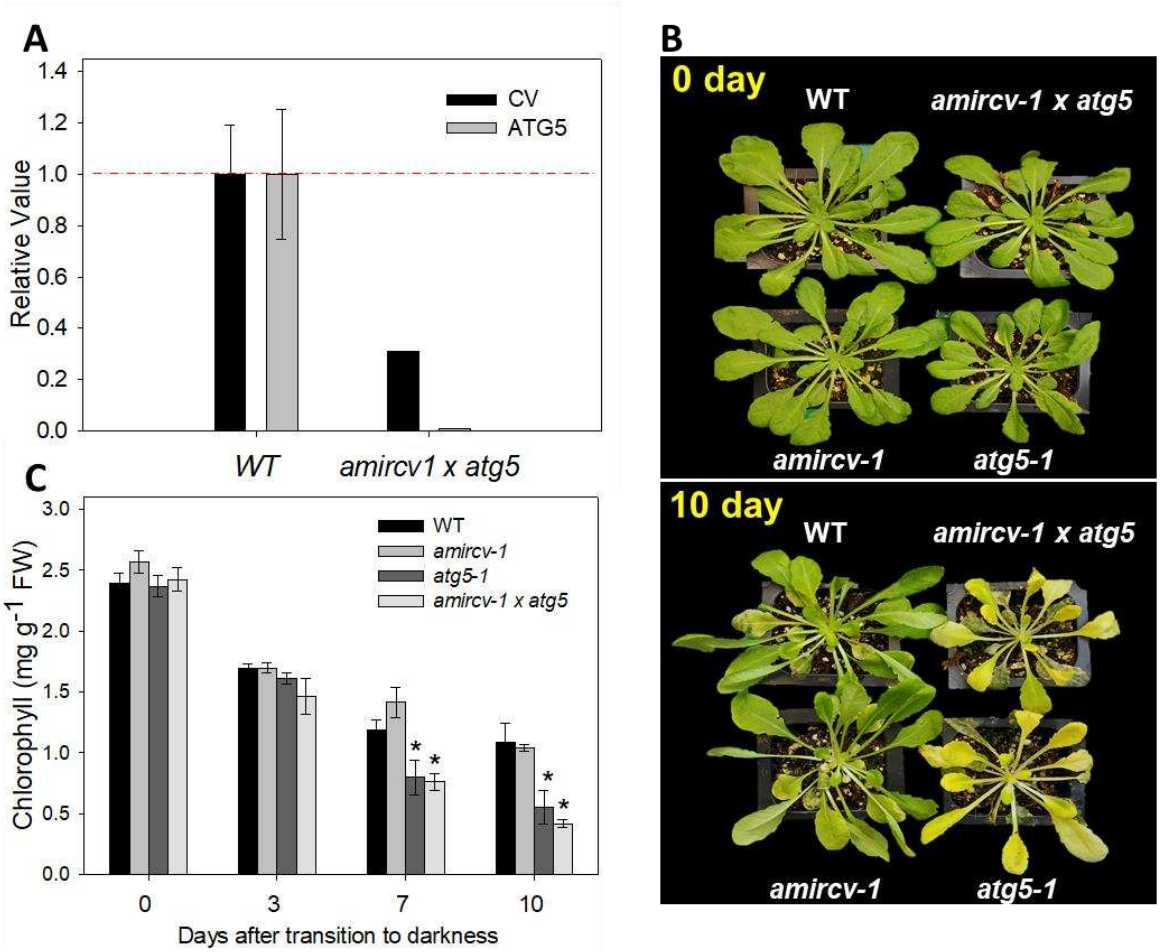

Figure 5: Phenotype of *Arabidopsis amircv1xatg5* mutants under extended darkness

(A) Confirmation of low expression of *CV* and *ATG5* genes in double mutant *amircv1xatg5*. (B) Representative images of 4-week-old, short-day-grown Arabidopsis plants immediately (0 d) and after further treatment for 10 days in darkness conditions. (C) Chlorophyll content of leaves of 4-week-old, short-day-grown. Values presented are means ± SE of five biological replicates. WT, wild-type; FW, fresh weight.

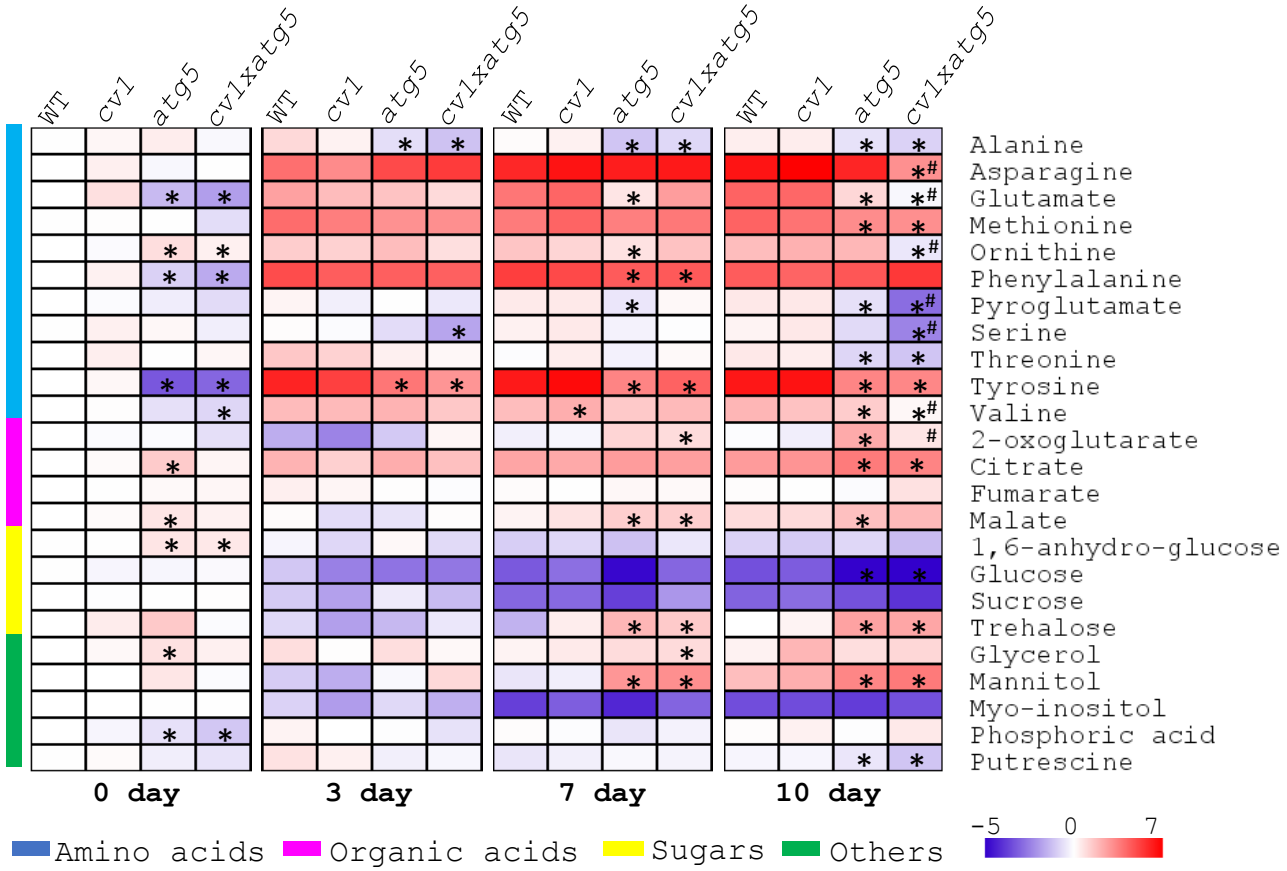

Figure 6: Metabolic effects of both CV and autophagy mutation during extended darkness conditions

Metabolite profile of Arabidopsis *amircv1xatg5* (cv1xatg5), *atg5, amircv-1* (cv-1) and wild-type (WT) genotypes during extended dark conditions. Data were normalized to the mean response calculated for the 0-d dark treated leaves of the WT. Values presented are means ± SE of three-five biological replicates per genotype; an asterisk (*) designate values that were determined by the Student's t-test to be significantly different ($P < 0.05$) from WT each time point. The hash (#) designate *amircv1xatg5* values that were determined by the Student's *t*-test to be significantly different ($P < 0.05$) from *atg5* each time point.

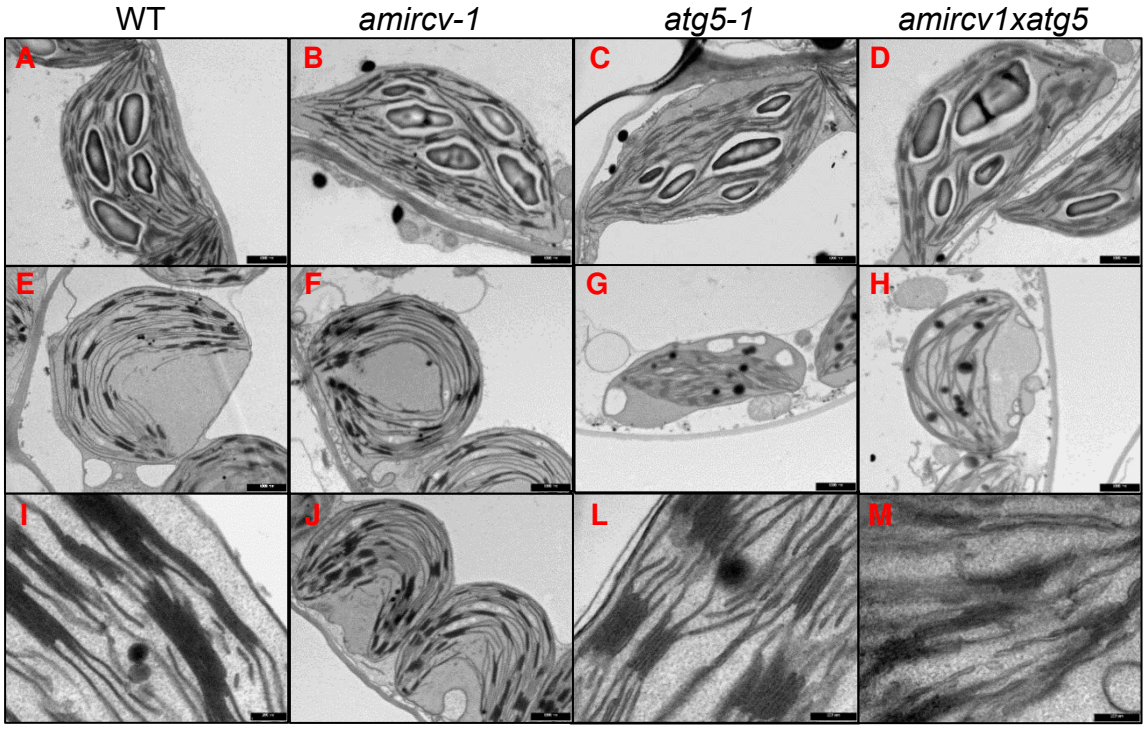

Figure 7: Abnormal chloroplast accumulation of *atg5-1* and *amicv1 x atg5* mutants

Transmission electron micrographs of control plants leaves (A-D) and leaves of WT, *amircv-1*, *atg5-1* and *amir1xatg5* plant exposed 7 days of darkness (E-M). Scale bar = 1 µm in images A-H and J; Scale bar = 0.2 µm in images I,L,M.

SUPPLEMENTAL DATA

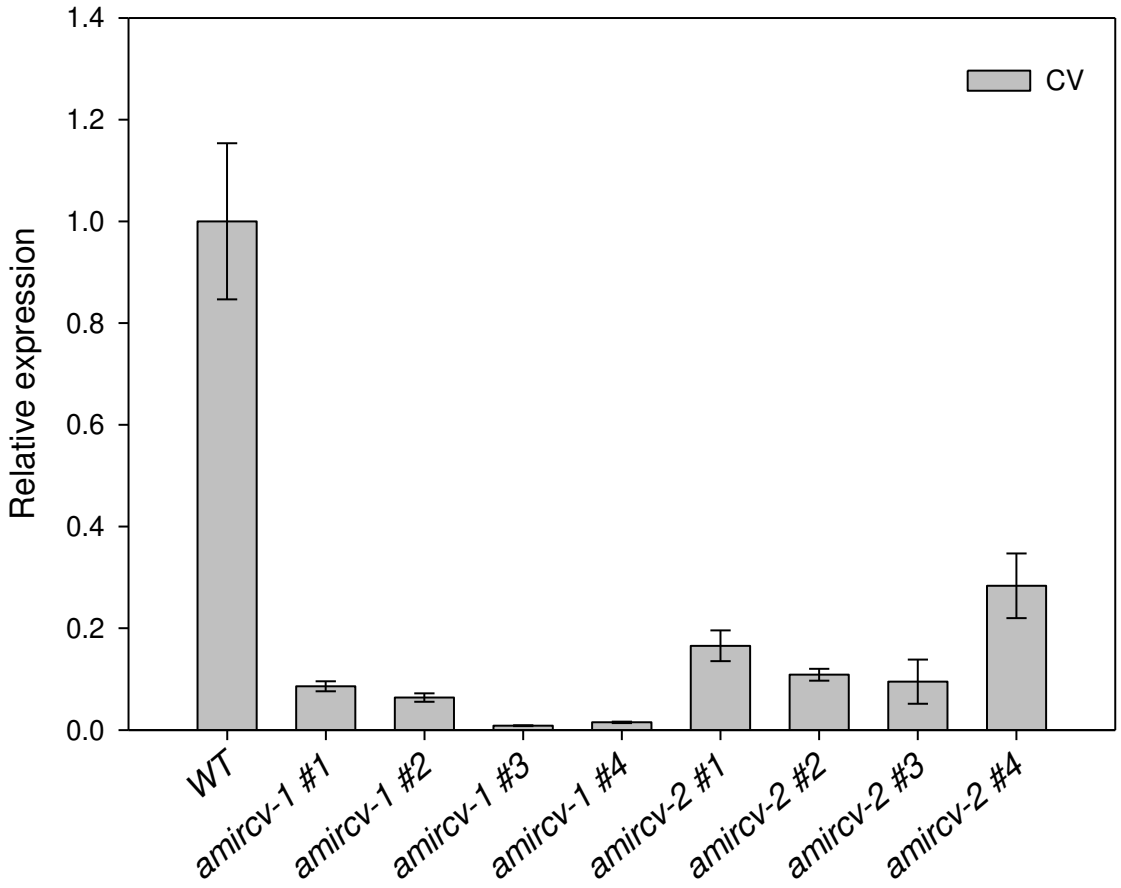

Figure S1- Confirmation of CV expression levels in *amircv* lines

Quantitative RT-qPCR analysis of *CV* expression in leaves of five week-old plants. Data were normalized to the mean calculated for the WT. Values are average of three independent technical replicates of each. Four individual plants of *amircv-1* and *amircv*-2 lines were evaluated.

Supplemental Table 1. Relative metabolite content of leaves of *Arabidopsis* knockout mutants *amircv-1*, *atg5-1, amircv1xatg5* and wild-type plants (WT) after further treatment for 0, 3, 7 and 10 days in darkness. Values are means ± SE of three-five independent samplings.

	WT				***amircv-1***				***atg5-1***				***amircv1xatg5***			
	0d	**3d**	**7d**	**10d**	**0d**	**3d**	**7d**	**10d**	**0d**	**3d**	**7d**	**10d**	**0d**	**3d**	**7d**	**10d**
2-oxoglutarate	1 ± 0.2	0.24 ± 0.07	0.81 ± 0.27	0.96 ± 0.29	1.11 ± 0.09	0.21 ± 0.03	0.89 ± 0.34	0.92 ± 0.17	0.95 ± 0.21	0.48 ± 0.04	2.55 ± 0.96	5.84 ± 0.86	0.65 ± 0.20	0.38 ± 0.16	2.41 ± 0.14	1.65 ± 0.32
Alanine	1 ± 0.2	2.06 ± 0.64	1.10 ± 0.11	1.40 ± 0.29	1.19 ± 0.26	1.3 ± 0.4	1.32 ± 0.29	0.28 ± 0.2	1.43 ± 0.5	0.64 ± 0.06	0.46 ± 0.14	0.68 ± 0.23	0.91 ± 0.41	0.44 ± 0.10	0.59 ± 0.17	0.54 ± 0.09
Asparagine	1 ± 0.2	6.19 ± 1.99	61.17 ± 24	109.1± 10.5	1.37 ± 0.37	4.29 ± 1.95	89.25 ± 7.8	88.87 ±7.58	0.9 ± 0.35	31.76 ±11.5	74.11 ± 31	79.27 ±9.06	1.02 ± 0.46	42.2 ± 30.5	79.2 ± 26	8.32 ± 3.80
Citrate	1 ± 0.1	2.61 ± 0.72	5.57 ± 1.38	7.85 ± 0.34	1.10 ± 0.19	2.49 ± 0.41	5.20 ± 0.36	7.78 ± 1.52	2.73 ±0.69	5.84 ± 0.46	6.69 ± 0.97	12.37 ± 0.9	1.22 ± 0.19	3.34 ± 0.88	6.24 ± 0.7	10.41 ± 1.04
Fumarate	1 ± 0.2	1.37 ± 0.30	1.09 ± 0.33	1.07 ± 0.07	0.99 ± 0.26	1.21 ± 0.23	1.03 ±0.06	0.99 ± 0.04	1.12 ± 0.18	1.04 ± 0.18	1.18 ±0.05	0.95 ± 0.11	1.20 ± 0.11	0.96 ± 0.07	1.13 ± 0.06	1.78 ± 0.71
Glutamate	1 ± 0.2	8.07 ± 1.89	13.6 ± 5.65	19.6 ± 4.32	1.45 ± 0.25	2.88 ± 1.34	18.7 ± 4.89	21.02 ± 4.3	0.63 ± 0.16	1.89 ± 0.76	1.65 ± 0.30	2.62 ± 0.30	0.44 ± 0.19	2.02 ± 0.66	8.57 ± 3.00	0.90 ± 0.38
Glucose	1 ± 0.1	0.56 ± 0.24	0.06 ±0.008	0.09±0.002	0.87 ± 0.22	0.18 ± 0.08	0.14±0.006	0.06 ±0.009	0.88 ± 0.22	0.15 ± 0.04	0.03 ±0.001	0.03 ±0.009	0.93 ± 0.07	0.03 ±0.004	0.05±0.002	0.02 ± 0.004
Glycerol	1 ± 0.1	1.54 ± 0.59	1.27 ± 0.34	1.63 ±0.20	1.15 ± 0.17	1.04 ±0.30	1.52 ± 0.43	1.45 ± 0.36	1.65 ± 0.21	1.91 ± 0.46	2.73 ±0.15	1.90 ± 0.27	1.34 ± 0.46	1.16 ± 0.49	2.00 ± 0.25	2.14 ±0.21
Malate	1 ± 0.2	0.64 ± 0.24	1.28 ± 0.28	1.96 ± 0.29	1.11 ± 0.22	0.62 ± 0.28	1.72 ± 0.14	1.98 ± 0.24	1.68 ± 0.26	0.68 ± 0.09	2.58 ± 0.26	3.38 ± 0.21	1.32 ± 0.19	0.47 ± 0.15	2.55 ± 0.11	3.84 ± 1.21
Manitol	1 ± 0.2	0.39 ± 0.13	0.71 ± 0.07	3.48 ± 1.53	1.01 ± 0.21	0.31 ± 0.10	0.80 ± 0.03	3.32 ±0.43	1.17 ± 0.28	1.12 ± 0.03	9.52 ± 0.44	10.13 ± 0.2	0.95 ± 0.21	0.70 ± 0.45	8.52 ± 0.43	12.64 ± 2.11
Methionine	1 ± 0.5	16.6 ± 8.59	12.45 ±4.59	19.55 ± 1.4	1.04 ± 0.41	11.7 ± 4.92	19.27 ±1.74	20.07 ±2.54	1.02 ± 0.62	8.18 ± 0.39	11.45 ±0.18	9.07 ±1.27	0.63 ± 0.22	8.50 ± 2.10	13.11±1.51	8.43 ± 2.13
Myo-inositol	1 ± 0.0	0.38 ±0.11	0.07 ±0.002	0.09±0.01	1.0 ± 0.03	0.26 ± 0.08	0.11 ±0.002	0.09 ±0.02	0.98 ± 0.03	0.60 ± 0.10	0.05 ±0.001	0.07 ± 0.01	1.02 ± 0.06	0.49 ± 0.22	0.12 ± 0.03	0.09 ± 0.004
Ornithine	1 ± 0.2	1.97 ± 0.5	3.42 ± 0.63	2.19 ± 0.59	0.94 ± 0.20	2.08 ± 0.55	2.26 ± 0.26	2.98 ± 0.69	2.14 ± 0.44	2.5 ± 0.32	1.74 ± 0.22	3.01 ±0.75	1.35 ± 0.13	1.84 ± 0.25	3.87 ± 0.85	0.72 ± 0.20
Phenylalanine	1 ± 0.1	25.1 ± 2.3	40.1 ± 3.93	13.72 ±0.32	1.30 ± 0.34	21.87 ±3.83	32.07± 8.33	24.68 ± 9.8	0.59 ± 0.11	21.3 ± 3.38	22.98 ±8.21	19.27 ±5.72	0.32 ± 0.08	20.86 ± 8.0	23.82 ± 6.8	44.54 ±11.2
Phosphoric acid	1 ± 0.0	1.06 ± 0.10	1.06 ± 0.10	1.07 ± 0.17	0.94 ± 0.06	1.01 ± 0.04	0.96 ± 0.18	1.01 ± 0.16	0.73 ± 0.09	0.97 ± 0.34	0.71 ± 0.18	0.97 ± 0.07	0.55 ± 0.06	0.68 ± 0.08	0.84 ± 0.11	0.81 ± 0.01
Pyroglutamate	1 ± 0.2	1.24 ± 0.27	1.5 ± 0.07	1.57 ± 0.03	0.95 ± 0.26	0.81 ± 0.20	1.54 ± 0.10	1.55 ± 0.09	0.88 ± 0.13	1.03 ± 0.23	0.72 ± 0.30	0.83 ± 0.03	0.74 ± 0.07	0.73 ±0.22	1.16 ± 0.22	0.14 ± 0.04
Putrescine	1 ± 0.1	1.74 ± 0.88	0.94 ± 0.19	0.87 ± 0.02	1.12 ± 0.11	1.35 ± 0.53	0.81 ± 0.04	0.88 ± 0.1	0.80 ± 0.26	0.80 ± 0.06	0.91 ± 0.03	0.71 ± 0.03	0.70 ± 0.09	0.89 ± 0.13	085 ± 0.08	0.46 ± 0.13
Serine	1 ± 0.2	1.08 ± 0.28	1.32 ± 0.29	1.26 ± 0.48	1.01± 0.24	0.95 ± 0.25	1.52 ± 0.01	1.77 ± 0.31	0.63 ± 0.19	0.78 ± 0.05	0.45 ± 0.18	0.75 ± 0.15	0.80 ± 0.10	0.30 ± 0.06	0.98 ± 0.29	0.19 ± 0.02
Sucrose	1 ± 0.0	0.57 ± 0.18	0.15 ± 0.02	0.14 ± 0.02	0.98 ± 0.02	0.27 ±0.06	0.13 ± 0.03	0.1 4±0.03	1.03 ± 0.03	0.76 ± 0.13	0.07 ±0.001	0.09 ± 0.02	1.05 ± 0.03	0.55 ± 0.13	0.15 ± 0.07	0.06 ± 0.01
Threonine	1 ± 0.3	2.93 ± 1.4	0.96 ± 0.35	1.56 ± 0.31	1.38 ± 0.16	1.55 ± 0.21	1.43 ± 0.04	1.43 ± 0.19	1.02± 0.19	1.35 ± 0.05	0.83 ± 0.03	0.58 ± 0.13	1.19 ± 0.26	1.16 ± 0.25	1.13 ± 0.25	0.45 ± 0.07
Trehalose	1 ± 0.2	0.69 ± 0.29	0.35 ± 0.04	1.01 ± 0.42	1.21 ± 0.28	0.27 ± 0.07	0.29 ± 0.11	1.27 ± 0.16	1.10 ± 0.29	0.46 ± 0.09	5.8 ± 1.47	5.88 ± 0.48	0.94 ± 0.25	0.72 ± 0.38	2.75 ± 0.46	7.68 ± 1.10
Tyrosine	1 ± 0.1	49.12 ±18.6	90.2 ± 12.7	91.02 ±2.64	1.45 ± 0.28	30.02 ±13.8	107.3 ±15.1	91.17 ±6.69	0.10 ± 0.01	10.94 ±2.92	10.4 ± 4.10	12.5 ± 0.13	0.13 ± 0.07	7.60 ± 2.05	25.3 ± 7.95	3.65 ± 1.78
Valine	1 ± 0.1	4.36 ± 0.83	3.54 ± 0.08	4.09 ± 0.44	1.22 ± 0.08	4.10 ± 0.66	4.71 ± 0.41	3.64 ± 0.38	0.82 ± 0.11	4.28 ± 0.88	2.81 ± 0.96	2.66 ± 0.58	0.58 ± 0.12	2.88 ± 0.66	3.74 ± 0.60	1.17 ± 0.38

Supplemental Table 2. Primers used in the RT-PCR analyses performed in this study.

Gene	Locus	Forward primer	Reverse primer
ATG5	AT5G17290	5'- GTGGCTGGACAAGTTAAGACAGC	5'- ACGAGATGTCATCCCAGGTATCG-3'
ATG8h	At3g06420	5'- CCACGAGACATGACTGTTGGAC-3'	5'- AGTCCATGCGACTAGCGGTTTG -3'
CV	AT2G25625	5'-CGGAGGTGGAGTGACAAGAG-3'	5'-GAGCAGACGGACGAGGAAGA-3'
ETFQO	At2g43400	5'- AAAGCTATCTTCTTCTTCTTCACC-3'	5'- GGTTGCAATCCCAACAACTT-3'
IVDH	AT3G45300	5'-AATGGGAAAGTTGACCCAAAGGAC-3'	5'-TAAAGCGACCTGCGTTGCTCTC-3'
LKR/SDH	AT4G33150	5'-TGATTGTCGCGTCTCTGTATC-3'	5'-ATCTAGCCGAACTGCTTCTAC-3'
ACT	AT2G37620	5'-CTTGCACCAAGCAGCATGAA -3'	5'-CCGATCCAGACACTGTACTTCCT-3'

ATG5 and *ATG8h*, autophagy genes; *CV*, chloroplast vesiculation; *ETFQO*, electron-transfer flavoprotein: ubiquinone oxidoreductase; *IVDH*, isovaleryl-CoA dehydrogenase; *LKR/SDH*, lysine-ketoglutarate reductase/saccharopine dehydrogenase; *ACT*, actin.

Chapter 4:

WRKY45 transcription factor is a key regulator of metabolic adjustments during dark-induced leaf senescence in *Arabidopsis thaliana.*

Title:

WRKY45 Transcription Factor is a Key Regulator of Metabolic Adjustments During Dark-induced Leaf Senescence in *Arabidopsis thaliana.*

Authors:

Jessica A. S. Barros[a, b], João Henrique F. Cavalcanti[c], Karla G. Pimentel[a], Taly Lapidot-Cohen[b], David B. Medeiros[d], Jorge A. Condori-Apfata[a], Yariv Brotman[d], Adriano Nunes-Nesi[a], Alisdair R. Fernie[d], Tamar Avin-Wittenberg[b] and Wagner L. Araújo[a]*

Affiliation:

[a] Departamento de Biologia Vegetal, Universidade Federal de Viçosa, 36570-900 Viçosa, Minas Gerais, Brazil

[b]Department of Plant and Environmental Sciences**,** Alexander Silberman Institute of Life Sciences, Hebrew University of Jerusalem, Givat Ram, 9190401, Jerusalem, Israel

[c] Instituto de Educação, Agricultura e Ambiente, Universidade Federal do Amazonas, 69800-000, Humaitá, Amazonas, Brazil

[d] Max Planck Institute of Molecular Plant Physiology, Am Mühlenberg 1, D-14476 Potsdam-Golm, Germany

ABSTRACT

Plants are constantly exposed to environmental changes that affects their performance. Metabolic adjustments are crucial to control energy homeostasis and plant survival, particularly under stress conditions. Under carbon starvation conditions, a coordinated response is initiated favoring the catabolism of proteins, lipids, and chlorophylls, which culminate in premature senescence. Notwithstanding, regulatory networks and signaling events that modulate transcriptional control during low energy stress is yet poorly understood. WRKY transcription factors have been characterized as key players during both developmental senescence and stress conditions. However, the association of WRKY with energy-related pathways remains unclear. Here, we identified that WRKY45 is not only important for developmental senescence, but it is also highly activated during carbon starvation induced by darkness. By using *Arabidopsis* overexpression mutants, we observed that the ectopic expression of WRKY45 resulted in an early senescence phenotype coupled with significant changes in amino acids and organic acids during dark-induced senescence. These changes were likely associated with the dysregulation of mitochondrial signaling rather than to the transcriptional activation of amino acids catabolic genes. Collectively, our results revealed WRKY45 as an important component of metabolic reprogramming during carbon starvation and highlights the potential role of WRKY in the regulation of mitochondrial signaling pathways.

Keywords: Carbon starvation, energetic metabolism, senescence, transcription factor.

INTRODUCTION

Plants have evolved multiple mechanisms to ensure their survival under sub-optimal conditions. Although leaf senescence is a natural developmental process, premature senescence is part of a 'escape' strategy by which plants cope with several stress (Sade et al., 2018). At the molecular level, signaling cascades responsible for inducing or repressing target gene expression are activated. Several classes of transcription factors (TFs) are able to control processes and modulate specific pathways, triggering metabolic and phenotypic changes in response to a given environmental stimulus (Mitsuda and Ohme-Takagi, 2009). Among such TFs, WRKYs are of particular significance since they participate in diverse (a)biotic stress responses as well as regulate plant developmental aspects (Finatto et al., 2018).

In *Arabidopsis thaliana,* the WRKY TF family comprises 75 members operating as either transcriptional activators or repressors through binding to the conserved W-box element (T)TGACC/T in the promoter regions of targets genes (Ülker and Somssich, 2004; Rushton et al., 2010). In addition to their crucial roles in several stress conditions, WRKY TFs have been extensively characterized to have central importance in the regulation of senescence related process. In this context, transcriptional analysis of Arabidopsis senescent leaves revealed that WRKY genes are the second largest group of TF found in the Arabidopsis senescence transcriptome (Breeze et al., 2011; Guo et al., 2004). To date, functional analyses have shown that several WRKY TFs positively or negatively regulate developmental leaf senescence in Arabidopsis (Miao et al., 2004; Besseau et al., 2012; Jiang et al., 2014; Guo et al., 2017; Zhang et al., 2017; Chen et al., 2017; Wang et al., 2020). For instance, WRKY53, a positive regulator of leaf senescence, is regulated by complex mechanisms (Zentgraf and Doll, 2019). Notably, WRKY25 is a positive regulator of WRKY53 expression, and WRKY25 itself negatively regulates leaf senescence (Zentgraf and Doll, 2019). In addition, WRKY57 operates in jasmonate induced leaf senescence (Jiang et al., 2014). WRKY42, WRKY55 and WRKY75 promote leaf senescence through the production of endogenous salicylic acid (Zhang et al., 2017; Niu et al., 2020; Wang et al., 2020), whereas WRKY45 and WRKY6 are involved in gibberellin-triggered leaf senescence by the activation of senescence associated genes (SAGs) (Chen et al., 2017; Zhang et al., 2018).

Members of the WRKY TF family have also been associated to energy and carbohydrate limitation responses (Bakshi and Oelmüller, 2014). Accordingly, Arabidopsis lines overexpressing OsWRKY72 displayed enhanced sensitivity to sucrose limitation

conditions (Song et al., 2010). The transcriptome analysis of Arabidopsi*s* suspension cells revealed the induction of WRKY6, WRKY45, and WRKY65 during sucrose deprivation (Contento et al., 2004). In addition, the expression of WRKY22 is enhanced by extended darkness treatment, and Arabidopsis plants overexpressing this TF exhibited an accelerated senescence phenotype under these conditions (Zhou et al., 2011). Furthermore, WRKY TFs were also associated with autophagy related genes during conditions of mitochondrial dysfunction triggered by the lack of FtSH4 protease (Zhang et al., 2017). Recently, it was verified that the overexpression of WRKY40 and WRKY45 genes conferred tolerance to submergence through a mechanism related to mitochondrial retrograde signaling (Meng et al., 2020). The aforementioned studies clearly revealed that WRKY TFs are part of several distinct environmental stress responses; however, to which extent WRKY TF controls the metabolic responses during low energy remains largely unclear. Given that, WRKY45 (*i*) plays a critical role in developmental senescence (Chen et al., 2017) and (*ii*) it is involved in the adaptation to low oxygen conditions (Meng et al., 2020), we investigated the potential role of WRKY45 in response to energy depletion. To this end, we generated three overexpression lines of WRKY45 TF and submitted them to extended darkness, a condition that mimics low energy stress and induces senescence in plants. Our results demonstrate that WRKY45 is a key regulator of metabolic reprogramming during dark-induced senescence in leaves by modulating amino acids and TCA cycle intermediates. Furthermore, transcript analyses indicate that WRKY45 likely participate on mitochondrial stress signaling pathways rather than directly regulate amino acid catabolic genes.

RESULTS

Identification of WRKY45 TF as candidate to regulate plant energetic response

In order to obtain a detailed expression profile of WRKY45 transcription factor, we initially evaluated the expression pattern of WRKY45 in different Arabidopsis tissues. Our findings demonstrate that WRKY45 is highly expressed in senescent leaves while a lower expression was observed in young and adult leaves, flowers, and seedlings (Fig. 1A). In agreement, the association of WRKY45 with age-triggered leaf was previously reported (Chen et al., 2017). It was postulated that WRKY45 operates as a component of gibberellin signaling pathway which positively regulates leaf senescence (Chen et al., 2017). Furthermore, we observed a concomitantly up-regulation of WRKY45 during carbon starvation induced by extended darkness (Fig. 1B). Further *in silico* analysis revealed that WRKY45 is also activated during short periods of starvation and hypoxia (Supplemental

Figure S1). Accordingly, a pivotal role of *At*WRKY45 in submergence tolerance was recently reported (Meng et al., 2020). Noteworthy, during hypoxia mitochondrial ATP production is compromised triggering an energetic stress. Collectively, these results pinpointed a potential role of WRKY45 on both age-triggered senescence and during short and long-term energy depletion.

Ectopic expression of WRKY45 results in enhanced dark-induced senescence

To further investigate the *in vivo* function of WRKY45 in energetic depletion responses, we generated three transgenic Arabidopsi*s* lines constitutively expressing WRKY45 TF under the control of the cauliflower mosaic virus (CaMV) 35S promoter (hereafter named *35S:wrky45-1***,** *35S:wrky45-3, 35S:wrky45-*4). Mutants plants were screened in kanamycin selection plates, and the overexpression of WRKY45 gene was further confirmed through qRT-PCR (Supplemental Figure S2). Thereafter, 4-week-old plants of *35S:wrky45* lines and its respective wild type (WT) were submitted to dark-induced senescence. After 10 days of continuous darkness, overexpression lines presented a more sensitive phenotype compared to WT plants, showing symptoms of early leaf senescence (Fig. 2A). To further investigate the senescence phenotype, chlorophyll and maximum photochemical efficiency of PSII (maximum variable fluorescence/ maximum yield of fluorescence [F_v/F_m]) were measured. In general, total chlorophyll and F_v/F_m decreased following dark treatment (Fig. 2B and C); however, both parameters were more reduced in *35S:wrky45* mutants lines (Fig. 2B and C). The lower levels of chlorophyll and F_v/F_m is consistent with the hypersensitive response of *35S:wrky45* lines observed during later stages of darkness.

In response to energy depletion events, carbon sources are exhausted, and plants must metabolize proteins and amino acids as alternative substrates (Araújo et al., 2011). Interestingly, *35S:wrky45* mutants showed higher rate of protein catabolism as evidenced by a lower levels of total protein and higher total amino acid accumulation in later stages of darkness (Fig. 3A and B). Accordingly, the reduced levels of proteins and altered amino acids have been described in mutants which present an early-sensitive phenotype under extended darkness (Araujo et al., 2010; Barros et al., 2017). Additionally, starch levels were more intensively, and quickly, reduced in *35S:wrky45-1* and *35S:wrky45-2* lines after 3 days of darkness (Fig. 3C), reinforcing the carbon starvation phenotype in these genotypes.

Not only proteins and amino acids but also lipids are important energetic reserves, which are mostly used during either seed remobilization stages or stresses conditions (Lu et al., 2020; Barros et al., 2020). To further investigate whether WRKY45 also affects lipid

metabolism, we analyzed alterations in the lipid profile in *35S:wrky45* lines during extended darkness treatment. Accordingly, the neutral lipids diacylglycerol (DAG) and triacylglycerol (TAG), as well as polar lipids including digalactosyldiacylglycerol (DGDG), monogalactosyldiacylglycerol (MGDG), and phospholipids, phosphatidylcholine (PC) phosphatidylethanolamine (PE) were determined. During extended darkness conditions, increased TAG levels coupled with a mixed pattern of increase and reduction of phospholipids (PC and PE) were observed (Supplemental Figures 3 and 4). Comparable responses were previously demonstrated during similar conditions of extended darkness (Barros et al., 2021). Nevertheless, only minor alterations of TAG and phospholipids were observed in *35S:wrky45* lines in comparison to WT (Supplemental Figures 3 and 4). On the other hand, notable changes were observed in the levels of galactolipids (MGDG and DGDG) (Fig. 4). Remarkably, this lipid class constitute the bulk of membrane lipids in chloroplasts, and lower levels are usually observed in plants under starvation or nutrient stress conditions (Barros et al., 2021; Have et al., 2019). Interestingly, an early decrease of DGDG was observed in *35S:wrky45* lines, yet both DGDG and MGDG were reduced after 10 days of extended darkness (Fig. 4). These findings suggests an intense degradation of chloroplasts membranes in *35S:wrky45* plants, most likely contributing to the reduced chlorophyll and *F*v/*F*m, and consequent higher sensitive of this genotype in response to dark-induced senescence conditions.

WRKY45 alters primary metabolites during dark-induced senescence

In order to obtain a detailed metabolite characterization of *35S:wrky* mutants, we next performed a metabolic profiling of rosette leaves using an established gas chromatography mass spectrometry (GC-MS) approach. The extended dark treatment led to a prompt decline of the sugars, namely fructose, glucose, sucrose, mannose, and myo-inositol, in all genotypes analyzed (Fig. 5). However, higher reductions of glucose and mannose were observed in *35S:wrk45* plants in the first days of darkness. The fast reduction of glucose might be correlated to higher consumption of starch in *35S:wrky45* plants (Fig. 3C). The vast majority of organic acids were reduced during darkness, as previously observed during extended darkness conditions (Ishizaki et al., 2006; Araujo et al., 2010; Barros et al., 2017; Kamafradan et al., 2018). Remarkably, the accumulation of the TCA cycle intermediates (e.g. malate, fumarate, and succinate) in all *35S:wrky45* lines at the end of dark treatment indicate an altered operation of the TCA cycle in these mutants (Fig.5).

We were also able to identify stress-related metabolite including putrescine, spermidine, and mannitol (Fig. 5). Interestingly, all *35S:wrky45* lines presented reduction of

spermidine levels after 10 days of darkness. Nevertheless, a slight higher levels of putrescine were observed in *35S:wrky45-1* and *35S:wrky45-4* plants after 7 days of darkness (Fig. 5). The levels of mannitol increased more than 10-fold after 10 days of darkness only in *35S:wrky45* plants. Mannitol, as well as other sugar alcohols, may be utilized to protect against ROS (Patel et al., 2016). It seems reasonable to assume that the accumulation of mannitol likely indicates a more severe stress status experienced by *35S:wrky45* plants.

WRKY45 shift amino acid metabolism

Since we have demonstrated that WRKY45 overexpression substantially affect the levels of total protein and total free amino acids (Fig. 3), we next analyzed the levels of individual amino acids. This analyze revealed an increase in the majority of the amino acids in all genotypes (Fig. 6). The accumulation of amino acids is a common response observed in natural or induced senescent leaves triggered by protein degradation (Araújo et al., 2010; Watanabe et al., 2013, Law et al., 2018). Notably, only proline and glycine levels strongly decreased during dark treatment (Fig. 6). Nevertheless, all *35S:wrky45* mutants lines displayed higher levels of glycine than WT plants at both 3 and 10 days after darkness, while no major differences were found in proline levels of *35S:wrky45* plants compared to WT (Fig. 6).

It is important to mention that the overexpression of *WRKY45* culminated with considerable changes in amino acids levels of *35S:wrky45* lines at the later stages of darkness (Fig. 6). In this context, it was observed lower accumulation of arginine, glutamine, isoleucine, lysine ornithine, and tyrosine in all mutants lines after 10 days of darkness (Fig. 6). BCAAs, aromatic amino acids, and lysine have been previously characterized as alternative substrates able to sustain respiration through a direct electron channeling to the ubiquinol pool within the plant mETC (Ishizaki et al., 2005, 2006; Araújo et al., 2010). Plants with disruption in either amino acid catabolism or amino acids supply were characterized by energetic failure under carbon depletion conditions (Ishizaki et al., 2005, 2006; Araújo et al., 2010; Barros et al., 2017). The reduced levels of energy-related amino acids in conjunction with the hyper-sensitive phenotype of *35S:wrky45* lines indicates that the WRKY45 most likely participate on the regulatory cascades of amino acid catabolism.

Thus we next investigated the expression of key genes related to the amino acid catabolism and alternative respiratory pathway. Overall, we observed an induction of amino acid catabolism pathways upon darkness treatment, although no differences were observed between WT and *35S:wrky45* mutants lines (Fig. 7). This induction was observed for genes related to BCAA (*IVDH, BCAT-2*), lysine (*LKR/SDH* and *D2HGDH*), and tyrosine

catabolism (*HGO*). Collectively, these results indicate that WRKY45 did not act directly in the transcriptional regulation of pathways of energetic amino acids catabolism.

WRKY45 induces senescence-related genes during dark-induced senescence

It was previously postulated that WRKY45 is a positive regulator of Gibberellin-mediated leaf senescence in Arabidopsis by the directly activation of senescence associated genes (SAGs) (Chen et al., 2017). Therefore, we further investigated the impact of WRKY45 overexpression on the common senescence marker gene, *SAG12*. During our experimental conditions, it was observed a marked activation of *SAG12* (Fig. 7). Interestingly, *35S:wrky45* plants presented lower transcripts levels of *SAG12* after 3 days of darkness. However, a higher induction of this gene was observed after 7 days of darkness in *35S:wrky45-3 and 35S:wrky45-4* lines (Fig. 7), suggesting that WRKY45 overexpression triggers an initial delay of *SAG12* activation, which was further compensated during the later stages of darkness.

During senescence process a massive dismantling of chloroplasts components is activated which triggers the typical "senescence phenotype" (Woo et al., 2018). Autophagy and chloroplast vesiculation (CV) pathways are known mechanisms involved in the degradation of chloroplast proteins in senescing leaves (Izumi and Nakamura 2018; Wang & Blumwald, 2014). While the disruption of autophagy-related genes (ATG) resulted in an early-senescence phenotype, the disruption of CV improved chloroplast maintenance under abiotic stress (Wang & Blumwald, 2014). Therefore, we also analyzed the expression of Autophagy 8e (*ATG8e*) and *CV* genes in 3*5S:wrky45* lines. Although both *ATG8e* and *CV* transcripts increased throughout darkness treatment, similar expression pattern of *ATG8e* was observed in WT and *35S:wrky45* lines, with significant differences only observed for *CV* expression (Fig. 7). Accordingly, an up regulation of *CV* gene was observed in both control conditions and after 10 days of darkness in *35S:wrky45-1* and *35S:wrky45-4* lines (Fig. 7). The promoter of *CV* contains a WRKY binding site upstream of the translation start codon (ATG) (Supplementary Figure S5), indicating *CV* as a direct target of WRKY TF. In agreement, the overexpression of *CV* leads to an early senescence phenotype in Arabidopsis (Wang and Blumwald, 2014) similar to the observed in WRKY45 overexpression lines.

WRKY45 plays role on mitochondrial signaling during dark-induced senescence

Plant mitochondria are crucial to support energy metabolism and the survival during dark periods (Ishizaki et al., 2006; Keech et al., 2007; Araujo et al., 2010). Plant mitochondria also play an important role in stress perception, by signaling its status to the nucleus to activate the expression of responsive genes, in a mechanism known as

mitochondrial retrograde regulation (MRR) (Selinski et al., 2018). Interestingly, WRKY TFs have been also related to act as either positive or negative regulators of mitochondrial stress-responsive genes (Van Aken et al., 2013). Several studies have shown the importance of alternative oxidase (AOX) induction for plant stress tolerance (Bartoli et al., 2005; Li and Xing 2010; Narsai et al., 2011; Saha et al., 2016; Wany et al., 2019). In addition, AOX1a is widely used as a marker gene of mitochondrial dysfunction and MRR (Selinski et al., 2018). Here, we verified that both isoforms *AOX1a* and *AOX1d* were initially downregulated after 3 days of darkness. However, their expression was further increased throughout darkness treatment (Fig. 7). Interestingly, higher induction of *AOX1a* and *AOX1d* transcripts was observed in *35S:wrky45* plants after 7 and 10 days of darkness. In addition, *35S:wrky45* lines present reduced levels of *AOX1d* gene under optimal growth conditions. These results indicate the potential role of WRKY45 in the regulation of mitochondrial protection mechanism under energy depletion conditions. The fact that *35S:wrky45* lines also exhibited reduced levels of *AOX1d* gene under optimal growth conditions further suggests a complex mechanism of *AOX1d* regulation mediated by WRKY45 TF.

In order to gain more insights on the relevance of WRKY45 TF on mitochondrial signaling, we further performed a phenotype assay of *35S:wrky45* lines submitted to mitochondrial dysfunctional conditions. To this end, WT and transgenic plants were germinated and grown on half-strength Murashige and Skoog (1/2 MS) medium supplemented with 10μM rotenone, an inhibitor of complex I extensively used to induce retrograde signaling (De Clercq et al., 2013; Van aken et al., 2016). Plants were grown for 14 days, and the primary root length and dry weight were measured (Fig. 8). As expected, under control conditions, no major differences were observed between *35S:wrky45* lines and WT plants. The addition of rotenone resulted in significant growth impairments in all genotypes. However, root length and dry weight was significantly lower in *35S:wrky45* lines compared to WT plants in rotenone treated plants (Fig. 8). By further using bioinformatic tools, we verified an induction of WRKY45 gene during either rotenone and oligomycin treatments (Supplementary Figure S6). Mutants with compromised MRR have been characterized by the sensitivity response to treatments with mitochondrial inhibitors (De Clercq et al., 2013; Van aken 2016). Collectively, these results coupled with the aforementioned ones, suggest that WRKY positively affects tolerance to stress induced by rotenone, and further reinforced our assumption that WRKY45 operates as a component of mitochondrial stress signaling.

The respiratory response of *35S:wrky45* mutants under dark-induced senescence

Given the severe phenotype observed in *35S:wrky45* lines coupled with both broad changes in TCA cycle intermediates and transcription activation of AOX mechanisms, we next investigated changes in respiration rates. To this end, we evaluated the rate of oxygen consumption of WRKY45 overexpression lines using a Clark oxygen electrode. Dark respiration rates concomitantly decreased during darkness treatment in all genotypes (Fig. 9A). Notably, the respiration rates were more affected in WT plants, with reductions ranging from 34% after 3 days to 71% after 10 days of darkness (Fig. 9B). On the other hand, lower changes were observed in *35S:wrky45-3* and *35S:wrky45-4* lines with respiratory rates decreasing 45% and 52% on the later stages of darkness. Reductions on respiration rates were previously reported in whole darkened plants (Keech et al., 2007; Barros et al., 2017; Law et al., 2018). This exquisite response was referred as a respiratory "stand-by" mode, and it ensures long-term survival of plants to low energy conditions (Keech et al., 2007; Law et al., 2018). Interestingly, the data obtained here suggests that the overexpression of WRKY45 impacts the fine-tune regulation of this mitochondrial response during extended darkness conditions.

DISCUSSION

The functional role of WRKY TFs during developmental senescence and stress conditions has been extensively demonstrated (Finatto et al., 2018). More specifically, WRKY45 TF has been associated to the regulation of age-triggered leaf senescence and submergence tolerance (Chen et al., 2017; Meng et al., 2020). Here, we provide compelling experimental evidence supporting an additional role of WRKY45 in metabolic reprogramming during energy deprivation events. First, we observed a transcriptional activation of *WRKY45* gene during both development senescence (Fig. 1A) and carbon starvation events induced by darkness (Fig. 1B). By using overexpression mutants, we further demonstrated the significance of WRKY45 TF as a positive regulator of distinct aspects related to plant energetic metabolism. The first evidence was the early onset of dark-induced senescence phenotype coupled with reduced chlorophyll and photosynthetic competence of *35S:wrky45* overexpression lines after 10 days of darkness (Fig. 2). During senescence events, increased catabolic processes such as the degradation of chlorophylls, proteins, carbohydrates, and lipids are observed, while anabolic processes decrease (Watanabe et al., 2013, Law et al., 2018). Notably, the overexpression of WRKY45 reduces the level of total leaf protein and increases the total amino acids content compared to WT

(Fig. 3). In addition to protein metabolism, our results shown the enhanced turnover of chloroplast lipids in *35S:wrky45* plants (Fig. 4). We further demonstrated, concomitantly with the enhanced protein and chloroplast lipids loss in *35S:wrky45* lines, a higher induction of the *CV* gene, which can be directly correlated to the early senescence phenotype observed in *35S:wrky45* lines (Fig. 2 and 7).

Our detailed metabolic analysis also revealed that WRKY45 is able to trigger a large impact on the metabolism of amino acids and organic acids under later stages of darkness (Fig. 5 and 6). Several amino acids accumulated in response to darkness, however, this accumulation was significantly lower in *35S:wrky45* lines, particularly after 10 days of darkness (Fig. 6). Glutamine and arginine, both used as nitrogen storage and transport compounds, accumulated less in *35S:wrky45 lines*, while asparagine levels increased similarly in all genotypes. Arginine degradation inside the mitochondria contributed to nitrogen remobilization, and the enzymes involved in this process are induced during senescence and germination phases (Witte, 2011). The complete arginine degradation results in α-ketoglutarate, ammonium and NADH (Hildebrandt et al., 2015; Winter et al., 2015). This process is mediated by ornithine intermediates which was also reduced in *35S:wrky45* lines. On the other hand, arginine and ornithine can also be metabolized in polyamines (Tiburcio et al, 2014). In plants, putrescine, spermidine, and spermine are the main polyamines, being involved in several physiological processes, including plant senescence and (a)biotic stress responses (Wang et al., 2019a). Although we observed slight higher levels of putrescine in *35S:wrky45-1* and *35S:wrky45-4* after 7 days of darkness, a marked reduction of spermidine was observed in *35S:wrky45* plants after 10 days of darkness (Fig. 5). Elevated levels of spermidine have been also related to chloroplast protection, restraining protein and chlorophyll degradation which results in delayed leaf senescence (Sobieszczuk-Nowicka & Legocka, 2014; Law et al, 2018). It seems reasonable to assume that the reduced levels of spermidine contributes to the chloroplast sensitive phenotype observed in *35S:wrky45* plants during late periods of darkness.

BCAA, aromatic amino acids, and lysine play a pivotal role on the maintenance of plant cell respiration by directly providing electrons to mETC under carbon starvation induced by darkness (Ishizaki et al., 2005, 2006; Araújo et al., 2010). Our results revealed a greater reduction of lysine, isoleucine, and tyrosine levels in *35S:wrky45* mutants after 10 days of darkness (Fig. 6). By contrast, valine and phenylalanine levels were virtually invariant between *35S:wrky45* and WT plants. The initial steps of leucine, isoleucine, and valine are identical being mediated by BCAT-2 and IVDH (Hildebrandt et al., 2015; Schertl

et al., 2017). Yet we observed transcriptional induction of these enzymes during darkness, no differential regulation was observed in *35S:wrky45* lines (Fig. 7). Accordingly, the solely accumulation of isoleucine in *35S:wrky45* mutants suggests that WRKY45 may regulate specific enzymes of isoleucine catabolism. Since the further steps involved in the degradation of the three BCAAs are not well known in plants (Hildebrant et al., 2015; Schertl et al., 2017), further investigation of BCCA catabolism will be clearly required to fully understand this fine tune regulation in response to changes in the expression of WRKY45.

Despite the divergent response of BCAA levels, *35S:wrky45* lines presented a clearly reduction in the levels of lysine after 10 days of darkness. Lysine degradation, which occurs via either D2HGDH or LKR/SDH enzymes, play a key role in the maintenance of energy metabolism by alternative respiratory pathways (Araujo et al., 2010; Hildebrandt et al., 2015; Cavalcanti et al., 2018; Batista-Silva et al., 2019). This fact aside, no differential up-regulation of lysine catabolism genes was observed in the WRKY45 overexpression lines. It is worth to mention that WRKY45 negatively regulated *LKR/SDH* gene under optimal growth conditions (Fig. 7). Interestingly, an over enrichment of WRKY45 transcript were previously observed in plants with impairment of lysine biosynthesis (Cavalcanti et al., 2018). Further studies are clearly required to disentangle this intrinsic connection between WRKY45 and lysine metabolism. Recent evidence also suggested that tyrosine is used as energetic substrate during dark-induced senescence (Wang et al., 2019b). Our results additionally revealed significantly reductions of this amino acid in *35S:wrky45* lines at 7 and 10 days after darkness (Fig. 6). Noteworthy, the complete oxidation of tyrosine result in acetoacetate and fumarate (Hildebrandt et al., 2015). Thus, it seems highly possible that the degradation of tyrosine may also play a role on energetic metabolism by feeding intermediates to the TCA cycle. Despite the lower levels of tyrosine along with accumulation of fumarate found in *35S:wrky45* plants, there is no further differences in transcripts levels of the tyrosine catabolic enzyme HGO in these plants, which reinforces the relatively minor importance of WRKY45 in the activation of these amino acids catabolism genes.

The significance of proline oxidation and its contribution to respiration during senescence was recently reported (Schertl et al., 2014; Launay et al., 2019). Proline has been suggested as an alternative energy source under low carbon conditions (Schertl et al., 2014; Launay et al., 2019). Furthermore, proline catabolism has been associated to transcriptional regulation by bZIP1, bZIP53 and bZIP63 TFs under energy depletion conditions (Dietrich et al., 2011; Mair et al., 2015). However, we did not observe any changes in the levels of proline in the WRKY45 overexpression plants. Thus, it seems reasonable to suggest that

WRKY and bZIPs modulate the catabolic pathways of different amino acids under energetic limitation. In fact, bZIPs are able to regulate the ASN1 gene that affect asparagine levels (Dietrich et al., 2011; Mair et al., 2015). Given that no further differences was observed in asparagine levels of *35S:wrky45* mutants, our results provide further support to the notion that WRKY45 do not share the same regulatory mechanisms of bZIPs TFs.

Catabolic products of free amino acids can be ultimately converted to precursors or intermediates of the TCA cycle (Araújo et al., 2011; Hildebrandt et al. 2015). Consistently, a higher accumulation of TCA intermediates including succinate, malate, and fumarate was observed in *35S:wrky45* plants at 10 days of darkness (Fig. 5). In fact, accumulation of TCA cycle intermediates during dark-induced senescence was previously associated with modifications in the pattern of different amino acids coupled with early-sensitive phenotypes (Araújo et al., 2010; Barros et al., 2017; Kamranfar et al., 2018). The higher accumulation of TCA cycle intermediates in *35S:wrky45* plants during extended darkness might be triggered by an enhanced amino acids catabolism and/or altered mitochondrial metabolism.

In addition to their effects on the metabolism, abiotic stresses can also perturb the functioning of organelles, including mitochondria and chloroplasts, that, in turn, activate feedback mechanisms by which nuclear gene expression is modified to restore the organellar functions (Ng et al., 2014). Although the role of mitochondria in the acclimation to various stresses is relatively well established (Vanlerberghe, 2013, Wang et al., 2018), the understanding of how mitochondrial signaling contributes to adaptive mechanisms remains rather unexplored. In plant mitochondria, AOX is commonly used as a marker for the MRR (Van Aken et al., 2009; Wang et al., 2018). The transcriptional regulation of *AOX1a* has been extensively studied, and it relies in the coordination of different TFs with a variety of other regulators that do not directly bind to the *AOX1* promoter (Selinski et al., 2018). Compelling evidence has further suggested the role of WRKY TFs on the regulation of mitochondrial responsive genes, including *AOX1a* and NADH dehydrogenaseB2 (*NDB2*) (Van Aken et al., 2009; 2013, Meng et al., 2020). This fact is most likely associated to the presence of the core binding sites of WRKY TF on the promoter regions of these genes (Van Aken et al., 2009; 2013). Accordingly, our results revealed an up-regulation of *AOX1a* and *AOX1d* genes in *35S:wrky45* plants after 7 and 10 days of darkness. This differential regulation was specially marked for *AOX1d* which increased about eight times more in *35S:wrky-3* and *35S:wrky-4* compared to WT. Other studies have shown that Arabidopsis *AOX1a* is under both negative and positive regulation of WRKY TFs (Dojcinovic et al., 2005; Vanderauwera et al., 2012; Van aken et al., 2013). In fact, the presence of W-box

motif was reported within the region of *AOX1a* promoter accountable for MRR (Dojcinovic et al., 2005). By using a promoter analysis approach, we were also able to identify a W-box motif in the promoter of Arabidopsis *AOX1d* gene (Supplementary Figure S5). Interestingly, low levels of *AOX1d* were observed in *35S:wrky45* lines under optimal conditions (Fig. 7). This finding highlights WRKY45 as a versatile regulator of *AOX1d*, operating as either positive or negative regulator according to starvation status of the cell.

Comparative transcriptome studies have further highlighted that the induction *AOX1d*, and in minor extent *AOX1a*, is associated with senescence process (Buchanan-Wollaston et al.2005, Clifton et al., 2006, Chrobok et al., 2016). In fact, *AOX1* isoforms present different expression patterns according with the tissue and developmental conditions (Clifton et al., 2006). To rule out the possibility that up-regulation of *AOX1a* and *AOX1d* observed here is an indirect effect of senescent phenotype, we evaluated the phenotype of *35S:wrky45* lines under mitochondrial dysfunctional stress induced by rotenone. Therefore, we observed that seedlings of WRK45 overexpression lines presented a better growth performance following rotenone treatment (Fig. 8). This response is likely triggered by the activation of mitochondrial stress related genes mediated by WRKY45, reinforcing the potential role of WRKY45 in the MRR. Accordingly, the importance of WRKY45 and WRKY40 to confer tolerance to hypoxia by the activation of mitochondrial stress signaling was recently reported elsewhere (Meng et al., 2020). The same study identified the expression of several WRKY TFs in a mitochondrial signaling mutant during hypoxia conditions, shedding new light on the activation of mitochondrial responses mediated by WRKY TFs (Meng et al., 2020). Here, we provided further evidence that WRKY45 is most likely a pivotal player involved in the mitochondrial-mediated stress responses in a dark-induced senescence context. Surprisingly, the changes in *AOX1* expression together with the accumulation of TCA cycle intermediates, did not culminate in higher respiratory rates. These findings highlight that the altered organic acids levels in *35S:wrky45* are mostly associated with changes in the flux within the TCA cycle. On the other hand, the fact that *35s:wrky45-3 and 35s:wrky45-4* lines presented a more invariant respiration rates after 7 and 10 days of darkness indicates that WRKY45 overexpression disturb the general mitochondrial activity response to dark-induced senescence.

CONCLUSIONS

Collectively, the results described here revealed the role of WRKY45 TF in mediating an exquisite metabolic reprograming following extended darkness conditions.

WRKY45 overexpression seems to activate a massive degradation of energetic amino acids associated with an early-senesce response. Surprisingly, rather than being involved in the regulation of amino acids catabolism pathways, WRKY45 is seemingly able to transcriptionally regulate the retrograde mitochondrial signaling associated to stress. Our results provide compelling evidence for the functional role played by WRKY45 under energetic constraints; however, there is still much work to fully uncover the molecular network that regulate plant energetic response during dark-induced senescence. Dissecting the intertwined pathway and regulatory proteins involved in such energetic response will provide a fully understanding of WRKY45 implications for plant metabolism and survival particularly in response to stress responses.

METHODS

Constructs and transformation

Arabidopsis thaliana WRKY45 gene (At3g01970) was amplified by PCR using specific primers that introduce the SalI and PstI restriction sites. The PCR product was purified and digested with *Sal*I e *Pst*I restriction enzymes, and it was inserted into the pUC19 vector, using T4 DNA ligase enzyme. The fragment insertion was confirmed trough clone sequencing. After, the construction was transferred to plant expression vector with CAMV 35S promoter and further used for *Agrobacterium tumefaciens* cloning and used to transform *Arabidopsis* using the floral deep method (Clough & Bent, 1998).

Plant Material and Dark Treatment

*35S:wrky*45 mutants plants previously genotyped by RT-PCR and its correspondent WT (Columbia-0 ecotype) were used in this study. Seeds were surface-sterilized and imbibed for 4 days at 4°C in the dark and subsequently germinated in selective medium containing kanamycin. Viable seedlings were selected and grown at 22°C under short-day conditions (8 h light/16 h dark), 60% relative humidity with 150 μmol photons m^{-2} s^{-1} for 4 weeks. Afterwards, plants were maintained in dark in the same growth cabinet. The rosettes were harvested at intervals of 0, 3, 7 and 10 days after transition to darkness and immediately frozen in liquid nitrogen and stored at –80°C until further analysis.

Biochemical assays

Leaf samples were harvested at the time points indicated, immediately frozen in liquid nitrogen, and stored at -80°C until further analysis. Extraction was performed by rapid grinding of tissue in liquid nitrogen and immediate addition of ethanol as described in Gibon et al. (2006). Photosynthetic pigments were determined as in Porra et al. (1989). The levels

of starch were determined exactly as described previously (Fernie et al., 2001). Proteins and amino acids were determined as described previously (Cross et al., 2006).

Metabolite profiling

Metabolite profiling was performed using approximately 50 mg of whole rosette material. The extraction, derivatization, standard addition, and sample injection were performed based on established gas chromatography-mass spectrometry (GC-MS)-based metabolite profiling protocol of Lisec et al. (2006). Peaks were annotated manually, and ion intensity was determined by the aid of TagFinder software (Luedemann et al., 2012), using a reference library from the Golm Metabolome Database (Kopka et al., 2005) and following the recommended reporting format (Fernie et al., 2011).

Lipid Profiling

Lipids and natural endogenic free fatty acid were extracted from six biological replicates using the MTBE method described by Salem et al. (2016). Vacuum-dried organic phases were processed using ultra-performance liquid chromatography (on a C8 reverse-phase column) coupled with Fourier transform mass spectrometry (exactive mass spectrometer; Thermo Fisher Scientific) in positive and negative ionization modes. Processing of chromatograms, peak detection, and integration were performed using REFINER MSH 10 (GeneData). Processing of mass spectrometry data included the removal of the fragmentation information, isotopic peaks, and chemical noise. Selected features were annotated using an in-house lipid database (Lapidot-Cohen et al., 2020). Five-six biological replicates were used for the analysis.

Expression analysis by RT-PCR

To expression analysis in different tissues and during darkness, as well to *35S:wrky* lines genotyping, it was used the protocol described below. Total RNA was isolated using TRIzol reagent (Ambion, Life Technology) according to the manufacturer's recommendations. The total RNA was treated with DNAse I (RQ1 RNase free DNase I, Promega, Madison, WI, USA). The integrity of the RNA was checked on 1% (w/v) agarose gels, and the concentration was measured using a Nanodrop spectrophotometer. Finally, 1 μg of total RNA were reverse transcribed with High Capacity cDNA Reverse Transcription Kit (thermos Fischer) according to the manufacturer's recommendations. Real-time PCR reactions were performed in a 96-well microlitre plate (Applied Biosystems Applera, Darmstadt, Germany), using Power SYBR Green PCR Master Mix (BioRad). The WRKY45 primer used here were designed using the open-source program QuantPrime-qPCR primer designed tool. ACTIN (AT2G37620) was used as internal standard. The relative levels of

mRNAs were determined using the $2^{-\Delta Ct}$ method (Livak and Schmittgen, 2001). Three biological replicates were processed for each experimental condition.

Statistical analyses

Unless otherwise stated, data were obtained from six-five plants in individual pots per genotype, each one representing a biological replicate. The experiments were designed and conducted in a completely randomized distribution design. Data were statistically examined using analysis of variance and tested for significant ($P < 0.05$) differences using Student's *t* tests. All statistical analyses were performed using the algorithm embedded into Microsoft Excel.

Authors contribution

J.A.S.B., J.H.F.C , and W.L.A. designed the research; J.A.S.B. performed most of the research with the support of J.H.F.C, K.G.P and J.A.C-A; W.L.A. supervised the project; T.L-C and L.R. performed lipid profile; D.B.M and A.R.F. performed metabolite profile; T.A-W., Y.B., A.N-N. and A.R.F. contributed with new reagents/analytic tools; T.A-W, D.B.M., A.N-N, and A.R.F. analysed the data, discussed the results, and complemented the writing. J.A.S.B. and W.L.A. analyzed the data and wrote the article, which was later approved by all the others.

REFERENCES

Araújo WL, Ishizaki K, Nunes-Nesi A, Larson TR, Tohge T, Krahnert I, Witt S, Obata T, Schauer N, Graham IA, Leaver CJ, Fernie AR (2010) Identification of the 2-hydroxyglutarate and isovaleryl-CoA dehydrogenases as alternative electron donors linking lysine catabolism to the electron transport chain of Arabidopsis mitochondria. Plant Cell **22:** 1549-1563

Araújo WL, Tohge T, Ishizaki K, Leaver CJ, Fernie AR (2011) Protein degradation – an alternative respiratory substrate for stressed plants. Trends Plant Sci. **16:** 489-498

Bakshi M, Oelmüller R (2014) WRKY transcription factor: Jack of many trades in plants. Plant Signal Behavior doi.org/10.4161/psb.27700

Barros JAS, Cavalcanti JHF, Medeiros DB, Nunes-Nesi A, Avi-Wittenberg T, Fernie AR, Araújo WL (2017) Autophagy deficiency compromises alternative pathway of respiration following energy deprivation. Plant Physiol **175:** 62–76

Barros JAS, Siqueira JAB, Cavalcanti JHF, Araújo WL, Avin-Wittenberg T (2020) Multifaceted Roles of Plant Autophagy in Lipid and Energy Metabolism. Trends Plan Sci. **25 (11):** 1141-1153

Barros JAS, Magen S, Lapidot-Cohen T, Rosental L, Brotman Y, Araújo WL, Avin-Wittenberg T (2021) Autophagy is required for lipid homeostasis during dark-induced senescence. Plant Physiol, kiaa120, https://doi.org/10.1093/plphys/kiaa120

Bartoli CG, Gomez F, Gergoff G, Guiamét JJ, Puntarulo S (2005) Up-regulation of the mitochondrial alternative oxidase pathway enhances photosynthetic electron transport under drought conditions. J Exp Bot **56**:1269-76

Batista-Silva W, Heinemann B, Rugen N, Nunes-Nesi A, Araújo WL, Braun HP, Hildebrandt TM (2019) The role of amino acid metabolism during abiotic stress release. Plant Cell Environ. **42:** 1630–1644.

Besseau S, Li J, Palva ET (2012) WRKY54 and WRKY70 co-operate as negative regulators of leaf senescence in Arabidopsis thaliana. J. Exp. Bot. **63**: 2667-2679

Breeze E, Harrison E, McHattie S, Hughes L, Hickman R, Hill C, Kiddle S, Kim YS, Penfold CA, Jenkins D (2011). High-resolution temporal profiling of transcripts during Arabidopsis leaf senescence reveals a distinct chronology of processes and regulation. Plant Cell **23**: 873-894

Buchanan-Wollaston V, Page T, Harrison E, Breeze E, Lim PO, Nam HG, Lin JF, Wu SH, Swidzinski J, Ishizaki K, Leaver CJ (2005) Comparative transcriptome analysis reveals significant differences in gene expression and signalling pathways between developmental and dark/starvation induced senescence in Arabidopsis. Plant Journal **42**: 567–585.

Cavalcanti JHF, Kirma M, Barros JAS, Quinhones CGS, Pereira-Lima ÍA, Obata T, Nunes-Nesi A, Galili G, Fernie A, Avin-Wittenberg T, Araújo WL (2018) An LL-diaminopimelate aminotransferase mutation leads to metabolic shifts and growth inhibition in Arabidopsis. Journal of Experimental Botany **69:** 5489–5506.

Chen L, Xiang S, Chen Y, Li D, Yu D (2017) Arabidopsis WRKY45 interacts with the DELLA protein RGL1 to positively regulate age-triggered leaf senescence. Molecular plant **10**: 1174-1189

Clifton R, Millar AH, Whelan J (2006) Alternative oxidases in Arabidopsis: a comparative analysis of differential expression in the gene family provides new insights into function of non-phosphorylating bypasses. Biochim Biophys Acta **1757**: 730–741

Clough SJ, Bent AF (1998) Floral dip: a simplified method for Agrobacterium-mediated transformation of Arabidopsis thaliana. The plant journal **16:** 735-743

Contento A L, Kim SJ, Bassham DC (2004) Transcriptome profiling of the response of Arabidopsis suspension culture cells to Suc starvation. Plant Physiol **135:** 2330-2347

Chrobok D, Law SR, Brouwer B, Lindén P, Ziolkowska A, Liebsch D, Narsai R, Szal B, Moritz T, Rouhier N, Whelan J, Gardeström P, Keech O (2016) Dissecting the metabolic role of mitochondria during developmental leaf senescence. Plant Physiol **172**: 2132–2153

Cross JM, von Korff M, Altmann T, Bartzetko L, Sulpice R, Gibon Y, Palacios N, Stitt M (2006) Variation of enzyme activities and metabolite levels in 24 Arabidopsis accessions growing in carbon-limited conditions. Plant Physiol **142**: 1574–1588

De Clercq I, Vermeirssen V, Van Aken O, Vandepoele K, Murcha MW, Law SR, Inze A, Ng S, Ivanova A, Rombaut D, et al (2013) The membrane-bound NAC transcription factor ANAC013 functions in mitochondrial retrograde regulation of the oxidative stress response in Arabidopsis. Plant Cell **25**: 3472-3490

Dietrich K, Weltmeier F, Ehlert A, Weiste C, Stahl M, Harter K, Dröse-Laser W (2011) Heterodimers of the Arabidopsis transcription factors bZIP1 and bZIP53 repro- gram amino acid metabolism during low energy stress. Plant Cell **23:** 381–395

Dojcinovic D, Krosting J, Harris AJ, Wagner DJ, Rhoads DM (2005) Identification of a region of the Arabidopsis AtAOX1a promoter necessary for mitochondrial retrograde regulation of expression. Plant Mol Biol **58**: 159-175

Fernie AR, Aharoni A, Willmitzer L, Stitt M, Tohge T, Kopka J, Carroll AJ, Saito K, Fraser PD, DeLuca V (2011) Recommendations for reporting metabolite data. Plant Cell **23**: 2477–2482

Fernie AR, Roscher A, Ratcliffe RG, Kruger NJ (2001). Fructose 2,6-bisphosphate activates pyrophosphate: fructose-6-phosphate 1-phosphotransferase and increases triose phosphate to hexose phosphate cycling in heterotrophic cells. Planta **212**: 250-63

Finatto T, Viana V E, Woyann LG, Busanello C, Maia LCD, Oliveira ACD (2018) Can WRKY transcription factors help plants to overcome environmental challenges? Genet. Mol. Biol. **41**: 533–544.

Gibon Y, Blaesing OE, Hannemann J, Carillo P, Hohne M, Hendriks JH, Palacios N, Cross J, Selbig J, Stitt MA (2006). Robot-based platform to measure multiple enzyme activities in arabidopsis using a set of cycling assays: comparison of changes of enzyme activities and transcript levels during diurnal cycles and in prolonged darkness. Plant Cell **16:** 3304-3325

Guo P, Li Z, Huang P, Li B, Fang S, Chu J, Guo H (2017) A tripartite amplification loop involving the transcription factor WRKY75, salicylic acid, and reactive oxygen species accelerates leaf senescence. Plant Cell **29**: 2854-2870

Guo Y, Cai Z, Gan S (2004) Transcriptome of Arabidopsis leaf senescence. Plant Cell Environ **27**: 521-549

Havé M, Luo J, Tellier F, Balliau T, Cueff G, Chardon F, Zivy M, Rajjou L, CacasJL, Masclaux-Daubresse C (2019) Proteomic and lipidomic analyses of the Arabidopsis atg5 autophagy mutant reveal major changes in endoplasmic reticulum and peroxisome metabolisms and in lipid composition. New Phytologist **223**: 1461–1477.

Hildebrandt TM, Nunes-Nesi A, Araujo WL, Braun HP (2015) Amino acid catabolism in plants. Mol Plant **8:** 1563-1579

Ishizaki K, Larson TR, Schauer N, Fernie AR, Graham IA, Leaver CJ (2005) The Critical Role of Arabidopsis Electron-transfer Flavoprotein:ubiquinone oxidoreductase During Dark-induced Starvation. The Plant Cell **17:** 2587–2600

Ishizaki K, Schauer N, Larson TR, Graham IA, Fernie AR, Leaver CJ (2006) The Mitochondrial Electron Transfer Flavoprotein Complex Is Essential for Survival of Arabidopsis in Extended Darkness. The Plant Journal **47:** 751-760

Izumi M, Nakamura S (2018) Chloroplast protein turnover: the influence of extraplastidic processes, including autophagy. Int. J. Mol. Sci . **19**: 828

Jiang Y, Liang G, Yang S, Yu D (2014) Arabidopsis WRKY57 functions as a node of convergence for jasmonic acid- and auxin-mediated signaling in jasmonic acid-induced leaf senescence. Plant Cell **26**: 230-245

Kamranfar I, Xue GP, Tohge T, Sedaghatmehr M, Fernie AR, Balazadeh S, Mueller-Roeber, B (2018). Transcription factor RD 26 is a key regulator of metabolic reprogramming during dark-induced senescence. New Phytologist **218**:1543-1557

Keech O, Pesquet E, Ahad A, Askne A, Nordvall D, Vodnala SM, Tuominen H, Hurry V, Dizengremel P, Gardeström P (2007) The different fates of mitochondria and chloroplasts during dark-induced senescence in Arabidopsis leaves. Plant Cell Environ **30:** 1523–1534

Kopka J, Schauer N, Krueger S, Birkemeyer C, Usadel B, Bergmüller E, Dörmann P, Weckwerth W, Gibon Y, Stitt M, Willmitzer L, Fernie AR, Steinhauser D (2005) GMD@CSB.DB: the Golm Metabolome Database. Bioinformatics **21**: 1635–1638

Lapidot-Cohen T, Rosental L, Brotman Y (2020) Liquid chromatography–mass spectrometry (LC-MS)-based analysis for lipophilic compound profiling in plants. Curr Protoc Plant Biol. 5 e20109. doi: 10.1002/cppb.20109

Launay A, Cabassa-Hourton C, Eubel H, Maldiney R, Guivarc'h A, Crilat E, Planchais S, Lacoste J, Bordenave-Jacquemin M, Clément G, Richard L, Carol P, Braun HP, Lebreton S, Savouré A (2019) Proline oxidation fuels mitochondrial respiration during dark-induced leaf senescence in Arabidopsis thaliana. Journal of Experimental Botany **70**: 6203–6214.

Law SR, Chrobok D, Juvany M, Delhomme N, Lindén P, Brouwer B, Ahad A, Moritz T, Jansson S, Gardestrom P, Keech O (2018) Darkened leaves use different metabolic strategies for senescence and survival. Plant Physiol **177**: 132–150

Li Z, Xing D (2010) Mechanistic study of mitochondria-dependent programmed cell death induced by aluminium phytotoxicity using fluorescence techniques. J Exp Bot **62**: 331-43

Lisec L, Schauer N, Kopka J, Willmitzer L, Fernie AR (2006) Gas-chromatography mass spectrometry-based metabolite profiling in plants. Nat Prot **1:** 387-396

Livak KJ, Schmittgen TD (2001) Analysis of relative gene expression data using real-time quantitative PCR and the 2(−ΔΔC(T)) method. Methods **25**: 402–408

Lu J, Xu Y, Wang J, Singer SD, Chen G (2020) The role of triacylglycerol in plant stress response. Plan Theory **9**: 472

Luedemann A, Strassburg K, Erban A, Kopka J (2008) TagFinder for the quantitative analysis of gas chromatography--mass spectrometry (GC-MS)-based metabolite profiling experiments. Bioinformatics **24:** 732-737

Mair A, Pedrotti L, Wurzinger B, Anrather D, Simeunovic A, Weiste C, Valerio C, Dietrich K, Kirchler T, Nâgele T, Carbajosa JV, Hanson J, Baena-Gonzalez E, Chaben C, Weckwerth W, Dröge-Laser W, Teige M (2015) SnRK1-triggered switch of bZIP63 dimerization mediates the low-energy response in plants. Elife **4:** doi: 10.7554/ eLife.05828

Meng X, Li L, Narsai R, De Clercq I, Whelan J, Berkowitz O (2020) Mitochondrial signalling is critical for acclimation and adaptation to flooding in Arabidopsis thaliana. Plant J. **103:** 227–247

Miao Y, Laun T, Zimmermann P, Zentgraf U (2004) Targets of the WRKY53 transcription factor and its role during leaf senescence in Arabidopsis. Plant Mol. Biol. **55**: 853-867

Mitsuda N, Ohme-Takagi M (2009) Functional analysis of transcription factors in Arabidopsis. Plant Cell Physiol. **50:** 1232–1248

Narsai R, Rocha M, Geigenberger P, Whelan J, van Dongen, J T (2011) Comparative analysis between plant species of transcriptional and metabolic responses to hypoxia. New Phytol. **190**: 472–487

Ng S, De Clercq I, Van Aken O, Law SR, Ivanova A, Willems P, Giraud E, Van Breusegem F, Whelan J (2014) Anterograde and retrograde regulation of nuclear genes encoding mitochondrial proteins during growth, development, and stress. Mol. Plant. **7**: 1075–1093

Niu F, Cui X, Zhao P, Sun M, Yang B, Deyholos MK, Li Y, Zhao X, Jiang YQ (2020) WRKY42 transcription factor positively regulates leaf senescence through modulating SA and ROS synthesis in Arabidopsis thaliana. Plant Journal **104**: 171-184.

Patel TK, Williamson JD (2016) Mannitol in plants, fungi, and plant-fungal interactions. Trends Plant Sci. **21**: 486–497

Porra RJ, Thompson WA, Kriedemann PE (1989) Determination of accurate extinction coefficients and simultaneous equations for assaying chlorophylls a and b extracted with four different solvents: verification of the concentration of chlorophyll standards by atomic absorption spectroscopy. Biochim Biophys Acta **975**: 384–394

Rushton PJ, Somssich IE, Ringler P, Shen QJ (2010) WRKY transcription factors. Trends Plant Sci. **15**: 247-258

Sade N, Del Mar Rubio-Wilhelmi M, Umnajkitikorn K, Blumwald E (2018) Stress-induced senescence and plant tolerance to abiotic stress. J. Exp. Bot. **69**: 845–853

Saha B, Borovskii G, Panda SK (2016) Alternative oxidase and plant stress tolerance. Plant Signal Behav 12:e1256530

Salem MA, Juppner J, Bajdzienko K, Giavalisco P (2016) Protocol: a fast, comprehensive and reproducible one-step extraction method for the rapid preparation of polar and semi-polar metabolites, lipids, proteins, starch and cell wall polymers from a single sample. Plant Methods **12:** 45

Schertl P, Braun, HP (2014) Respiratory electron transfer pathways in plant mitochondria. Front Plant Sci **5:** 163-167

Schertl P, Danne L, Braun HP (2017) 3-Hydroxyisobutyrate Dehydrogenase is involved in Valine and Isoleucine degradation in A. thaliana. Plant physiology **175**:51-61

Selinski J, Scheibe R, Day DA, Whelan J (2018) Alternative oxidase is positive for plant performance. Trends Plant Sci **23**: 588–597

Sobieszczuk-Nowicka E, Legocka J (2014) Plastid-associated polyamines: their role in differentiation, structure, functioning, stress response and senescence. Plant Biol **16:** 297-305

Song Y, Ai CR, Jing SJ, Yu DQ (2010) Research progress on function analysis of rice WRKY gene. Rice Sci **17:** 60-72

Tiburcio AF, Altabella T,Bitrian M, Alcazar R (2014)The roles of polyamines during the life span of plants: from development to stress. Planta **240**:1–18

Ülker, B. and Somssich, I. E. (2004). WRKY transcription factors: from DNA binding towards biological function. Curr. Opin. Plant Biol**. 7**: 491-498

Vanderauwera S, Vandenbroucke K, Inze A, van de Cotte B, Muhlenbock P, De Rycke R, Naouar N, Van Gaever T, Van Montagu MC, Van Breusegem F (2012) AtWRKY15 perturbation abolishes the mitochondrial stress response that steers osmotic stress tolerance in Arabidopsis. Proc. Natl Acad. Sci. **109:** 20113– 20118.

Van Aken O, Zhang B, Carrie C, Uggalla V, Paynter E, Giraud E, Whelan J (2009) Defining the mitochondrial stress response in Arabidopsis thaliana. Molecular plant **2**: 1310-1324.

Van Aken O, Zhang B, Law S, Narsai R, Whelan J (2013) AtWRKY40 and AtWRKY63 modulate the expression of stress- responsive nuclear genes encoding mitochondrial and chloro- plast proteins. Plant Physiol **162:** 254–271

Van Aken O, De Clercq I, Ivanova A, Law SR, Van Breusegem F, Millar AH, Whelan J (2016) Mitochondrial and chloroplast stress responses are modulated in distinct touch and chemical inhibition phases. Plant Physiol **171**: 2150–2165

Vanlerberghe GC (2013) Alternative Oxidase: A Mitochondrial Respiratory Pathway to Maintain Metabolic and Signaling Homeostasis during Abiotic and Biotic Stress in Plants. Int J Mol Sci. **14**: 6805-6847

Wany A, Gupta AK, Kumari A, Mishra S, Singh N, Pandey S, et (2019) Nitrate nutrition influences multiple factors in order to increase energy efficiency under hypoxia in Arabidopsis. Ann. Bot. **123:** 691–705

Wang S, Blumwald E (2014) Stress-induced chloroplast degradation in Arabidopsis is regulated via a process independent of autophagy and senescence-associated vacuoles. Plant Cell **26:** 4875–488

Wang W, Paschalidis K, Feng JC, Song J, Liu JH (2019a) Polyamine catabolism in plants: A universal process with diverse functions. Front. Plant Science **10**: 561

Wang M, Toda K, Block A, Maeda HA (2019b) TAT1 and TAT2 tyrosine aminotransferases have both distinct and shared functions in tyrosine metabolism and degradation in Arabidopsis thaliana. Journal of Biological Chemistry **294**: 3563–3576

Wang Y, Berkowitz O, Selinski J, Xu Y, Hartmann A, Whelan J (2018) Stress responsive mitochondrial proteins in Arabidopsis thaliana. Free Radical Biology and Medicine **122**: 28-39.

Wang Y, Cui X,Yang B, Xu S, Wei X, Zhao P, Niu F, Sun M, Wang C, Cheng H, JiangYQ (2020) WRKY55 transcription factor positively regulates leaf senescence and the defense response by modulating the transcription of genes implicated in the biosynthesis of reactive oxygen species and salicylic acid in Arabidopsis. Development doi: 10.1242/dev.189647

Watanabe M, Balazadeh S, Tohge T, Erban A, Giavalisco P, Kopka J, Mueller-Roeber B, Fernie AR, Hoefgen R (2013) Comprehensive dissection of spatio-temporal metabolic shifts in primary, secondary and lipid metabolism during developmental senescence in Arabidopsis thaliana. Plant physiology **162:** 1290-1310

Winter G, Todd CD, Trovato M, Forlani G, Funck D (2015) Physiological implications of arginine metabolism in plants. Front Plant Sci **6:** 534

Witte CP (2011) Urea metabolism in plants. Plant Science **180**: 431–438

Woo HR, Masclaux-Daubresse C, Lim PO (2018) Plant senescence: how plants know when and how to die. Journal of Experimental Botany **65**: 715–718.

Zentgraf U, Doll J (2019) Arabidopsis WRKY53, a Node of Multi-Layer Regulation in the Network of Senescence. Plants 8

Zhang S, Li C, Wang R, Chen Y, Shu S, Huang R, Zhang D, Li J, Xiao S, Yao N, Yang C (2017) The Arabidopsis mitochondrial protease FtSH4 is involved in leaf senescence via regulation of WRKY-dependent salicylic acid accumulation and signaling. Plant Physiol **173**: 2294–2307

Zhang Y, Liu Z, Wang X, Wang J, Fan K, Li Z, Lin W (2018) DELLA proteins negatively regulate dark-induced senescence and chlorophyll degradation in Arabidopsis through interaction with the transcription factor WRKY6. Plant Cell Rep. **37**: 981–992.

Zhou X, Jiang YJ, Yu DQ (2011) WRKY22 transcription factor mediates dark-induced leaf senescence in Arabidopsis. Mol. Cells **31**: 303–313

FIGURES

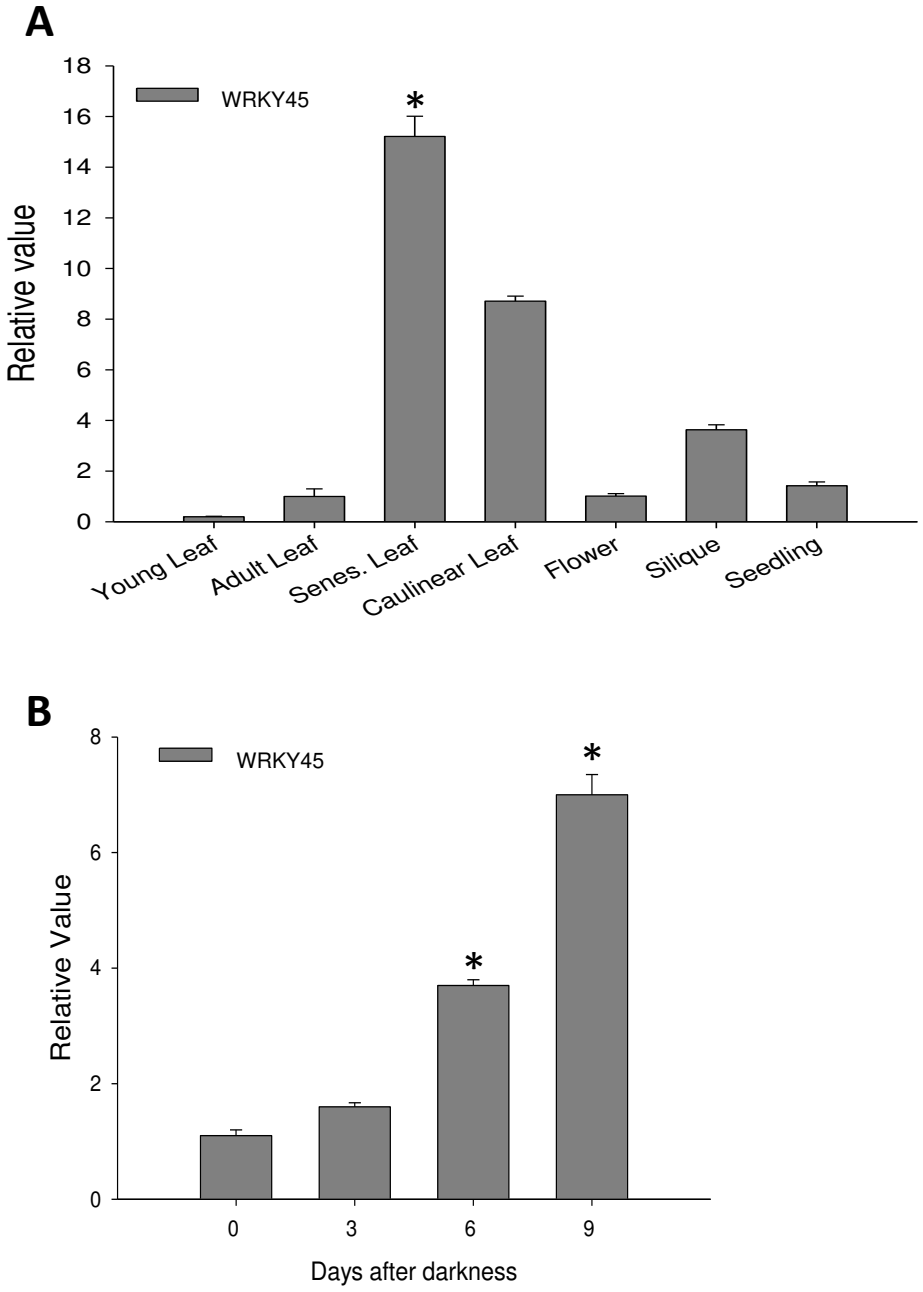

Figure 1- WRKY45 is induced during developmental and dark-induced senescence in Arabidopsis.

Transcript levels of *WRKY45* gene in different *Arabidopsis* tissues (A); and during darkened-induced senescence (B). The y axis values represent the transcript level relative to young leaf (A) and to 0d dark-treated leaves (B). Values are average of three independent biological replicates. (*) indicates values that were determined by the Student's t test to be significantly different ($P < 0.05$)

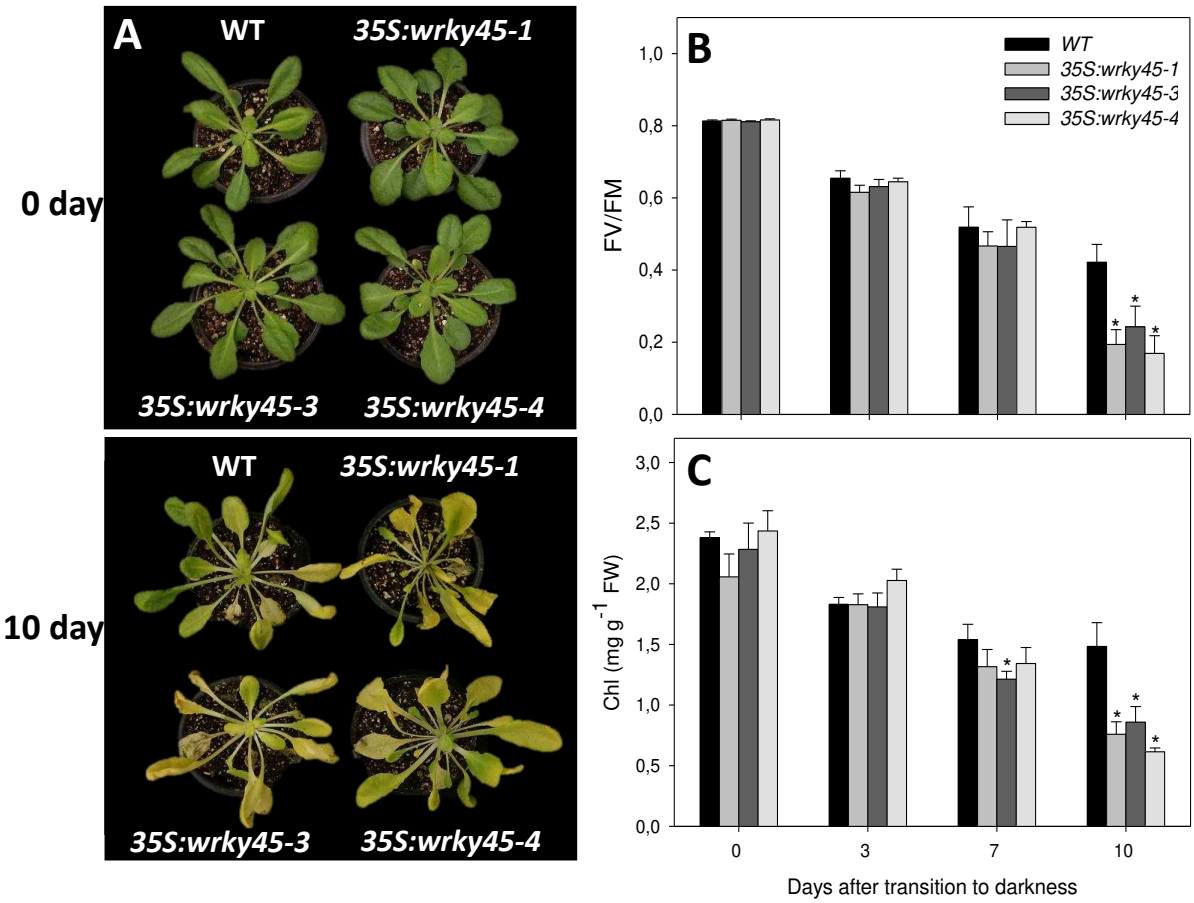

Figure 2- Phenotype of *Arabidopsis 35S:wrky45* mutants during dark-induced senescence

(A) Images of 4-week-old, short-day-grown Arabidopsis plants immediately (0 d) and after treatment for 10 days in darkness conditions; (B) Fv/Fm, the maximum quantum yield of PSII; (C) Chl, Chlorophyll content of leaves of 4-week-old, short-day-grown plants after further treatment for 0, 3, 7 and 10 days in darkness. Values are means ± SE of five independent samplings; an asterisk indicates values that were determined by the Student's t test to be significantly different ($P < 0.05$) from WT each time point analyzed; FW, fresh weight.

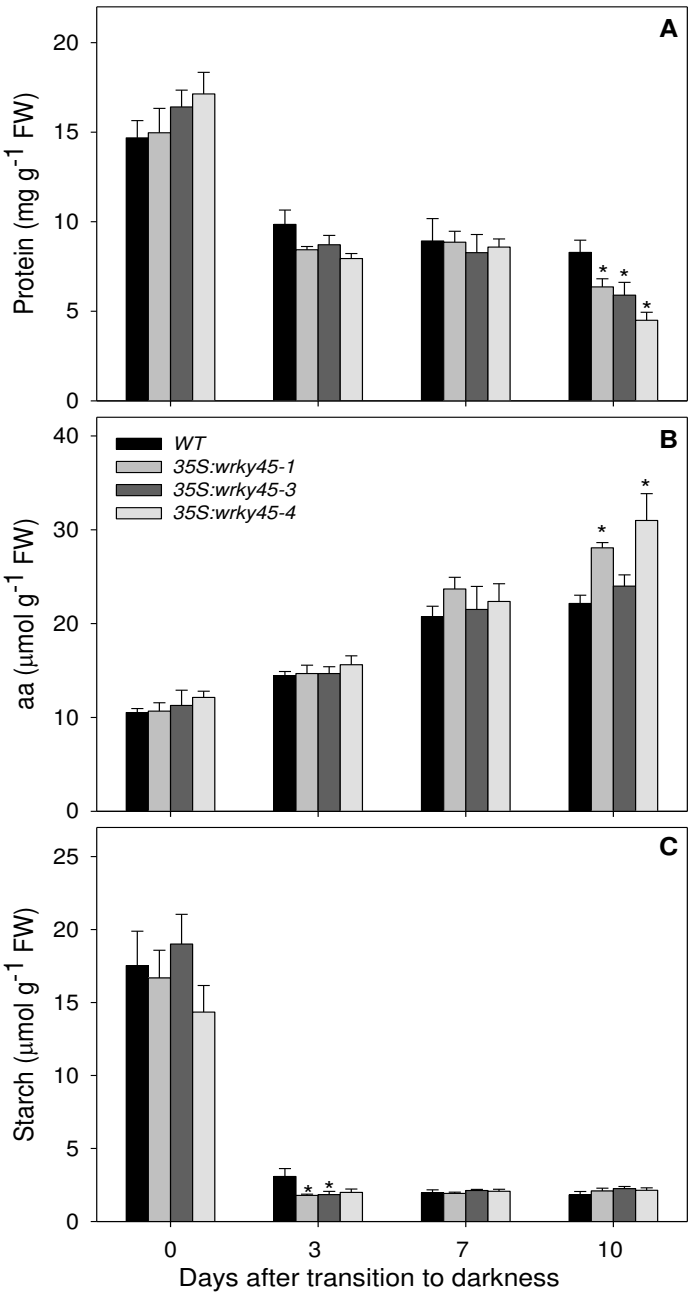

Figure 3- Metabolite levels in *Arabidopsis 35S:wrky45* mutants during dark-induced senescence

Metabolites were measured using whole rosette of 4-week-old short-day-grown *Arabidopsis* plants after further treatment for 0, 3, 7 and 10 days in extended darkness. **(A)** Protein, **(B)** Amino acids, **(C)** Starch. Values presented are means ± SE of five biological replicates per genotype; an asterisk (*) designate values that were determined by the Student's *t*-test to be significantly different ($P < 0.05$) from the wild-type.

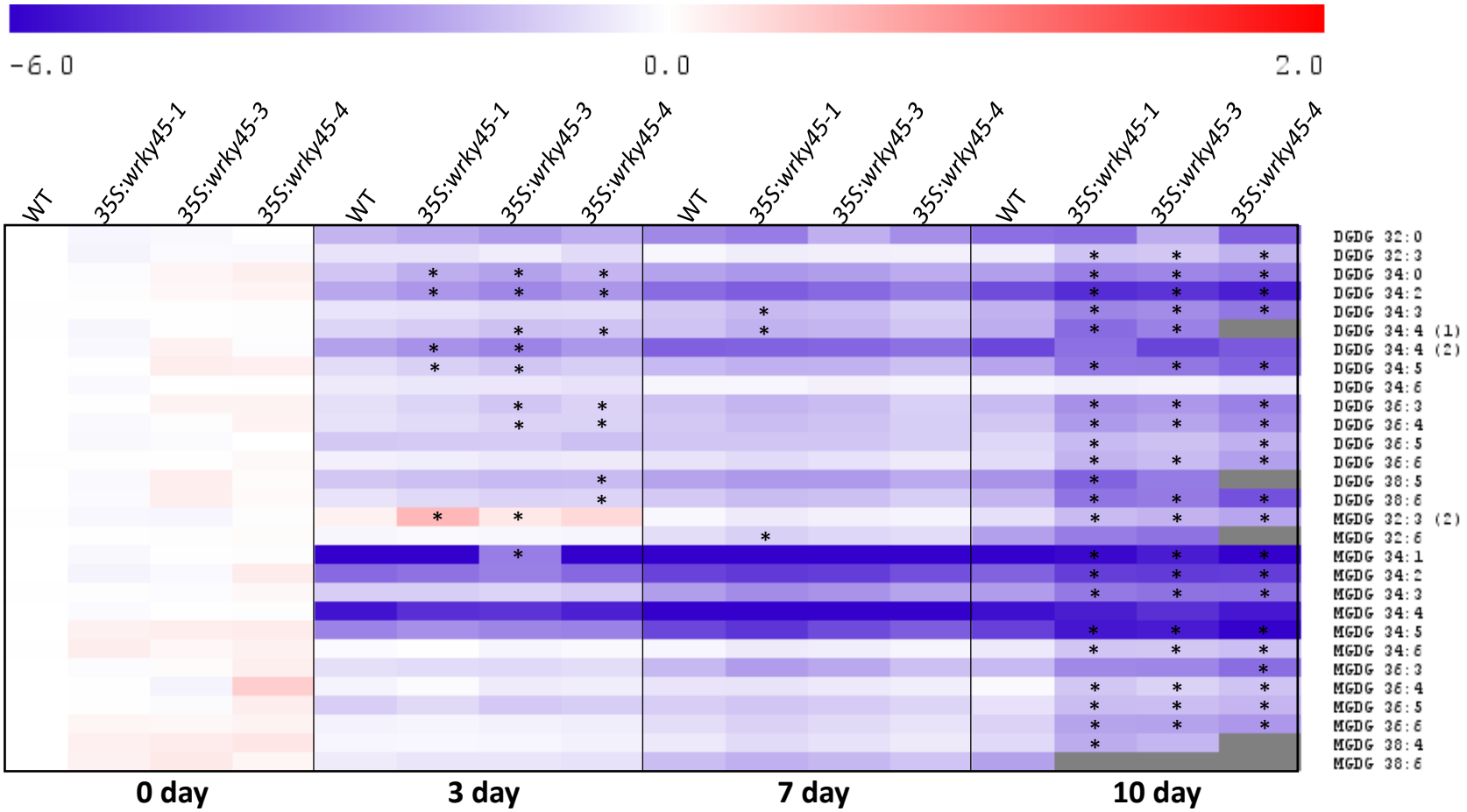

Figure 4- Chloroplast lipids are substantially reduced in *Arabidopsis 35S:wrky45* mutants during dark-induced senescence

Monogalactosyldiacylglycerol (MGDG) and Digalactosyldiacylglycerol (DGDG) values plotted are $\log_2$fold change. Data were normalized to the mean response calculated for the 0-d dark treated leaves of the wild type (WT). Values presented are means ± SE of five-six biological replicates per genotype; an asterisk (*) designate values that were determined by the Student's t-test to be significantly different ($P < 0.05$) from WT at each time point analyzed.

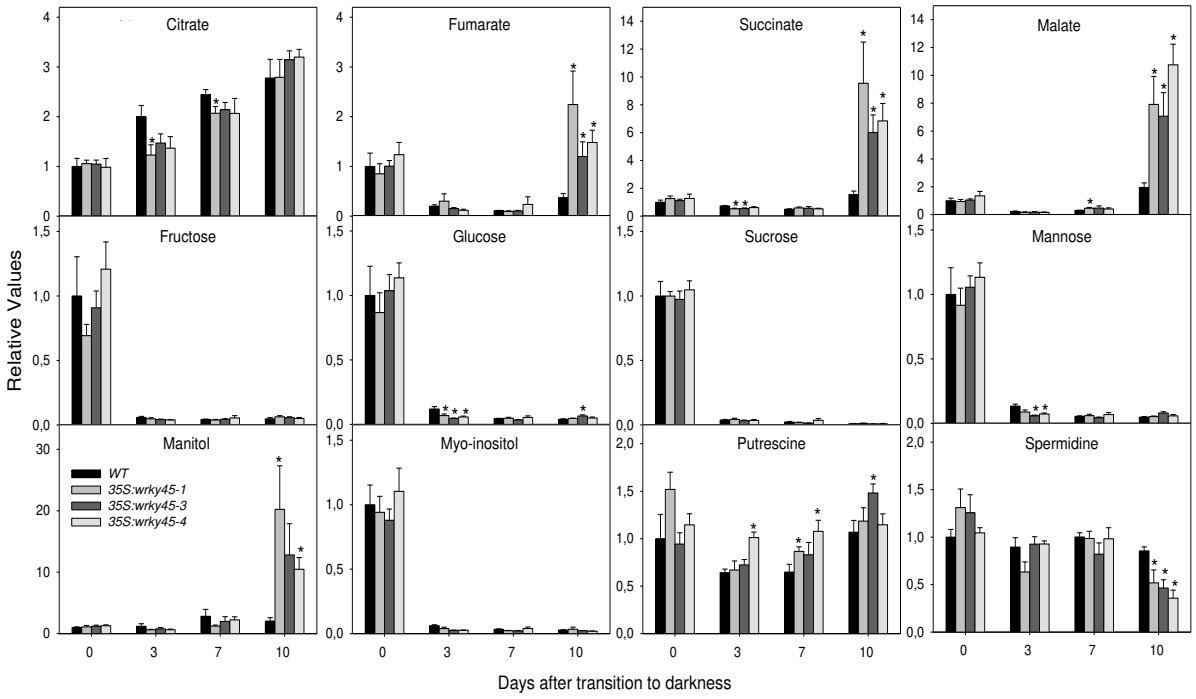

Figure 5- Relative levels of metabolites in *Arabidopsis 35S:wrky45* mutants during dark-induced senescence.

The y axis values represent the metabolite level relative to the wild type (WT). Data were normalized relative to the mean content calculated for the WT at 0d. Values presented are means of five-six biological replicates per genotype. Asterisks designate values that were determined by the Student's *t* test to be significantly different ($P < 0.05$) from the WT at each time point analyzed

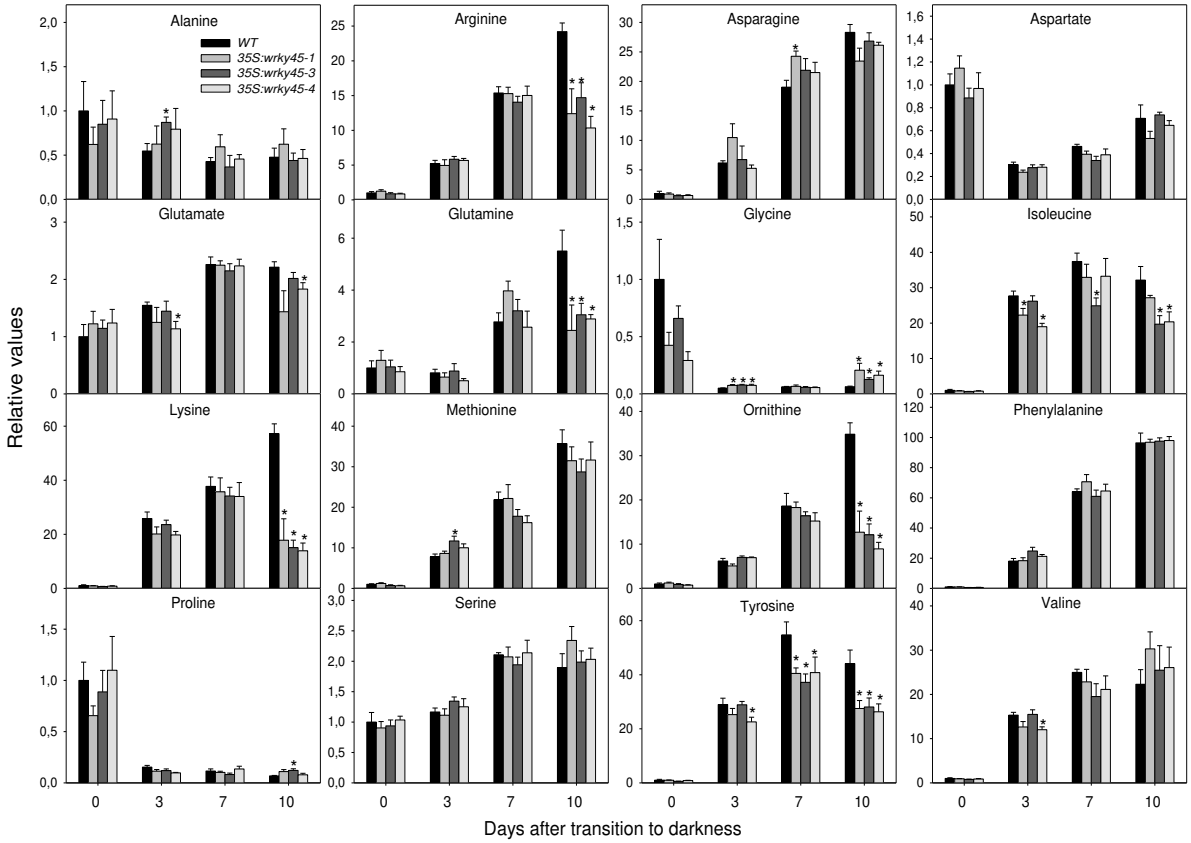

Figure 6- Relative levels of amino acids in *Arabidopsis 35S:wrky45* mutants during dark-induced senescence.

The y axis values represent the metabolite level relative to the wild type (WT). Data were normalized to the mean response calculated for the WT at 0-d. Values presented are means of five-six biological replicates per genotype. Asterisks designate values that were determined by the Student's *t* test to be significantly different ($P < 0.05$) from the WT at each time point analyzed.

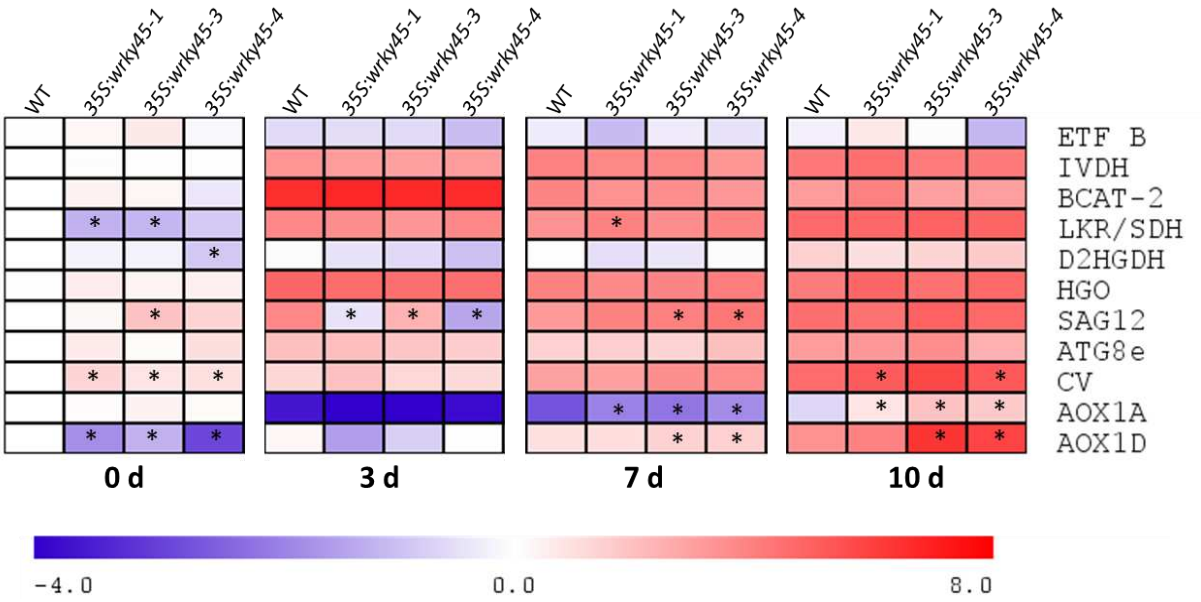

Figure 7 - Changes in transcript levels in WT and *35S:wrky45* mutants during dark-induced senescence.

Transcript abundance is shown for genes associated with amino acid catabolism, protein degradation and alternative respiratory pathways. The y-axis values represent the expression level relative to the wild type (WT). Data were normalized with respect to the mean response calculated for the 0-d dark-treated leaves of the WT. Values presented are means ± SE of three independent biological replicates. An asterisk (*)

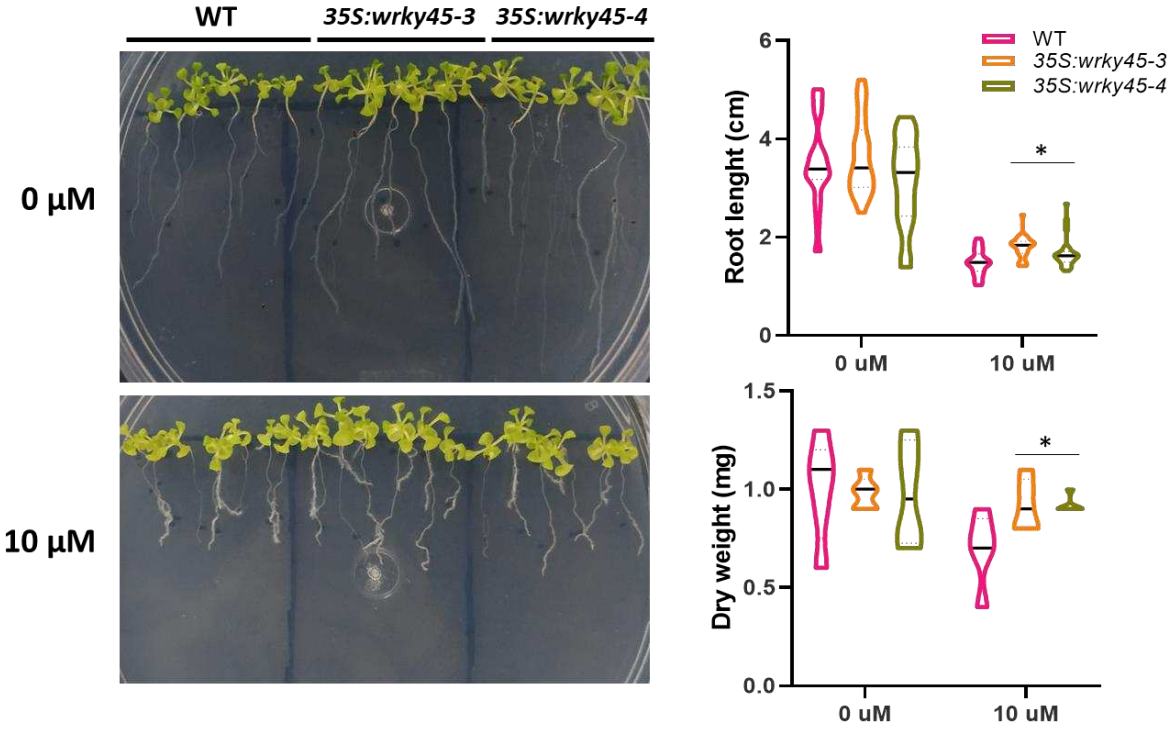

Figure 8- Increased rotenone tolerance of *Arabidopsis 35S:wrky45* mutants

(A) Two-week-old wild-type (WT), *35S:wrky45-3*, and *35S:wrky45-4* seedlings germinated and grown on 1/2MS medium supplemented with 10 µM rotenone and 10 µM DMSO (control = 0 µM rotenone) (B) primary root length (C) fresh weight. Data represent average of five individual experiments (n = 25 to 30 plants). Asterisk indicates significant differences from WT (Student's t test; *P < 0.05)

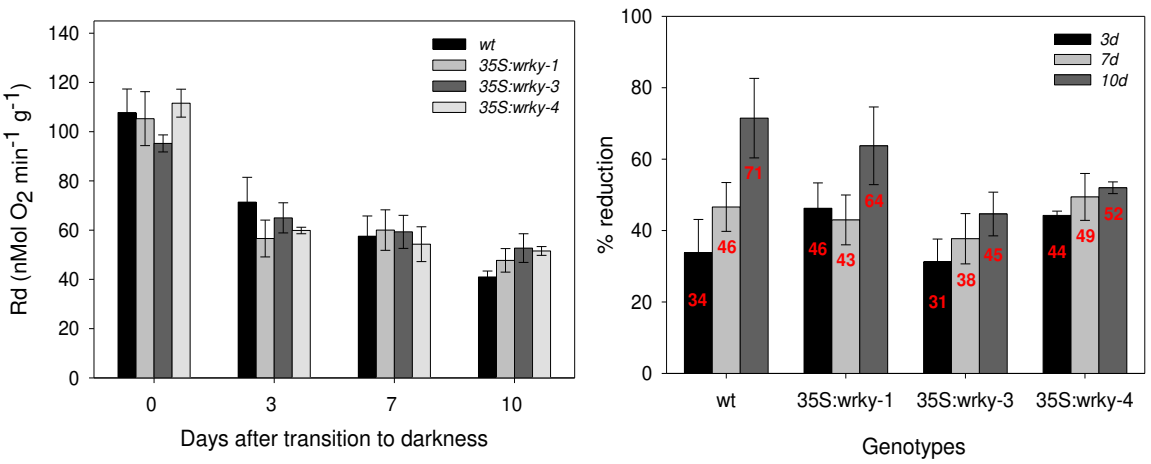

Figure 9- Dark respiration of *35S:wrky45* mutants during dark-induced senescence.

(A) Senescent leaf respiration was measured as oxygen consumption rate in liquid phase. (B) % reduction of respiratory rates calculated from the mean response of the 0-d dark-treated for each genotype. Values presented are means of four-five biological replicates per genotype Asterisks designate values that were determined by the Student's *t* test to be significantly different ($P < 0.05$) from the wild type (WT).

SUPPLEMENTAL DATA

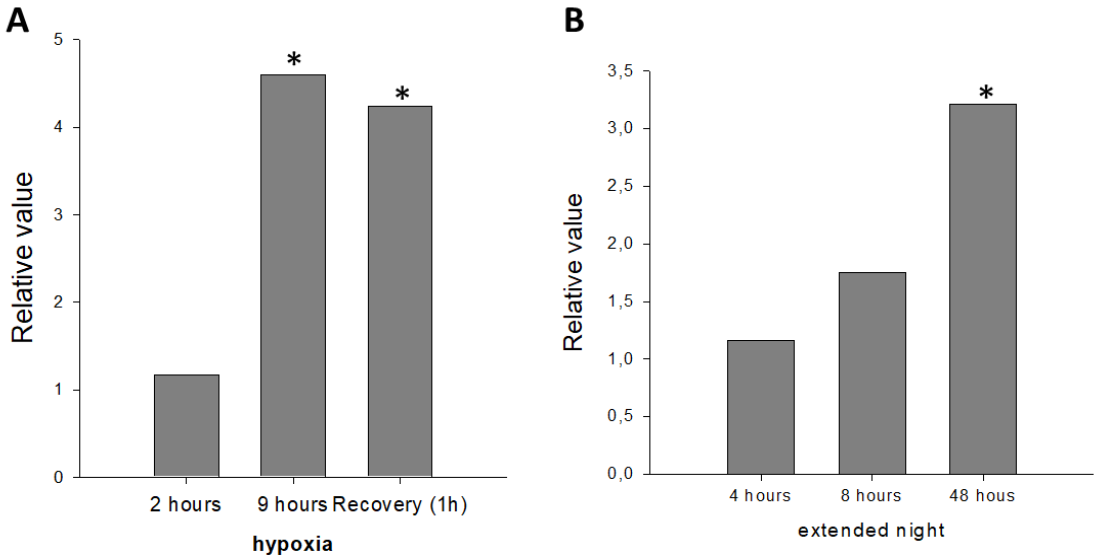

Figure S1- WRKY45 is induced hypoxia and extended night conditions

In silico analysis of WRKY45 transcript levels in different low energy conditions (A) Hypoxia (B) Extended night. (*) indicates values that were determined by the Student's t test to be significantly different ($P < 0.05$)

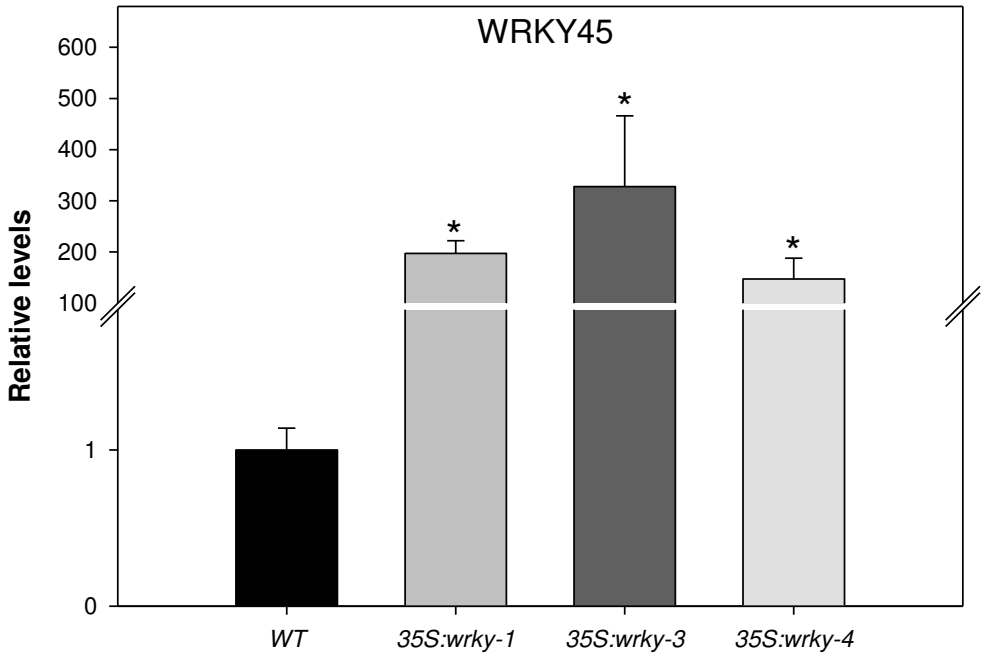

Figure S2- Confirmation of WRKY45 transcript levels in *35S:wrky45* overexpressing lines

Transcript expression levels of *WRKY45* gene in 4-week-old WT and *35S:wrky45* lines. Data were normalized to the mean calculated for the WT. Values are average of three independent biological replicates. (*) indicates values that were determined by the Student's t test to be significantly different ($P < 0.05$)

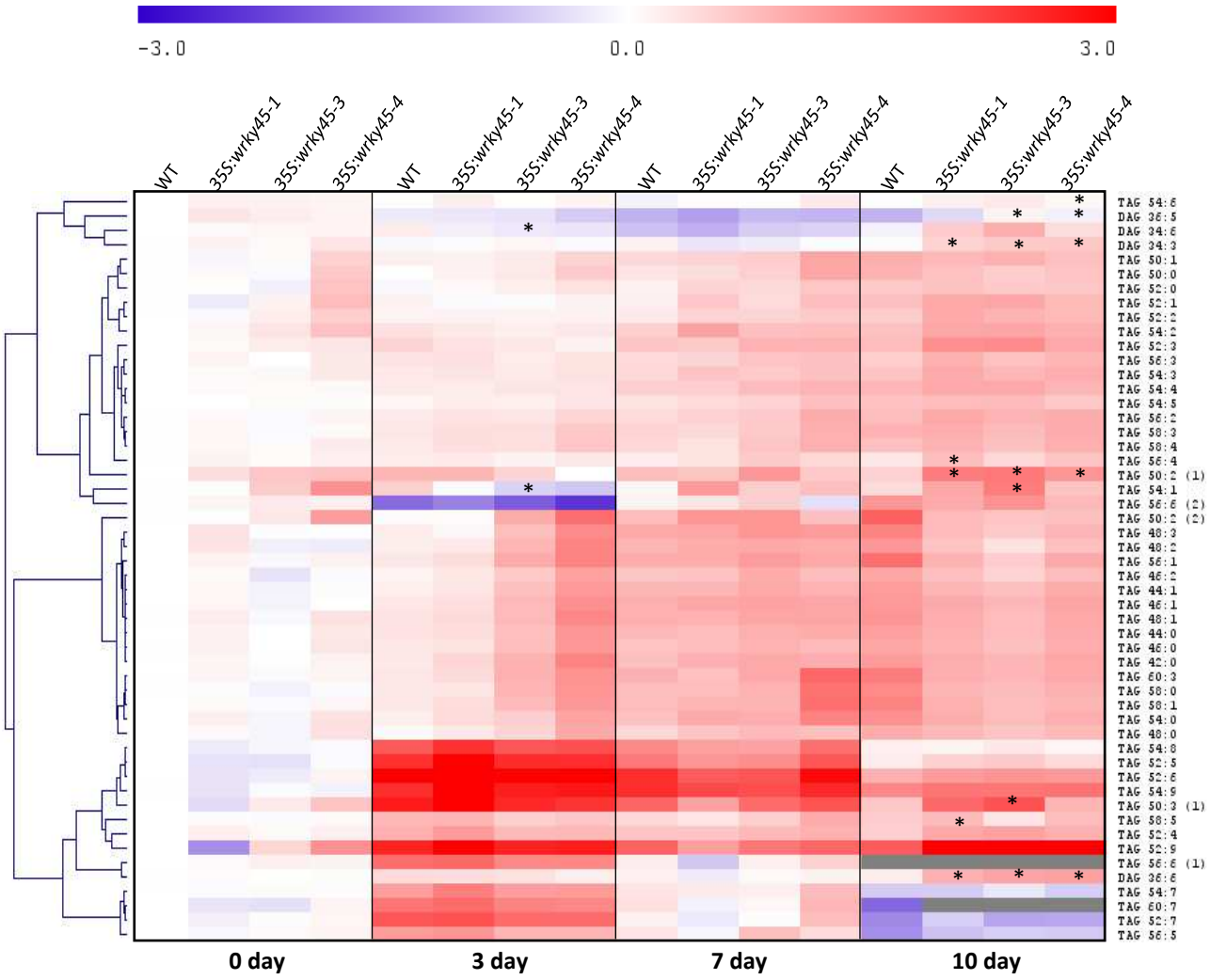

Figure S3: Neutral lipids profile of *35S:wrky45* lines during dark-induced senescence.

Triacylglycerol (TAG) and Diacylglycerol (DAG) values plotted are log_2 fold change. Distances were measured by Pearson correlation using MeV 4.9.0 software. Data were normalized to the mean response calculated for the 0-d dark treated leaves of the wild type (WT). Values presented are means ± SE of five-six biological replicates per genotype; an asterisk (*) designates values that were determined by Student's t-test to be significantly different ($P < 0.05$) from WT each time point analysed.

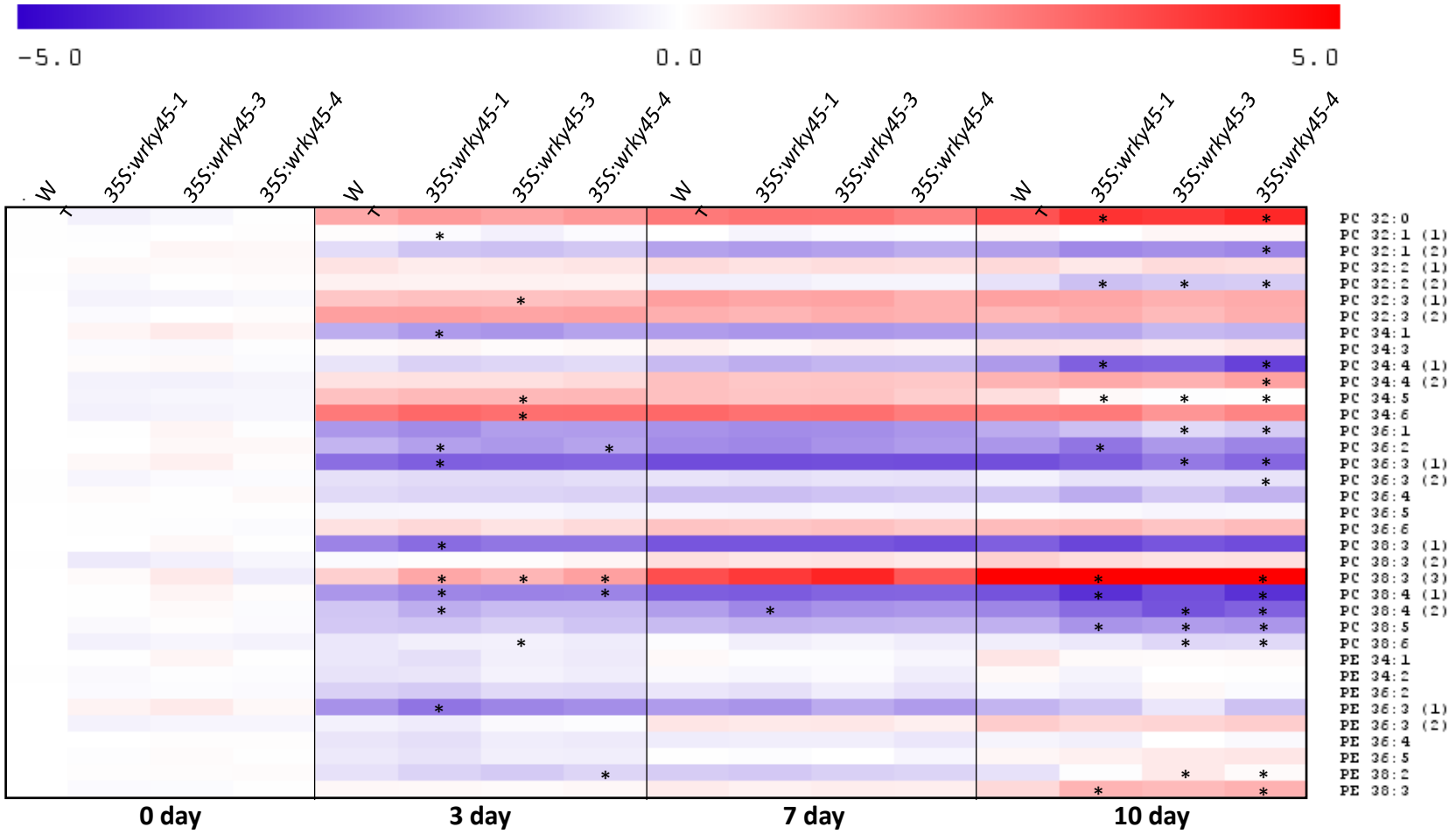

Figure S4: Phospholipid profile of *35Swrky45* lines during dark-induced senescence.

Phosphatidylcholine (PC) and Phosphatidylethanolamine (PE) values plotted are $\log_2$ fold change. Data were normalized to the mean response calculated for the 0-d dark treated leaves of the wild type (WT). Values presented are means ± SE of five-six biological replicates per genotype; an asterisk (*) designates values that were determined by Student's t-test to be significantly different ($P < 0.05$) from WT each time point analysed.

Figure S5: WRKY45 binding sites in the promoters of target genes.

Upper panel shows schematic representation of *AOX1b* and *CV* promoter regions (1 Kb) containing W box clusters. Only perfect W boxes (T/CTGACC/T, red bar) are depicted. The relative position of W boxes in respective promoters relative to the ATG start codon are indicated.

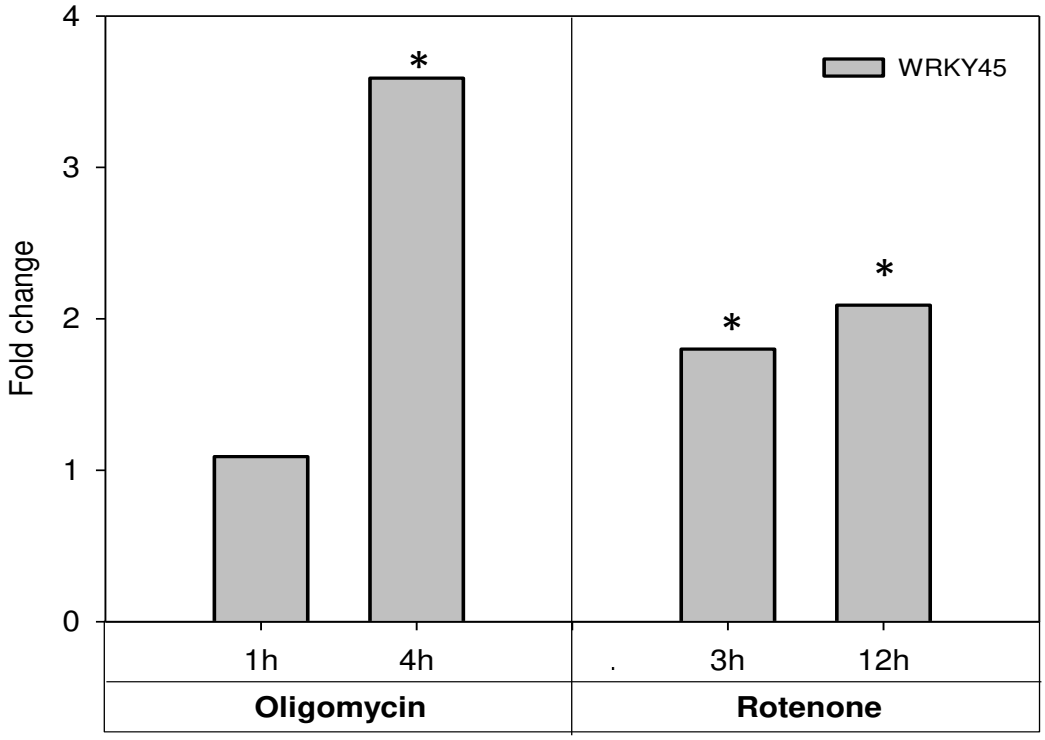

Figure S6- Mitochondrial dysfunction induces WRKY45 transcripts

In silico analysis of *WRKY45* transcript levels in different mitochondrial inhibitors treatments. (*) indicates values that were determined by the Student's t test to be significantly different ($P < 0.05$)

Supplemental Table 1. Relative metabolite content of leaves of Arabidopsis WRKY45 overexpression lines and wild type plants (WT) after further treatment for 0, 3,7 and 10 days in darkness as measured by GC-MS. Values are means ± SE of five independent samplings. Bold numbers indicate values that were determined by the Student's t test to be significantly different ($P < 0.05$) from the wild type (WT).

	WT				***35S:wrky45-1***			
	0d	**3d**	**7d**	**10d**	**0d**	**3d**	**7d**	**10d**
Alanine	1 ± 0.3	0.54 ± 0.1	0.42 ± 0.04	0.47 ± 0.1	0.62 ± 0.19	0.89 ± 0.2	0.62 ± 0.17	0.28 ± 0.2
Arginine	1 ± 0.2	5.29 ± 0.4	15.37 ± 0.9	24.2 ± 1.25	1.25 ± 0.2	4.45 ± 0.69	15.28 ± 0.9	**12.4 ± 3.5**
Asparagine	1 ± 0.4	6.18 ± 0.4	19.02 ± 1.2	28.31± 1.3	0.89 ± 0.2	7.78 ± 2.2	24.27 ± 0.9	23.44 ± 2.4
Aspartate	1 ± 0.1	0.3 ± 0.02	0.46 ± 0.18	0.71± 0.12	1.14 ± 0.1	0.24 ± 0.02	0.39 ± 0.03	0.53 ± 0.06
Citrate	1 ± 0.1	1.99 ± 0.2	2.44 ± 0.1	2.99 ± 0.32	1.05± 0.07	**1.22 ± 0.2**	**2.14 ± 0.14**	2.79 ± 0.35
Fructose	1 ± 0.3	0.05±0.006	0.04 ±0.003	0.05 ±0.01	0.69 ±0.08	0.05±0.008	0.04 ±0.004	0.06 ±0.008
Fumarate	1 ± 0.2	0.2 ± 0.02	0.11 ± 0.01	0.37 ± 0.08	0.85 ± 0.20	0.3 ± 0.14	0.09 ±0.01	**1.31 ± 0.35**
Glutamate	1 ± 0.2	1.55 ± 0.06	2.26 ± 0.13	2.21 ± 0.09	1.22 ± 0.21	1.25 ± 0.26	2.25 ± 0.07	1.69 ± 0.3
Glutamine	1 ± 0.2	0.81 ± 0.13	3.44 ± 0.36	5.50± 0.8	1.29 ± 0.38	0.65 ± 0.16	3.65 ± 0.16	**2.44 ± 0.98**
Glucose	1 ± 0.2	0.10 ± 0.01	0.04±0.002	0.04±0.003	0.87 ± 0.15	**0.07 ± 0.01**	0.05±0.007	0.04±0.002
Glycine	1 ± 0.3	0.05±0.002	0.06 ±0.003	0.06 ±0.004	0.42 ± 0.11	**0.07 ±0.007**	0.06 ±0.012	**0.21 ± 0.06**
Isoleucine	1 ± 0.2	27.70 ± 1.3	35.92 ±1.9	32.16 ± 3.8	0.84 ± 0.08	**22.26 ± 1.9**	32.92 ± 3.7	27.17 ± 0.6
Lysine	1 ± 0.3	24.62±2.28	48.6 ± 12.5	57.22 ±3.64	0.93 ± 0.09	18.64 ±2.27	35.71 ±5.17	**17.82 ± 7.9**
Malate	1 ± 0.2	0.24 ± 0.03	0.30 ± 0.01	1.95 ± 0.33	0.94 ± 0.14	0.16 ± 0.03	0.49 ± 0.05	**7.91 ± 2.0**
Manitol	1 ± 0.1	1.19 ± 0.41	2.82 ± 1.12	2.04 ± 0.55	1.1 ± 0.23	0.63 ± 0.07	1.23 ± 0.16	**20.22 ±7.08**
Mannose	1 ± 0.2	0.13 ± 0.01	0.05 ±0.004	0.05 ±0.005	0.91 ± 0.13	0.09 ± 0.01	0.06 ±0.01	0.05 ±0.004
Methionine	1 ± 0.1	6.51 ± 0.63	21.85 ±1.91	35.69 ±3.4	1.20 ± 0.18	8.63 ± 0.55	22.17 ±3.42	31.49 ±3.41
Myo-inositol	1 ± 0.1	0.06±0.006	0.33 ±0.003	0.03±0.002	0.94 ± 0.12	0.04 ±0.01	0.02 ±0.002	0.02±0.001
Ornithine	1 ± 0.2	6.18 ± 0.6	18.61 ±2.87	34.85 ±2.87	1.22 ± 0.18	5.08 ± 0.43	18.27 ±1.25	**12.7 ± 4.78**
Phenylalanin	1 ± 0.2	19 ± 1.60	62.41± 0.85	91.87 ±4.61	0.93 ± 0.12	18.37 ±1.94	73.78 ± 3.7	96.87 ± 2.0
Proline	1 ± 0.2	0.14 ± 0.01	0.11 ± 0.02	0.07 ±0.005	0.66 ± 0.09	0.12 ± 0.01	0.10 ± 0.01	**0.12 ± 0.02**
Putrescine	1 ± 0.3	0.67 ± 0.04	0.65 ± 0.08	1.07 ± 0.13	1.52 ± 0.18	0.67 ± 0.09	**0.87 ± 0.04**	1.18 ± 014.
Serine	1 ± 0.2	1.16 ± 0.06	2.10 ± 0.03	1.89 ± 0.22	0.9 ± 0.10	1.11 ± 0.10	2.07 ± 0.16	2.34 ± 0.23
Succinate	1 ± 0.1	0.73 ± 0.03	0.49 ± 0.03	1.55 ± 0.25	1.26 ± 0.19	**0.53 ± 0.05**	0.59 ± 0.07	**9.54 ± 2.95**
Sucrose	1 ± 0.1	0.04 ±0.004	0.19±0.003	0.008±0.00	0.99 ± 0.03	0.04 ±0.009	0.17 ±0.004	0.01±0.003
Spermidine	1 ± 0.1	0.89 ± 0.1	1 ± 0.04	0.85 ± 0.04	1.31 ± 0.19	0.7 ± 0.008	0.98 ± 0.07	**0.52 ± 0.13**
Tyrosine	1 ± 0.3	30.18 ±2.17	54.73 ± 4.8	44.13±4.99	0.98 ± 0.09	25.27 ±2.26	**40.5 ± 2.03**	**27.51±2.96**
Valine	1 ± 0.1	15.3 ± 0.63	24.45 ±0.47	22.29 ±3.31	0.92 ± 0.06	12.65 ±1.22	22.83 ±2.82	30.28 ±3.84

Supplemental Table 1 (continuation). Relative metabolite content of leaves of Arabidopsis WRKY45 overexpression lines and wild type plants (WT) after further treatment for 0, 3,7 and 10 days in darkness as measured by GC-MS. Values are means ± SE of five independent samplings. Bold numbers indicate values that were determined by the Student's t test to be significantly different ($P < 0.05$) from the wild type (WT).

	35S:wrky45-3				***35S:wrky45-4***			
	0d	**3d**	**7d**	**10d**	**0d**	**3d**	**7d**	**10d**
Alanine	0.85 ± 0.27	**0.87 ± 0.06**	0.36 ±0.13	0.44 ±0.08	0.9 ± 0.3	0.79 ± 0.23	0.45 ± 0.05	0.46 ±0.1
Arginine	0.88 ± 0.15	5.84 ± 0.4	14.04 ± 0.8	**13.46 ± 1.8**	0.85 ± 0.1	5.89 ± 0.18	15.02 ± 1.3	**10.34 ±1.7**
Asparagine	0.61 ± 0.13	6.75 ± 2.3	21.88 ±1.2	26.83 ±1.4	0.66 ± 0.1	5.26 ± 0.55	**21-5 ±1.73**	26.14 ±0.5
Aspartate	0.88 ± 0.08	0.27 ± 0.02	0.34 ± 0.03	0.74 ± 0.02	0.97 ± 0.14	0.28 ± 0.02	0.39 ±0.05	0.64 ± 0.0
Citrate	1.04 ±0.08	1.59 ± 0.13	2.14 ± 0.12	3.03 ± 0.15	0.98 ± 0.17	1.5 ± 0.2	2.06 ± 0.3	3.09 ± 0.1
Fructose	0.91 ± 0.13	0.04±0.002	0.04 ±0.005	0.56 ±0.006	1.21 ± 0.21	0.04±0.001	0.05 ±0.01	0.05±0.007
Fumarate	1 ± 0.11	0.15 ± 0.02	0.10±0.011	**1.07 ± 0.3**	1.23 ± 0.24	0.12 ± 0.02	0.21 ± 0.12	**1.48 ± 0.25**
Glutamate	1.14 ± 0.14	1.44 ± 0.17	2.15 ± 0.12	2.01 ± 0.10	1.24 ± 0.24	**1.33 ± 0.13**	2.23 ± 0.11	**1.83 ± 0.11**
Glutamine	1.04 ± 0.26	0.88 ± 0.28	3.20 ± 0.43	**3.05 ± 0.43**	0.85 ± 0.2	0.51 ± 0.08	2.57 ± 0.62	**2.88 ± 0.17**
Glucose	1.03 ± 0.12	**0.04 ±0.003**	0.03 ±0.003	0.06 ±0.008	1.13 ± 0.11	**0.06 ±0.006**	0.05±0.012	0.05±0.008
Glycine	0.67 ± 0.11	**0.08 ±0.005**	0.06 ±0.006	**0.12 ±0.01**	0.29 ± 0.08	**0.07 ±0.009**	0.05±0.004	**0.16 ±0.03**
Isoleucine	0.66 ± 0.05	26.2 ± 1.52	**24.91 ± 2.2**	**19.70 ± 2.4**	0.79 ± 0.11	**18.98 ± 0.9**	33.2 ±5.03	**20.35 ± 2.8**
Lysine	0.68 ± 0.07	23.57 ±1.66	34.17 ±3.23	**15.08 ±2.75**	0.83 ± 0.14	19.76 ±1.31	34 ± 5.16	**11.65 ±1.65**
Malate	1.04 ± 0.08	0.15 ± 0.02	0.37 ± 0.13	**7.06 ± 1.69**	1.35 ± 0.32	0.15 ± 0.02	0.41 ± 0.07	**10.75 ± 1.48**
Manitol	1.20 ± 0.18	0.78 ± 0.2	1.99 ± 0.77	12.8 ± 5.1	1.29 ± 0.14	0.63 ± 0.10	2.24 ± 0.5	**10.47 ± 1.9**
Mannose	1.05 ± 0.09	**0.06±0.006**	0.04 ±0.004	0.08 ±0.01	1.13 ± 0.11	**0.07 ±0.008**	0.07 ±0.01	0.06 ±0.01
Methionine	0.71 ± 0.17	**12.5 ±0 .86**	17.78 ±1.66	28.71 ±3.19	0.63 ± 0.11	10.51 ±0.88	16.21±1.68	31.66±4.45
Myo-inositol	0.88 ± 0.08	0.02±0.002	0.02±0.002	0.02±0.001	1.10 ± 0.18	0.02±0.002	0.04±0.01	0.02±0.002
Ornithine	0.88 ± 0.19	7.01 ± 0.32	16.4 ± 0.92	**12.11±2.45**	0.73 ± 0.10	6.95 ± 0.15	15.22±1.87	**8.93±1.48**
Phenylalanin	0.59 ± 0.04	24.78 ±2.43	58.16 ±3.08	97.57 ±2.18	0.6 ± 0.08	21.20± 1.24	64.56 ± 4.5	97.98 ±2.64
Proline	0.89 ± 0.21	0.12 ± 0.01	0.08 ± 0.01	**0.012 ±0.01**	1.1 ± 0.33	0.09 ±0.001	0.10 ± 0.02	0.08 ± 0.016
Putrescine	0.94 ± 0.12	0.72 ± 0.05	0.83 ± 0.13	**1.38 ± 0.13**	1.14 ± 0.11	**1.01 ± 0.06**	**1.08 ± 0.11**	1.14 ± 0.11
Serine	0.94 ± 0.09	1.34 ± 0.07	1.94 ± 0.12	1.98 ± 0.18	1.03 ± 0.06	1.4 ± 0.11	2.14 ± 0.2	2.03 ± 0.18
Succinate	1.11 ± 0.10	**0.54 ± 0.04**	0.57 ± 0.12	**6.0 ± 0.26**	1.27 ± 0.31	0.62 ± 0.06	0.52 ± 0.04	**6.84 ± 1.25**
Sucrose	0.97 ± 0.06	0.03 ±0.004	0.12 ±0.001	0.007±0.00	1.05 ± 0.07	0.03 ±0.005	0.04±0.01	0.008±0.00
Spermidine	1.26± 0.19	0.92 ±0.08	0.82 ± 0.12	**0.46 ± 0.08**	1.04 ± 0.05	0.93 ±0.03	0.98 ± 0.11	**0.35 ± 0.08**
Tyrosine	0.57 ± 0.05	28.88 ±1.25	**37.18 ±3.12**	**28.09±3.3**	0.85 ± 0.09	**22.55 ±1.74**	**40.79±5.76**	**26.29±2.92**
Valine	0.78 ± 0.05	15.48 ±1.03	19.52± 2.9	21.07 ±3.06	0.88 ± 0.09	**12.01± 0.66**	21.1 ± 3.04	22.77 ±3.23

Supplemental Table 2. Primers used in the RT-PCR analyses performed in this study

Gene	Locus	Forward primer	Reverse primer
AOX1A	AT1G34190	5'-GCCTACCGATTTGTTCTTCCAGAG-3'	5'-CGTCGAAGCGATTTGCAGTGTAG-3'
AOX1D	AT1G32350	5'-AAAGCTTTGCTCGAAGAGGCTGAG-3'	5'-ACAATCGCTCGTTCGTACCATTTG-3'
ATG8E	AT2G45170	5'-ACCCTGATCGAATTCCTGTGATTG-3'	5'-ACTGTTAGGTCTGATGGCACAAGG-3'
BCAT-2	AT1G10070	5'-TCTTTTGTTTCGTCCGGATCA-3'	5'-CAACCGAAGGAGAAGGCATGA-3'
CV	AT2G25625	5'-CGGAGGTGGAGTGACAAGAG-3'	5'-GAGCAGACGGACGAGGAAGA-3'
D2HGDH	AT4G36400	5'-GAAGCTGTCATATCGGTGGA-3'	5'-TCGTACCCAGTATTGTCTTTGC-3'
ETF(beta)	AT5G43430	5'-TTCTTAGGGAAACAGGCGATA-3'	5'-GCTTGTGGCCAACCAAGTAA-3'
ETFQO	AT2G43400	5'-TTGGCCATTAGTGCTATGGAACAC-3'	5'-TCCCATGCTTGAGCGTGAAAGG-3'
HGO	AT5G54080	5'-TGTTAGTTCCTCAAACAGGAAGGC-3'	5'-ACAGCAATCTCACCAGGAGTTACC-3'
IVDH	AT3G45300	5'-AATGGGAAAGTTGACCCAAAGGAC-3'	5'-TAAAGCGACCTGCGTTGCTCTC-3'
LKR/SDH	AT4G33150	5'-TGATTGTCGCGTCTCTGTATC-3'	5'-ATCTAGCCGAACTGCTTCTAC-3'
SAG12	AT5G45890	5'-ACAAAGGCGAAGACGCTACTTG-3'	5'-ACCGGACATCCTCATAACCTG-3'
WRKY45	AT3G01970	5'-TGCACAGAAGAAGGATGCAG-3'	5'-TGGTATGTCGTCACCACCAC-3'
ACT	AT2G37620	5'-CTTGCACCAAGCAGCATGAA -3'	5'-CCGATCCAGACACTGTACTTCCTT-3'

AOX, alternative oxidase*; ATG8,* autophagy related gene *8; BCAT,* branched chain amino acid transferase*; CV,* chloroplast vesiculation*; D2HGDH*, 2-hydroxyglutarate dehydrogenase; *ETFß*, electron-transfer flavoprotein; *ETFQO*, electron-transfer flavoprotein: ubiquinone oxidoreductase; HGO, homogentisate 1,2-Dioxygenase; *IVDH*, isovaleryl-CoA dehydrogenase; *LKR/SDH*, lysine-ketoglutarate reductase/saccharopine dehydrogenase; *SAG12*, senescence-associated genes; *ACT*, actin.

GENERAL CONCLUSIONS

This thesis was largely focused on investigating unexplored aspects governing plant response to carbon starvation conditions. Briefly, the mains goals of the work presented here were: *(i)* to gain additional insights into how and to which extent autophagy affects starvation response, in terms of lipid turnover and its interconnections with other degradative pathways *(ii)* to identify novel players operating on the transcriptional regulation of energy deprivation response. In attempt to reach these aims, different and complementary experimental approaches were undertaken, and the results obtained were divided in four independent research chapters.

Among the features characterizing the starvation response, the importance of autophagy and amino acids degradation pathways have been extensively investigated (Araujo et al., 2010, 2011; Barros et al., 2017; Hirota et al., 2018). However, much less is currently known regarding the contribution of lipid substrates to energetic maintenance during carbon depletion conditions. In the chapter 1, we summarized and discussed novel findings that reveals the potential roles of autophagy in lipid metabolism. Compelling evidence suggested that autophagy is a versatile player in lipid metabolism, either meditating lipid droplet biogenesis or turnover, in addition to autophagy requirement for membrane turnover. Current evidence also highlights the complexity of this system, given that autophagy participates in the maintenance of energy-producing organelle under stress conditions (Marshall and Vierstra, 2018). Although the significant advances on the connections between autophagy and lipid metabolism, efforts to further enhance our understanding of how exactly autophagy mechanisms are involved in lipid metabolism are clearly required.

That being said, in chapter 2 we further contribute to the improve this knowledge by using a lipidomic approach to investigate how autophagy contribute to lipid turnover, specifically under carbon starvation conditions. Our findings showed that the lack of autophagy affects proper membrane turnover and TAG accumulation, while induce the massive degradation of chloroplast lipids. Microscopy analysis revealed that *atg* mutants fails to produce lipid droplet, instead, it channels lipid substrates to Plastogoluli storage in chloroplast. By further comparing our data with a previous study using dark-treated leaves of maize *atg*12 mutants (McLoughlin et al., 2020), similarities and differences were observed highlighting that lipid changes mediated by autophagy might diverge between different species. Collectively, the chapters 1 and 2 clearly pinpoint to the requirement of further studies to fully establish the mechanism governing autophagy, membrane recycling,

and organellar maintenance. This knowledge is a potential target for metabolic engineering in the management of plant oil reserves.

During nutrient starvation, autophagy aids to the recycling of metabolites. The importance of autophagy to overcome starvation conditions is evident by the early-senescence phenotype commonly observed in *atg* mutants during these conditions (Thompson et al., 2005; Lee et al., 2013; Barros et al., 2017; Hirota et al., 2018). This fact implies that chloroplast degradation is actually faster in the absence of autophagy, which is an intriguing feature since autophagy plays a key role in chloroplast turnover. Our previous study suggested connections between autophagy and other catabolic pathway, the chloroplast vesiculation (CV), which can promote the chloroplast degradation response in the absence of autophagy (Barros et al., 2017). Thus, in the chapter 3 we investigated how autophagy and CV interact to ensure adequate chloroplast maintenance under low energy conditions induced by darkness. Firstly, we demonstrated that CV has a relatively minor importance on chloroplast degradation in presence of autophagy. Further characterization of double mutants for both CV and autophagy pathways revealed that CV mainly contributes to release of amino acids and chloroplast structural response of *atg* mutants during extended darkness. Our further results suggest that the differential chloroplast protein degradation mediated by CV and autophagy is most likely able to orchestrate the chloroplast structural changes. It will be especially important and interesting to identify proteins involved in this process. Therefore, elucidating how multiple processes of chloroplast turnover respond to different stresses and stimuli might be useful strategies to improve both yield and stress tolerance in crop plants.

Finally, the chapter 4 is mostly focused to unravel the regulatory factors which govern the early senescence phenotype and metabolic response during carbon starvation. The transcription factor WRKY45 was proposed to mediate metabolic reprogramming in response to starvation. Indeed, the overexpression of WRKY45 was associated with a differential accumulation of amino acids and organics acids, and it additionally impacts the proper respiration adjustment under extended darkness. Intriguingly, our findings indicate that WRKY45 operates mostly in the activation of mitochondrial signaling responses rather than by a direct regulation amino acid catabolic pathways. The fine-tuning of mitochondrial signaling integrate their function with overall cellular processes and reveals WRKY45 as an important modulator of plant stress responses. Additional studies are clearly required to determine the pathways involved in the transduction of low-energy signals into gene regulation and cellular adaptation.

In summary, this thesis presented and discussed novel and exciting results underlying the metabolic adjustments taking place during carbon starvation. At the same time that our findings disclose unexplored aspects involved in the regulation of plant stress response, it further adds more layers of complexity to this process. There are still many unsolved questions about the complexity between energetic metabolism, senescence, and stress response in plants. Particularly, we can name three outstanding questions that still need to be explored: (i) how and to which extent lipid substrates contributes to alternative respiratory pathways and energy generation?; (ii) what is the relevance of other chloroplast catabolic pathways, including senescent associated vacuoles, for the recycling of proteins and energy homeostasis?; and (ii) how and in which level the ETF/ETFQO system and amino acid catabolic pathways are regulated to ensure energy provision during sub-optimal growth conditions? Dissecting these mechanisms is clearly required to fully understand the key components of energetic reprogramming of plant metabolism.

REFERENCES

Araújo WL, Ishizaki K, Nunes-Nesi A, Larson TR, Tohge T, Krahnert I, Witt S, Obata T, Schauer N, Graham IA, Leaver CJ, Fernie AR (2010) Identification of the 2-hydroxyglutarate and isovaleryl-CoA dehydrogenases as alternative electron donors linking lysine catabolism to the electron transport chain of Arabidopsis mitochondria. Plant Cell **22:** 1549-1563

Araújo WL, Tohge T, Ishizaki K, Leaver CJ, Fernie AR (2011) Protein degradation – an alternative respiratory substrate for stressed plants. Trends Plant Sci. **16:** 489-498

Barros JAS, Cavalcanti JHF, Medeiros DB, Nunes-Nesi A, Avi-Wittenberg T, Fernie AR, Araújo WL (2017) Autophagy deficiency compromises alternative

Hirota T, Izumi M, Wada S, Makino A, Ishida H (2018) Vacuolar protein degradation via autophagy provides substrates to amino acid catabolic pathways as an adaptive response to sugar starvation in Arabidopsis thaliana. Plant & Cell Physiology **59:** 1363–1376

Lee TA, Vande-Wetering SW, Brusslan JA (2013) Stromal protein degradation is incomplete in Arabidopsis thaliana autophagy mutants undergoing natural senescence. BMC Research Notes **6**: 17–17

Marshall RS,Vierstra RD (2018) Autophagy: the master of bulk and selective recycling. Annu. Rev. Plant Biol. **69**: 173-208

McLoughlin F, Marshall RS, Ding X, Chatt EC, Kirkpatrick LD, Augustine RC, Li F, Otegui MS, Vierstra RD (2020) Autophagy Plays Prominent Roles in Amino Acid, Nucleotide, and Carbohydrate Metabolism During Fixed-carbon Starvation in Maize. Plant Cell. DOI: 10.1105/tpc.20.00226

Thompson AR, Doelling JH, Suttangkakul A, Vierstra RD (2005) Autophagic nutrient recycling in Arabidopsis directed by the ATG8 and ATG12 conjugation pathways. Plant Physiol **138**: 2097–2110